The Comprehensive Insight of Relationships between Mechanical Properties, Structural and Biochemical Changes in Corneal UVA/riboflavin Cross-linking

By

Shao-Hsuan Chang

A thesis submitted in application for the degree of

Doctor of Philosophy

University of Liverpool

June 2019

Declaration

I hereby certify that this dissertation constitutes my own product, that where the language of others is set forth, quotation marks so indicate, and that appropriate credit is given where I have used the language, ideas, expressions or writings of another.

I declare that the dissertation describes original work that has not previously been presented for the award of any other degree of any institution.

Signed,

Shao-Hsuan Chang

“This dissertation contains material that is confidential and/or commercially sensitive. It is included here on the understanding that this will not be revealed to any person not involved in the assessment process”.

List of Publications

Shao-Hsuan Chang, Ashkan Eliasy, Dong Zhou, Sherif Hasaan, Kevin J. Hamill, Colin E. Willoughby, Ahmed Elsheikh. Experimental Evaluation of Stiffening Effect Induced by Corneal UVA/Riboflavin Cross-Linking Using Intact Porcine Eye Globes. *In progress*

Shao-Hsuan Chang, Colin E. Willoughby, Kevin J. Hamill, Ahmed Elsheikh. The Efficacy of Conventional Versus Accelerated Collagen Cross-linking for Progressive Keratoconus: Systemic Review and Meta-analysis. *In progress*

Shao-Hsuan Chang, Ashkan Eliasy, Kai-Jung Chen, You-Ren Ji, Tai-Horng Young, Tsung-Jen Wang, Colin E. Willoughby, Kevin J. Hamill*, Ahmed Elsheikh. The Relationship Between Mechanical Properties, Ultrastructural Changes, and Intra-fibrillar Bond Formation in Corneal UVA/Riboflavin Cross-linking Treatment for Keratoconus. *J Refract Surg.* 2018;1:34(4):264-272.

Abstract

UVA/riboflavin corneal cross-linking (CXL) is a common therapeutic approach used to prevent progression in keratoconus. However, the understanding of how changes to the mechanical behaviour in cross-linked corneas relate to changes in the ultrastructure is limited. The aim of this study was to determine the correlation between the mechanical properties and ultrastructural changes induced by UVA/riboflavin CXL, and hence understand the possible stabilisation mechanism of this therapeutic approach in keratoconus.

Porcine corneas were treated following the current gold standard CXL called "Dresden" protocol, consisting of dropwise application of 0.1% riboflavin in 20% dextran followed by 30 min of UVA irradiation. The uniaxial tensile testing and inflation were performed to investigate the changes in mechanical properties and presented as the tangent modulus. The alterations in ultrastructure induced by CXL were assessed using transmission electron microscopy and Fourier Transform Infrared Spectroscopy. In addition, the protein interactions were examined using liquid chromatography-mass spectrometry and western blotting with results compared against corneas treated with each of the treatment solution components individually.

Data revealed that UVA/riboflavin cross-linked corneas displayed a significant increase in the material properties. Comparisons concentrated on tangent modulus ratios at a stress of 0.03 MPa, the tangent modulus measured in the corneas treated with the full Dresden protocol ($Et_{Cross\text{-}linking}$) were 2.09 ± 0.17 and 2.48 ± 0.69 using uniaxial tensile testing and inflation, with a 28±17% and 43±24% increase comparing to its corresponding control respectively. The altered collagen architecture was observed within the first 300 μm of stromal depth consisting of 5% increase ($p < 0.01$) in the thickness of collagen fibrils with no significant changes to intra-fibrillar spacing, resulting in an 8% to 12% decrease in number of fibrils per unit area. Furthermore, Fourier Transform Infrared Spectroscopy confirmed formation of inter-fibrillar amide bonds induced by UVA-mediated CXL. Although dextran contributed to a 13±9% increase in stiffness accompanied with a reduced fibrillar thickness

($p < 0.05$) and potential C-O stretching force, it did not cause additional protein interactions on proteoglycans or collagens according to the western blot analysis and Coomassie blue staining.

The data support a model wherein collagen fibril diameter and structural density are fundamental parameters in defining tissue stiffening following UVA/riboflavin corneal CXL, and provide the key benchmarks against which modifications to the Dresden CXL protocol can be evaluated.

Key words: Collagen Cross-linking, Dresden Protocol, Tangent Modulus, Ultrastructure, Proteoglycans, Riboflavin, Keratoconus

Table of Contents

List of Figures

List of Tables

Abbreviations

CXL: Cross-linking

ICRS: Intrastromal Corneal Ring Segments

IOP: Intraocular Pressure

UVA: Ultraviolet-A

LASIK: Laser Assisted in Situ Keratomileusis

PPK: Photorefractive Keratectomy

PK: Penetrating Keratoplasty

ORA: Ocular Response Analyser

TEM: Transmission Electron Microscopy

SEM: Scanning Electron Microscopy

FTIR: Fourier Transform Infrared Spectroscopy

AFM: Atomic Force Microscopy

ATR: Attenuated Total Reflection

LC-MS: Liquid Chromatography-Mass Spectrometry

FE: Finite Element

IFE: Inverse Finite Element

DIC: Digital Image Correlation

PIV: Particle Image Velocimetry

PSO: Particle Swarm Optimisation

TMD: Thickness Measurement Device

CHT: Circular Hough Transform

LED: Light Emitting Diode

MCM: Monte Carlo Method

μ: Shear Modulus

α: Strain Hardening Exponent

ε: Strain

σ: Stress

Et: Tangent Modulus

ROS: Reactive Oxygen Species

PG: Proteoglycan

GAG: Glycosaminoglycan

ECM: Extracellular Matrix

KS: Karatan Sulfate

CS: Chondroitin Sulfate

DS: Dermatan Sulfate

MMP: Matrix Metalloproteinase

LOX: Lysyl Oxidase

TIMP: Tissue Inhibitors of Metalloproteinase

ChonABC: Chondroitinase ABC

Kase: Keratanase

IL: Interleukin

TNF-α: Tumor Necrosis Factor-α

PBS: Phosphate Buffered Saline

D_2O: Deuterium Oxide

PMSF: Phenylmethylsulfonyl Fluoride

PVDF: Polyvinylidene Difluoride

HPMC: Hydroxypropyl Methylcellulose

SDS: Sodium Dodecyl Sulfate

SDS-PAGE: Sodium Dodecyl Sulfate Polyacrylamide Gel Electrophoresis

D: Dioptre

CDVA: corrected Distance Visual Acuity

UCVA: Uncorrected Visual Acuity

CCT: Central Corneal Thickness

MRSE: Mean Refractive Spherical Equivalent

SE: Spherical Equivalent

K: Keratometry

NOS: Newcastle Ottawa Quality Assessment Scale

RMS: Root Mean Square

SD: Standard Deviation

ANOVA: One Way Analysis of Variance

I^2: Heterogeneity

SMD: Standard Mean Difference

Chapter 1. Introduction

1.1. Background

Cornea is the outermost, transparent structure that protects the eyes from external influences and provides most of the eyes' refractive power (Campbell and Gubisch 1966, DelMonte and Kim 2011). Any abnormality of the cornea can affect the eye sight significantly. Corneal ectatic disorder, such as keratoconus, is a progressive degenerative corneal disease in which structural changes progress to become a thin and more cone-shaped cornea. Keratoconus affects roughly 1 in 375 in the general population (Godefrooij, de Wit et al. 2017). However, difficulties with differential diagnosis result in the uncertainty and its prevalence. The exact aetiology of keratoconus remains unclear, which may be associated with certain connective tissue disorders and inheritance (Davidson, Hayes et al. 2014, Gordon-Shaag, Millodot et al. 2015, Woodward, Blachley et al. 2016). Environmental and genetic factors are both decisive causes (Mao and Bristow 2001). In the early to moderate stages of keratoconus, rigid contact lenses and intrastromal corneal ring segments (ICRS) are the usual treatments (Alio, Pinero et al. 2011). However, they do not affect the corneal tissue nor do they arrest or slow down the progression of keratoconus. As the disease advances, contact lenses and ICRS can no longer be effective in improving visual acuity, penetrating keratoplasty (PK) is required to restore visual functions in 20% of cases (Waller, Steinert et al. 1995). Therefore, keratoconus becomes one of the most common indications for keratoplasty worldwide (Al-Yousuf, Mavrikakis et al. 2004).

One of the key features of keratoconus is the loss of corneal mechanical stability, with the reduced stiffness of the cornea compared to a normal cornea (Wollensak 2006). Cross-linking (CXL) with ultraviolet-A (UVA) and photosensitizer riboflavin is a new strategy that has been reported to be effective in arresting keratoconus progression in the majority of treated eyes in a number of randomised controlled trials (O'Brart, Chan et al. 2011, Wittig-Silva, Chan et al. 2014). Theoretically, CXL is a procedure that creates chemical bonds between the substrates e.g. collagen, proteoglycans, and other proteins in the corneal stroma by means of photo-polymerization using UVA and riboflavin to strengthen the structure (Wollensak, Spoerl et al. 2003, Coskunseven, Jankov et al. 2009). The

change in corneal biomechanical properties is postulated to initiate immediately after CXL treatment. Therefore, the determination of biomechanical properties of the cornea tissue requires reliable and accurate measurements *ex vivo*, which is an important indicator for the advancement of corneal biomechanics. Numerous modifications to the standard CXL protocol such as accelerated and trans-epithelial CXL have been developed in clinical setting. Although these clinical results are promising, the long-term efficacy of current treatment regimens remains uncertain. The lack of a suitable study platform to evaluate CXL methodologies in clinical practice worldwide is also a limitation. Therefore, the current study aimed to improve this understanding and develop a systematic testing method that includes the *ex vivo* inflation tests on the whole eye globe. The investigation on the effect of UVA/riboflavin CXL and the variables/modifications that may determine the treatment outcome is of scientific and clinical value.

1.1.1. The Eye

The ocular globe is a complex organ responsible for processing the light from the environment through specialized cells in retina which induce the electro-chemical impulses to the brain to create visual sensations (Stryer 1987, Passaglia, Dodge et al. 1997). The outmost protective tunic is made up of the sclera and cornea, which is pressurized shell structure of varying thickness. Sclera is opaque and constitutes about five-sixths of the eye (Watson and Young 2004). Cornea is the transparent segment located at the front of the eye and forms approximately one sixth of its total surface area. The cornea and lens both are responsible for the refraction of light. Cornea acts as the principal refractive component and accounts for about 70% the total refractive power (DelMonte and Kim 2011, Sridhar 2018). The lens has the ability to alter its shape and focal distance in order to focus an object with varying distance (Land 2015). As a result, those tissues and transparent media including aqueous humour in the anterior chamber and vitreous body in the posterior chamber have to remain optically clear to obtain good eyesight.

The inner layer of the eye is consisting of the choroid, ciliary body and iris. The iris modifies the amount of the light entering the eye by adjusting the size of the pupil. Behind the iris is the lens which is attached to the ciliary body via a series of zonular fibres (Land 2015). The retina is the innermost surface of the eye, which contains photo-receptive nervous elements required to generate cellular signals and action potentials. Finally, the complex cascades within the retina are transmitted along the optic nerve extending to the visual cortex of the brain (Erskine and Herrera 2014). The gross structure of the eye is illustrated in figure 1.1.

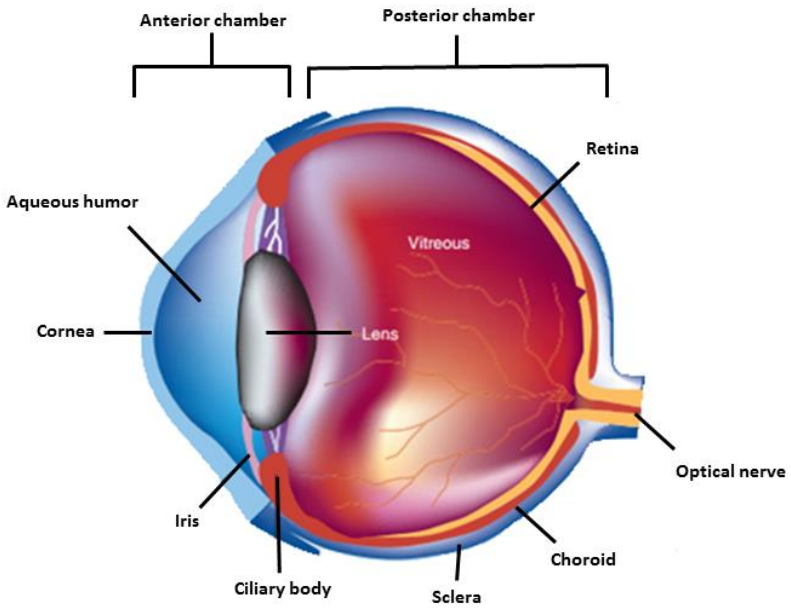

Figure 1.1. Cross-sectional illustration of ocular globe. Reproduced from (Mason, Stewart et al. 2011)

1.1.2. Corneal Extracellular Matrix and Ultrastructure

1.1.2.1. Epithelium and Bowman's Layer

The function and structure of the cornea are of significant importance for maintaining physiological visual capability. As a protective element of the eye, the cornea shields the intraocular structures from external influences. It consists of five basic layers: epithelium, Bowman's layer, stroma, Descemet's membrane, and endothelium, as shown in figure 1.2 (DelMonte and Kim 2011). Epithelium is the outmost surface of the cornea, a stratified non-keratinizing squamous layer, constituting about 10% of the corneal thickness. Bowman's layer is a specialised corneal membrane and described as a modified region of anterior stroma. A study that applied transmission electron microscopy (TEM) has shown that lower mammals have a thin Bowman's layer whereas higher mammals display a thicker layer (Hayashi, Osawa et al. 2002). Ultrastructurally, it is 8-12 μm thick in human, consisting of fine collagen fibrils with around 25 nm in diameter and interweaving with fibrils of the anterior stroma (figure 1.3) (Komai and Ushiki 1991). Although the anatomical structure of Bowman's layer has been well explored, its physiological function is inconclusive (Wilson and Hong 2000).

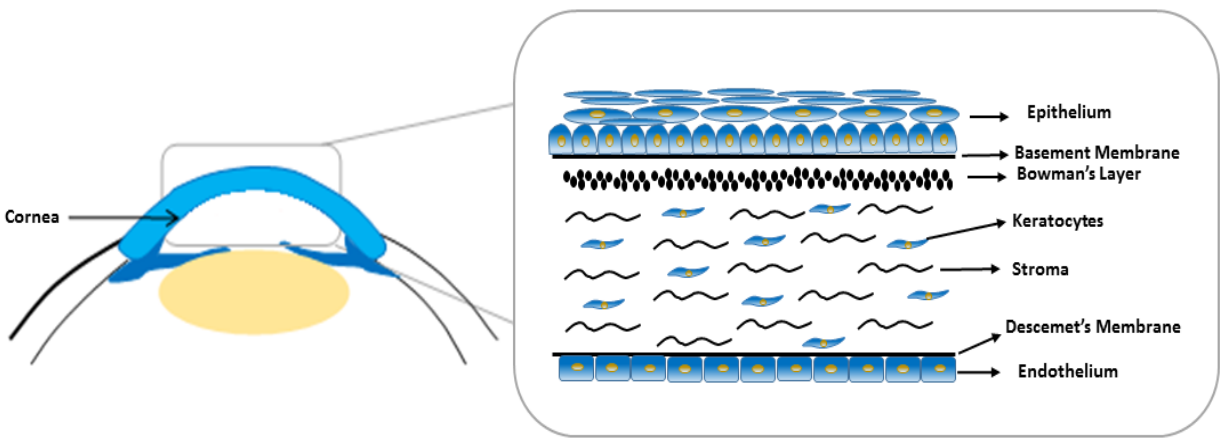

Figure 1.2. Structure of cornea. Reproduced from (Parekh, Ferrari et al. 2016)

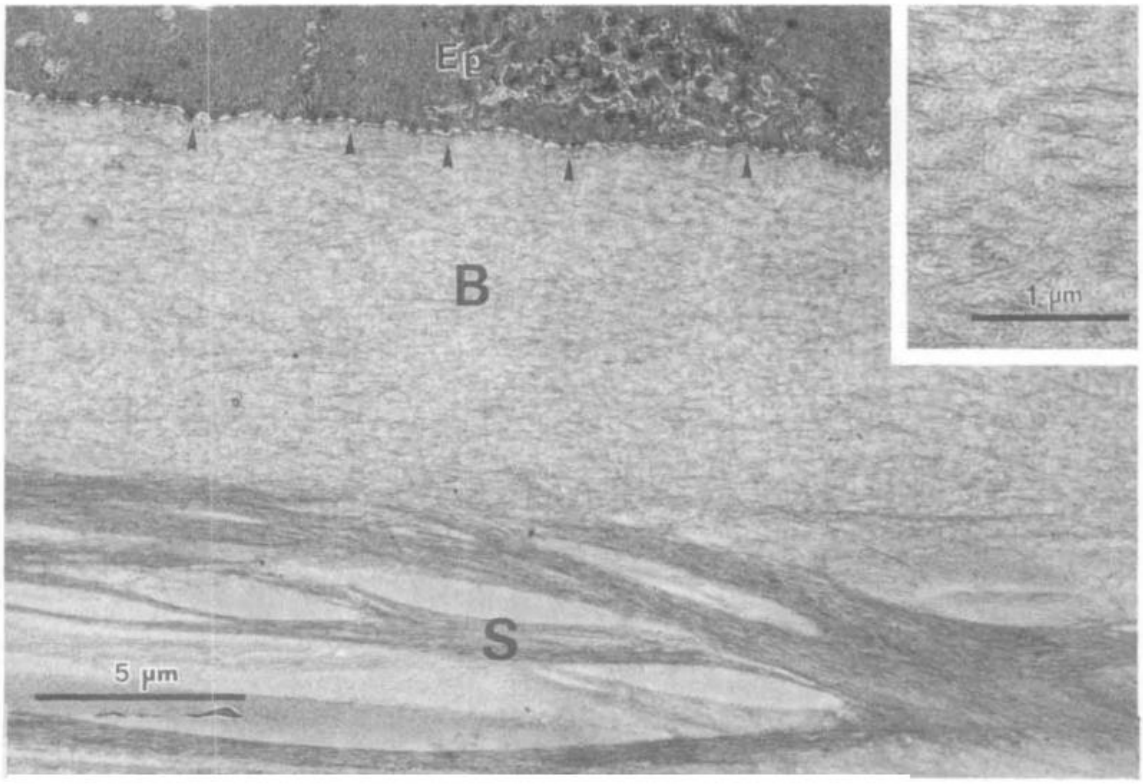

Figure 1.3. Transmission electronic micrograph of cross-section of Bowman's layer in human cornea. Arrowheads show the irregular profile in anterior surface. B = Bowman's layer, Ep = epithelium, S = stroma (x6300). Inset: higher magnification of the collagen fibrils (x23000). Source (Komai and Ushiki 1991)

1.1.2.2. Stroma and Keratocytes

Stroma comprises almost 90% of the corneal thickness and acts as the main contributor for light scattering, corneal transparency, corneal mechanical strength and curvature (Bergmanson, Sheldon et al. 1999, DelMonte and Kim 2011). Basically, stroma is a structure of a matrix of cellular, proteoglycan and collagenous components. The stroma consists of approximately 200-300 lamellae layers of mainly type I collagen fibril (figure 1.4). The orientation of collagen fibrils and spacing arrangement in each lamella are critical for the corneal transparency, corneal strength and rigidity (Meek 2009, Meek and Knupp 2015). Keratocytes are the predominant cellular component in stroma, responsible for synthesizing collagen and regulating the corneal constituents and extracellular matrix (ECM) compositions between the lamellae (Chen, Mienaltowski et al. 2015). However, the direct contribution of keratocytes to the corneal biomechanical properties is unclear, but the role of

keratocytes can imply the underlying involvement in mechanical stability that stems from the highly organized collagen structure. In normal physiological states, keratocytes are quiescent but become mitotically active fibroblasts in response to injury or damaged areas to assist in healing (Kuo, Broman et al. 2006, DelMonte and Kim 2011).

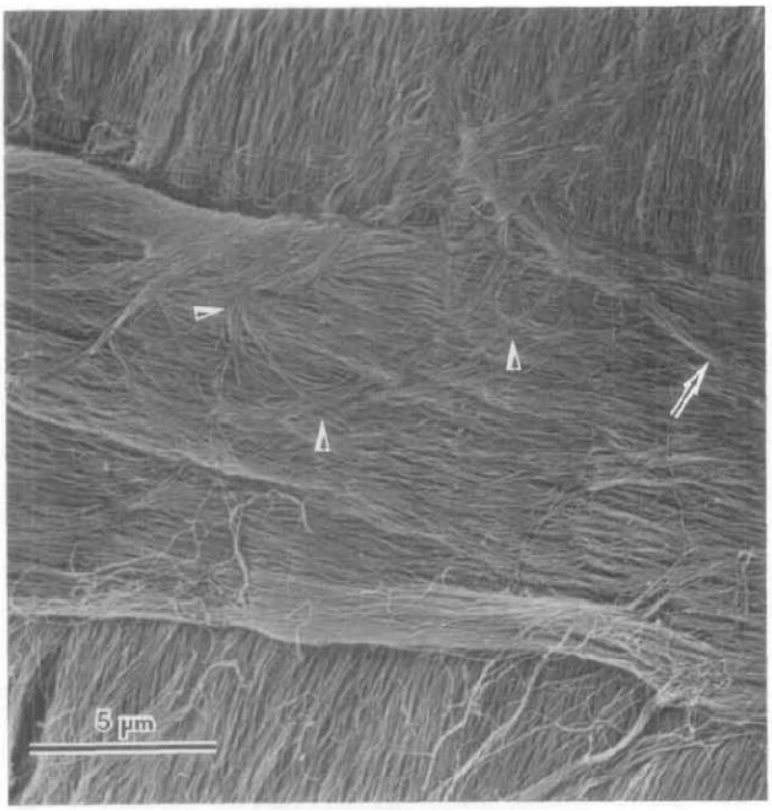

Figure 1.4. Lamellae surface of cornea. Collagen fibrils of each bundle are arranged in the same direction (arrows). Source (Komai and Ushiki 1991)

1.1.2.3. Stroma and Proteoglycans

Stroma contains keratocan, lumican, mimecan, and decorin, the core proteins of major proteoglycans that play important roles in corneal hydration and transparency (Iozzo 1999, Chakravarti, Petroll et al. 2000). Proteoglycans (PGs) are macromolecules covalently bonded to oligosaccharides and glycosaminoglycan (GAG) side chains (Chan, Cogan et al. 1993). The GAG side chains include keratan sulfate (KS) and chondroitin/dermatan sulfate (CS/DS) (figure 1.5). These small leucine-rich repeat proteoglycans play a pivotal role in modifying the structure and function of collagen fibrils. Evidence from experimental results indicate that KS is important in the regulation of collagen fibril diameter, while DS is not involved in determining the fibril diameter but participating in modulating

inter-fibrillar spacing and lamellar adhesion, suggesting that proteoglycan-collagen interactions may be important in fibril assembly and matrix organization (Chan, Cogan et al. 1993, Kuo, Broman et al. 2006). Another supported study from Wollensak and colleagues have reported that the digestion of PGs by alpha-amylase led to a significant decrease in inter-lamellar cohesion force, which showed the importance of PG complexes in inter-lamellar stabilization (Wollensak, Sporl et al. 2011). The types of PGs and their amount in different structures of the cornea are shown in Table 1.1.

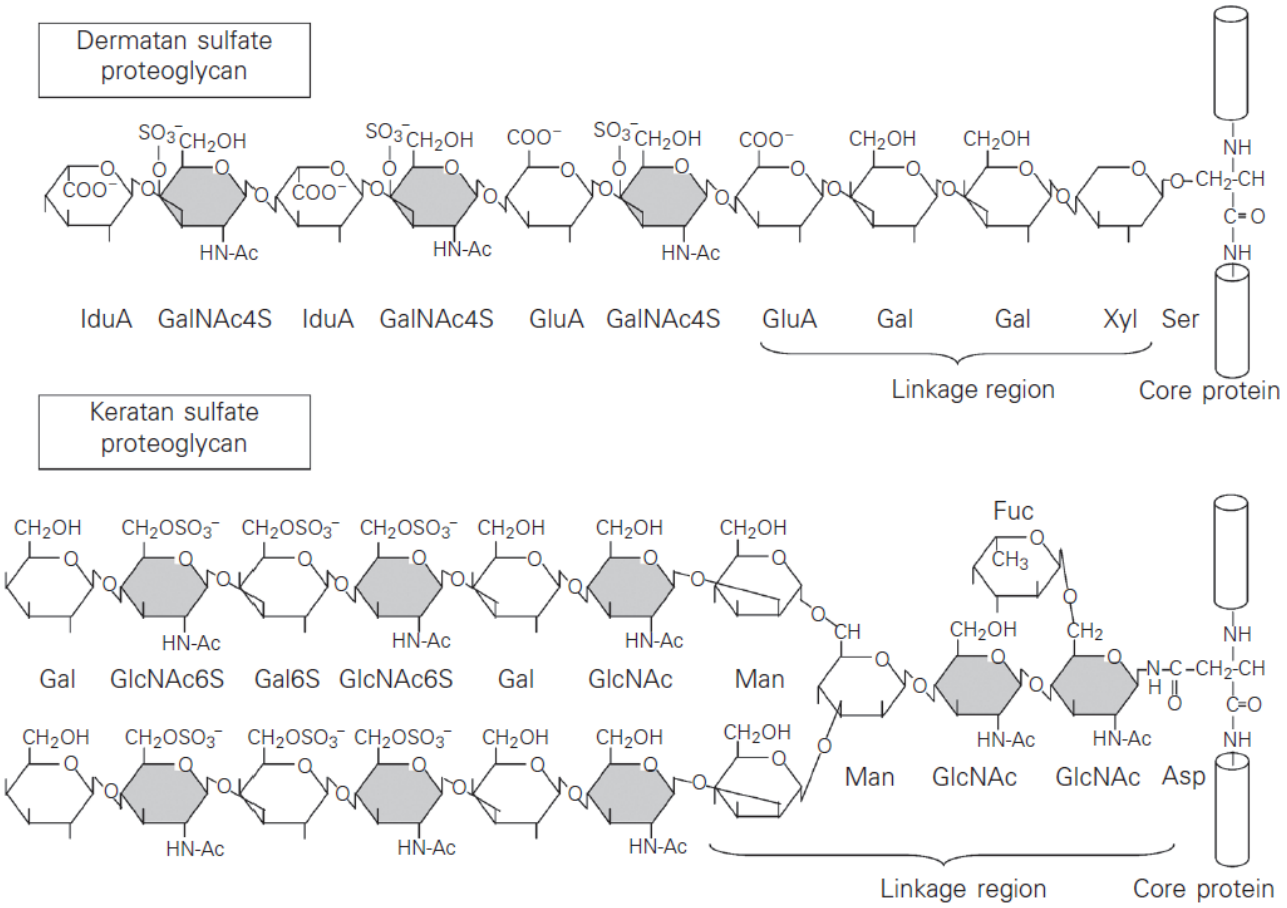

Figure 1.5. Structure of corneal matrix glycosaminoglycans (GAGs). Source (Michelacci 2003)

Table 1.1. Distributions of proteoglycan types and their amount in corneal structure. Source (Michelacci 2003)

Corneal structure	Proteoglycan types and their level		
	Keratan S	Heparan S	Chondroitin S
Epithelium	low	Low	High
Bowman's	Low	High at interface with epithelium	Low
Stroma	high	Low	Low
Descemet's	Low	High at interface with endothelium	Low
Endothelium	Low	Low	High
Keratocyte	Low	Low	High

1.1.2.4. Stroma and Collagen

The primary stromal constituent is collagenous networks with remarkably uniform diameter and inter-fibrillar spacing (Quantock and Young 2008, Meek 2009). Corneal collagen fibrils are composed of type I molecules incorporated with type V molecules into heterotypic fibrils (Birk, Fitch et al. 1988). Collagen fibrils in each lamellae run parallel to each other and to the surface of the cornea. They are of similar diameter and relatively uniformly spaced. The internal structure of the stroma is classified into anterior and posterior regions. The orientation and densely-packed interwoven lamellae within anterior stroma contribute to corneal rigidity and curvature maintenance (DelMonte and Kim 2011, Morishige, Takagi et al. 2011). Whereas, lamellae are less interwoven and loosely-packed in posterior stroma (Wang, Rabinowitz et al. 2000). Due to the structural characteristics, the posterior stroma is known to have the capabilities in controlling hydration and swelling with a lower refractive index compared to anterior stroma (Freund, McCally et al. 1995, Wang, Rabinowitz et al. 2000). Indeed, it has been reported that swelling is confined to the posterior stroma and anterior stroma does not swell perceptibly under conditions of extreme hydration (Lee and Wilson 1981, Castoro, Bettelheim et al. 1988, Cristol, Edelhauser et al. 1992, Muller, Pels et al. 2001). Stromal swelling is due to the pressure exerted by the presence of negative charged PGs which is observed in the anterior and posterior

stroma. Therefore, the differential swelling behaviour between anterior and posterior, and the special feature of posterior stroma for constraining swelling can be considered to relate to the fibril number density, stromal interweave and differences in PGs (Lee and Wilson 1981, Castoro, Bettelheim et al. 1988, Abahussin, Hayes et al. 2009). In the bovine corneal stroma, the KS/CS ratio is higher in posterior stroma than that in anterior stroma (Bettelheim and Plessy 1975). It may be explained that the water affinity of KS is higher than CS. Additionally, the anterior interweave of the stromal lamellae has been reported to contribute to the non-swelling property of anterior stroma (Muller, Pels et al. 2001, Alanazi, Almubrad et al. 2015). The isotropic arrangement in the anterior cornea and organizational differences of the anterior and posterior lamellae may play an important role in structural stability in the maintenance of corneal curvature and these specified physiological properties (Abahussin, Hayes et al. 2009).

In-depth studies of collagen fibril orientation using x-ray diffraction indicate two preferred directions of collagen in the central cornea along horizontal (nasal-temporal) and vertical (superior-inferior) meridians in human (Daxer and Fratzl 1997, Meek and Boote 2009). Another study reveals approximately 30% of collagen fibrils throughout the stromal depth tended to lie in the diagonal direction (Boote, Dennis et al. 2005). Additionally, vertically and horizontally orientated strip specimens are found to exhibit similar stiffness stretching at low extension rate (1%/min) within physiological range (Elsheikh, Brown et al. 2008). This suggests that the collagen fibrils are populated equally in orthogonal directions at the centre of the cornea to provide corneal elasticity in order to withstand intraocular pressure (IOP). In summary, collagens within corneal stroma are highly organised, display preferred orthogonal arrangement and a high degree of spatial organisation with uniform diameter of fibrils (Daxer and Fratzl 1997, Newton and Meek 1998, Boote, Dennis et al. 2003).

1.1.2.5. Descemet's Membrane and Endothelium

Descemet's membrane is the basement membrane of endothelium. Its abnormality can affect the health of the endothelial cells, which is known as Fuch's endothelial dystrophy (Bergmanson,

Sheldon et al. 1999). Endothelium is formed of a 5-μm thick monolayer of polarized cells in hexagonal shape. Different from the epithelium which is a self-renewing layer and harbours a resident stem cell population at its periphery. Endothelium is normally quiescent and not considered self-regeneration (Polisetti and Joyce 2013). The essential function of endothelium is to maintain stromal deturgescence and corneal clarity by actively pumping ions, which draws water osmotically from the stroma into aqueous humour (Hodson and Mayes 1978).

1.1.2.6. Summary

Although these components and critical structures are important in regulating thickness, transparency, and physiological function (Bourne 2003), the mechanical behaviour of cornea is essential for maintaining its dimensions and stable shape for a good vision. The cornea maintains its shape by balancing IOP with a transverse swelling pressure which results from the presence of collagen, salts and proteoglycans (Hodson and Mayes 1978). The normal physiological IOP value ranges between 10 to 20 mmHg (Eysteinsson, Jonasson et al. 2002). Together, the cornea and sclera form the outermost fibrous tunic wall which is capable of withstanding both internal and external forces to retain the shape of the eye globe.

This thesis performed the experimental designs on porcine corneas, in which corneal dimensions, collagen preferred orientation, stromal thickness and radius of curvature are significantly different from human corneas. The use of animal corneas as approximate models for human corneas to assess biomechanical properties has been necessary and widely studied in comparative analysis. The porcine corneas show a primarily circumferential orientation of fibrils, whereas the fibrils in human corneas have a preferential orientation in the superior-inferior and temporal-nasal direction (Meek and Newton 1999, Zeng, Yang et al. 2001, Wollensak, Spoerl et al. 2003, Hayes, Boote et al. 2007, Elsheikh, Alhasso et al. 2008). It is acceptable that the porcine cornea is a suitable model for human cornea in mechanical measurement. Although there exists some differences in corneal thickness (the average porcine cornea is 1.2 times thicker than the human cornea), stiffness (the porcine cornea is

more elastic than the human cornea), and ultrastructure of fibril orientation. They exhibit similar stress-strain behaviour and react similarly to sustained loading.

1.1.3. Corneal Mechanics

Corneal mechanics is an important field to study the refractive function and material properties (Dupps and Wilson 2006). In recent years, there has been an increased scientific interest in assessing biomechanical properties of the cornea due to its potential clinical applications, such as the measurement of IOP, the surgical outcome prediction, and the diagnosis of keratoconus. Cornea is considered as a viscoelastic material and exhibits a response from its viscous (fluid property such as the content of PGs and GAGs) and elastic (solid property such as collagen fibrils and lamellae layers) characteristics. Therefore, any specific mechanical changes occurring in the cornea can be linked to the alternations in its viscous and elastic components. A complete understanding of corneal biomechanical properties is needed and will be helpful for developing effective simulation models for a more accurate surgical outcome prediction.

It is commonly accepted that the overall biomechanical properties of the cornea are largely determined by the corneal stroma, and a summation of many factors related to the lamellae structure and its physiological states (Maurice and Monroe 1990). The measurement of mechanical behaviour of the cornea depends on its thickness, curvature, topography, IOP, hyper-elasticity and hydration state of the tissue. Clinically, studies have focused on measuring corneal biomechanical properties *in vivo* by using Ocular Response Analyser (ORA) (Medeiros and Weinreb 2006). ORA is the standard biomechanical characterization method by exerting a high-speed air puff onto the cornea that results in consequent corneal deformation. The deformation of the cornea is recorded through the measurement of applanation pressure signals (figure 1.6). The two pressure signals which occur when cornea deforms inwardly at the onset of the airpuff and when it returns back to original state are used to calculate biomechanical parameters (Ahearne, Yang et al. 2007). IOP increases have been reported in patients after CXL treatment, which may reflect the increase in corneal rigidity (Coskunseven, Jankov et al. 2009, Kymionis, Grentzelos et al. 2010, Vinciguerra, Albe et al. 2010). However, it may

be an effect on the measurement method, the corneal stiffening due to CXL might be responsible for IOP overestimation (Krueger and Ramos-Esteban 2007). In addition, it lacks the correlations to standard mechanical property measurements such as stress and strain, and elasticity for direct comparison (Ahearne, Yang et al. 2007).

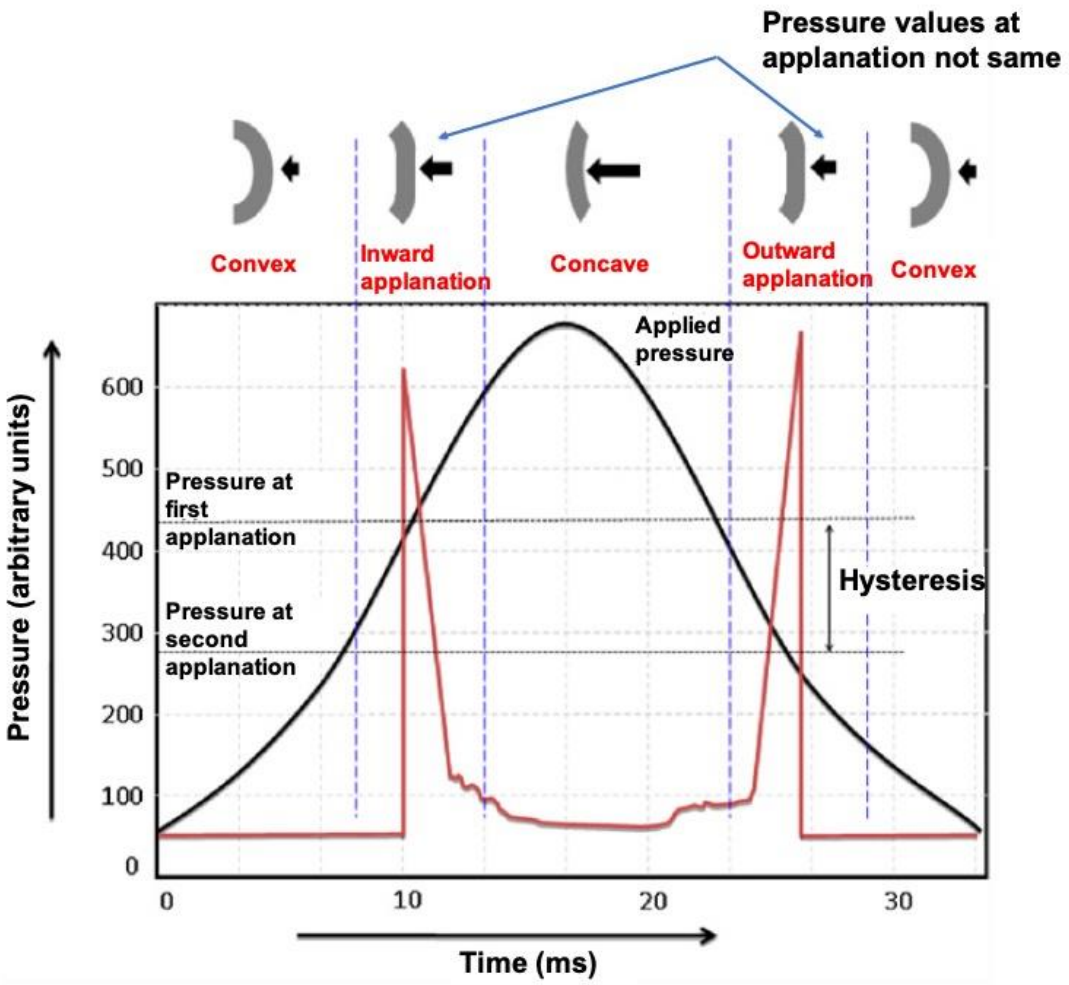

Figure 1.6. Measurement of corneal mechanical properties using ORA. Source (Ambekar, Toussaint et al. 2011)

Although some biomechanical behaviours can be measure *in vivo*, the decisive properties largely rely on *ex vivo* mechanical tests. The classic biomechanical properties include Young's modulus of elasticity, creep, stress-relaxation and hysteresis. The Young's modulus is the proportion between the applied stress and the resultant strain values, which reflects the stiffness or elasticity of the tissue (Wollensak, Spoerl et al. 2003, Kohlhaas, Spoerl et al. 2006). Creep is defined as the changes in

deformation of the material under constant loading force, which will be useful information to reveal the biomechanical abnormality due to the impaired extracellular matrix. Hysteresis is characterised during cyclic loading of soft biological tissues. It describes the stress-strain difference in loading and unloading states and represents a dissipation of energy within the material (Lombardo, Serrao et al. 2014). A more accurate term is viscous damping, which indicates the result of the interaction between PGs and extracellular matrix in biological tissues. The tissue viscoelasticity can be attributed to fluid movement within the tissue, the reorientation of the collagen fibrils, and the flow-dependent viscoelasticity of the proteoglycans. In addition, due to the depth-dependent preferred collagen orientation, the comprehensive understanding of spatial-mechanical variations within the stroma is of importance for the advancement of corneal mechanics.

The mechanical properties of the cornea are governed by the composition, dimensions, and arrangement of its structural components, which can be determined by its stress-strain behaviour. Uniaxial tensile testing is the traditional and most commonly used *ex vivo* testing to determine the tangent modulus or elasticity of cornea. The collagen fibrils are mainly responsible for cornea stiffness and strength. They bear the load at moderate to elevated strain levels (linear region of the stress-strain curve) (figure 1.7) (Freed and Doehring 2005). This method involves in isolating the cornea *ex vivo* and applying certain pressure or loading under constant humidity and temperature (figure 1.8) (Wollensak, Spoerl et al. 2003, Boyce, Jones et al. 2007). However, in this technique, cornea is excised into strips and flattened without considering the thickness variations between centre and periphery. The mechanical measurements may be inaccurate due to its technique destructive specimen preparation with disrupted fibril orientations, inconsideration of corneal curvature, and non-uniform stress distribution while applied the stretching force along the corneal strip (Elsheikh and Anderson 2005, Ahearne, Yang et al. 2007, Ruberti, Sinha Roy et al. 2011).

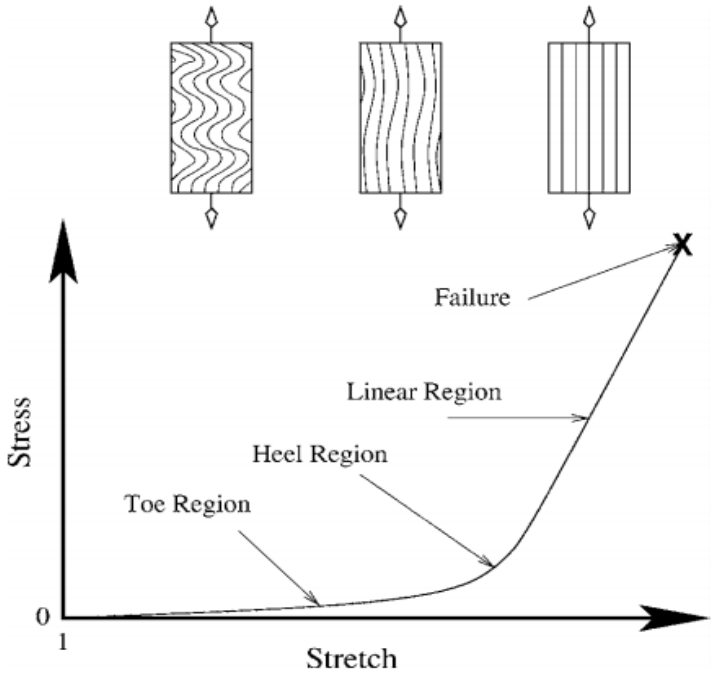

Figure 1.7. The strain-stress curve of typical collagenous tissue. The collagen fibril recruitment shows as a function of the deformation. Source (Freed and Doehring 2005)

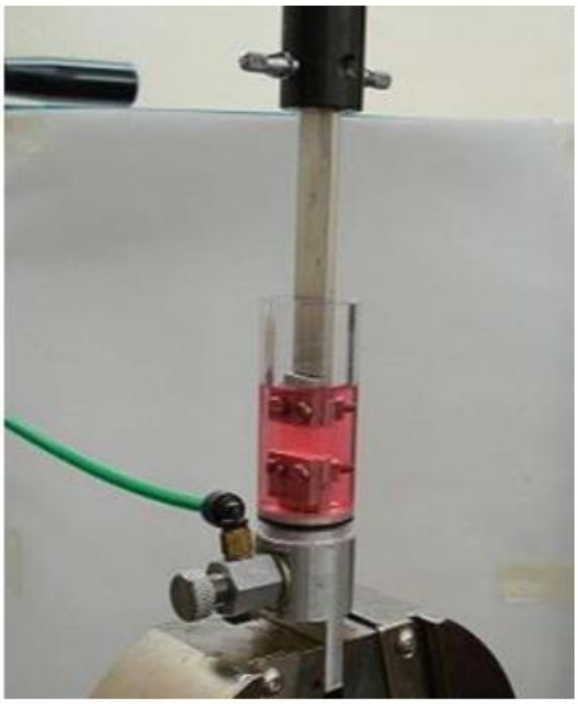

Figure 1.8. Uniaxial tensile specimen hydration technique with a custom-made enclosure designed to allow the full immersion of tensile specimens in organ culture during uniaxial extensometry and prevent tissue dehydration. Source (Elsheikh, Alhasso et al. 2008)

Although these factors affect the accuracy and reliability of the uniaxial testing as cornea shows regional variations in strain and deformation, the results can still be further improved by mathematical modifications (Elsheikh and Anderson 2005). However, it is unclear how the *ex vivo* measurement of tensile test corresponds to its mechanical properties *in vivo*. Therefore, the inflation test (figure 1.9) with intact cornea or whole eye globe has been developed and attempted to address this issue by mimicking the *in vivo* loading conditions of the eye (Elsheikh, Wang et al. 2007, Boyce, Grazier et al. 2008, Elsheikh, Alhasso et al. 2008). The test is considered to be more reliable and closely related to *in vivo* conditions than uniaxial tensile test. It is expected to produce the average behaviour of intact corneas due to the stromal anisotropy resulting from the preferred collagen fibril orientation. Inflation test analyses the degree of extension of the cornea in response to the change in IOP. When the IOP is increased by injecting the saline from the posterior, the corneas become stretched. The stretched corneas will induce a stress to prevent additional extension to the surface. However, most of the deformation occurs in the peripheral region, the curvature of the central cornea only changes by a small amount with elevated IOP (Whitford, Studer et al. 2015). The stress and strain can then be calculated according to the parameters including the IOP, corneal radius, curvature and thickness.

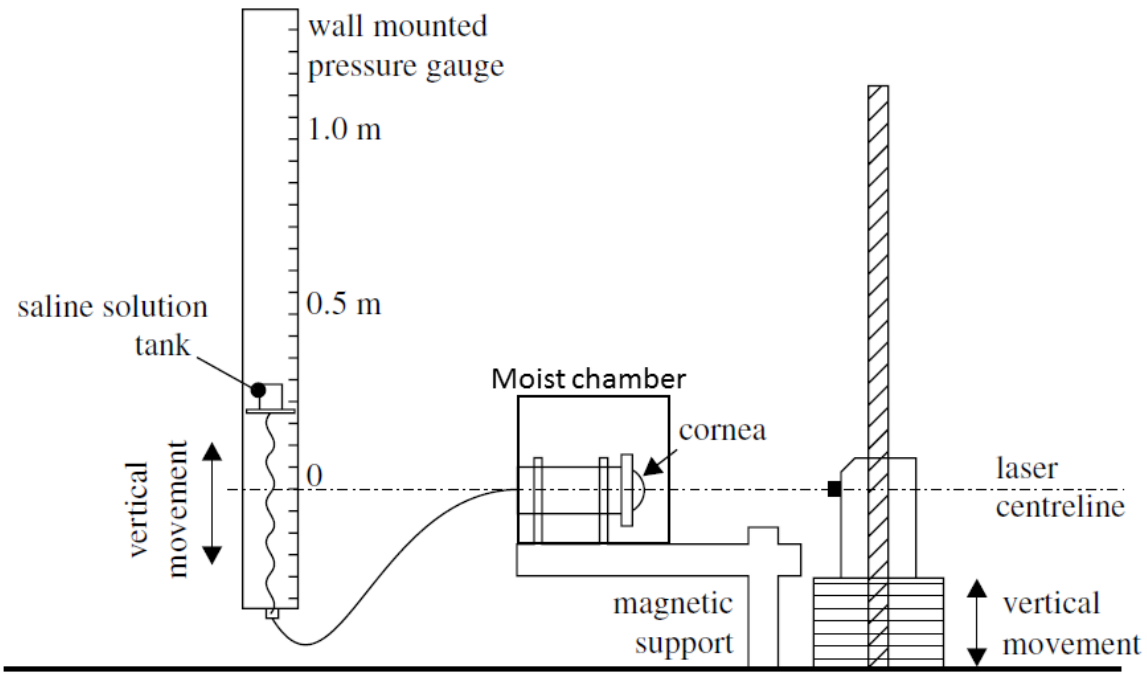

Figure 1.9. Inflation test rig. Source (Elsheikh and Anderson 2005)

In the field of vision science, corneal mechanical properties can be estimated precisely using inverse finite element (IFE) analysis in a finite element (FE) model. The FE model can be used as a reliable tool for the prediction of surgery outcome (Sinha Roy and Dupps 2011, Sinha Roy, Rocha et al. 2013). FE models have been used for decades to study the biomechanical effects of refractive surgery and to analyse the corneal optical changes with reasonable accuracy (Hanna, Jouve et al. 1992, Pinsky and Datye 1992). Many applications are developed for lamellar keratoplasty, corneal transplantation as well as disease modelling such as keratoconus (Alastrue, Calvo et al. 2006, Cabrera Fernandez, Niazy et al. 2006). Recently, the anisotropic and collagen fibril-based FE models have been studied and attempted to analyse the effects of different mechanical properties on deformation of the cornea (Nguyen, Jones et al. 2008, Pandolfi and Holzapfel 2008, Grytz and Meschke 2010, Studer, Larrea et al. 2010).

1.1.4. Keratoconus and UVA/riboflavin CXL

Keratoconus, the most common ecstatic disorder of the cornea, is a non-inflammatory progressive thinning disease (figure 1.10). The clinical sign of this disease is characterised by distorted radius of curvature, anterior protrusion, and reduced thickness and stiffness (Scroggs and Proia 1992). These features impair vision due to the development of irregular astigmatism.

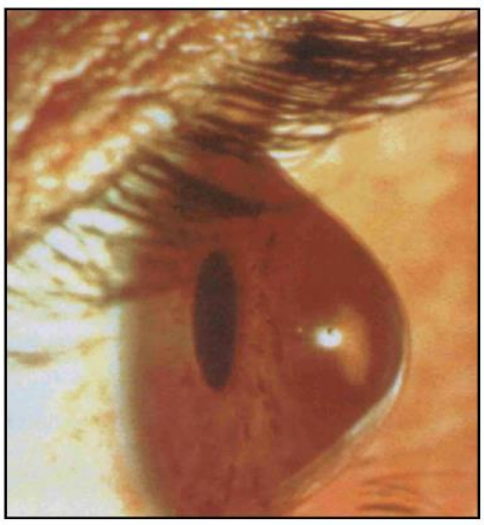

Figure 1.10. Keratoconus as a result of central thinning. Source (Kim, Rabinowitz et al. 1999)

The frequency of keratoconus varies widely but occur in all races (Kim, Rabinowitz et al. 1999). It appears to be a geographical influence on prevalence rate for the disease. As a result, the prevalence ranges from 1 in 375 in the general population (Godefrooij, de Wit et al. 2017). It is observed more frequently in certain ethnic and geographical groups such as South Asians and Middle Eastern areas (Tabbara, Al-Omar et al. 1999). The disease usually manifests in patient's adolescent years in most cases (Krachmer, Feder et al. 1984, Kennedy, Bourne et al. 1986). However, the progression is slow and taking up to several years to develop, thereafter remaining stationary for many years (Duke-Elder 1965). However, the corneal curvature, ultrastructure and material properties alter often in an unpredictable manner as the disease progresses. Therefore, the period between the onset of disease and the first clinical sign or symptom is very difficult to detect.

Genetic factors and mechanical trauma such as eye rubbing can be considered possible causes for keratoconus, but the exact cause is uncertain. It has been associated with detrimental enzyme activity within the cornea (Wang, Rabinowitz et al. 2000, McMonnies 2008). In histopathological studies, keratoconic corneas are characterized by increased amount of proteases, decreased levels of the tissue inhibitor of metalloproteinases (TIMPs), increased expression of IL-4 receptors, changed distribution and reduced activity of lysyl oxidase (LOX), apoptotic of keratocytes, and dramatic alternations in orientations and arrangements of collagen fibrils and lamellae (Ihalainen, Salo et al. 1986, Wilson, He et al. 1996, Kim, Rabinowitz et al. 1999, Wong, Sethi et al. 2002, Meek, Tuft et al. 2005, Dudakova, Liskova et al. 2012, Akhtar, Almubrad et al. 2013). In addition, the production of collagen, the content and distribution of PGs and the compositions of ECM are altered in keratoconus (Wollensak and Buddecke 1990, Snyder, Bergmanson et al. 1998, Meek, Tuft et al. 2005). A defect in glycoprotein synthesis has been found in keratoconic cornea (Wollensak and Buddecke 1990). Abnormal PGs are reported to accumulate in keratoconus lamellae and arranged parallel to collagen fibrils, unlike crosswise arrangement to the fibril in normal corneal tissue (Fullwood, Meek et al. 1990, Sawaguchi 1998). It is suspected that enzymatic degradation of KS may alter the inter-fibrillar cohesion and viscoelastic properties (Funderburgh and Conrad 1990). These changes result in an increase degradative enzyme release and ultimately leading to corneal stromal loss.

It is commonly known that the corneal transparency and mechanical properties are regulated by the uniform distribution of collagen fibrils which assemble into well-organized lamellae layers (Maurice 1957, Michelacci 2003). The organization of corneal collagen is critical to the maintenance of the shape of the cornea, therefore, whenever the corneal collagen fibril mesh is altered or disrupted, abnormal corneal refraction occurs and mechanical properties change, finally leading to visual impairment. Although the pathogenesis of the disease remains unknown and unpredictable, the studies of structural changes have provided valuable information using laboratory tools such as light microscopy, confocal microscopy and scanning or transmission electron microscopy (SEM / TEM) (Randers, Kristensen et al. 1998, Sherwin, Labuza et al. 2002). It has been noted a thin or rupture in Bowman's layer in keratoconus (figure 1.11), and sometimes distortions in the stroma beneath these defects (Scroggs and Proia 1992, Sawaguchi 1998, Akhtar, Almubrad et al. 2013). TEM studies of keratoconic tissue showed that the number of collagen fibrils and amount of lamellae appear to be less than in normal tissue (figure 1.12) (Takahashi, Murakami et al. 1999, Morishige, Wahlert et al. 2007). Another x-ray diffraction study reveals no difference in collagen diameter and inter-fibrillar spacing but a reduction in inter-molecular spacing (Fullwood, Meek et al. 1990). A loosely-packed and randomly-oriented collagen fibrils arrangement in keratoconus have been observed through SEM micrograph (Sawaguchi 1998, Akhtar, Almubrad et al. 2013). In summary, these ultrastructural studies and x-ray diffraction on keratoconus have shown that the native collagen fibril network is disorganized and loses the preferred directions (Meek, Tuft et al. 2005, Akhtar, Almubrad et al. 2013).

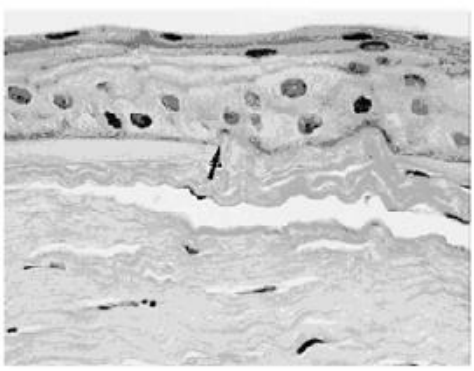

Figure 1.11. Characteristic features of keratoconus. Breaks in the Bowman's layer. Source (Rabinowitz 1998)

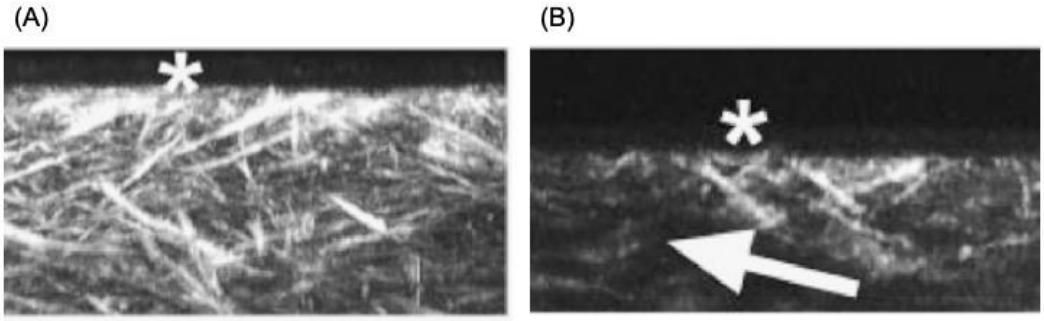

Figure 1.12. TEM images of collagen lamellae in keratoconus. Normal cornea (A) is characterised by numerous collagen fibrils in the stroma, while keratoconic cornea (B) shows reduced amount of collagen lamellae (asterisks). Source (Morishige, Wahlert et al. 2007)

Together with the instability of Bowman's layer, reduced number of lamellae and disorganized stromal collagen fibrils could contribute to the development of keratoconus. As the disease progresses, the redistribution of collagen fibril mesh occurs due to the slippage of collagen lamellar. The slippages and alternations may be promoted by the reduced lamellar cohesiveness and mechanical failure in keratoconic corneas, which leads to mechanical instability (Hayes, Boote et al. 2007, Wollensak, Sporl et al. 2011). As a result, the keratoconic corneas lose their rigidity and their mechanical strength reduces to approximately 60-70% of the normal cornea (Spoerl and Seiler 1999, Shah, Laiquzzaman et al. 2007). The altered biomechanical behaviours have been implied to be resulting from the changes in orientation and alignment of collagens (Edmund 1988, Elsheikh, Alhasso et al. 2008).

Clinically, it has been attempted to determine the biomechanical properties of the cornea and their response to IOP. A study measuring corneal hysteresis in normal and keratoconic corneas using an ocular response analyzer (ORA) showed an average of 9.6 mmHg and 8.1 mmHg in normal and keratoconic population, respectively (Luce 2005). Their results also indicate that the keratoconic corneas demonstrate a general decrease in hysteresis compared to normal corneas. The corneas become unusually thin at the centre in all cases of keratoconus. Consequently, the cornea is weakened and unable to withstand the IOP due to the reduced stiffness and elasticity (Luce 2005).

In recent years, the new treatment using UVA/riboflavin CXL has been introduced for progressive keratoconus. It is the only method designed to arrest disease progression currently (figure 1.13) (Wollensak 2006, Hovakimyan, Guthoff et al. 2012). Laboratory studies have showed that this treatment significantly increases the stiffness of corneas (Andreassen, Simonsen et al. 1980, Akhtar, Almubrad et al. 2013). Researchers have consistently demonstrated the qualitative trend of an increase in corneal stiffness after CXL treatment (Spoerl and Seiler 1999, Wollensak, Spoerl et al. 2003, Kohlhaas, Spoerl et al. 2005, Kohlhaas, Spoerl et al. 2006). Various methods including uniaxial tensile testing, inflation test, optical coherence elastography, supersonic shear wave, atomic force microscopy (AFM) and scanning acoustic microscopy (SAM) all have been successfully introduced for measuring the stress-strain and tangent modulus of corneas following CXL (Kling, Remon et al. 2010, Beshtawi, Akhtar et al. 2014, Lombardo, Serrao et al. 2014, Nguyen, Aubry et al. 2014, Seifert, Hammer et al. 2014, Twa, Li et al. 2014). Despite the differences in the nature of these methods, all of these studies demonstrate a statistically significant increase in tangent modulus of cross-linked corneas. More recently, Seifert et al. reported the distribution of tangent modulus by investigating different depth intervals using AFM (Seifert, Hammer et al. 2014). These studies not only provided significant evidence but also enhanced comprehensive insight on corneal CXL treatment.

Figure 1.13. Picture of a UVA/riboflavin CXL treatment administered to a patient. Source (Wollensak, Spoerl et al. 2003)

CXL treatment has been demonstrated to have a long-term impact on stiffening of the cornea. It has been reported that the Young's modulus of elasticity significantly increased over a time period of up

to 8 months after CXL treatment on rabbit corneas (Wollensak and Iomdina 2009). Furthermore, the tear film study from keratoconic patients who had undergone UVA/riboflavin CXL treatment demonstrates a significant increase in the level of total proteins, decrease in the expression of IL-4, 5, 6 and TNF-α, compared to non-treated keratoconus patients during a postoperative period ranging from 3 to 6 months (Balasubramanian, Mohan et al. 2012). However, the long-term stabilities of CXL on molecular characterizations and possible implications of these changes have not been reported.

Other evidences related to CXL strategy including the increased diameter of collagen fibrils, the resistance to enzyme digestion, changed shrinking temperature and swelling behaviours all have been reported (Spoerl, Wollensak et al. 2004, Spoerl, Wollensak et al. 2004, Wollensak, Wilsch et al. 2004, Hayes, Kamma-Lorger et al. 2013). Ultrastructural studies have demonstrated that collagen CXL significantly improves the collagen architecture with an increase in collagen diameter and density (Wollensak, Wilsch et al. 2004, Akhtar, Almubrad et al. 2013). However, literature on studying the correlation between ultrastructural changes and biomechanical behaviour of cross-linked cornea is scant, and specific contribution of the dextran within riboflavin solution has not been reported (Choi, Lee et al. 2013, Seifert, Hammer et al. 2014). The understanding of these networks will be of importance and help to establish the optimized CXL protocol in clinical practice.

1.1.5. Applications of CXL and Complications on Clinical Practice

1.1.5.1. Keratoconus

The available evidence suggests that CXL is capable of halting progression of keratoconus, particularly in patients with less advanced disease and relatively preserved corrected visual acuity. Although flattening of corneal curvature and improved visual acuity are observed, the improvement is often in an unpredictable manner, and may not impact appreciably on binocular visual function.

For the patients who experience the ICRS implantation with more advanced progression, the additional CXL treatment would be applied to enhance the flattening effect as well as lessen corneal steepening (Alio, Shabayek et al. 2006, Chan, Sharma et al. 2007, Ertan, Karacal et al. 2009). It has been reported that the patients treated with Intacs following CXL had a significantly greater reduction

in cylinder power than the Intacs only group (Chan, Sharma et al. 2007, Ertan, Karacal et al. 2009). Another similar 7 months follow-up study shows a greater improvement in corrected distance visual acuity (CDVA), spherical equivalent (SE), and mean keratometry (K) in the group treated with ICRS first and subsequent CXL treatment (Coskunseven, Jankov et al. 2009). The patients with marked thinning of the cornea and significant apical scarring should be excluded from CXL surgery. However, consensus has not been achieved yet due to the optimal timing of CXL or the impact of CXL on the insertion of the corneal ring segments.

1.1.5.2. Post-operative Ectasia

Due to its ability of stabilizing biomechanical properties of cornea, CXL has been proposed as a therapeutic method of arresting ectasia progression that is often encountered after excimer laser refractive surgery or LASIK (Laser-Assisted in Situ Keratomileusis). Halting the progression of ectasia in a patient after LASIK using CXL is firstly reported by Kohlhaas et al. and showed an increase in biomechanical stability to prevent the post-LASIK ectasia progression (Kohlhaas, Spoerl et al. 2005).

Another refractive surgical procedure that has been combined with CXL treatment is photorefractive keratectomy (PRK). The positive impact of CXL in conjunction with PRK has been shown in a case of post-LASIK ectasia (Kymionis, Portaliou et al. 2011). Another study has reported an improvement in vision and K readings on patients with keratoconus treated with CXL and followed by PRK 12 months later (Kanellopoulos and Binder 2007). Despite these promising results, studies with longer follow-up and larger patient numbers are needed to evaluate the effectiveness and safety of CXL in the management of post-operative ectasia.

1.1.5.3. Infectious Keratitis

Infectious keratitis is a corneal disease that results from infection with microorganisms or immunological disorders (sterile keratitis). Attempts have been made in recent years to evaluate the effects of CXL in infectious keratitis to make it a treatment option. The antibacterial effectiveness of CXL has been examined *in vitro* against some common pathogens which are selected from a panel of

clinical ocular isolates obtained from patients with severe keratitis (Martins, Combs et al. 2008). Several studies have demonstrated the effect of UVA/riboflavin CXL on patients with infectious keratitis. The progression of ulcers has been halted, as well as corneal re-epithelialization and resolution of the infectious process are also reported (Iseli, Thiel et al. 2008, Micelli Ferrari, Leozappa et al. 2009, Moren, Malmsjo et al. 2010).

However, there has been a debate about the action mechanisms of UVA/riboflavin CXL in infectious keratitis, and so several hypotheses have been proposed: (i) the inhibition of proteolytic enzymes by the photochemical process; (ii) strengthened structure of corneal collagen induced by CXL resulting in the increased resistance to infectious process; and (iii) photo-initiated sterilization effect of the UVA/riboflavin. A later study has confirmed these hypotheses and demonstrated symptomatic relief and the arrest of corneal melting progression due to bacterial keratitis (Makdoumi, Mortensen et al. 2010). The ability of CXL to inhibit pathogen growth makes it a potential tool in the management of infectious keratitis.

1.1.5.4. Corneal Edema

Persistent corneal edema is another indication for CXL (Krueger and Ramos-Esteban 2007, Ehlers and Hjortdal 2008, Wollensak, Aurich et al. 2009, Bottos, Hofling-Lima et al. 2010, Cordeiro Barbosa, Barbosa et al. 2010). It has been demonstrated that conventional CXL procedure alters the swelling property of the cornea and minimizes tissue hydration. Therefore, it is hypothesized that CXL may reduce the space for fluid accumulation and so increase the optical clarity of the cornea. The potential anti-edematous effect of CXL makes it a useful tool in the clinic for treating corneal edema. Reduced edema, increased corneal clarity, and improved visual acuity have been demonstrated during a 2 months follow-up study after CXL treatment associated with corneal ulcer or infectious keratitis (Kozobolis, Labiris et al. 2010). However, it has been noted that the improved corneal transparency and visual acuity, as well as a decrease in central corneal thickness are typically seen after CXL, but return to preoperative levels within months, suggesting that this procedure does not have a lasting effect in patients with corneal edema. This might be explained by the fact that the pre-treatment with

dextran prior to CXL, allowing dehydration of the cornea and reduced corneal thickness. The importance of dehydrating the swollen cornea before CXL has also been demonstrated in patients with Fuchs dystrophy with various degrees of edema (Hafezi, Dejica et al. 2010).

1.1.5.5. Complications

Although UVA/riboflavin CXL is considered as a safe and well-tolerated procedure, the possible complications have been reported (Table 1.2). According to a study involving 117 eyes of 99 patients, the complication rate is defined as loss of 2 or more Snellen lines (2.9%), and the failure rate is defined as continued progression of ectasia (7.6%) (Koller, Mrochen et al. 2009). Age and CDVA are considered as risk factors for the complications, while maximum K is defined as risk factor for failure rate (Koller, Mrochen et al. 2009). In spite of the use of CXL, systemic conditions such as pregnancy and neurodermatitis have been proposed to be risk factors for progression of ectasia (Hafezi and Iseli 2008, Raiskup-Wolf, Hoyer et al. 2008).

Most commonly seen post-operative complications is corneal haze which normally does not affect the vision significantly (Mazzotta, Balestrazzi et al. 2007). Sever stromal haze after CXL is rarely developed and has been observed on the patients with preoperative increased K value and reduced corneal thickness (Raiskup, Hoyer et al. 2009). In addition, the epithelium removal is required while using conventional CXL procedure, therefore the sterile infiltrates and stromal scarring both have been reported with the incidence rate of 7.6% and 2.8%, respectively (Dhawan, Rao et al. 2011). Sterile infiltrates cause stromal melt, and usually resolved with stromal scars resulting in reduction of visual acuity (Eberwein, Auw-Hadrich et al. 2008, Angunawela, Arnalich-Montiel et al. 2009). Infectious keratitis is also a known complication associated with epithelial defects or bandage contact lens wearing, both of which are presented after the conventional CXL with epithelial debridement (Perez-Santonja, Artola et al. 2009, Pollhammer and Cursiefen 2009, Sharma, Maharana et al. 2010).

Table 1.2. Reported complications of UVA/riboflavin corneal CXL. Reproduced from (Letko, Majmudar et al. 2011).

Complication	References
Vision significant stromal haze	Mazzotta et al. (2007), Raiskup et al. (2009)
Infection	
Bacterial keratitis	Micelli Ferrari et al. (2009), Pollhammer et al. (2009), Sharma et al. (2010), Perez-Santonja et al. (2009), Zamora et al. (2009)
Acanthamoeba keratitis	Rama et al. (2009)
Herpes simplex keratitis and uveitis	Kymionis et al. (2007)
Sterile inflammation	
Keratitis and corneal scaring	Koppen et al. (2009)
Stromal infiltrates and melt	Angunawela et al. (2009), Eberwein et al. (2008)
Diffuse lamellar keratitis	Kymionis et al. (2007)

1.2. Scope of Study

CXL strategy has been used to increase stiffness of corneal stroma and stabilize the structures. Mechanical properties of biological tissues are established as being largely dependent upon the intertwining of collagen fibrils, linked lamellae layers and inter-fibrillar spacing (Boote, Dennis et al. 2003, Depalle, Qin et al. 2015, Whitford, Studer et al. 2015). Therefore, the efficacy of the CXL is believed to rely on changes to the mechanical properties of the tissue induced through modifying the characteristics of collagen fibrils within the cornea, and the induction of intra-fibrillar bonds, with the overall effect on the treatment depth (Schumacher, Mrochen et al. 2012, Raiskup and Spoerl 2013, Raiskup and Spoerl 2013). However, the stabilisation mechanisms and underlying molecular processes remain unclear. The topics of interest include the understanding of how changes to the mechanical behaviours in cross-linked corneas relate to changes in ultrastructure and biochemistry, and determining of these relationships. It is clinically relevant when evaluating the efficacy of UVA/riboflavin CXL and designing modifications to the CXL procedure for the optimal protocols.

1.3. Aim and Objectives

It is known that the organization of collagen fibrils, expression of protein levels, and the mechanical properties of corneal stroma are altered in keratoconus. The proteolytic enzymes cause the instability of Bowman's layer, reduced number of lamellae, and disorganized collagen fibrils, which are responsible for the mechanical instability and resulting in reduced stiffness. Corneal CXL with riboflavin and UVA is the current therapeutic approach that halts disease progression. Therefore, the primary goal of this research is to gain a greater understanding of the relationship between biomechanical behaviour and biological aspects by systematically investigating the effect of UVA/riboflavin CXL using Dresden protocol, hence to explore the mechanisms and provide a reference against which modifications to CXL approaches may be compared.

The effects of these induced cross-links have been variously reported as increases in tissue stiffness, resistance to enzymatic digestion, changes to ultrastructure and swelling behaviour. However, these studies have generally evaluated the overall effects of the full CXL protocol without separating the contribution of individual aspects of the treatment which may cause the differences in outcomes reported. In addition, numerous modifications to the Dresden protocol are being tested in clinical settings; therefore, defined knowledge of the effect of the current treatment regimen is needed to provide a benchmark against which these modifications can be compared, and moreover for rationale design of alternative approaches. To fulfil the purpose, biomechanical characterization provides quantitative measurements to assess the efficacy of CXL. Biological and ultrastructural changes present evidence for evaluating the degree of CXL and the interactions between proteins. This requires a number of objectives to be accomplished and is illustrated in figure 1.14.

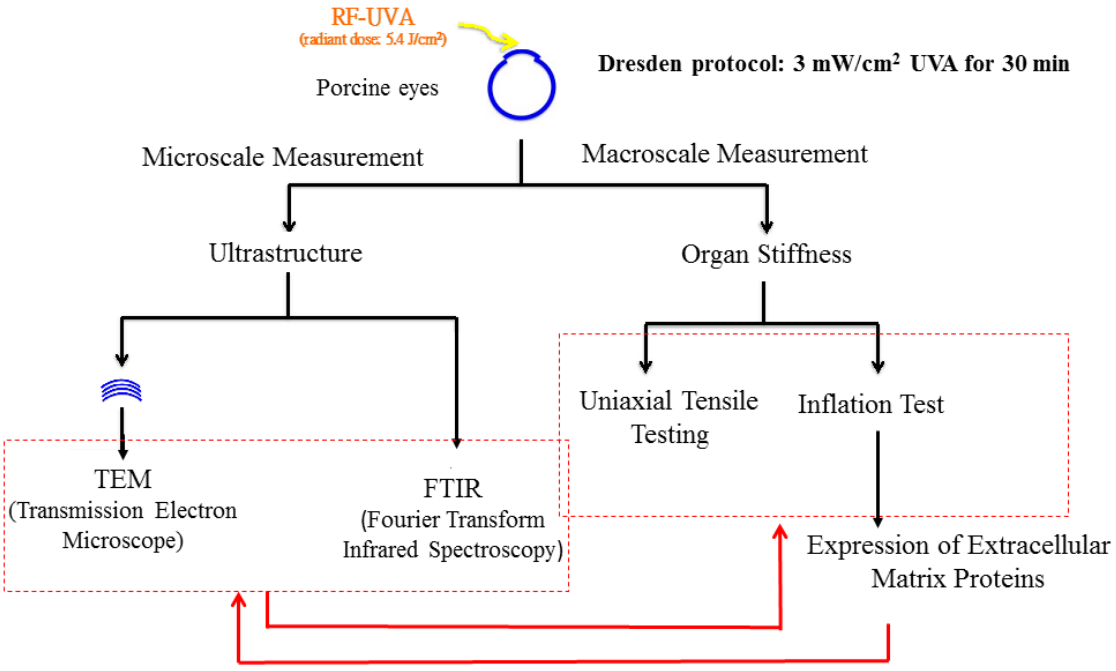

Figure 1.14. Plan of Investigation.

First aim is to enable characterization of corneal mechanical properties

The measurement of changes in corneal mechanical behaviour is performed using uniaxial tensile testing and inflation test. The purpose of applying two different mechanical measurements is due to the anisotropic and viscoelastic properties of the ocular tissue. The procedure involved in the tensile test has some inherent deficiencies which may reduce the reliability of this method especially when the measurements are performed under high stress or maximum loading. Therefore, inflation is considered more accurate for determining material properties than tensile testing due to its experimental design that is representative of *in vivo* conditions. Additionally, tensile and inflation tests follow different loading orientations in the measurement of corneal mechanical properties. Tensile testing induces a change in the alignment of collagen fibrils towards the load direction. In the inflation testing, as the tissue is loaded similar to the *in vivo* conditions, therefore, no change in the fibrils' orientation would be expected.

Second aim of this study is to identify the alterations in corneal ultrastructure and possible interactions between Extracellular Matrix (ECM) proteins

In this corneal CXL procedure, chemical bonds are created between substrates within the corneal stroma by means of photo-polymerisation induced by UVA radiation. There has been hypothesized, but not directly provided evidence regarding the proteins involved and possible locations where cross-links may occur after UVA/riboflavin CXL. To confirm the findings in ultrastructure and understand the chemical and biological interactions induced by UVA/riboflavin CXL, the ultrastructural parameters including diameter of collagen fibrils, inter-fibrillar spacing and density of collagen is analysed using the Transmission Electron Microscope (TEM). Fourier Transform Infrared Spectroscopy (FTIR) is used to evaluate the formation of new chemical bonds induced by UVA/riboflavin CXL. The expression level of ECM proteins such as collagens and PGs of corneal stroma is examined using Liquid Chromatography-Mass Spectrometry (LC-MS) and Western Blotting analysis.

Third aim is to define the relationship between biomechanical behaviour, biochemical and structural changes

Understanding the mechanical behaviours of the cornea and its corresponding biological and ultrastructural alterations is clinically relevant. In the third aim, possible mathematical methods and statistical analysis are performed to define those relationships and fundamental parameters in determining tissue stiffening following UVA/riboflavin corneal CXL, as well as provide the key benchmarks against which modifications to the Dresden CXL protocol can be evaluated.

Forth aim is to evaluate the efficacy of conventional CXL and accelerated CXL used in clinical settings by Meta-analysis

In the previous aims, normal porcine specimens are used for experimental design and conventional Dresden is performed to define the fundamental parameters in determining tissue stiffening and

structural changes. However, the CXL effects on keratoconic eyes and its clinical efficacy could not be manifested on porcine corneas. Therefore, we evaluate the CXL efficacy in clinical practical using specific statistical analysis which called meta-analysis. Although Dresden protocol is widely adopted, alternative protocols have been developed due to different clinical purposes. Such efforts have resulted in the development of accelerated CXL which have also been widely studied in laboratory and clinical practice. These accelerated techniques maintain the same energy density of the standard corneal CXL procedure (5.4 J/cm^2) by creating different combinations of irradiance levels and exposure time according to Bunsen-Roscoe law of reciprocity. In this aim, the meta-analysis is performed to compare the effectiveness of conventional Dresden protocol (3 mW/cm^2, 30 min) and different accelerated protocols with 9 mW/cm^2, 18 mW/cm^2, and 30 mW/cm^2 irradiances. The compared follow-up duration is at 12 months through the direct comparison clinical trials on the changes in refractive powers and topographic outcomes for progressive keratoconus.

Chapter 2. Literature Review

2.1. Introduction

The formation of collagen cross-links in corneal stroma is based on enzymatic and non-enzymatic processes. The enzyme-regulated process involving lysyl oxidase (LOX) induces the oxidation of lysine and hydroxylysine and aldehyde condensation to form covalent bonding of intra- and inter-molecular cross-links (Eyre 1987, Hovakimyan, Guthoff et al. 2012). The non-enzymatic CXL procedure is related to the glycation of collagen (Lapolla, Traldi et al. 2005). This glycation-mediated crosslinking is the main contributor to the increase in corneal strength with age, and consistent with the observation that diabetes may protect against the development of keratoconus (Seiler, Huhle et al. 2000, Dahl, Spotts et al. 2012). In keratoconus, the decreased corneal mechanical strength is resulted from the reduced number in stromal collagen crosslinks and molecular bonds between stromal ECM (Hovakimyan, Guthoff et al. 2012). Therefore, actively increasing the covalent bonding or cross-links between collagen molecules and ECM within stroma could be reasonable to enhance corneal rigidity, hence potentially halt the disease progression. Due to this reason, a German research group at Dresden Technical University in the 1990s, led by Theo Seiler, conceived the treatment of corneal CXL using UVA/riboflavin (Spoerl and Seiler 1999, Mazzotta, Balestrazzi et al. 2007). The impressive clinical results initially achieved in Germany have prompted use of UVA/riboflavin CXL worldwide (Wollensak, Spoerl et al. 2003, Wollensak 2006).

The general procedure of corneal crosslinking involves epithelium removal, a pre-treatment of 0.1% riboflavin solution in 20% dextran via drops onto the cornea every 2 to 5 minutes for 30 minutes to ensure adequate penetration of riboflavin into the stroma, followed by a 30-minute treatment of UVA irradiation with a total energy of 5.4 J/cm^2 (370 nm, 3 mW/cm^2). This procedure, known as Dresden protocol, is the standard corneal CXL treatment. Researchers and companies have been working on many modifications to improve the effectiveness and clinical feasibility of the standard corneal CXL procedure. However, the exact mechanism for Dresden protocol has not been understood clearly,

which is of important value for developing optimal and improved protocols for the treatment of progressive keratoconus in clinical practice.

An efficient CXL treatment must achieve two criteria, safety and efficacy, which compensates the reduced stiffness without harming the endothelium and other posterior structures of the eye (Wollensak, Spoerl et al. 2003, O'Brart, Chan et al. 2011). Many researches have been investigated for fine-tuning the treatment conditions, such as the UV power, radiant dose, the absorption of riboflavin, and duration of treating time (Spoerl and Seiler 1999, Schumacher, Oeftiger et al. 2011). According to Beer-Lambert's law, the irradiance decreases with increasing depth due to the absorption in a certain thickness of stroma saturated with riboflavin, which also results in a depth-dependent decrease in CXL effect. In this procedure, riboflavin also serves as a protective substance, limiting UVA penetration to the stromal layer, thereby avoiding photo-oxidative damage to endothelium and the inner structures of the eye (Wollensak, Aurich et al. 2010). Because of the reduction and the shielding effect of riboflavin, 70% of the UV irradiation is absorbed in the first 200 μm (figure 2.1) (Kohlhaas, Spoerl et al. 2006). Therefore, the corneal endothelium, as well as the deeper structure such as lens and retina, is theoretically exposed to a residual UV intensity less than 0.35 mW/cm^2 with a 400 μm-thick stroma, which not reach the cytotoxic threshold of endothelium (Wollensak, Sporl et al. 2003). However, the keratocyte damage has been observed and the stroma is depopulated of keratocyte down to 300 μm depth using *in vivo* confocal microscope, and the repopulation of this area takes up to 6 months (Wollensak, Spoerl et al. 2004, Mazzotta, Balestrazzi et al. 2007).

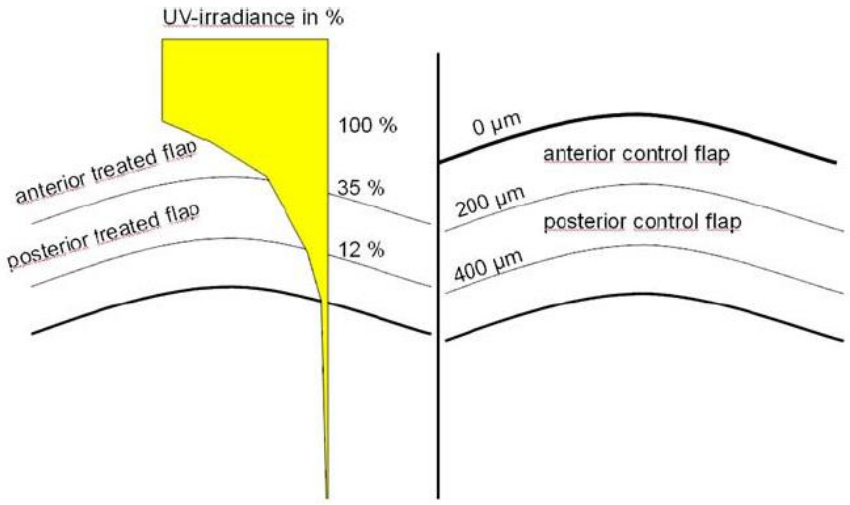

Figure 2.1. Schematic of the cornea thickness and UVA irradiation. Source (Kohlhaas, Spoerl et al. 2006)

2.2. Rationale of UVA/riboflavin CXL

Corneal CXL with UVA and riboflavin induces a photo-oxidative reaction to increase the rigidity of stromal collagen fibrils and the overall mechanical strength of the stromal layer. Riboflavin (vitamin B2) functions as the photosensitizing substance that increases the absorption coefficient of the cornea so that CXL reaction can take place (Wollensak, Aurich et al. 2010, Iseli, Popp et al. 2011).

In a photo-oxidative reaction, the photosensitizer absorbs the energy from the proper light source, followed by generating electron to form an excited photosensitizer. The excited photosensitizer may transfer either charge or energy by interacting with other molecules. The mechanisms responsible for photosensitized oxidative reactions are classified into two categories. There is a general agreement that for a reaction generating free radicals from substrates or excited sensitizer will be classified as Type I mechanism which is favoured at low oxygen condition. Similarly, for a reaction that involves in the generation of singlet oxygen should be classified as Type II mechanism. In Type II mechanism, the reaction usually occurs under aerobic condition (Lubart, Lavi et al. 2006).

The common understanding of CXL therapy is that the exposure of riboflavin to UVA light in order to generate free radicals or reactive oxygen species (ROS) in mediating the collagen crosslinking in terms of the stiffening of the cornea. Therefore, in the presence of light, riboflavin that exhibits photosensitizing properties can form an excited state by absorbing the energy from light and cause the formation of chemical bonds between substrates (collagen, proteoglycans and other extracellular matrix proteins) in the corneal stroma through mixed Type I-II photochemical mechanism (Zhang, Conrad et al. 2011). The type of mechanisms largely depends on the level of oxygen concentration during the CXL process.

The major kinetic reactions involved in Type I and Type II mechanisms include the formation of excited triplet riboflavin (Rf^*_3), the free radicals from excited riboflavin and substrates, and the generation of singlet oxygen ($^1O_2$) as shown in figure 2.2 (Raiskup and Spoerl 2013). Briefly, riboflavin is activated by UVA light and forms excited singlet riboflavin (Rf^*_1, lifetime 10^{-8}s). Through intersystem energy crossing, the excited singlet riboflavin will quickly transform to excited triplet riboflavin (Rf^*_3, lifetime 10^{-2}s) (Huang, Kim et al. 2006). The excited states with longer lifetime are more likely to interact with other molecules to initiate photochemical reactions, where the onset of the separation of Type I and Type II reactions. For Type II mechanism, oxygen is necessary to form singlet oxygen ($^1O_2$), which is the physically excited form of oxygen molecule. If the oxygen is depleted by UVA light, then Type I mechanism dominates the reaction, which represents the formation of free radicals and the direct interaction between triplet riboflavin and substrates. Therefore, in a standard clinical CXL treatment, both reactions take place. It depends on the level of oxygen in the cornea and the diffusion rate of oxygen into the cornea during the procedure (Kamaev, Friedman et al. 2012).

The diffusion rate of oxygen is time-dependent and one of the main factors to model the photodynamic reactions. The standard clinical CXL chooses continuous UVA mode as the light source to initiate the reaction, which may cause the intraoperative oxygen depletion during the process. Pulsed light modality turns out to be an alternative for CXL light source due to its on/off cycle of

oxygen delivery (Kamaev, Friedman et al. 2012). Pulsing the UVA light allows the oxygen reuptake, which releases singlet oxygen as the main driver in mediating the collagen crosslinking. The optimization of oxygen availability is determined on the diffusion rate of oxygen into the tissue. Therefore, CXL with pulsed energy may be considered to optimize the intraoperative oxygen availability and achieve the improved postoperative functional outcomes (Mazzotta, Traversi et al. 2014).

In summary, the Type I mechanism occurs when the oxygen is depleted and this represents that the free radical reactions mediate the CXL in the cornea. Otherwise, the Type II mechanism implies the replenishment of oxygen in the system and the singlet oxygen plays a predominant role in mediating the collagen CXL.

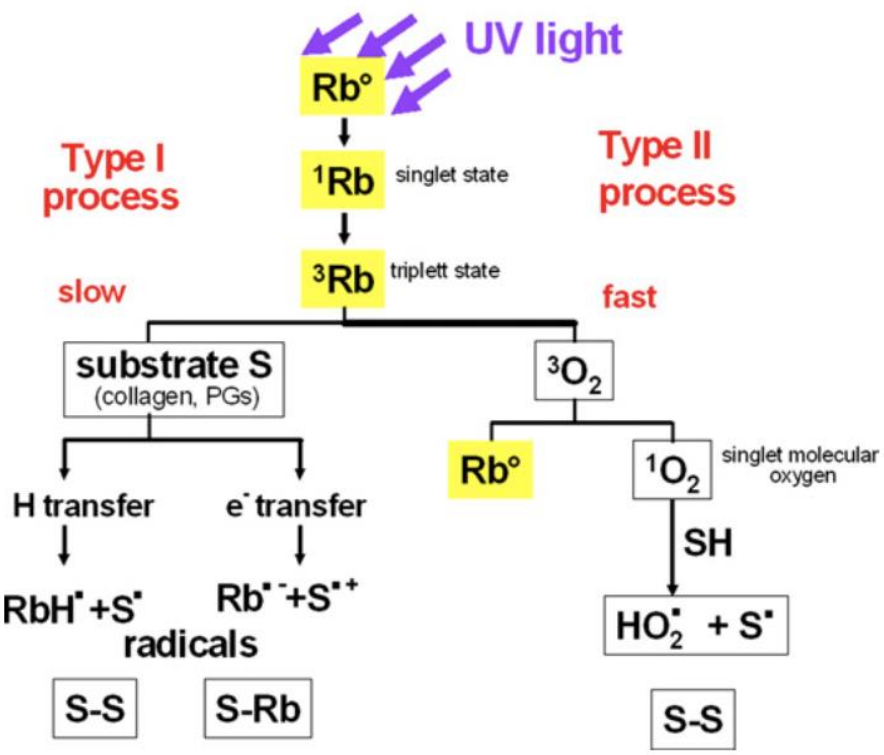

Figure 2.2. Excitation of riboflavin and the two possible reaction mechanisms. Source (Raiskup and Spoerl 2013)

2.3. Efficacy of UVA/riboflavin CXL (Laboratory Studies)

The structure of collagen plays an important role in providing mechanical support and matrix accumulation. Under physiological state, collagen molecules self-assemble into fibrils which provide elasticity, and then go through enzymatic CXL to stabilise fibril structure (i.e. maturation) (Snedeker and Gautieri 2014). Collagen is synthesised in the form of its procollagen molecule. Collagen molecule is processed by removing the extension peptides from procollagen, and then undergoes post-translational modification to form collagen fibrils. Cross-links happen between adjacent tropo-collagen helices and micro-fibrils through enzyme regulated process (Sung, Chang et al. 2003). The enzymatic collagen CXL is primarily mediated by the enzyme LOX which is a copper-dependent amine oxidase. It oxidizes the ε-amino groups of lysines or hydroxylysines into reactive aldehydes which spontaneously react with contiguous aldehyde groups or ε-amino groups, forming insoluble fibrils (figure 2.3) (Eyre 1987, Shetty, Sathyanarayanamoorthy et al. 2015, Takaoka, Babar et al. 2016). Therefore, the stability of fibrils, collagen inter-connectivity, and mechanical strength are all enhanced. On the other hand, there is a family of proteinases that dominate the degradation of the ECM called matrix metalloproteinases (MMPs). MMPs are calcium-dependent zinc-containing endopeptidases which play a key role in tissue remodelling and decompose ECM including gelatins, elastins, collagens, and matrix glycoproteins. In normal physiological conditions, MMPs can be inhibited by tissue inhibitors of MMPs (TIMPs) through forming an inactive enzyme-inhibitor complex (Riley, Harrall et al. 1995). Previous studies suggest that the weakening strength of corneal stroma could be due to the dysfunction of these enzymes responsible for the remodelling of collagen structure. The detailed pathology, however, has not be clarified (Collier 2001, Dudakova, Liskova et al. 2012).

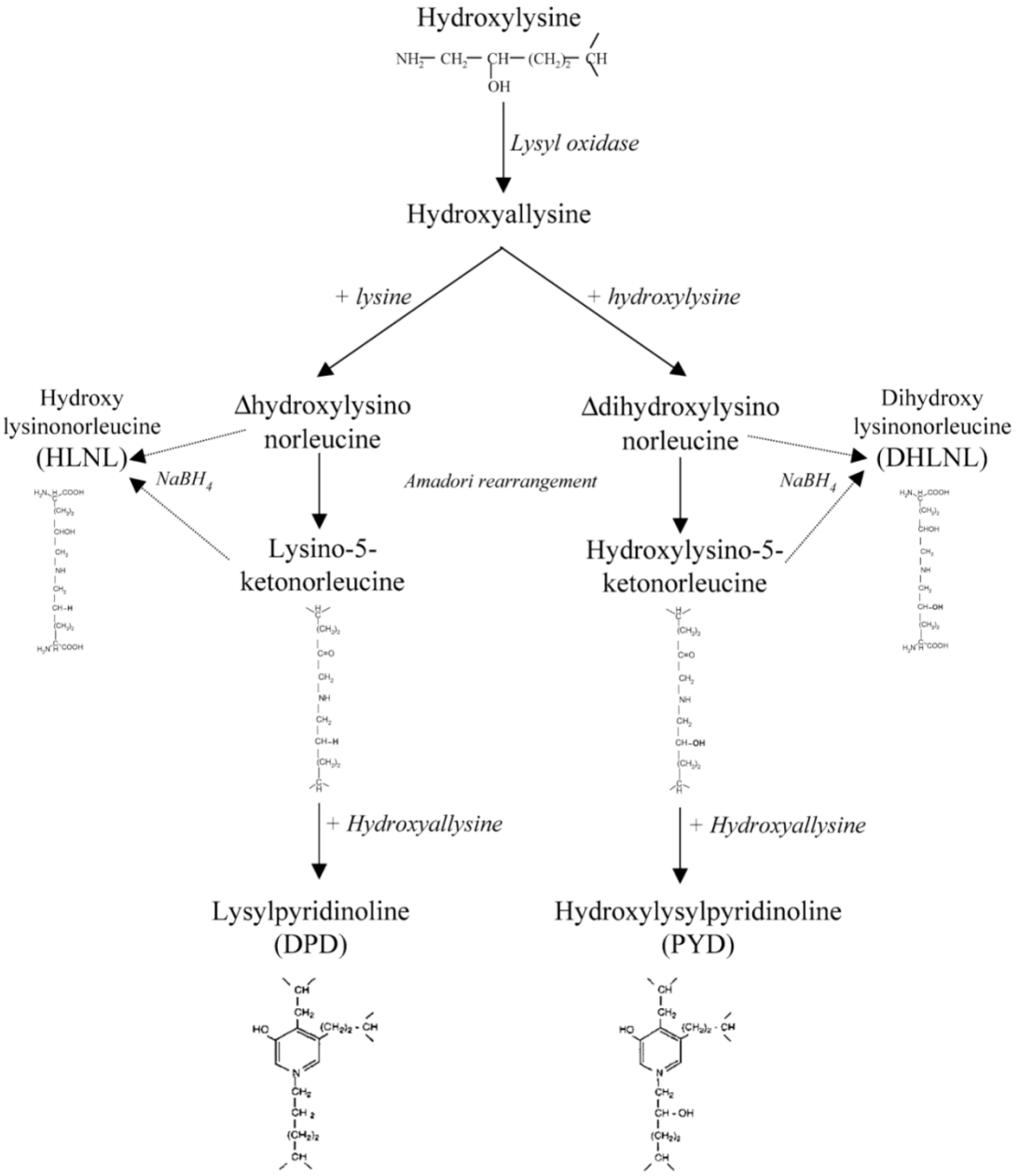

Figure 2.3. Pathways of collagen enzymatic cross-links. Source (Eyre 1987)

Another mechanism that changes the strength of the stromal tissue is non-enzymatic glycation, a phenomenon that occurs through the reaction of collagen with glucose and its oxidation products (figure 2.4) (Seiler, Huhle et al. 2000, Lapolla, Traldi et al. 2005, Elsheikh, Wang et al. 2007). Although the nature of collagen CXL pathways may not be the major factor in the aetiology of keratoconus, the mechanical strength of the keratoconic cornea is significantly reduced compared to normal corneas (Cannon and Foster 1978, Andreassen, Simonsen et al. 1980). In addition, there is no

definite findings that UVA/riboflavin CXL treatment produces cross-links between or within collagen and proteoglycans as the molecular bonds can not be seen microscopically.

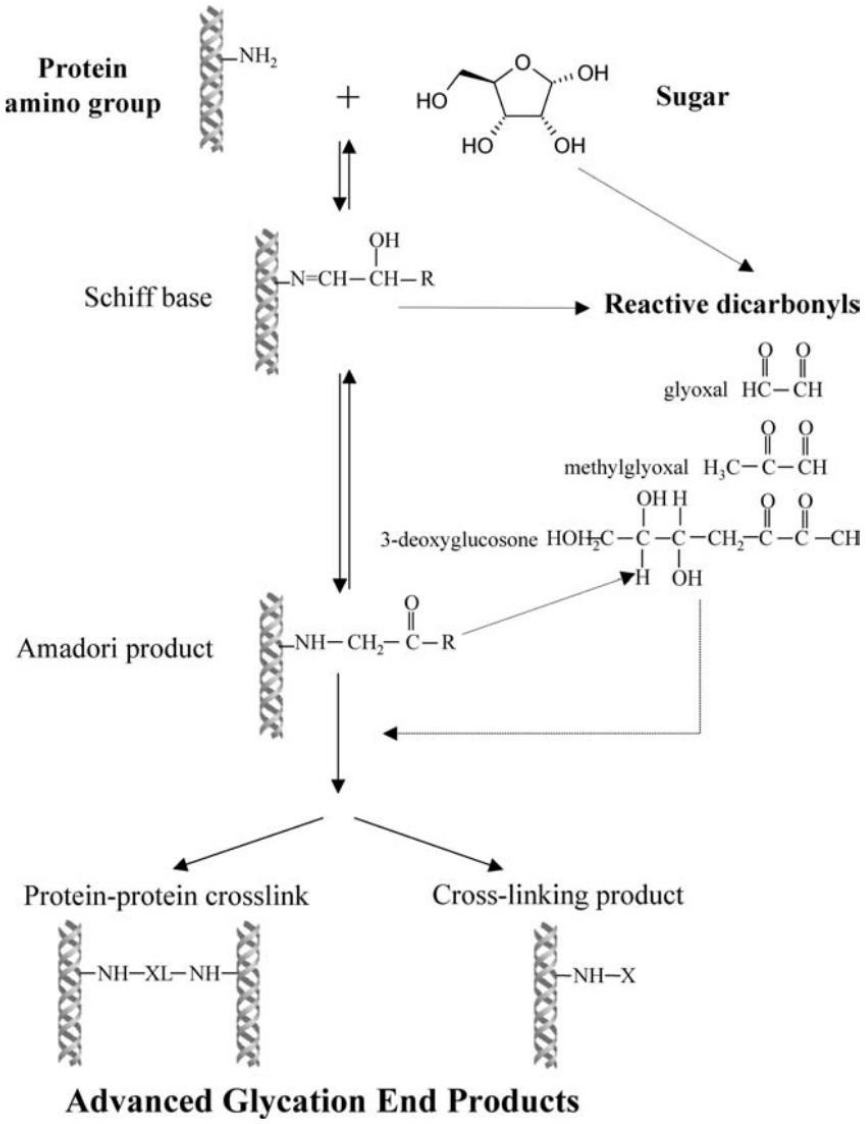

Figure 2.4. Pathways of advanced glycation end products formation. Source (Lapolla, Traldi et al. 2005)

Many laboratory studies have reported changes in corneal physiochemical properties induced by CXL (Table 2.1). A remarkable positive effect of CXL using UVA/riboflavin on mechanical properties of porcine and human has been demonstrated (Wollensak, Spoerl et al. 2003, Kohlhaas, Spoerl et al. 2006, Tanter, Touboul et al. 2009). The mechanical measurements of cross-linked corneal stroma

show an immediate increase in stress for a given level of strain, which indicates that the stiffening effect lasts for several months following the procedure in animal studies (Wollensak, Spoerl et al. 2003, Wollensak and Iomdina 2009). These changes have been shown to occur in the anterior 200 μm of the stroma where the most of the UVA absorption takes place (Kohlhaas, Spoerl et al. 2006). In addition to the stiffening effect of CXL, an alteration in the swelling properties, a more compact anterior stroma, increased resistance to enzymatic digestion and stromal shrinking temperatures, as well as reduced corneal permeability of solutes all have been described after the CXL treatment (Spoerl, Wollensak et al. 2004, Spoerl, Wollensak et al. 2004, Stewart, Schultz et al. 2009, Bottos, Hofling-Lima et al. 2010). A higher shrinkage temperature has been demonstrated in the anterior stroma following CXL (Spoerl, Wollensak et al. 2004). Increased resistance to enzymatic digestion has been confirmed, with a dose-dependent response to riboflavin concentration and in relation to the UVA intensity (Spoerl, Wollensak et al. 2004, O'Brart, O'Brart et al. 2018). The laboratory evidence including biomechanical, biophysical and chemical molecular changes while evaluating the efficacy of CXL will be discussed in detail in the following section.

Table 2.1. Published laboratory studies of changes in corneal stroma induced by CXL. Source (Subasinghe, Ogbuehi et al. 2018)

Table 1 Laboratory studies on conventional crosslinking treatment

Author (reference)	Investigative techniques	Type of study	Animal model	No. of eyes	Key findings
Tabibian et al. [48]	Biomechanical testing	In vivo	Mice	18	No differences in the stress-strain curves following repeated CXL
Hatami-Marbini and Rahimi [49]	Biomechanical testing	Ex vivo	Bovine	25	Post-CXL—increase equilibrium stress, maximum stress, and tangent modulus ($p < 0.01$).
					Increasing the hydration—decrease in equilibrium stress, maximum stress, and tangent modulus ($p < 0.01$).
Matteoli et al. [50]	OCT	Ex vivo	Porcine	24	Reduction of CT (34%) immediately after CXL treatment.
					Treated CS effect 42% compared with control corneas.
Beshtawi et al. [51]	SAM	Ex vivo	Human	6	Speed of sound measurement increase (square foot of thickness) by a factor of 1.039× in CXL cornea
					AS and PS increased by factor of 1.019×
Labate et al. [34]	AFM	Ex vivo	Human	7	YM increased at AS (1.1–1.5×), mean hysteresis decrease—0.9×–1.5×
Seifert et al. [52]	AFM	Ex vivo	Porcine	16	YM maximum at the corneal surface and decreased within next 200 µm
					Maximum CS higher ($p < 0.01$) than posterior 100 µm
					MSF at the corneal surface 8.1, MSE—1.7×
Hayes et al. [53, 54]	Enzymatic digestion studies and X-ray scattering study	Ex vivo	Porcine, sheep, and rabbit	117	CT decrease after riboflavin application and UVA exposure
					CXL treatment induces crosslinks within collagen molecules and/or between collagen fibrils and the proteoglycan
					CXL do not effect on hydrodynamic behavior of cornea
					CXL increase enzymatic digestion
Dias et al. [55]	AFM	Ex vivo	Human	24	CXL increase AS stiffness 1.9 times than the control corneas
					PS not significantly affected
Akhtar et al. [56]	TEM	In vivo	Human	9	Diameter of CXL treated corneas increased
					CXL treatment has no effect on hemidesmosomes, BM, Bowman's layers CFs diameter smaller than normal but larger than KC
					Interfibrillar distance increased
					CXL treatment normalizes PG synthesis
Lanchares et al. [57]	Biomechanical testing/uniaxial tensile testing	Ex vivo	Porcine	17	30-min UVA CXL with riboflavin increased stiffness
					60-min UVA-radiated decrease stiffness
Wollensak et al. [40]	Biomechanical testing, pachymetry, and histology (H&E, PAS)	Ex vivo	Porcine	72	CXL mainly occur at intra- and interfibrillar CF, absent interlamellar CXL
					Crosslinking effect on interlamellar cohesion, upheld by interlacing collagen lamellae and PG

(continue)

Table 1 (continued)

Author (reference)	Investigative techniques	Type of study	Animal model	No. of eyes	Key findings
Kling et al. [58]	Biomechanical testing and Scheimpflug imaging	Ex vivo	Porcine	38	Immediate decrease in CT following riboflavin installation CXL effective in preventing an increase in anterior corneal radius in the horizontal than in the vertical meridian 1.54 reduction in corneal thinning, 2.8 reduction in corneal apical rise Increase IOP, YM (1.096 ±0.30 kN/m^2)
Mencucci et al. [59]	TUNEL assay, Western blot analysis, immunohistochemistry, and light microscopy	In vivo	Human	15	CXL stimulates keratocyte apoptosis and repopulation CF diameter increased by 22.6% compared with control, 16.1% compared with KC. Not significantly different on PS
Wollensak and Iomdina [60]	Biomechanical testing	In vivo	Rabbits	9	Increase YM by 78.4–87.4%, ultimate stress by 69.7–106.0% Decrease ultimate strain by 0.57–78.4%
Dhaliwal and Kaufman [61]	Confocal microscopy, TEM, histology, and light microscopy	Pilot study	Human	5	Keratocyte apoptotic changes a depth of 300 µm with demarcation line Spherical structures evident until the depth of 300 µm
Bottós et al. [62]	Immunofluorescence confocal microscopy	Ex vivo	Porcine	25	Maximum CXL of CF in anterior stroma CXL effect is more in de-epithelialized than corneas with epithelium intact Keratocyte apoptosis up to 250–300 µm depth
Wollensak and Redl [63]	Pepsin extraction of collagen type I and sodium dodecyl sulfate-polyacrylamide gel electrophoresis	Ex vivo	Porcine	40	CFs has a very strong chemical stability following CXL treatment High molecular weight collagen polymers present at crosslinked corneas
Wollensak et al. [64]	Light microscopy, biomicroscopy, and OCT	Ex vivo	Porcine	25	Swelling pattern—intense in AS (242 µm), for next 238 µm (hydration factor 2.2), non-crosslinked posterior 135 µm (hydration factor 2.7) Sensitivity of swelling response is in relation with degree of CXL OCT not suitable for clinical control of CXL effect
Kohlhaas et al. [65]	Biomechanical testing	Ex vivo	Porcine and human	40 and 10	Significant stiffening in AS (200 µm). 75–70% of UVA irradiation absorbed within 200 µm and next 20% absorbed in the next 200 µm of cornea Endothelium preserved
Schilde et al. [66]	Biomechanical testing	Ex vivo	Porcine	20	Resistance to enzymatic digestion is high in CXL corneas CXL of the CFs extends pass the first anterior 200 µm to next 200 µm of cornea

(continue)

Table 1 (continued)

Author (reference)	Investigative techniques	Type of study	Animal model	No. of eyes	Key findings
					65% of riboflavin absorbed in anterior 200 μm and 25–30% absorbed in next 200 μm
Spoerl et al. [13]	Micrometer and histology (H&E)	Ex vivo	Porcine	30	Shrinkage temperature—AS (75 ± 1.2 °C) than PS (70 ± 0.8 °C)
Wollensak et al. [41]	TUNEL assay, TEM, and histology	Ex vivo	New Zealand white rabbits	38	Keratocyte apoptosis present at anterior 50 μm 4 h post-treatment
					Cytotoxic UVA irradiation range from 0.5–0.7 mW/cm^2
Wollensak et al. [41]	Morphometric computer software	In vivo	NZ white albino rabbit	10	CF diameter increased 12.2% (3.96 nm) in AS and 4.6% (1.63 nm) in PS
					Average increase of anterior CF with CF—9.3% (3.1 nm)
Spoerl et al. [13]	Enzymatic assay (collagenase, pepsin, and typsin) and light microscopy	Ex vivo	Porcine	80	CXL treatment significantly increases resistance to collagenase, pepsin, and trypsin digestion in the anterior half of the cornea
Wollensak et al. [67]	Biomechanical testing	In vivo	Porcine and human	20 and 5	Increased in YM by factor 1.8 in porcine and 4.5 in human corneas
					Mean CT—850 μm ± 70 (SD) in porcine, 550 ± 40 μm in human corneas
					Increase stress by 71.9% in porcine and 328.9% in human corneas

CXL, crosslinking; YM, Young's modulus; OCT, optical coherence tomography; SAM, scanning acoustic microscopy; AFM, atomic force microscopy; TEM, transmission electron microscopy; UVA, ultraviolet A; PG, proteoglycan; CFs, collagen fibrils; CF, collagen fiber; BM, basement membrane; H&E, hematoxylin and eosin; PAS, periodic acid-Schiff; NZ, New Zealand; IOP, intraocular pressure; TUNEL, TdT-mediated dUTP nick-end labeling; AS, anterior corneal stroma; PS, posterior corneal stroma; MSF, mean stiffening factor; MSE, mean stiffening effect; CT, corneal thickness; CS, corneal stiffening

2.3.1. Mechanical Evidence

The intended goal of CXL is to strengthen the intrinsic mechanical properties of corneal stroma. Therefore, the evaluation of mechanical properties of cross-linked corneas is of much importance. Among other methods to test the efficacy of this treatment, biomechanical characterization provides an objective and quantitative measurement to assess the degree of CXL. Due to this reason, the measurement of biomechanical property of cross-linked cornea have been conducted, and demonstrated consistent qualitative trend of statistically significant increase in corneal stiffness through many studies (Spoerl, Huhle et al. 1998, Spoerl and Seiler 1999, Wollensak, Spoerl et al. 2003, Kohlhaas, Spoerl et al. 2006, Tanter, Touboul et al. 2009, Lanchares, del Buey et al. 2011, Schumacher, Oeftiger et al. 2011). The characterization techniques have been reported to describe corneal stiffness following CXL including tensile testing (Wollensak, Spoerl et al. 2003, Kohlhaas, Spoerl et al. 2006), AFM (Choi, Lee et al. 2013, Dias, Diakonis et al. 2013), inflation testing (Lombardo, Serrao et al. 2014) and SAM (Beshtawi, Akhtar et al. 2013, Beshtawi, Akhtar et al. 2014). Results reveal that the majority of the stiffening effects often occur in the anterior stroma with a depth-dependence manner (Kohlhaas, Spoerl et al. 2006, Dias, Diakonis et al. 2013, Sondergaard, Ivarsen et al. 2013). These studies have provided important evidence and implied structure-dependent relationship on the corneal material properties.

The stiffening effect of CXL treatment has been examined on human, porcine, and rabbit corneas as well as on collagen hydrogels (Jue and Maurice 1986, Wollensak, Spoerl et al. 2003, Ahearne, Yang et al. 2008, Kling, Remon et al. 2010, McCall, Kraft et al. 2010). The results are dependent on the thickness of cornea and difference between species. A study compares the stress strain measurement using tensile testing on human and porcine corneas before and after CXL (Wollensak, Spoerl et al. 2003). The increase in rigidity is 328.9% and 71.9% in human and porcine corneas, respectively (figure 2.5). The difference in results between human and porcine corneas is due to the higher absorption coefficients in human cornea, and thinner central thickness of human (550 mm and 850 mm in human and porcine respectively). Additionally, the anterior stroma in human corneas is much

stiffer than its posterior stroma without any treatment, whereas the anterior and posterior stromal strips of porcine corneas do not appear to differ significantly (figure 2.6) (Kohlhaas, Spoerl et al. 2006). This result demonstrates that a larger portion of human cornea is cross-linked compared to porcine cornea. Indeed, the UVA/riboflavin CXL often occurs in the anterior 200 μm of corneal thickness as approximately 70% of UVA is absorbed within the anterior portion and only 20% in the next 200 μm (Kohlhaas, Spoerl et al. 2006).

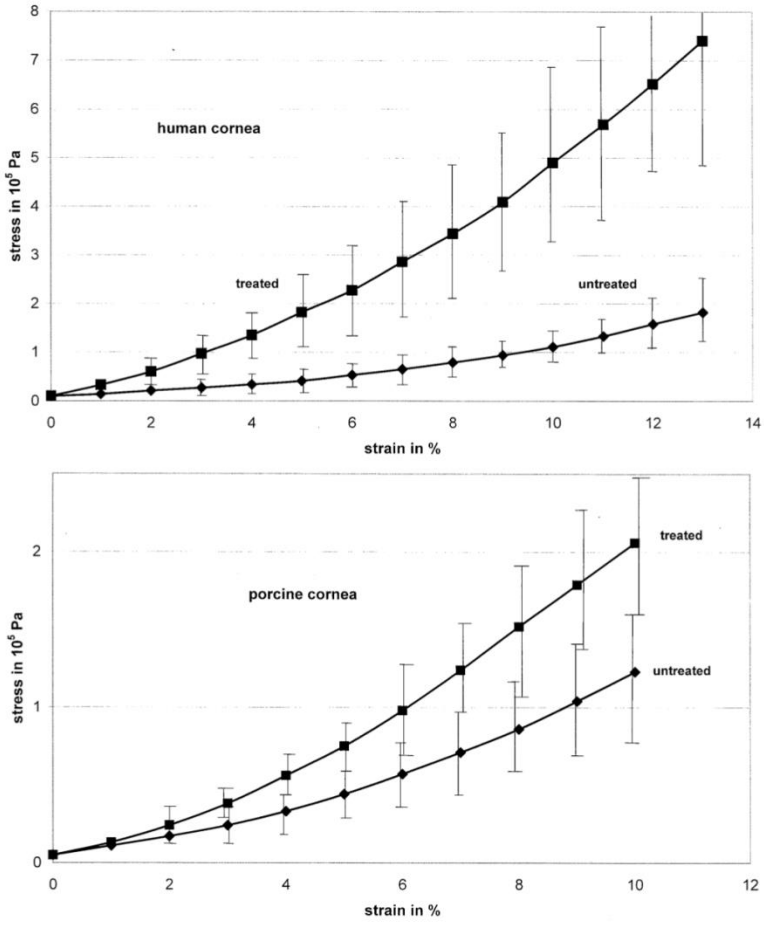

Figure 2.5. Stress-strain measurements of cross-linked corneas. *Top:* human corneas treated with UVA/riboflavin CXL (irradiance 3 mW/cm^2). *Bottom:* porcine corneas treated with UVA/riboflavin CXL (irradiance 3 mW/cm^2). Source (Wollensak, Spoerl et al. 2003)

Other factors may also contribute to this between-species difference, such as the orientation of the collagen fibrils providing different structural properties (Muller, Pels et al. 2001). The tangent modulus at 6% strain increases by factors of 1.5 in rabbit, 1.8 in porcine, and 4.5 in human corneas

(Wollensak, Spoerl et al. 2003, Wollensak and Iomdina 2009). This difference can be explained by the anterior localization of the main CXL effect. However, the reduced biomechanical effect in rabbit cornea compared with the human cornea may be due to the intrinsic properties of collagen matrix. The tangent modulus at 6% strain is 1.81 and 1.3 in normal rabbit and human corneas, respectively (Wollensak and Iomdina 2009). Additionally, the UVA absorption coefficient is significantly lower in rabbit than that in human cornea after riboflavin application, which indicates the less UV-induced cross-links in rabbit corneal stroma (Spoerl, Mrochen et al. 2007).

In summary, the overall mechanical stiffness can be considered as a combination effect of internal geometry and material property itself. Therefore, the formation of cross-links between collagens at the intra-helical, inter-helical, and intra-fibrillar levels following CXL is believed to induce subsequent mechanical strength of collagens (Wollensak, Wilsch et al. 2004, Abad 2008).

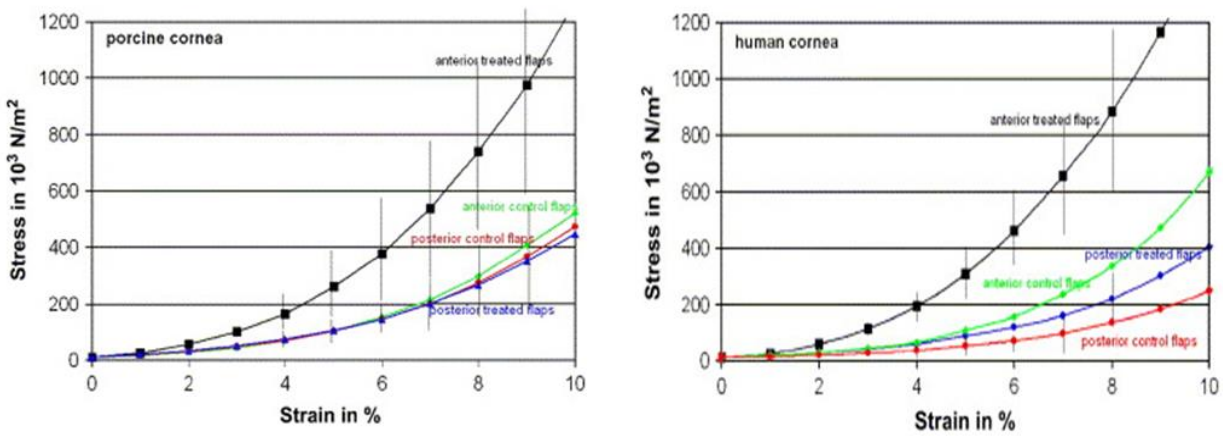

Figure 2.6. Stress-strain measurements of treated and untreated strips. *Left:* porcine corneal anterior and posterior strips treated with UVA/riboflavin (irradiance 3 mW/cm^2). *Right:* human corneal anterior and posterior strips treated with UVA/riboflavin (irradiance 3 mW/cm^2). Source (Kohlhaas, Spoerl et al. 2006)

Collagen CXL is initially thought to affect the mechanical properties, ultrastructure, hydrodynamic and enzymatic behaviour of the cornea (Wollensak, Aurich et al. 2007, Kling, Remon et al. 2010, Chai, Gaster et al. 2011, Zhang, Conrad et al. 2011, Akhtar, Almubrad et al. 2013, Wang, Huang et

al. 2015). The components within the treatment protocols could have also resulted in the difference in corneal stiffness measured. In Dresden CXL procedure, 20% dextran is used as the thickening agent during the application of riboflavin solution. In the original corneal cross-linking procedure, dextran, is also used to prevent corneal swelling during the procedure.

However, most of previous comparative studies have not been done with matched corneal pairs, and the control group should have a placebo treatment with saline or riboflavin or dextran to ensure the more reliable comparisons. Recently, it has been reported that the role of dextran in tensile mechanical testing and that mechanical outcomes change in response to tissue hydration states (Annaka 2012, Hatami-Marbini and Rahimi 2016). The results demonstrate that dextran causes a reduction in tissue hydration and therefore a reduction in thickness which significantly affected the outcomes of uniaxial tensile test and the overall stiffness of the treated corneas (Hayes, Kamma-Lorger et al. 2013, Hatami-Marbini and Rahimi 2016). Higher tensile stiffness is observed in less hydrated corneal specimens, and part of this stiffening effects following corneal CXL could be due to the changes in corneal hydration state instead of CXL therapy itself (figure 2.7).

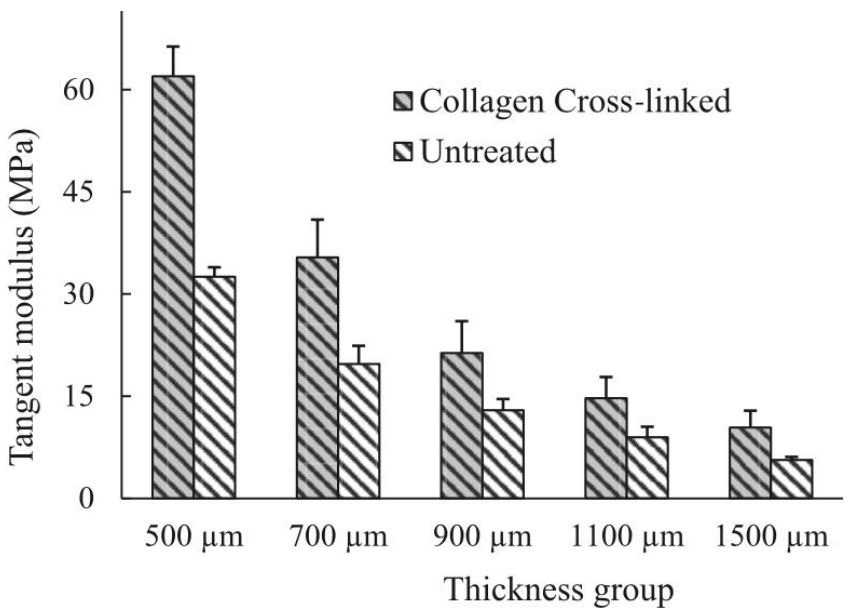

Figure 2.7. Tangent modulus of the collagen cross-linked corneal strips at different levels hydration (thickness) compared to those of the untreated bovine corneas. Source (Hatami-Marbini and Rahimi 2016)

In a photo-assisted CXL process, the efficacy of the CXL also relies on the concentration of photosensitizer and the irradiation of light source. The depth-dependent profile of riboflavin and UVA induced CXL efficacy has been studied recently. The process of CXL requires spatial and temporal distribution of photosensitizer and illuminating light, which can be simulated by Monte Carlo (MC) method. The MC method is a stochastic technique and the "gold standard" for biophotonic simulation and has been developed to solve the problem of light transportation and distribution within biological tissues (Qu, Macaulay et al. 1994). The light propagation through living tissue is of complication due to the very high scattering characteristic of the living tissues, and a photon generally will scatter many times before its absorption. Thus, the optical properties such as tissue absorption and scattering coefficients as well as the degree of anisotropy of the tissue must be considered when investigating light penetration and distribution through a tissue (Jones, Preyer et al. 2009, Nan and He 2013). Understanding the light delivery in corneal stroma also plays a notable role in standardizing more precise protocol for clinical CXL treatment. MC is especially helpful in a multi-layered tissue which has different photosensitizer concentration. To model this process using MC method, it requires principle parameters including the diffusion of riboflavin, distribution of UVA, the rate of photo-polymerization, and the stiffening effect of tissue. In a study of Schumacher and colleagues establishes a MC model to optimize the UVA/riboflavin corneal CXL, in which they used Fick's law of diffusion and Beer's law of light absorption, equations of polymerization rate, and integrated with tangent modulus, calculating its spatial and temporal distribution. The distribution of biomechanical properties can be then predicted with the combination effects of varied concentration and pre-soaking time of riboflavin, and the illumination intensity and duration. The riboflavin concentration, UV intensity, the rate of polymerization (or the rate of induced cross-links), and the increase in stiffness can then be generated as a depth-dependent function. In their derived model, the increase in stiffness is not the same under equal amount of accumulated energy dose due to the rate of cross-links dependent on the square root of illumination intensity. Their study demonstrates that higher intensity with a shorter illumination time results in a more even distribution of induced cross-links and

biomechanical stabilities, when comparing the UV intensity of 3 mW/cm^2 and 10 mW/cm^2 (figure 2.8) (Schumacher, Oeftiger et al. 2011).

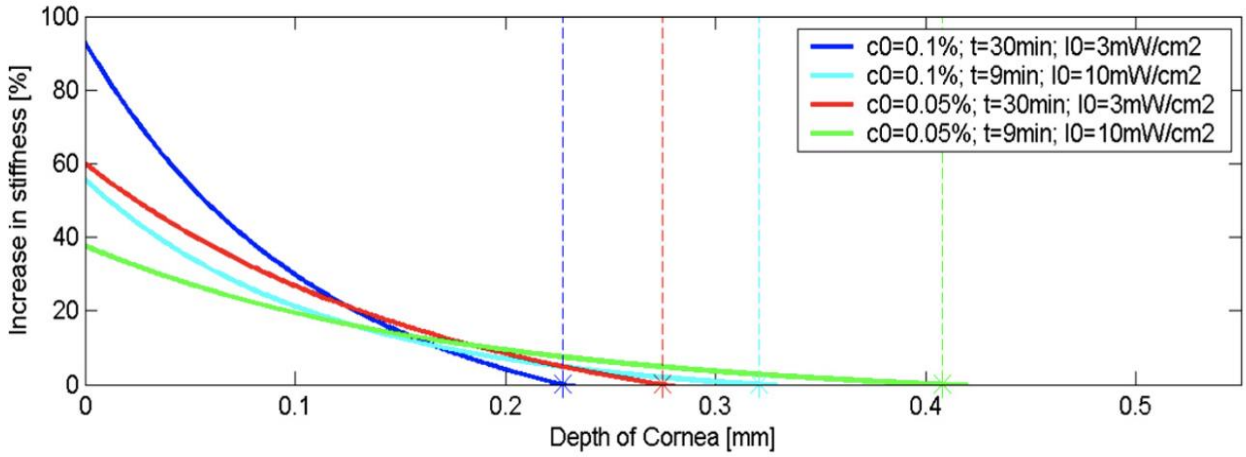

Figure 2.8. The increase in stiffness as a function of the corneal depth following four different cross-linking treatment protocols. The treatment protocols differed in terms of riboflavin concentrations (c0), UVA exposure time (t) and UVA intensity (I0). Four different cases are shown: c_0 = 0.1%, treatment time 30 minutes with UV intensity 3 mW/cm^2; c_0 = 0.1%, treatment time 9 minutes with UV intensity 10 mW/cm^2; c_0 = 0.05%, treatment time 30 minutes with UV intensity 3 mW/cm^2; and c_0 = 0.05%, treatment time 9 minutes with UV intensity 10 mW/cm^2. The pre-treatment time of riboflavin was set to 30 minutes. *Dotted lines*: the threshold for the onset of induced cross-links. Source (Schumacher, Mrochen et al. 2012)

Another photodynamic model considering the photo-initiation rate of riboflavin and Beer's law of light absorption for predicting the penetration depth of cross-links reports a good agreement with the clinical outcome (Laggner, Pollreisz et al. 2015, Lin 2015). The model demonstrates that longer and deeper riboflavin diffusion may result in an increase in biochemical stability. Moreover, they have shown that the most effective zone of UVA/riboflavin CXL is confined to 150-250 μm irrespective of the riboflavin concentration and diffusion time. The depth threshold of CXL can then be explained using this photodynamic model. It is possible to calculate the amount of induced cross-links in corneal stroma and predict the relative increase in stiffness at an experimental scale. However, the CXL

photodynamic model still exists some limitations as monitoring of the spatial distribution in the corneal tissue would be a challenge, therefore the concentration of photosensitizer was idealized and assumed the same as the initial amount. The average amount of riboflavin which is actually 50% less than assumed in the model corresponds to the initial concentration. The model postulates that the amount of riboflavin consumed by the photochemical reaction is refilled through the continuous riboflavin instillation during the CXL treatment, which stays the same amount as the initial concentration. The uneven light distributions were also neglected in the model. All these assumptions have unknown effects on the outcomes.

In recent years, researchers have attempted to increase the intensity of UV power by reducing the treating time, which is called accelerated CXL. The initial assumption is to examine the equivalence of biomechanical properties regarding the stiffening effect of CXL on corneas treated with Dresden protocol or accelerated method. The stiffening effect using an irradiation of 3 mW/cm^2 for 30 minutes and 9 mW/cm^2 for 10 minutes has been examined and reported no significant difference (Schumacher, Oeftiger et al. 2011). Another study comparing different intensity from 2 mW/cm^2 to 15 mW/cm^2 with corresponding illumination time to maintain the constant total energy dose of 5.4 J/cm^2 shows an equivalent stiffness, which validate the Bunson-Roscoe law of reciprocity (Krueger and Ramos-Esteban 2007). However, not all studies consist with the law of reciprocity. It has been demonstrated that no significant increase in Young's modulus is found in the corneas treated with same intensity of 3 mW/cm^2 but doubled illumination time (Lanchares, del Buey et al. 2011). In addition, other ten different irradiances between 3 mW/cm^2 and 90 mW/cm^2 with constant energy dose are tested, the results demonstrate that the Bunsen-Roscoe law is only valid when the illumination intensity is lower than 45 mW/cm^2 (Wernli, Schumacher et al. 2013). More recently, the biomechanical effect of CXL has been reported to decrease significantly with increased intensity and reduced irradiation time while comparing three different conditions including 3 mW/cm^2 for 30 minutes, 9 mW/cm^2 for 10 minutes, and 18 mW/cm^2 for 5 minutes (Hammer, Richoz et al. 2014). Based on these findings, it is difficult to conclude the validity of Bunsen-Roscoe law, and the failure of the law is probably due to the complex photodynamic process which is not fully understood.

2.3.2. Biological Evidence

Cornea tissue is a dynamic and continuously remodelling environment in which is primarily coordinated by several enzymes including MMPs and LOX. These enzymes not only involve in the development of normal tissue maintenance but also play an important role in the pathogenesis of keratoconus. Previous studies have shown that proteinase activity is more active and proteinase inhibitor activity is reduced in keratoconus (Zhou, Sawaguchi et al. 1998, Davidson, Hayes et al. 2014). Researches have suggested that α and β chains which are smaller peptide chains consisting of collagen might form higher molecular weight polymers after UVA/riboflavin CXL treatment. These high molecular weight polymers are uneasy to be digested by MMPs as the cleavage site of MMPs are blocked during the CXL. In addition, another possible explanation is the transform of tertiary structure of cross-linked collagen that prevent MMPs to reach their cleavage sites (Zhang, Conrad et al. 2011, Zhang, Mao et al. 2013). Therefore, the enzyme digestion resistance is also an important indicator in evaluating the efficacy of CXL. Effective CXL in the stroma can stabilise the structure of collagen and possibly result in a steric hindrance which block the cleavable site of enzyme digestion such as collagenase, pepsin, and trypsin (Spoerl, Wollensak G Fau - Seiler et al. 2009, Hayes, Kamma-Lorger et al. 2013, Aldahlawi, Elshal et al. 2016, Aldahlawi, Hayes et al. 2016). Increased activity of collagenase in keratoconus has been recognized which had led researchers to focus on the ability of resistance to enzymatic digestion after CXL treatment (Rehany, Lahav et al. 1982). The resistance to collagenases, pepsin, trypsin, and MMPs including subtypes MMP-1, 2, 9, and 13 degradation all have been reported following CXL (Spoerl, Wollensak et al. 2004, Zhang, Mao et al. 2013). Particularly, the increased resistance of collagen and PGs from MMP degradation is likely to be important in the potential of CXL in arresting progression in keratoconus (Zhou, Sawaguchi et al. 1998, Zhang, Mao et al. 2013, Aldahlawi, Hayes et al. 2016). However, the ability seems to vary with the UVA irradiation intensity and different CXL protocols. Although the higher UVA irradiation ($30mW/cm^2$) tends to create more intense cross-links on the most superficial layers, which may result in the higher resistance to enzymatic digestion compared to standard protocol ($3mw/cm^2$) (figure 2.9)

(Aldahlawi, Hayes et al. 2016). The standard CXL protocol shows the highest measurement of corneal disk dry weight midway through the digestion process. Their finding indicates that the amount of cross-links may be less when the higher UVA intensity was used in the accelerated CXL with the same cumulative dose (5.4J/cm^2) as standard CXL protocol.

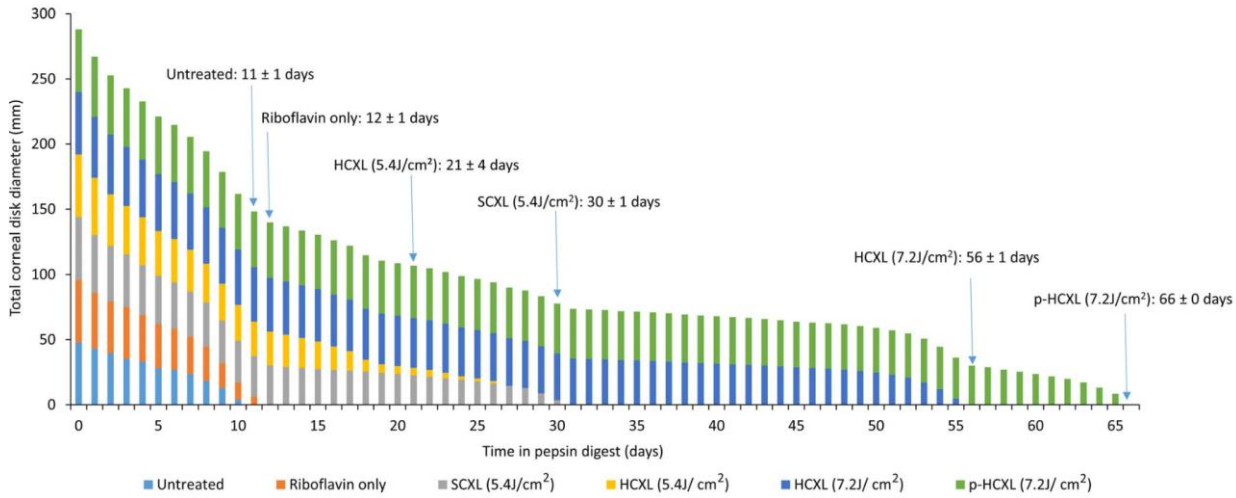

Figure 2.9. The summed diameter of corneal disks within each cross-linked and non-cross-linked treatment group in pepsin digest solution. Source (Aldahlawi, Hayes et al. 2016)

Other study has been observed intense type I collagen molecules, which is proved to be chemically stable to pepsin and heat treatment after CXL treatment (Wollensak and Redl 2008). The authors attempt to attribute the stabilising effect of CXL to the alterations in the tertiary structure of collagen fibrils. This finding also explains the corneal resistance to enzymatic digestion and increased diameter of collagen fibrils after CXL, which may contribute as an important factor in determining biomechanical changes.

Two-photon microscopy has been used in rabbit corneas to visualize the effect of CXL on cells and collagens by detecting its auto-fluorescence (Steven, Hovakimyan et al. 2010). The grade of CXL can then be quantified by auto-fluorescence lifetime measurements. Other experimental studies have demonstrated a dose-dependent damage on keratocytes in a rabbit model with different irradiation intensity ranging from 0.75 to 4 mW/cm^2 (Wollensak, Spoerl et al. 2004). In standard CXL procedure, an irradiance of 3mW/cm^2 is reported to lead to cell loss within the anterior 300 μm of the corneal

stroma (Wollensak 2010). It is known that quiescent corneal keratocytes adjacent to the injury transform into an activated, fibroblastic repair phenotype during wound healing process (Jester, Petroll et al. 1999, Stramer, Zieske et al. 2003). Studies have confirmed and shown numerous Ki-67 positive fibroblasts expression after CXL treatment (Wollensak, Iomdina et al. 2007, Hovakimyan, Guthoff et al. 2011, Hovakimyan, Guthoff et al. 2012), including a few α-SMA positive myofibroblasts detected (Mencucci, Marini et al. 2010, Salomao, Chaurasia et al. 2011). This evidence indicates that the activation of keratocytes after corneal CXL occurs by means of transformation into fibroblasts. In a rabbit model, the keratocyte repopulation can be observed by day 7. This repopulation commences in the posterior stroma, with activated keratocytes in the adjacent untreated stroma (Wollensak, Iomdina et al. 2007). According to these studies, there is no observable toxic effect of CXL at a depth beyond this level. The inference might be insufficient UV energy and oxygen radical production to cause further damage to inner structure of corneal stroma, which is also supported by theoretical constructs and experimental evidence.

2.3.3. Ultrastructural Evidence

In keratoconus, the elasticity of the collagen fibril is reported to decrease, leading to a general corneal weakness (White, Lewis et al. 2017). Therefore, the change in structure of collagen becomes one of the important parameters in morphological changes after CXL. The measurement of collagen fibril diameter has been examined in an animal model following CXL treatment. TEM images show an increase of 12.2% in collagen fibril diameters within the first 50 mm anterior region but only 4.6% increase in posterior segments (Wollensak, Wilsch et al. 2004). The collagen diameter is significantly larger in the anterior stroma than in the posterior stroma in the treated corneas, which suggests that the CXL induces a localisation effect in collagen structure with a depth-dependent manner. Collagen fibril diameter has also been evaluated in normal healthy rabbit corneas after CXL treatment, and more recently in human keratoconic corneas *ex vivo* (Wollensak, Wilsch et al. 2004, Akhtar, Almubrad et al. 2013). Wollensak and Wilsch demonstrate the increased fibril diameter in the anterior stroma in rabbit. In Akhtar's TEM study, the collagen fibril diameter and inter-fibrillar spacing are

significantly increased, and areas of PGs show a more uniform distribution in CXL treated keratoconic corneas, in which the overall ultrastructure is more similar to normal human corneas. However, X-ray scattering studies have not found the increase of fibril diameters in cross-linked corneas (Hayes, Kamma-Lorger et al. 2013). It is hypothesised that larger fibril diameters may be observed in cross-linked corneas using TEM technique, as the newly formed cross-links may increase the resistance to the tissue shrinkage during tissue processing for TEM imaging (figure 2.10) (Hayes, Kamma-Lorger et al. 2013).

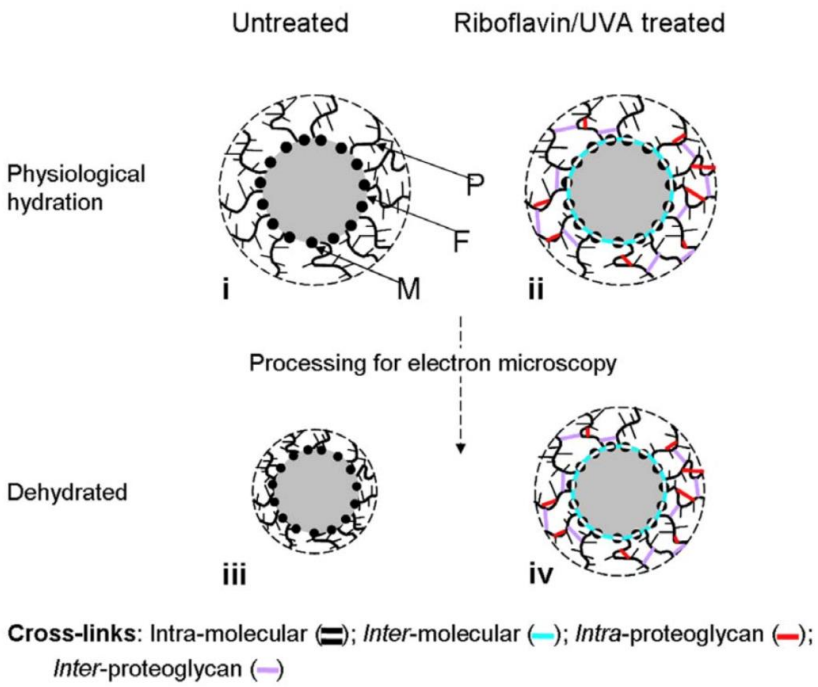

Figure 2.10. Schematic showing likely collagen shrinkage during TEM processing of cross-linked and non-cross-linked corneas. (i) the theoretical structure, (ii) the riboflavin/UVA induced cross-linked structure, (iii and iv) the shrinkage structure associated with tissue dehydration during TEM processing. (F) collagen fibril, (M) collagen molecules, (P) proteoglycans. Source (Hayes, Kamma-Lorger et al. 2013)

The morphological effect of CXL has also been investigated using immune-histochemical analysis in normal, keratoconic, and cross-linked keratoconic human eyes (Mencucci, Marini et al. 2010). The reported increase in collagen diameter of treated corneas in human is 22.6% anteriorly and 16.1% posteriorly. The difference between species may be due to the higher CXL percentage induced in

human corneas (Spoerl, Mrochen et al. 2007, Wollensak and Iomdina 2009). A more recent study evaluates the protective effect of additional soluble collagen in CXL procedure using enzyme-treated ectasia models (Wang, Huang et al. 2015). However, CXL does not restore the collagen ultrastructural damage caused by enzymatic treatment. The additional soluble collagen may provide an important role in protecting the ultrastructure during CXL process.

2.3.4. Biophysical Evidence

Collagen is composed of triple helix peptide chains held by hydrogen bonds. As the collagen is gradually heated up to reach a critical temperature, the hydrogen bonding in the collagen fibrils begin to be disrupted and the tissue shrinks rapidly. This critical temperature is known as thermal shrinkage temperature or denaturation temperature which has been used for decades as an effective technique in studying collagen CXL (Xu 2009). As the cross-linked structure of collagen fibrils become more stable, the more heat is required to disrupt the tertiary protein structure resulting in the increase in thermal shrinkage temperature.

Thermal damage is expected to occur after CXL as the treatment duration is long and UVA is absorbed in the corneal tissue. Many studies have demonstrated a higher shrinkage temperature in the anterior stroma where the CXL mainly affects and a strengthened thermomechanical behaviour of cross-linked corneas (Spoerl, Wollensak et al. 2004, Kohlhaas, Spoerl et al. 2006). In a porcine study, CXL significantly increases the tolerance to hydrothermal shrinkage temperature up to 75°C in the anterior portion of the corneas. However, the maximal shrinkage temperature in the posterior stroma and untreated corneas can only be up to 70°C (Spoerl, Wollensak et al. 2004). Corneal surface temperature is measured using an infrared thermos-camera in keratoconic human eyes during the CXL procedure (Mencucci, Mazzotta et al. 2007). A constant temperature increase is observed during the treatment but it has not exceed the threshold of thermal damage for corneal collagen fibrils, which suggests that UVA/riboflavin CXL is a safe procedure (Mencucci, Ambrosini et al. 2005). The shrinkage of the cornea is believed to occur as a result of collagen fibril denaturation and unwinding due to the increased heat (Spoerl, Wollensak et al. 2004).

Another important biophysical feature is the swelling behaviour which regulates the hydration state of stroma (Huang and Meek 1999). The hydration of corneal stroma has been widely studied as it correlates with corneal transparency. Many studies report that the hydration behaviour of stroma is largely dependent on the collagen arrangements and KS/CS ratio of PGs (Bettelheim and Plessy 1975, Muller, Pels et al. 2001, Hayes, White et al. 2017). PGs are macromolecules consisting of a core protein with covalently attached with GAG chains. Dermatan sulfate (DS), chondroitin sulfate (CS) and keratan sulfate (KS) are the dominant GAG chains found in the cornea forming inter-fibrillar bridges (figure 2.11). At physiological pH condition, these GAG components, DS, CS, and KS, carry with negative charges. The repulsive forces between these negative charges give rise to strong intermolecular forces which significantly affect the swelling properties of cornea (Hedbys 1961, Xi Cheng, Hamed Hatami-Marbini et al. 2013). It has been reported that KS side chains can create an open network capable of absorbing bulk of water, whereas CS side chains are able to form a tight network structure by interacting with other side chain, Ca^{2+} bridges, and hydrogen bonding to retain water in the other hand (Bettelheim and Plessy 1975). All these studies satisfy with the phenomenon that the diameter of fibrils in edema cornea is no different from that of normal cornea but the volume increase of inter-fibrillar substance leads to the swelling of cornea (Maurice 1957).

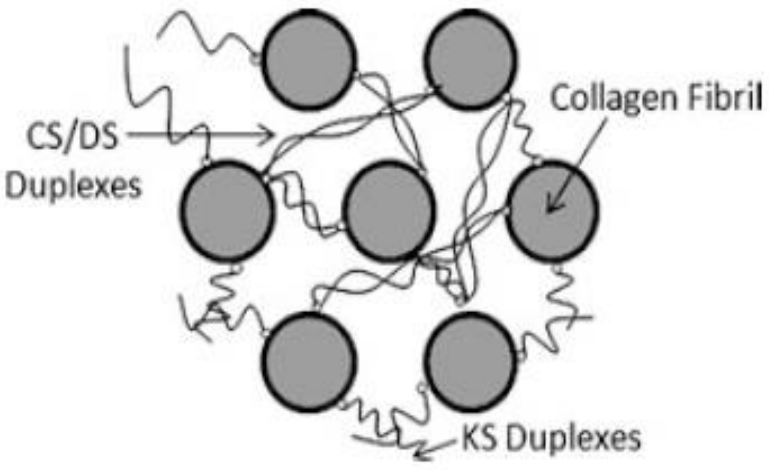

Figure 2.11. Collagen-Proteoglycan arrangement in the corneal stroma. Source (Scott 1992)

Therefore, it is considered important to examine the hydration of corneas after UVA/riboflavin CXL which is believed to affect the swelling of tissue. The effect of CXL on the alteration of corneal

swelling behaviour has been examined on 20 porcine corneas in a moist chamber for 24 hours after CXL treatment (Wollensak, Aurich et al. 2007). The difference between the treated and untreated corneas is statistically significant. Their results show that the swelling behaviour is dependent on the degree of CXL. The swelling degree of corneas is reduced when the cross-links increase. In another study, researchers further divide the cornea into three layers (cross-linked area, partial cross-linked, and non-cross-linked region) based on the CXL percentage, and examine the swelling behaviour using light microscopy. After hydration, no significant change in thickness is observed in the first layer which is cross-linked area, while the second and third layers are thickened by a factor of 2.2 and 2.7, respectively. Although the increased resistance to hydration has led to the proposal that CXL might have a role in the management of corneal decompensation. However, recent investigations have demonstrated that the changes in hydration performance are unlikely to be permanent alterations due to the osmolality of the 20% dextran solution used in the conventional Dresden protocol instead of the consequences of CXL itself (Hayes, Boote et al. 2011, Hayes, Kamma-Lorger Cs Fau - Boote et al. 2013).

2.3.5. Chemical and Molecular Evidence

Researchers have showed the riboflavin mediated photochemical reactions to be associated with the creation of singlet oxygen, with the CXL involving tyrosine residues, glycation end products, and alterations in secondary and tertiary protein structures (Kato, Wang et al. 1994, Choe and Min 2006, Huang, Kim et al. 2006, D'Agati, Yan et al. 2010). However, those findings have not been studied on corneas. Photochemical collagen CXL reaction within corneal stroma is hypothesized to be achieved by utilising the UVA light-triggered free radicals, which then would activate the adjacent aldehyde groups (Wollensak, Spoerl et al. 2003, McCall, Kraft et al. 2010). Lysine-based cross-links following UVA/riboflavin corneal CXL have previously been postulated but not been reported chemically (Spoerl, Huhle et al. 1998, Wollensak, Spoerl et al. 2003).

Recently, a study demonstrated that the effectiveness of riboflavin/UVA can be inhibited by blocking singlet oxygen using azide, and promoted by prolonging the half-life of oxygen radicals (Wright,

Bubb et al. 2002, Choe and Min 2006, Huang, Kim et al. 2006, McCall, Kraft et al. 2010). In addition, the effect of CXL on mechanical strength is prevented when carbonyl groups are blocked, while the mechanical strength remains when amine groups are blocked (McCall, Kraft et al. 2010). The results provide the evidence that the UVA/riboflavin CXL reactions may occur via the formation of imidazole intermediates, and the triggering of endogenous of carbonyl groups such as allysine and hydroxyl-allysine to form new covalent bonds. The degradation of riboflavin itself to react with the carbonyl groups is also supposed as another possible mechanism (figure 2.12) (McCall, Kraft et al. 2010).

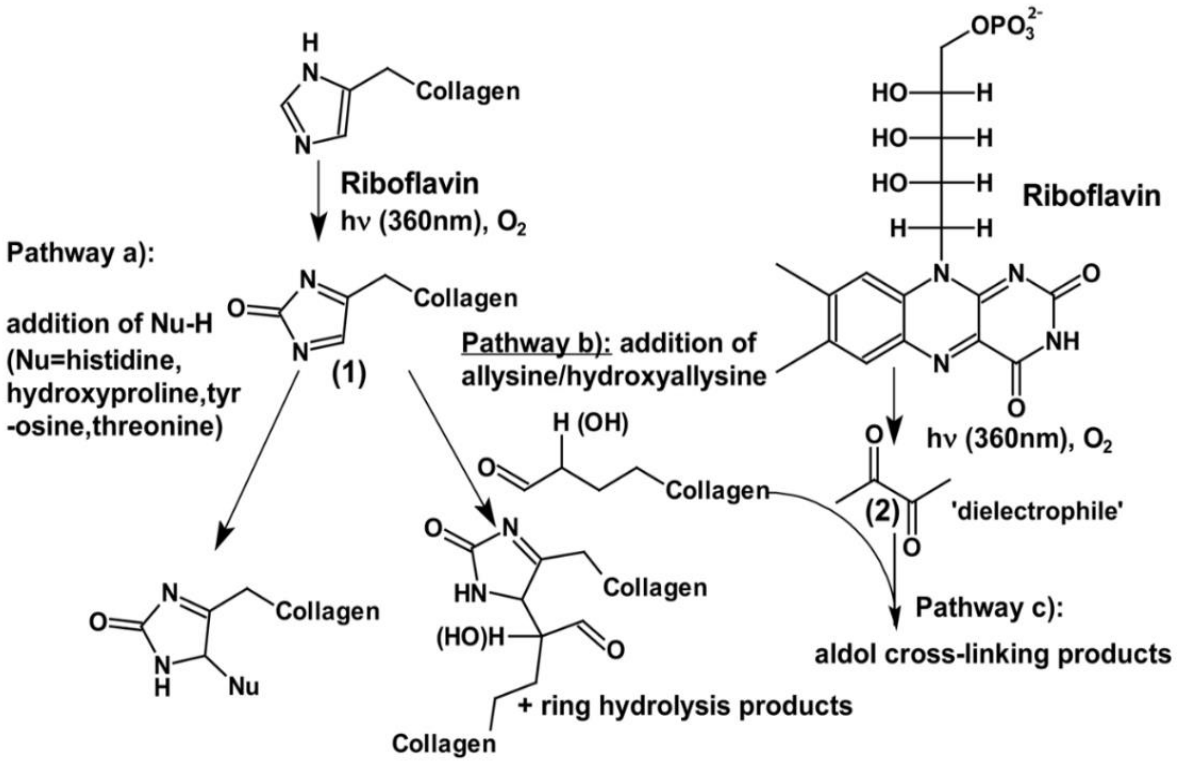

Figure 2.12. Proposed mechanisms by which riboflavin can induce CXL of collagen molecules in the presence of UVA. Source (McCall, Kraft et al. 2010)

The significance of oxygen in UVA/riboflavin CXL has also been studied, which suggests a significant increase in tensile mechanical measurement in cross-linked corneas under normal oxygen levels. No increase in mechanical measurement is found in untreated corneas in a low-oxygen condition (Richoz, Kling et al. 2014). Moreover, it has been noted that these photochemical CXL

changes is associated with loss of tyrosine and histidine residues within the collagen molecules, which could be inhibited by the level of oxygen (Kato, Wang et al. 1994). However, the precise mechanism of CXL at the molecular level has not been elucidated completely. Currently, all evidence for CXL is indirect and chemical proof is awaited. The plausible mechanism of UVA/riboflavin CXL is considered to be involved in the formation of chemical bonds between histidine, hydroxyproline, hydroxylysine, tyrosine, and threonine amino acid residues (Kato, Wang et al. 1994, McCall, Kraft et al. 2010).

In addition to the uncertainty regarding the precise chemical bond reactions in UVA/riboflavin CXL, the locations where the cross-links occur at the molecular level is also uncertain. The most commonly accepted hypothesis is proposed by Hayes et al. through a series of experiments including stromal ultrastructure, hydrodynamic behaviour, and enzymatic digestion (Hayes, Kamma-Lorger et al. 2013). They hypothesize that the most likely CXL scenarios are thought to occur within and between the collagen molecules at the surface of the fibrils and within the proteoglycan-rich matrix surrounding them (figure 2.13 A,B,C,F,G), these interactions contribute to the increased stiffens, enzymatic resistance, and hydrodynamic behaviour accordingly. In addition, cross-links are not possible to be formed between the collagen fibrils themselves, as the distance between individual fibrils is too large for the formation of fibril to fibril bonds (figure 2.13 D,E)

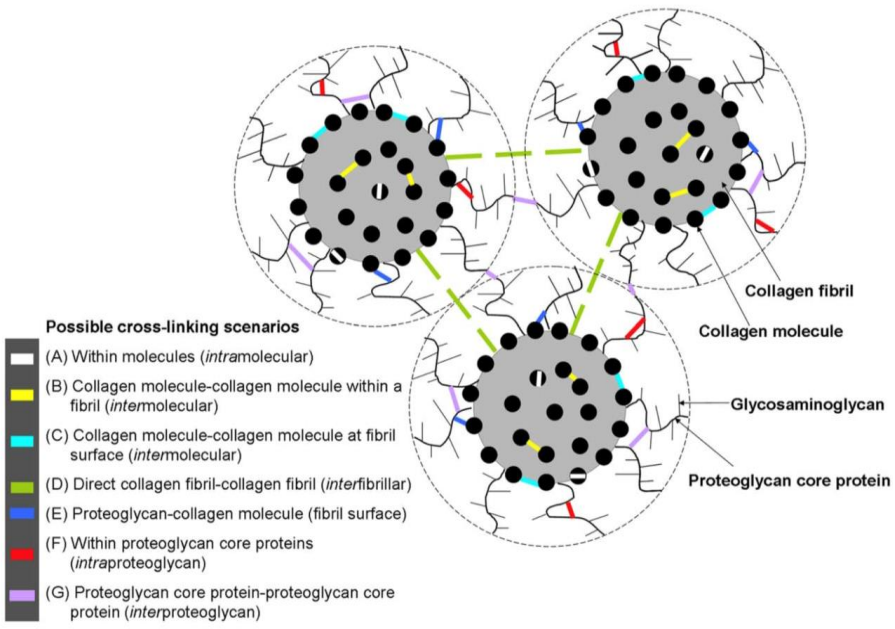

Figure 2.13. Schematic showing possible CXL scenarios. Source (Hayes, Kamma-Lorger et al. 2013)

2.4. UVA/riboflavin CXL in Clinical Trials

The first clinical study in human eyes was published in 2003, in a series of 23 eyes that underwent an epithelium-off CXL procedure, reported stabilisation of keratoconus with up to 5 years follow-up (Wollensak, Spoerl et al. 2003). In addition, the endothelial cell counts were not statistically significant changed and no loss of transparency of the cornea is reported in this trial. The so-called Dresden protocol is the current clinical approach (Wollensak, Spoerl et al. 2003), which has been available for many years in Europe and recently approved by the U.S. Food and Drug Administration for use in the United States.

Several clinical parameters are proposed to define the progression of corneal ectasia or keratoconus, as an increase more than 1.0 dioptre (D) in the steepest keratometry measurement, an increase of 0.50 D or more in manifest refraction spherical equivalent (SE) in one year, and a reduction of central corneal thickness over 5% in three consecutive tomographies in 6 months (Raiskup and Spoerl 2013, Alhayek and Lu 2015). Therefore, the improvement was documented with an average reduction in SE of 1.0 D and maximum keratometry (Kmax) of 2.0 D. Other clinical studies have been performed to assess the efficacy of CXL after this non-randomised pilot study conducted by the work of Wollensak, including series of paediatric patients and advanced keratoconus (Arora, Gupta et al. 2012, Vinciguerra, Albe et al. 2012, Ivarsen and Hjortdal 2013). Those studies reported similar results with stabilisation of disease in the majority of treated eyes, with few sight-threatening complications and improvement in visual performance, topographic keratometry, corneal shape, and higher-order aberrations (Arbelaez, Sekito et al. 2009, Coskunseven, Jankov et al. 2009, Vinciguerra, Albe et al. 2010, Asri, Touboul et al. 2011, Hersh, Greenstein et al. 2011, Kampik, Koch et al. 2011, Goldich, Marcovich et al. 2012). In a larger case-series study with 12-month follow-up, 142 eyes were included and exposed to CXL treatment. The results showed the improvement of visual acuity in 40% of patients after 12 months. However, it should be noted that while the results of these clinical studies have been supportive for this treatment, inclusion criteria have been varied considerably, with differing follow-up parameters.

Although the effiectiveness and safety of the conventional Dresden protocol has been proven in several clinical tirals, long exposure time to UV radiation and corneal epithelium removal have caused unbearable pain and unavoidable complications. Due to these reasons, many modifications have been made to achieve better outcomes using higher radiation intensity with shorter treatment duration, which is the acccelerated CXL proccedure (Table 2.2) (Rocha, Ramos-Esteban et al. 2008). Although all of these clinical studies have confirmed the acceptable efficacy of accelerated protocols without serious complications reported. These modified CXL procedures are controversial whether these accelerated protocols display equivalent efficacy on halting progression of keratoconus comparing to conventional Dresden protocol. (Bouheraoua, Jouve et al. 2014, Cinar, Cingu et al. 2014, Hashemian, Jabbarvand et al. 2014, Chow, Chan et al. 2015, Hashemi, Miraftab et al. 2015, Konstantopoulos and Mehta 2015, Cummings, McQuaid et al. 2016). In some ccomparative clinical studies, it is reported no difference in visual acuity improvement between two treating modelaties. However, a shallower demarcation line and reduced biomechanical stiffness in accelerated CXL may imply that conventional Dresden protocol might be more favorable on halting the progression of disease (Hammer, Richoz et al. 2014, Kymionis, Tsoulnaras et al. 2014, Tomita, Mita et al. 2014, Chow, Chan et al. 2015, Hashemi, Miraftab et al. 2015). The corneal stability after conventional Dresden or accelerated CXL protocols should be reviewed thoroughly with long term follow-up.

Table 2.2. Summary of methods and results of accelerated CXL reported in clinical studies. Source (Mohammadpour, Masoumi et al. 2017)

Reported outcomes for Accelerated CXL in the literature (ACXL: Accelerated CXL, UCVA: uncorrected visual acuity, BCVA: Best corrected visual acuity).

Author	Type of Study	Study features	Results
Waszczykowska et al.	Prospective interventional case series	16 eyes with ACXL (6 mW/cm2 for 15 min) followed for 2 years	- Significant flattening of the cornea in 18.7% of patients with a higher preoperative Kmax value (>50 D) and corneal steepening in patients with a lower Kmax value (<50 D) - Persistent corneal haze in 25% of patients
Shetty et al.	Prospective randomized interventional study	138 eyes with four irradiation protocols (3, 9,18, and 30 mW/cm2) at one year follow up	- Better visual, refractive, and tomographic improvements in the conventional and irradiations of 9 mW/cm^2 and 18 mW/cm^2. - Greater flattening effect in the conventional method
Tomita et al.	Prospective comparative interventional case series	30 eyes with ACXL and 18 eyes with conventional CXL	- Shallower demarcation line in ACXL - Both methods appear to be safe and effective.
Kymionis et al.	Prospective comparative interventional case series	12 eyes with ACXL (9 mW/cm2 for 10 min) and 9 eyes with standard protocol	Deeper demarcation line in the conventional group
Hashemi et al.	Prospective randomized clinical trial	31 eyes with ACXL (18 mW/cm2 for 5 min) and 31 contralateral eyes with conventional method	Comparable in outcome, safety and stopping the progression Better corneal flattening in the conventional method
Chow et al.	Prospective comparative interventional case series	19 eyes with ACXL (18 mW/cm2 for 5 min) and 19 eyes with conventional method	No significant difference in the improvement of UCVA, BCVA, and spherical equivalent
Elbaz et al.	Retrospective comparative interventional case series	16 eyes with ACXL (9 mW/cm2 for 10 min) followed for 12 months	- Improvement in the UCVA - Stabilization of all tested corneal parameters
Kymionis et al.	Prospective comparative interventional case series	10 eyes with ACXL (9 mW/cm2 for 10 min) followed for 3 months	- No endothelial cell loss - No intraoperative or early postoperative complication
Hashemian et al.	Prospective comparative interventional case series	77 eyes with ACXL and 76 eyes with conventional method	BCVA, UCVA, refraction, maximum keratometry, endothelial cell density, anterior and posterior stromal keratocyte density, and subbasal nerve density all were comparable and acceptable in the two groups
Shetty et al.	Prospective comparative interventional case series	30 eyes below 14 years of age with ACXL followed for 24 months	Safe and effective procedure in pediatric patients
Bozkurt et al.	Prospective comparative interventional case series	47 eyes with ACXL (30 mW/cm2 for 3 min) followed for 24 months	Improved UCVA, BCVA, corneal topography, total HOA, and coma aberrations
Sadoughi et al.	Prospective randomized interventional study	15 eyes with ACXL (9 mW/cm2 for 10 min) and 15 contralateral eyes with conventional method	- Similar refractive, visual, keratometric, and aberrometric results - Less adverse effects on the corneal thickness and endothelial cells in ACXL

ACXL: Accelerated CXL; UCVA: Uncorrected visual acuity; BCVA: Best corrected visual acuity.

2.5. Meta-Analysis Research

Meta-analysis is a quantitative, formal, epidemiological study design used to systematically assess the results from previous individual studies for integrating the findings to estimate an effect more precisely and derive conclusions about the body of research (Ferrer 1998). The aim of meta-analysis is to deal with the controversy or inconsistent conclusions between individual studies, and improve the estimates of size of effects. In medical research or clinical trials, meta-analysis refers to a systematic statistical procedure to estimate a net effect for a specific therapy when similar treatment

effects exist. This technique has become increasing popularity due to the large increase in the number of clinical trials published in past few decades. These multiple small studies which address same issue are usually diverse and conflicting because those clinical trials are typically studied in different locations with different patients' ages, gender, races, severe level of diseases and other pre-existing conditions. The variations resulting from clinical and methodological diversity may cause treatment effects differ substantially for a therapy from independent clinical studies, and make the clinical decision-making difficult. Therefore, meta-analysis can then be used to examine the factors that may explain the differing effects (Petitti, Contreras et al. 2000). Meta-analysis integrates the results of several independent studies and quantifies more accurately the effectiveness of the therapies evaluated. Therefore, outcomes from a meta-analysis may provide useful medical information hence generating new hypotheses for further clinical studies (Lau, Ioannidis et al. 1998).

The key characteristics and steps involved in performing a meta-analysis include a clearly stated objective with defined eligibility criteria (formulating question and defining eligibility criteria), a systematic search that attempts to identify all studies that meet the eligibility criteria (identifying pertinent studies), an assessment of the validity of the findings of the included studies (determining the outcome parameters), and a systematic presentation and synthesis of the attributes and findings from the studies used (data extracting, analyzing, and interpreting results). Clinical studies ideally include the diagnosis, patient characteristics, treatment groups and outcomes which should be clearly defined. However, studies satisfying these standards usually limited in number, exclusion of the studies which are not clearly defined for methodological reasons may increase the statistical validity of the analysis but may limit the ability to generalize the findings. Therefore, the use of weighting techniques during the analysis is considered to minimizing the effects of variable quality in many research (Lau, Ioannidis et al. 1998).

In analysis of studies in which the outcome of interest is continuous, the treatment effect can be calculated by $Y = \overline{X_T} - \overline{X_C}$ with variance of

$$Var(Y) = \frac{(n_T-1)S_T^2+(n-1)S_C^2}{n_T+n_C-2} \quad (2.1)$$

where $\overline{X_T}$, S_T^2 , n_T and $\overline{X}_C$, S_C^2 , n_C represents the sample mean, variance and sample size for the treatment group and control group, respectively.

Once effect estimates and their variance from individual studies are obtained, the overall estimate of treatment effect can be determined as $\overline{Y}$ with the variance of

$$Var(\overline{Y}) = \frac{1}{\sum_{i=1}^{n} w_i} \quad (2.2)$$

where weight w_i is the inverse of the estimated variance of Y_i for study i, and n is the number of studies. The confidence interval can then be determined assuming normality

$$(\overline{Y} - 1.96 * \sqrt{Var(\overline{Y}),} \overline{Y} + 1.96 * \sqrt{Var(\overline{Y})}) \quad (2.3)$$

It is a common practice to examine and quantify heterogeneity (I^2) between study characteristics (clinical and methodological diversity) and treatment effects. The data can only be combined if there is no significant or small heterogeneity, i.e. $I^2 < 30\%$.

$$I^2 = \max(1 - \frac{n-1}{\sum_{i=1}^{n} w_i(Y_i-\overline{Y})^2}, 0) \quad (2.4)$$

Metrics have been proposed to quantify heterogeneity, because the heterogeneity across studies always exists and depends on the number of studies included (Higgins, Thompson et al. 2003).

Overall, meta-analysis is designed to answer a scientifically valid question, and has evolved as a useful technique for summarizing large numbers of clinical trials and attempting to resolve discrepancies raised by these trials.

2.6. Summary

Experimental results such as the increase in corneal rigidity, a compact and organised collagen structure, the increased resistance to heat degradation, enzymatic digestion, and tissue swelling show the promising results of UVA/riboflavin CXL. All together the evaluations of CXL efficacy from laboratory studies, the comprehensive insights of the relationships between biomechanical, physiochemical and structural changes are clinical relevant and important indicators in optimising CXL protocols. Clinically, UVA/riboflavin CXL has developed as a favourite tool and first-line treatment for progressive keratoconus, as well as for other corneal issue such as post-LASIK ectasia. Corneal edema and infectious keratitis have also been reported to benefit from UVA/riboflavin CXL. Although current clinical outcomes suggest that UVA/riboflavin CXL administered with widely adopted treatment parameters is considered safe and effective, further improved protocols with optimised UVA/riboflavin CXL and minimised risks are likely to be designed in near future. Trans-epithelial CXL is one of the major improvements in alternative protocol, which can largely reduce the risk of infectious keratitis, stromal scarring, and patient discomfort (Ertan, Karacal et al. 2009, Kissner, Spoerl et al. 2010). Another improvement might come from changing of riboflavin solution. A recent study demonstrates the enhanced effect of UVA/riboflavin CXL with riboflavin dissolved in deuterium oxide (D_2O) as D_2O is known to increase the half-life of singlet oxygen species in the photo-chemical reaction (McCall, Kraft et al. 2010). Ultimately, the development of topical drops with chemical compounds capable of inducing CXL would further revolutionise the treatment for keratoconus and related corneal issue to clinical practice (Doillon, Watsky et al. 2003, Wollensak and Iomdina 2008, Paik, Wen et al. 2009).

Chapter 3. Methodology

3.1. Introduction

The current literature have demonstrated that the UVA/riboflavin corneal CXL alters the material behaviour, ultrastructure, biophysical properties and molecular bonding within corneal stroma, which significantly increase the overall mechanical response. Due to the viscoelastic and anisotropic properties of load-bearing tissue, the methods for the measurement of its mechanical properties can have significant impact on the resulting outcomes. In this work, two different mechanical measurement methods including uniaxial tensile test and inflation were employed to evaluate the effect of CXL on material behaviour. The induced ultrastructural changes were examined using TEM. Possible molecular bond formation was confirmed with FITR. Mass spectrometry and western blotting was performed to investigate the protein interactions involved in CXL reaction.

This chapter provides a detailed description of preparation of specimens, experimental setting and design, data analysis qualitatively and quantitatively including computational algorithm in order to understand the relationships between each parameter and underlying mechanisms of CXL treatment following Dresden protocol.

3.2. CXL Procedure and Experimental Design

3.2.1. Dresden Protocol

Conventional Dresden protocol is the gold standard used clinically to halt progression of keratoconus (Wollensak, Spoerl et al. 2003). The procedure in this study followed Dresden protocol with the cornea treated with 5 mL of 0.1% riboflavin in 20% dextran at 3-minute intervals for 30 minutes, followed by UVA (370 nm) illumination with the beam diameter of 10 mm at 3 mW/cm^2 (Opto Xlink; Mehra Eyetech Pvt. Ltd., Delhi, India) for a further 30 minutes. Topical dosing of riboflavin with dextran drops was continued every 3 minutes during the UVA irradiation (Table 3.1). The whole procedure was performed in a dark room.

Table 3.1. Full CXL details following the conventional Dresden protocol.

Parameter	Condition
Treatment Target	Porcine Cornea
Fluency (Total) (J/cm^2)	5.4
Soak time and interval (min)	30
Intensity (mW/cm^2)	3
Treatment time (min)	30
Epithelium status	off
Chromophore	Riboflavin-5-phosphate (Sigma, Dorset, United Kingdom)
Chromophore carrier	20% dextran
Chromophore concentration	0.10%
Osmolarity	Hyper-osmolar
Light source	Opto-Xlink (Mehra Eyetech Pvt. Ltd., Delhi, India)
Irradiation mode (Interval)	Continuous

3.2.2. CXL Treatment on Intact Whole Cornea and Half Corneal Segments

Fresh porcine eyes collected from a local abattoir (Morphets, Tan house farm, Widnes) within 6-9 hours after death were used to study the efficacy of Dresden CXL protocol and the individual contributions induced by UVA and photosensitizer riboflavin. The eyes were washed with PBS (Sigma-Aldrich, Dorset, United Kingdom), the central corneas were excised and the corneal

epithelium was mechanically removed using a blunt hockey knife. Each cornea was cut into two segments along the superior-inferior centreline with one half used as the test sample and the other as its corresponding control. The comparisons between the two segments were used to avoid inter-animal variation for uniaxial mechanical testing and TEM ultrastructural analysis (figure 3.1).

The treatment corneal segments were assigned to four groups:

Group 1 (PBS vs. PBS): contained six corneas, all segments were topically treated with PBS in 3-minute intervals for 1 hour and used to examine the intrinsic differences between the two segments of each porcine cornea.

Group 2 (PBS vs. Riboflavin+PBS): contained six corneas, corneal segments were topically treated in 3-minute intervals for 1 hour with either PBS or 0.1% riboflavin (Sigma-Aldrich, Dorset, United Kingdom) prepared in PBS.

Group 3 (PBS vs. Riboflavin+Dextran): contained six corneas, treatment was the same as for the Group 2, except that the riboflavin was prepared in 20% dextran (Sigma-Aldrich, Dorset, United Kingdom).

Group 4 (Dextran vs. Riboflavin+Dextran+UVA): contained ten corneas, half were treated following the conventional Dresden protocol. Cross-linked corneal segments were compared to fellow half segments treated with 20% dextran only.

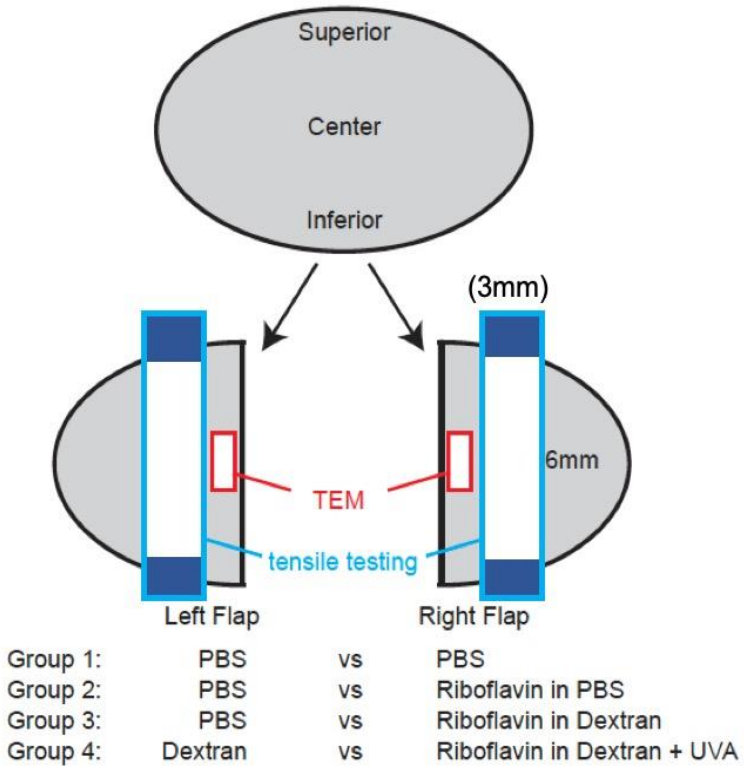

Figure 3.1. Experimental scheme. Each cornea was cut into two segments in a superior-inferior fashion. Specimens were dissected and processed for tensile testing (white solid rectangle) and TEM scanning (red hollow rectangle). The excised strips including part of the sclera (dark blue solid rectangle) were shown in figure.

Additionally, other intact corneas were prepared for inflation testing, protein analysis and infrared spectroscopy examination separately. For protein analysis and infrared spectroscopy studies, three groups (PBS, Riboflavin+Dextran, and Riboflavin+Dextran+UVA) including thirty-six intact corneas were collected in total for both examinations (n = 6 per group). For inflation testing, seven paired eye globes were used to examine the intact corneal behaviours, with one as the test sample with CXL treatment and the other as its non-treated control in PBS.

3.3. Uniaxial Tensile Testing

Uniaxial tensile testing involves subjecting a material strip with uniform width to a one dimensional tensile force. The load-elongation measurements are then used to calculate the stress-strain behaviour and hence the stiffness (tangent modulus) of the material. This is the most commonly used

experimental technique due to its simple set-up and post-test mathematical analysis (Elsheikh and Anderson 2005). However, there are a number of inherent deficiencies when used on biological tissues including the initial stresses caused by the ocular tissue's natural curvature (Rubinoff and Greener 1985, Elsheikh and Anderson 2005). In addition, the complex collagen arrangement within the ocular globe and orientation can have a significant impact on its mechanical response when subjected to loading (Lari, Schultz et al. 2012).

Several methods can be used to attach specimens to the testing machine, all of which aim to eliminate slippage of specimens during testing. Common methods include cyanoacrylic glue, pins, and mechanical clamps (Nyquist 1968, Nash, Greene et al. 1982, Uchio, Ohno et al. 1999, Lari, Schultz et al. 2012). As the hydration state of biological tissue has been shown to have a significant effect on the mechanical outcome measured, maintaining specimen hydration is of great importance during the conditioning and loading cycles (Hoeltzel, Altman et al. 1992, Downs, Suh et al. 2003, Elsheikh and Anderson 2005, Girard, Suh et al. 2007), thereby reducing environmental effects on the test results.

Due to the viscoelastic nature of ocular tissues, another crucial parameter in this testing protocol is the strain rate at which the specimen is tested. Various strain rates have been examined and therefore, a direct comparison between studies is not easily made and may not be reliable. The mechanical response of the cornea has been assessed using both uniaxial tensile and inflation test methods. Studies of mechanical stiffness (as measured by the tangent modulus) using uniaxial testing showed higher stiffness estimations compared to inflation testing, which can be attributed in part to the non-physiological loading conditions and the extraordinarily high strain rates adopted in strip tests (Elsheikh and Anderson 2005). Although the mechanical response observed in uniaxial tests may not be representative of *in vivo* behaviour, it remains a valuable method for comparative studies such as the current work on CXL.

3.3.1. Specimen Preparation and Test Rigs

A total of twenty-eight porcine eyes were obtained and separated into four groups as shown in Fig 3.1 (PBS vs. PBS; PBS vs. Riboflavin+PBS; PBS vs. Riboflavin+Dextran; Dextran vs.

Riboflavin+Dextran+UVA). The specimens were examined at room temperature and not frozen at any stage. The soft muscular tissue was removed with surgical tongs and curved scissors. The superior location was marked as strip centres on the intact specimens followed by conducting experimental conditions of different treatment regimes. Preparation involved detachment of the cornea from the extraocular muscles and sclera, extracted with curved scissors and placed on a rubber base where the

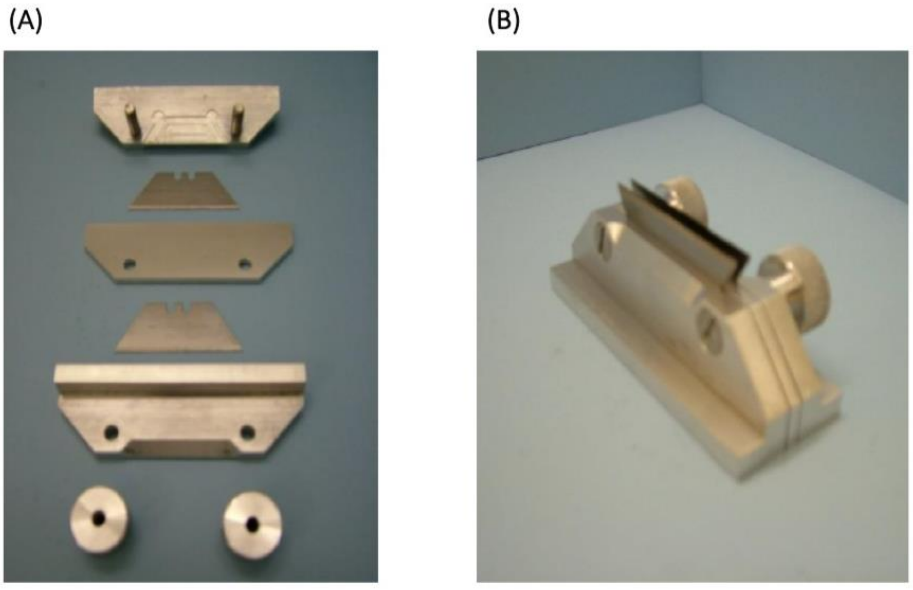

strips were isolated for uniaxial testing using a double blade cutting tool (figure 3.2).

Figure 3.2. Double blade cutting tool used for strip extraction. (A) individual component and (B) assembled tool. Source (Geraghty 2012)

The cutting tool was designed to accommodate the desire for strips. Two strips of 3 mm width were cut in the superior-inferior direction at the central cornea, and inserted vertically into custom designed clamps (figure 3.3). The distance between the clamps was 6 mm. The extracted specimens were then preserved in PBS. Prior to test commencement, a Perspex tube was placed around the specimen and filled with PBS to maintain hydration throughout the duration of the test.

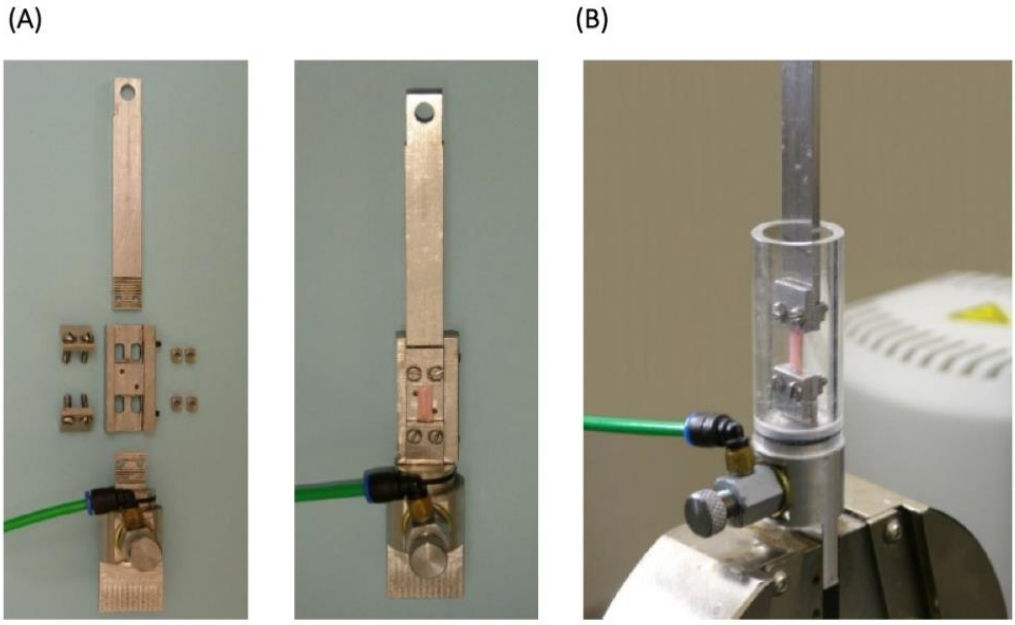

Figure 3.3. Tensile test setting. (A) clamp components and mechanical clamps for 12 mm sclera specimens attached to the assembled clamps, (B) mechanical clamps connected to the testing machine. Source (Geraghty 2012)

3.3.2. Testing Control and Protocols

Corneal stiffness was examined using a uniaxial tensile tester, Instron 3366 machine (Instron Engineering Corp., MA, USA), equipped with a 10N load cell (Instron, Part No. 2530-428). The material testing machine was controlled using the proprietary Bluehill3 software (Instron, UK). Information including tissue thickness, width and length were recorded, and the system was calibrated before testing started. The test protocol was set to apply a maximum loading stress of 0.125 MPa which was slightly above the stress expected under an intraocular pressure of 80 mmHg (Elsheikh, Wang et al. 2007). A constant extension of 1 mm/min was applied and the corresponding stress (applied force divided by cross-sectional area) and strain (extension over original length) were measured continuously. Five conditioning cycles with a four-minute recovery period between each cycle were performed (Geraghty, Jones et al. 2012).

3.3.3. Experimental Data Analysis

The uniaxial tensile test produced results in the form of axial load and elongation. Stress (σ) was calculated by dividing the applied load by the initial cross-sectional area (thickness x width) of the specimen. Strain (ε) was obtained by dividing the specimen elongation by the initial length. The tangent modulus (Et), the gradient of a tangent of the stress-strain behaviour pattern at any measurement point, was calculated at different stress levels to present the stiffness of the tissue (Wollensak, Spoerl et al. 2003, Boyce, Jones et al. 2007). Plots depicting the tangent modulus ratio ($Et_{Experimental}/Et_{Control}$) versus stress were used to demonstrate the biomechanical behaviour of specimens in each group. Comparisons in this thesis, concentrated on tangent modulus ratios at a stress of 0.03MPa, which is equivalent to a physiological IOP of around 25 mmHg (Anderson, El-Sheikh et al. 2004). The internal pressure within a thin spherical shell was converted into resisting stress using Laplace's law for a spherical shell analysis from Equation 3.1.

$$\sigma = PR/2t \tag{3.1}$$

where P is internal pressure; R is radius of curvature; t is the thickness of spherical shell.

3.4. Inflation

Inflation testing of ocular tissues for determining material properties has become the most desirable experimental method due to its representation of *in vivo* conditions. This stems from the similarities between the way in which the tissue is loaded during the test and that experienced *in vivo*. As the internal hydraulic pressure is increased, the tissue is subjected to mainly membrane tension, and this is similar to loading under IOP. However, accurate experimental setting is more demanding than uniaxial tensile testing.

The precise control of pressure loading rates can be operated manually or through a digital controlling system developed earlier (Elsheikh, Wang et al. 2007, Whitford, Joda et al. 2016). During the test, a variety of monitoring techniques including the use of laser or digital image correlation (DIC) can be

applied to track displacements (Smolek, Oshika et al. 1998, Elsheikh, Wang et al. 2007, Girard and Rigali 2011). For post-test analysis, the FE modelling technique is employed to construct numerical models of whole corneas or eye globes, and the material stress-strain relationships can be adjusted until the predicted surface deformations of the models matched those observed experimentally. This technique has provided an accurate means of determining the tissue's tangent modulus (Girard, Suh et al. 2009, Whitford, Studer et al. 2015).

The inflation testing requires a more sophisticated analysis approach which involves a combination of ultrasound pachymetry, geometric modelling, DIC and inverse FE analysis. This section of the study aimed to understand the biomechanical behaviour of cornea through testing under physiological state which represent the *in vivo* condition using inflation. The results are then analysed to derive constitutive corneal model. The following subsections present a detailed description of these techniques.

3.4.1. Specimen Preparation

Seven pairs of fresh porcine eyes were collected from a local abattoir and tested within 6-9 hours after death. Soft muscular tissue was removed with surgical tongs and curved scissors. The right eye globes of the pared specimens were cross-linked prior to inflation testing. The superior direction was marked and the eye globe was placed in a 3D printed component to allow for accurate needle insertion through posterior pole. The internal eye components were removed through the posterior pole with a 14G needle. The needle was then lightly glued around the posterior pole and the intra-ocular cavity was washed with 5 to 6 ml PBS (Sigma, Dorset, United Kingdom). During this procedure, the outer surface of the globe was kept hydrated by applying PBS drops every 2-5 minutes. Random speckles were applied on the globe by lightly spraying a waterproof and fast drying black paint to facilitate deformation tracking in post-analysis (figure 3.4). The prepared specimen was then placed into a custom-designed eye chamber filled with PBS, and transferred onto the inflation rig (figure 3.5). Due to the time-consuming specimen preparation, dextran becomes difficult to control the tissue thickness and hydration state. Only PBS was considered and used as control group.

Figure 3.4. Intact porcine eye globe prepared for testing. Noted the proper alignment of the needle along with corneal apex.

3.4.2. Test Rig

The inflation test rig provided full-field observation of ocular response to IOP changes. The physical test equipment was built in-house and fully bespoke (figure 3.5). The equipment features closed loop control software written in LabVIEW (version 10.0.1) to regulate IOP while collecting real-time data by triggering cameras to take pictures of the globe. The obtained images are used for measurement of deformation across the globe. The specimen was clamped in a horizontally placed eye chamber with high precision real-time laser (LK-2001, Keyence, UK) pointing towards the corneal apex. An array of six high resolution digital cameras (18.0 megapixels, 550D, Canon, Tokyo, Japan) surrounding the eye chamber and a pressure adjusting tank was placed vertically to inflate the eye while taking synchronous images. The camera setup shown in figure 3.6 allows an angle of 25° within each pair and an angle of 120° between each two pairs. Additionally, an LED light system was used to help increase the clarity of the images produced and all equipment was housed inside a tailored-fit tent to assure no light disturbance would affect the rig while testing.

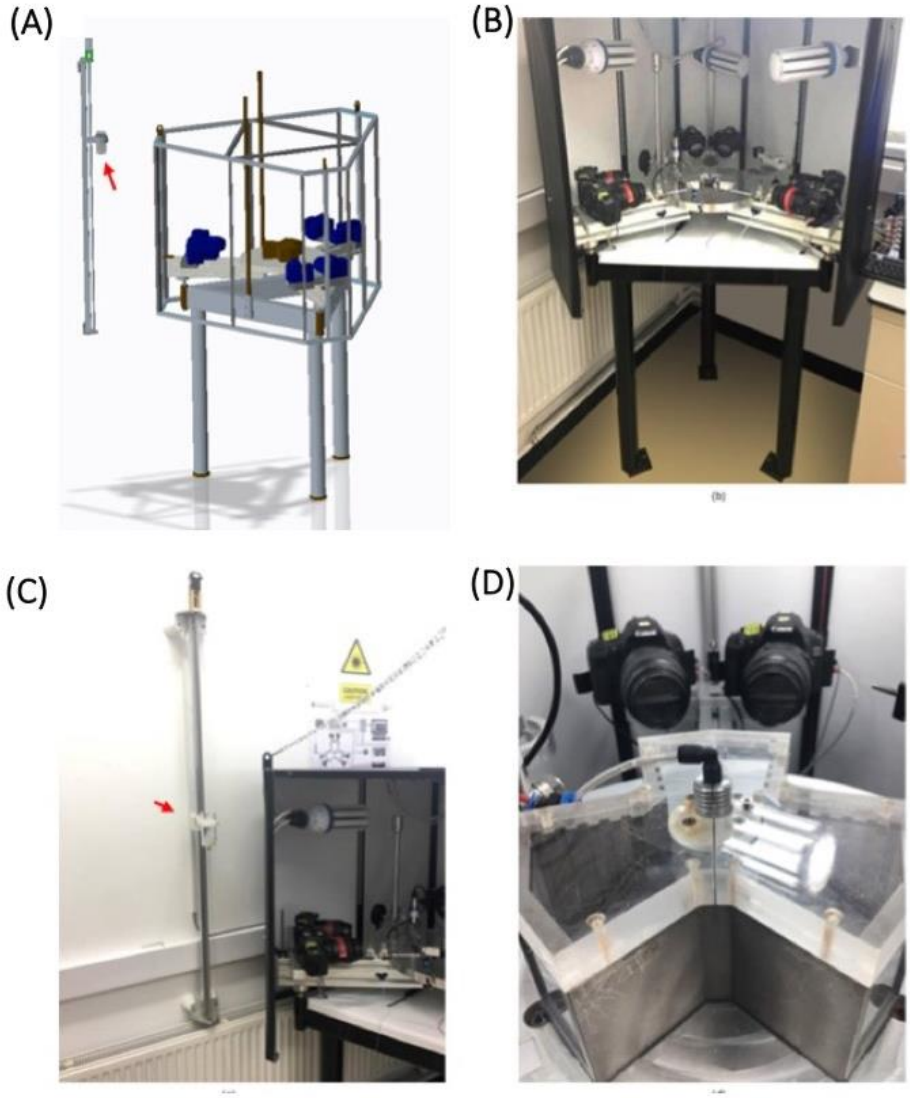

Figure 3.5. Inflation test equipment. (A, B) inflation setup with front cover removed, (C) location of pressure adjustment tank (arrow), (D) eye chamber with angled piping fixation.

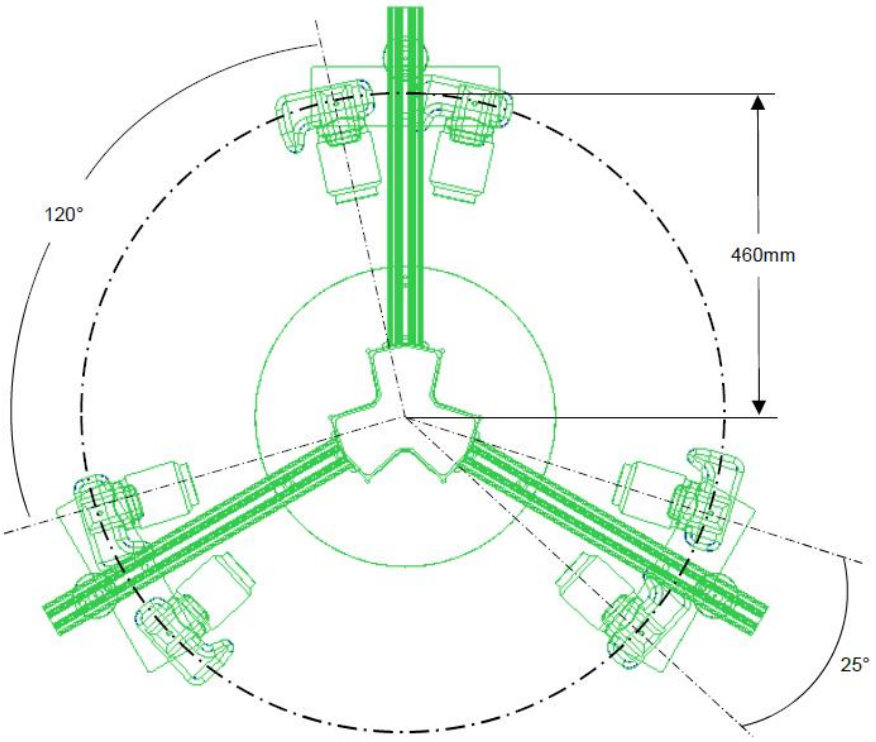

Figure 3.6. Camera array showing angles between cameras and distance from cameras to eye chamber (placed in the centre).

3.4.3. Testing Control and Protocols

A custom-built LabVIEW software was used to tightly control the pressure. The experiments started by 4 pre-conditioning cycles as shown in figure 3.7, in which the white lines represent the loading cycles with desired values of max IOP, and the yellow tick marks represent the camera firing times. The pre-conditioning cycles were to ensure the eye was sitting comfortably on the needle, and the tissue behaviour was repeatable (Elsheikh, Wang et al. 2007). An initial pressure of 2.5 mmHg was used to balance the external pressure applied by PBS in the pressure chamber, and was therefore considered a zero pressure point for the inflation test.

Specimens were pressurized to a maximum internal pressure at a rate of 2.75 mmHg/s, 0.55 mmHg/s, and 0.23 mmHg/s for fast, medium, and slow cycles, respectively. During each cycle the eye was allowed to relax for a period of 2 min. This time was obtained experimentally to allow tissue to fully

recover to its relaxation state. The behaviour of specimen in the fourth loading cycle was used for post-analysis.

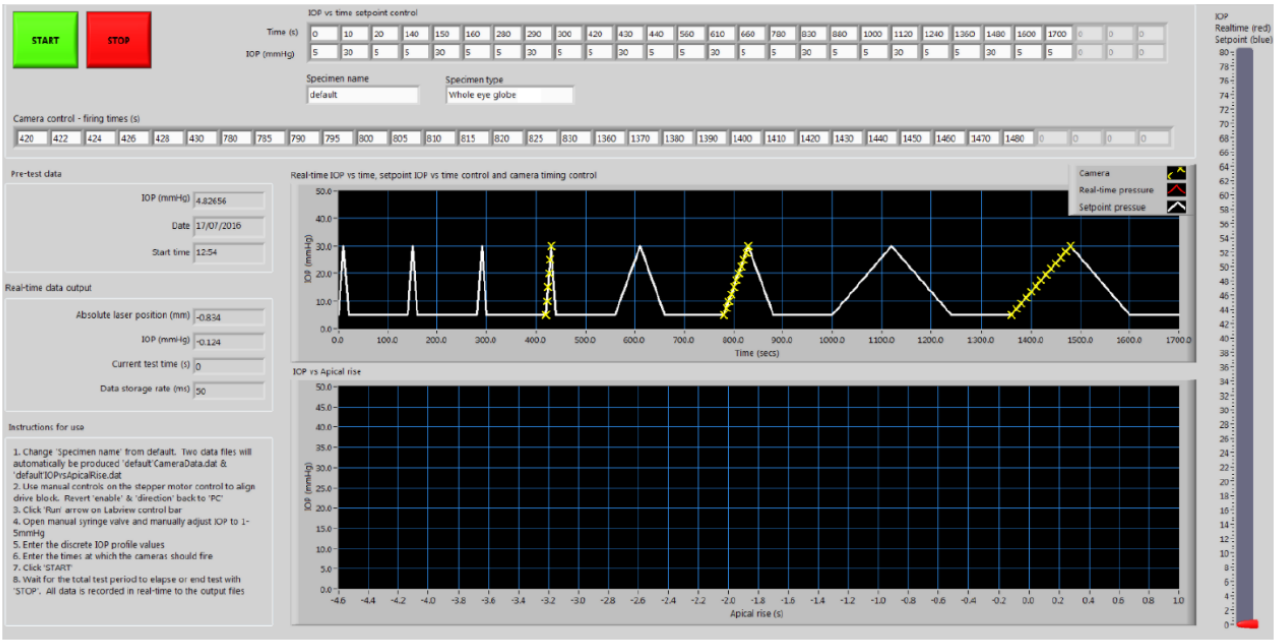

Figure 3.7. LabVIEW interface. IOP and camera firing times are shown in top graph in white and yellow tick marks, respectively.

3.4.4. Thickness Measurement

After the experiment was completed, the eye was removed from the test rig and dissected into an anterior and a posterior part as shown in figure 3.8A. Eight meridian profiles of discrete thickness measurements were selected. The thickness was measured at 2 mm intervals along each meridian from pole to pole (Elsheikh, Geraghty et al. 2010). The thickness at each desired point on each meridian line was determined using an in-house developed thickness measurement device (LTA-HS, Newport, Oxfordshire, UK) (figure 3.8B). The TMD was designed and developed by the Biomechanical Engineering group to measure the thickness of biological tissue. A vertical measurement probe was located at a height of about 30 mm above the centre point of the support. The probe moved down with a controlled velocity until it reached the surface of the tissue. By precisely knowing the original distance between the initial position of probe and the surface of support, the measured value was recorded as the thickness of the tissue.

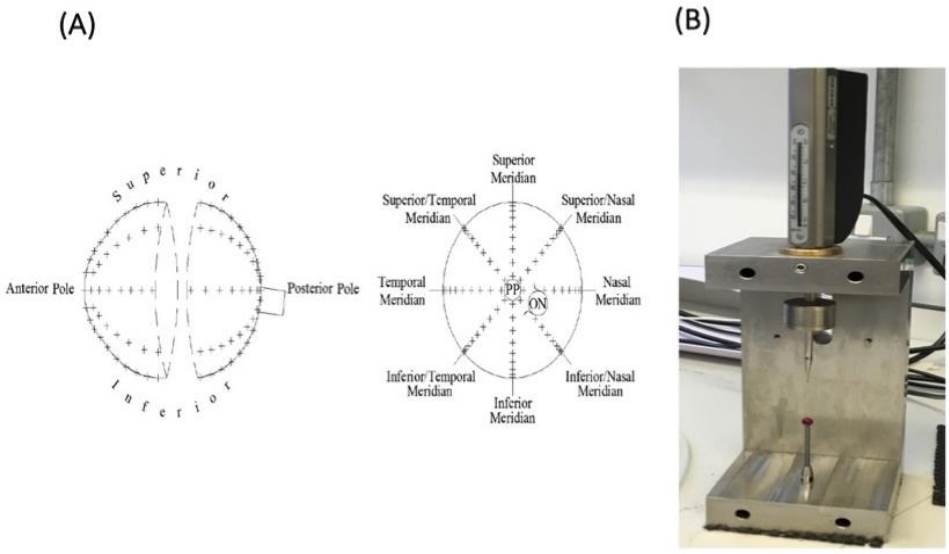

Figure 3.8. Thickness measurement (A) was performed on anterior and posterior segments along eight meridian lines with eight points per line using an in-house developed thickness measurement device (B).

3.4.5. Geometric Modelling

The reliability of the derived material properties largely depends on the accurate representation of geometry. The images taken during the inflation tests were used for reconstructing a 3D FE geometry as well as obtaining deformations which can then be used for inverse FE analysis to estimate the material properties. This section describes the methods used to recreate the geometry of the cornea in a FE model.

To obtain the external topography from six individual profiles taken by the six cameras, the first images of the eye taken at zero pressure were selected. The location of limbus was distinguished as the border of cornea and sclera as a transition zone when building the geometry. The contour line of the eye globe was extracted by selecting the region of interest, the edge of object inside the region was automatically segmented using bespoke MATLAB codes. After the external outline was determined, the needle axis was extended to intersect the cornea. The needle (reference) was glued around the posterior pole to prevent rotation. Therefore, this intersection point was assumed as the

corneal apex, as demonstrated in figure 3.9. Therefore, the acquired results included the edge profile of each initial image of the eye, the corneal apex and limbus points.

The internal topography was based on the external topography and the eight meridian profiles of discrete thickness measurements of cornea as shown in figure 3.10. The internal and external 3D topography was interpolated based on the spherical coordinates between the discrete points of measurement using bespoke MATLAB codes. In addition, a calibration ratio of mm/pixel was used to convert the obtained data into millimetre before the images were used to construct the geometry. For calibration, a steel ball with a diameter close to the size of eye (25mm) was used. Similar to above step, the region of interest around the steel ball was selected followed by segmenting the object. The best fitted circle was determined using the least square method. The mm/pixel ratio (Table 3.2) was then obtained by dividing the diameter of steel ball over the diameter of fitted circle in pixel.

Due to the non-uniform curvature with variable thickness, the external and internal geometry of eye globe were obtained to generate the corneal model. A model developed for the cornea using entire eye globe allowed appropriate realistic displacement at the limbus, the displacements at the limbus were tracked during the experiment and then introduced at the boundary of the corneal FE model. The purpose of building up corneal only model was to understand the effect of CXL treatment on corneas where the application of interest is. In addition, the approach of performing a cornel only model was to decrease the geometrical complexity and increase the efficiency of the computational calculation. Generally, to conduct a FE analysis in building up geometry, a given body is divided into elements which are interconnected at nodes. The nodes and elements create a network referred to as a mesh. Each element is assigned specific structural property and assembled together to give the globe response, the body is then analysed under certain boundary conditions. Therefore, the number, shape and type of elements are important factors in determining the accuracy of analysis.

In our corneal model, the mesh of geometry was constructed with Abaqus 6.13 (Dassault Systèmes Simulia Corp., Rhode Island, USA) using bespoke software. The model was meshed using C3D15H fifteen node elements arranged in rings across the ocular surface and layers across the thickness. This

element type is a second-order triangular prism with nodes at the corners and in the middle of each edge, which is capable of modelling a smooth geometric representation of variable thickness. The cornea was modelled as a homogenous, non-linear isotropic and hyper-elastic material that undergoes large deformation. Therefore, the FE was incorporated in the corneal model to capture its non-linear response under deformation.

The displacements at the limbus contributed to the deformed shape of the cornea. Therefore, the boundary conditions were provided to avoid the model from rigid-body rotation around Z-axis. Corneal apex was restrained against displacement in X- and Y-directions, whereas limbus was restrained in the X-, Y-, and Z-direction. The apical displacement of the entire cornea was extracted by the displacement of corneal apex minus the average displacement of limbus in the anterior-posterior direction. The resulting FE model was shown in figure 3.11, showing the cornea model that employed 8611 nodes and 2592 fifteen-node elements, organised in twelve-element ring with three-element layer. The development of numerical simulations was to generate the unique geometry of specific and generic cornea including their non-rotational symmetry and non-uniform thickness.

Table 3.2. The calibration factors (mm/pixel ratio) of all six cameras.

CAMERA NUMBER	MM/PIXEL RATIO
CAMERA 1	0.010661338507880614
CAMERA 2	0.01064330280139778
CAMERA 3	0.010917309328010596
CAMERA 4	0.010881594434167113
CAMERA 5	0.010956512285074006
CAMERA 6	0.010984206666706693

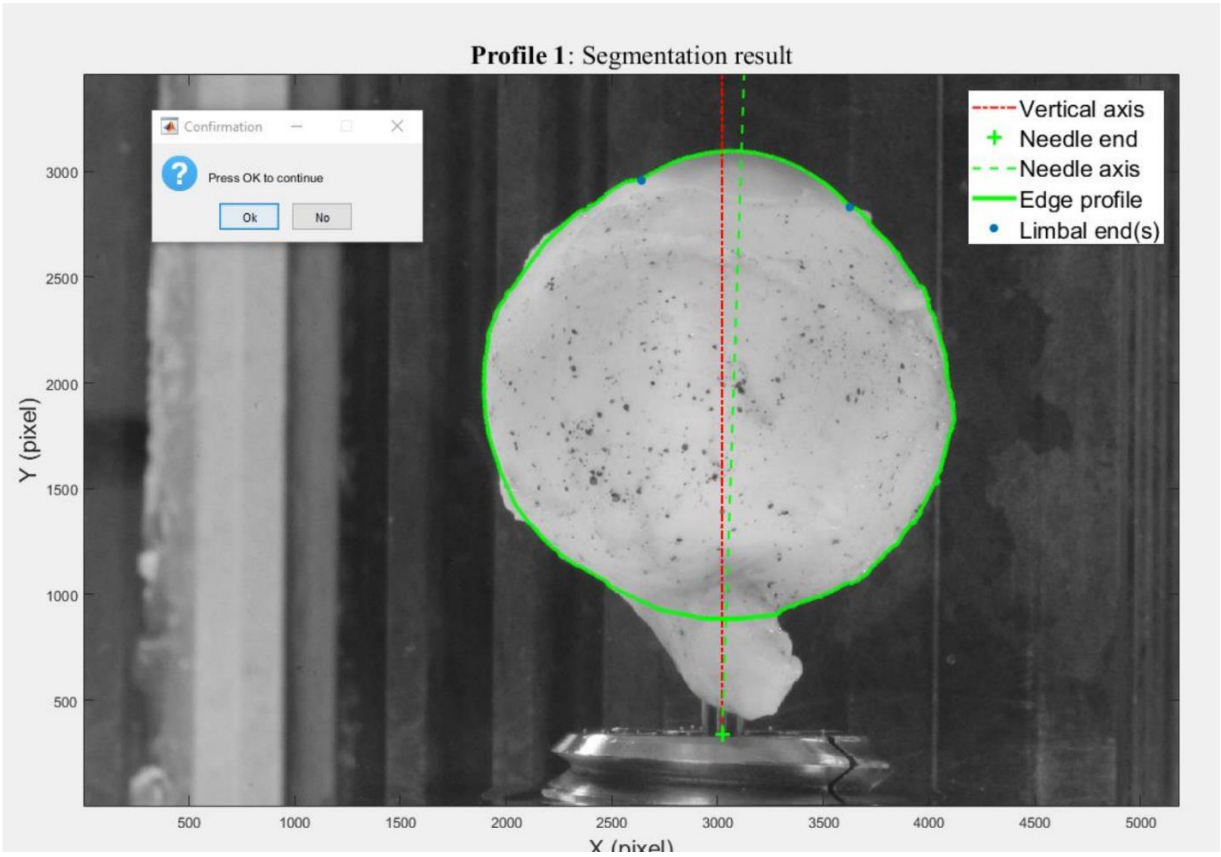

Figure 3.9. Segmentation results of eye globe topography

	THICKNESS MEASUREMENT IN ANTERIOR PART (mm)							
Angle	0°	45°	90°	135°	180°	225°	270°	315°
APEX	1.306	1.290	1.260	1.270	1.270	1.230	1.230	1.300
	1.305	1.270	1.260	1.250	1.250	1.270	1.200	1.250
	1.310	1.310	1.240	1.230	1.250	1.260	1.200	1.310
LIMBUS	1.580	1.340	1.380	1.370	1.650	1.420	1.320	1.440
	2.060	2.270	1.430	1.540	1.860	1.580	1.590	2.020
	0.750	1.630	1.690	1.680	1.400	0.799	0.560	0.790
	0.490	0.780	0.880	0.920	0.398	0.486	0.790	0.715
	0.930	0.820	0.880	0.704	0.550	0.558	0.970	1.030

Figure 3.10. Non-uniform thickness measurement of cornea with respect to the eight meridian lines.

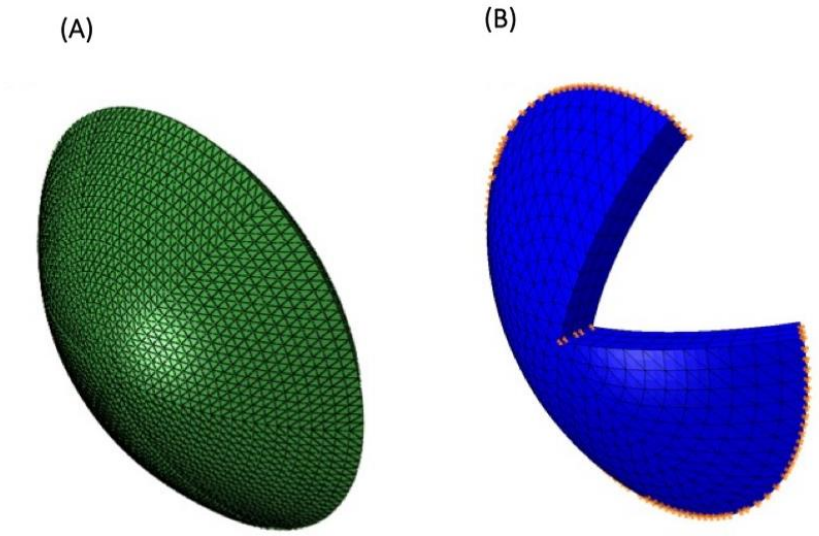

Figure 3.11. FE model of a tested porcine cornea. Image viewed from front (A) and cross-section (B). Orange dots represent the points at which there were boundary conditions.

3.4.6. Deformation Measurement by Digital Image Correlation (DIC)

The profiles obtained from the six sets of images of the six cameras were analysed using a 2D DIC method named Particle Image Velocimetry (PIV) to obtain deformations on the surface of the eye (figure 3.12) (Kohgo, Isoda et al. 2006, Sinha Roy and Dupps 2011). DIC is an established technique that relies on the analysis of successive camera images taken for a test specimen to derive the deformation distribution across the specimen surface (Sinha Roy and Dupps 2011). This technique was used to track the movement of the subsets between successive images resulting in displacement vectors, measured in pixels (Boyce, Grazier et al. 2008, Elsheikh, Geraghty et al. 2010, Myers, Coudrillier et al. 2010). PIV is based on DIC and compares an un-deformed and deformed image pairs of specimen surface which was speckled to present the local displacements within the selected subsets.

Three discrete locations including corneal apex and limbus on the left and right sides of the images were measured from each camera (figure 3.12B). The total displacement of the cornea at each pressure level was calculated using the displacement of corneal apex minus the average displacement of limbus.

The one-material corneal region was then determined based on this total displacement within an inverse analysis process to provide unique values of material parameters for the cornea.

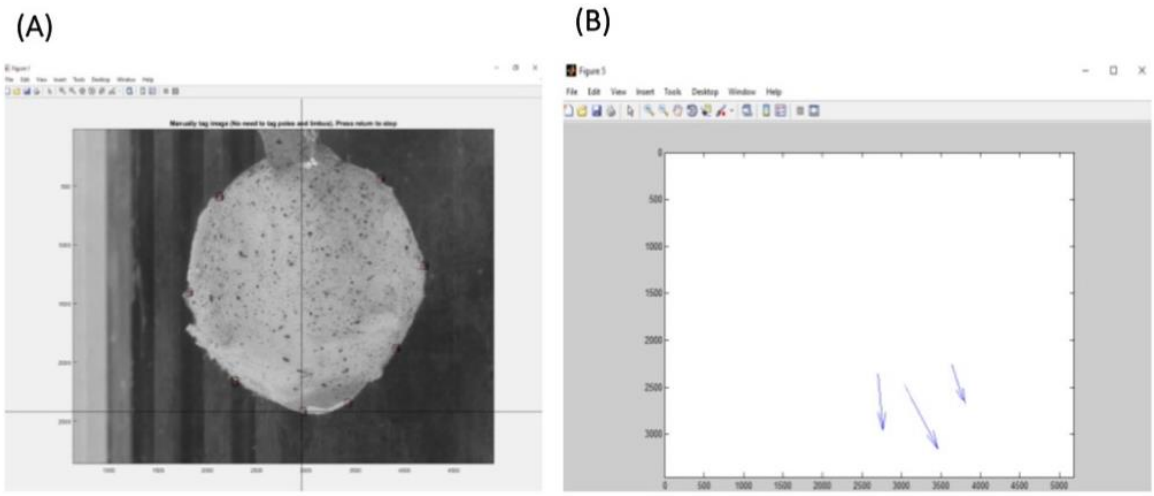

Figure 3.12. A demonstration of Particle Image Velocimetry (PIV). (A) screen capture of the manual tagging of desired points. (B) result of deformed tagged points (corneal apex and limbus).

3.4.7. Determining the Material Properties

Data from the test procedure was combined with a numerical simulation in a method known as IFE analysis. Inverse simulation is a mathematical approach to determine unknown model parameters to match observed physical response, which has been proven a valuable tool for obtaining mechanical properties of ocular material (Alastrue, Calvo et al. 2006, Linder-Ganz, Yarnitzky et al. 2009). In inverse FE analysis, an optimisation algorithm is coupled with an FE model to find optimal values of material properties. The optimisation is based on determining material parameters that provide the best possible match between experimental observations and numerical prediction of deformation under IOP.

An in-house built software that uses Particle Swarm Optimisation (PSO) as an optimisation strategy was developed to conduct the inverse analysis optimisation (Ivekovic, Trucco et al. 2008, Lim, Buyamin et al. 2014). The material constitutive model chosen to describe the material behaviour of the ocular tissue during loading was Ogden model as presented in Equation 3.2, utilised in a number

of previous studies on soft tissue (Yu, Bao et al. 2013, Whitford, Joda et al. 2016, Whitford, Movchan et al. 2018).

$$W\ (\lambda_1, \lambda_2, \lambda_3) = \sum_{i=1}^{N} \frac{2\mu_i}{\alpha_i^2}\left(\bar{\lambda}_1^{\alpha_i} + \bar{\lambda}_2^{\alpha_i} + \bar{\lambda}_3^{\alpha_i} - 3\right) + \sum_{i=1}^{N} \frac{1}{D_i}(J^{el} - 1)^{2i} \quad (3.2)$$

where W is the strain energy density; $\bar{\lambda_\iota}$ are the deviatoric principal stretches, $\bar{\lambda_\iota} = J^{-\frac{1}{3}}\lambda_i$; λ_i are the principal stretches; J denotes the volume ratio; α_i and μ_i are material parameters; N is the function order.

The Ogden material model order one relies on two parameters of μ (shear modulus) and α (strain hardening exponent) to define the non-linear material behaviour. The use of first order material model (N=1) reduced the computational time by reducing the number of variables. The values of material parameters α and μ represented the output of the inverse modelling process. The objective function was to minimise the root mean squared (RMS) of deformation (Equation 3.3).

$$RMS\ \% = \frac{1}{M}\sum_{j=1}^{M} \frac{\sqrt{\frac{1}{N}\sum_{i=1}^{N}(\delta_{i,j}^{experimental} - \delta_{i,j}^{numerical})^2}}{\delta_{\max j}^{experimental}}\ X\ 100 \quad (3.3)$$

where N is the number of pressure levels; M is the number of measurement locations and $\delta_{i,j}$ is the deformation at each particular pressure, at each location.

The design optimisation process adjusts the value of μ and α within the constitutive model while setting a wide lower and upper boundary range (lower boundary = [0.005, 50]; upper boundary = [0.2, 200]). With these parameters, stress and strain could then be extracted from the numerical modelling results and then tangent modulus was calculated from the gradient of the resulting stress-strain curve. The whole inflation process and post-test analysis are shown in figure 3.13.

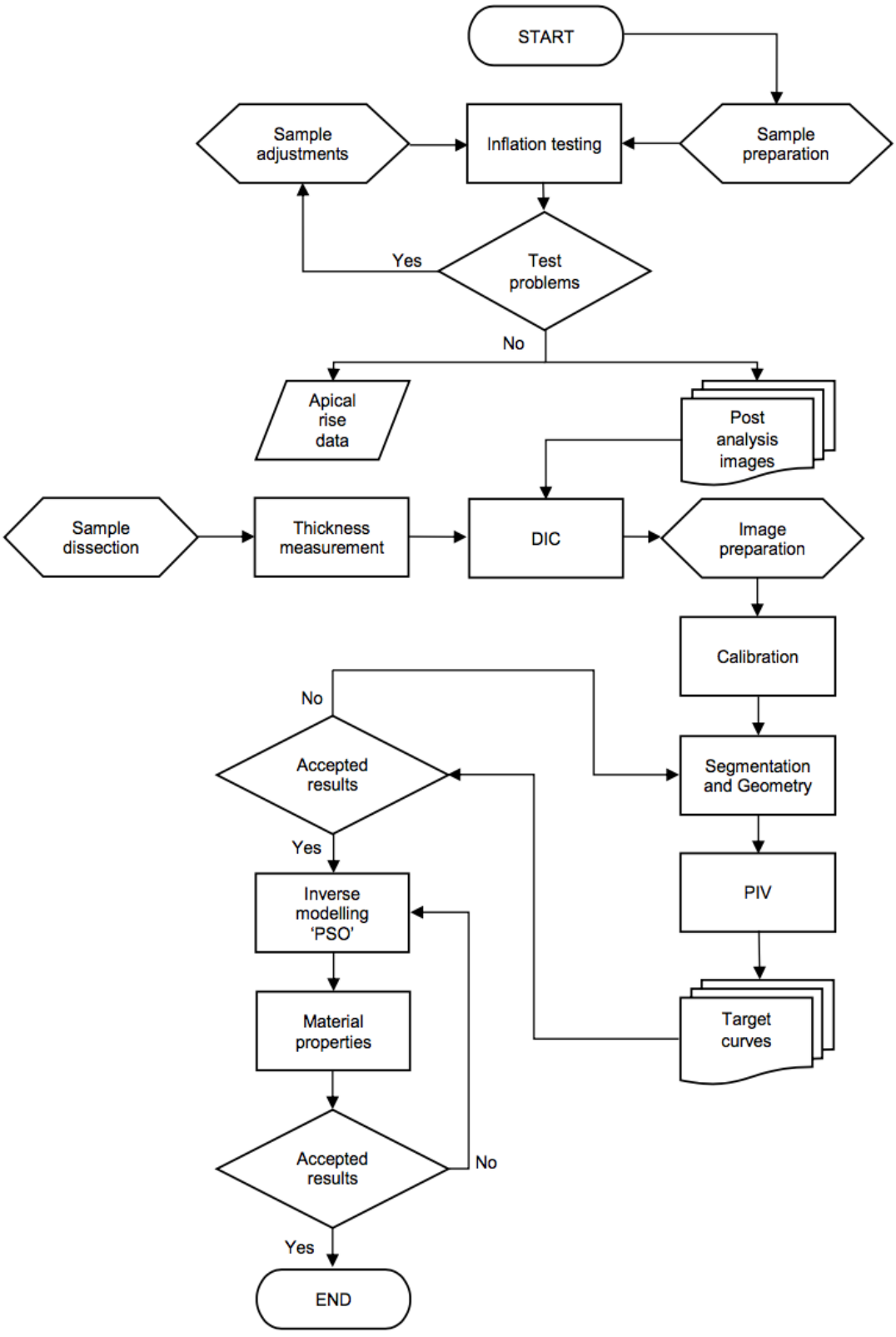

Figure 3.13. Flow chart of the complete inflation testing of intact ocular globe and subsequent inverse analysis.

3.5. Transmission Electron Microscopy (TEM) and Imaging Analysis

This experimental design aimed to understand the mechanical behaviour of the cross-linked cornea and its corresponding ultrastructural changes regarding the collagen diameter, density, and inter-fibrillar spacing. The ultrastructural and mechanical data was obtained from the same individual specimen in order to find out their correlations and the determinative ultrastructural parameters that may define the amount of stiffness.

CXL treatment is believed to induce structural alternations of corneal stroma and tissue remodelling, ultimately resulting in corneal stiffening. TEM is a standard histology technique for studying ultrastructure on nanoscale level, which allows the visualization of dense meshwork of collagen fibrils. Longitudinal (filamentous), frontal (circular), and oblique (ellipsoid) of collagen fibrilds are what can be found from TEM images. In order to obtain orientation independent fibril diameters, the minimal transverse diameter is usually measured by researchers as useful information. The orientation within the images is shown in figure 3.14. These fibrils are organised into lamellae, each lamellae layer containing parallel fibrils aligned in one direction. The lamellae are stacked and interwoven, always lie roughly parallel to the surface with various in-plane orientations (figure 3.15).

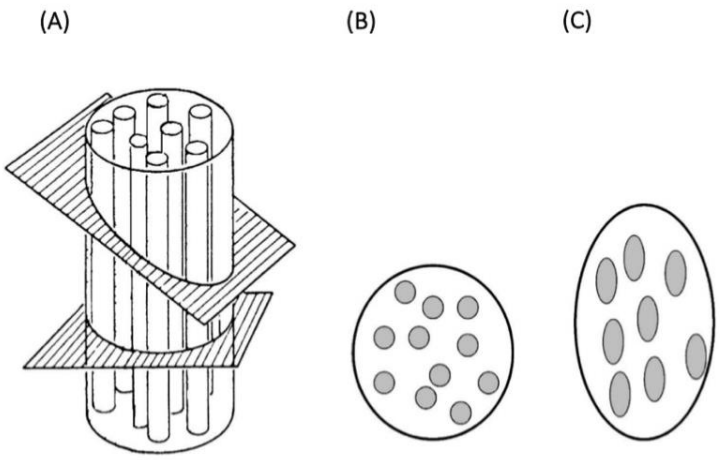

Figure 3.14. The minimum fibril diameter identified in two different section profiles (A). Rectangular section with circular section profiles (B), and oblique section with ellipsoidal section profiles (C). Source (Wollensak, Wilsch et al. 2004)

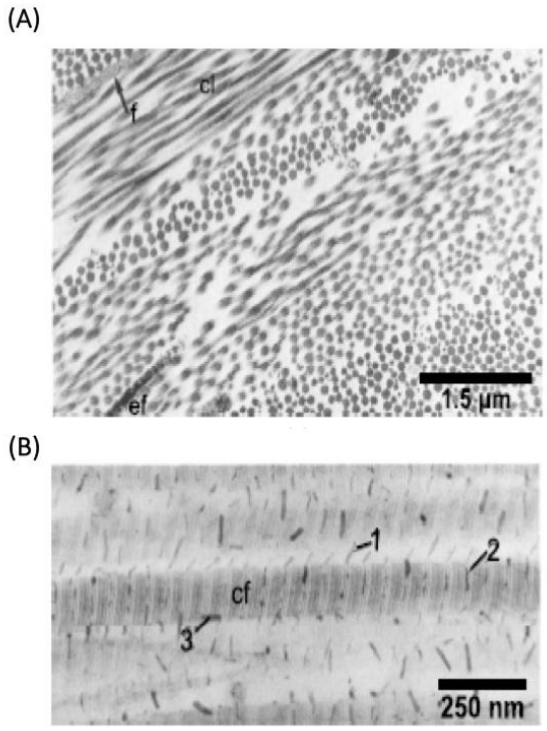

Figure 3.15. TEM images of collagen lamellae. (A) TEM images with different orientations of collagen fibrils (cf), fibroblast (f) and elastin fibrils (ef). (B) collagen fibrils (cf) and proteoglycans with different orientation; 1) radiating form fibrils, 2) around fibrils, 3) along fibrils. Source (Young 1985)

3.5.1. Sample Preparation and Experimental Procedure

A total of twenty-four porcine eyes were obtained for the study, separated into four groups (PBS vs. PBS; PBS vs. Riboflavin+PBS; PBS vs. Riboflavin+Dextran; Dextran vs. Riboflavin+Dextran+UVA. Preparation involved detachment of the cornea from the extraocular muscles and sclera. The specimens of experimental or control groups were isolated from the central regions of cornea with size of 1 mm x 2 mm. The whole procedure was illustrated in figure 3.16.

The ultrastructure was studied using TEM as described previously (Akhtar, Almubrad et al. 2013). Briefly, the tissues were fixed overnight with 2.5% glutaraldehyde (TAAB Laboratories Equipment Ltd, Reading, UK) in 0.1% tannic acid solution. Thereafter, specimens were incubated with 4% osmium (TAAB Laboratories Equipment Ltd), followed by serial dehydration through an acetone

(Sigma) gradient (30%, 50%, 70%, 90%, 100%), 15 min on each occasion. Specimens were then infiltrated and embedded in medium resin (TAAB Laboratories Equipment Ltd) with gentle agitation, followed by polymerisation overnight at 60°C overnight. The specimen blocks were then trimmed to expose the corneal surface using a razor blade followed by glass knife. The ultrathin 70 nm-thickness sections were cut using a diamond knife microtome with sections collected onto 200 mesh copper grids (Ted Pella, Inc., CA, USA). Sections were examined using a Tecnai G2 spirit BioTWIN Transmission electron microscope (FEI Company, OR, USA) operated at 120kV and 60k-fold magnification with a CCD camera. Tissues were sampled at five depth intervals from top of the anterior stroma 0-50 μm, 80-150 μm, 200-250 μm, 300-350 μm, 400-450 μm. The obtained images from each section were measured using imaging analysis software (ImageJ) and bespoke MATLAB codes for quantitative analysis, which is introduced in next section.

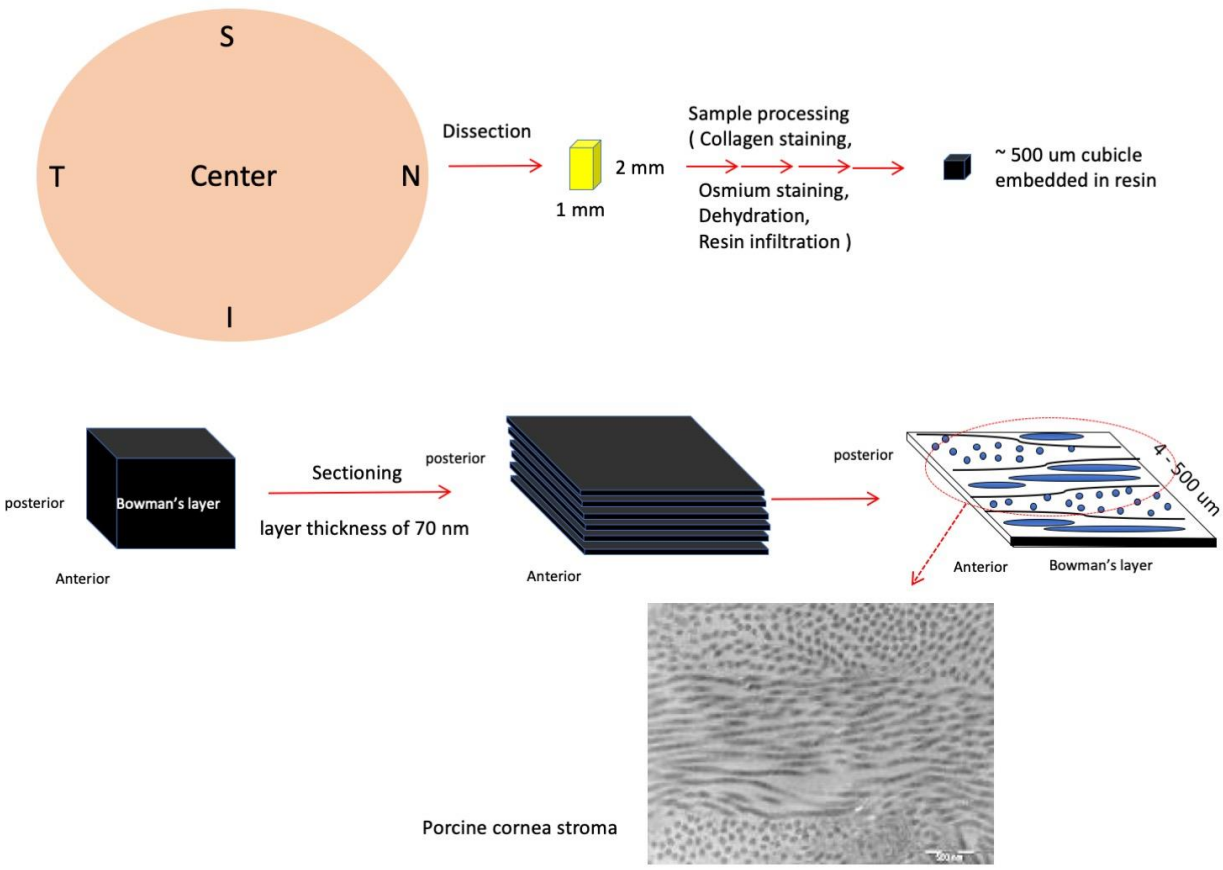

Figure 3.16. Experimental procedure of TEM technique.

3.5.2. Imaging Analysis (ImageJ/Fiji Software)

Ultrastructural parameters evaluated in this study included mean diameter of collagen fibrils, inter-fibrillar spacing and fibril density. Collagen fibrils in longitudinal, frontal and oblique profiles were observed in TEM images; only the frontal profiles were used for quantitative analysis with analyses performed using Fiji software (National Institutes of Health, Bethesda, MA, USA). Area measurement and counting function of the software were selected. Three random areas in each image were generated based on the uniform distribution using Matlab. A randomly chosen square was shown at higher magnification with an example of the selected circular area (figure 3.17). If the measured circular area does not match the circular cross-section of fibril bundles in original TEM image, the threshold needs to be reset until the best match has been found, the analytic steps were shown in figure 3.18. Results of measured particle areas were exported into corresponding excel data sheets and proceeded for average diameters. For each depth interval, ten fields were analysed and data were given as mean ± SD. Apart from the fibril diameter, other important structural parameters including the density of collagen and inter-fibrillar spacing were investigated and described as below. The calculation of inter-fibrillar spacing was generated from Equation 3.4 while assuming that the collagen fibrils were evenly distributed.

$$\mathrm{R} + \mathrm{D} = \sqrt{A/N} \tag{3.4}$$

Here R was defined as inter-fibrillar spacing (nm), D as mean diameter of collagen fibrils (nm), A as the area of selected zone of measurement (nm^2), N as the number of fibrils (circular spots) within the selected zone. For the quantification of collagen fibril density, a window of fixed unit size (300 x 300 nm^2) was randomly localised, and the number and area of circular spots were measured.

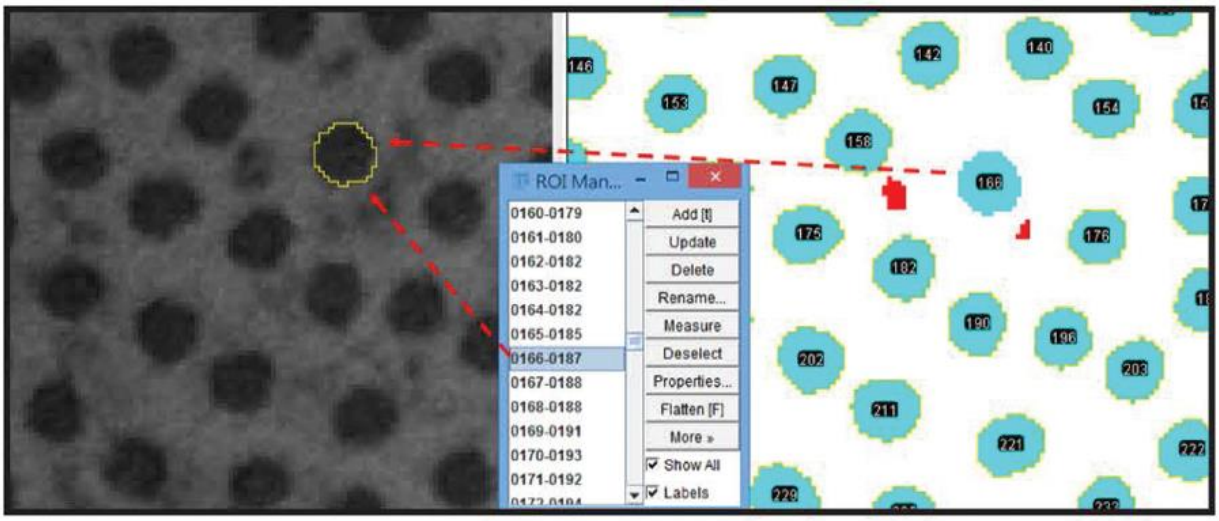

Figure 3.17. TEM images of porcine corneas imaged at a depth of 80 to 150 μm. An area of 300 x 300 nm^2 is shown with an example of the selected circular area and number of collagen fibrils.

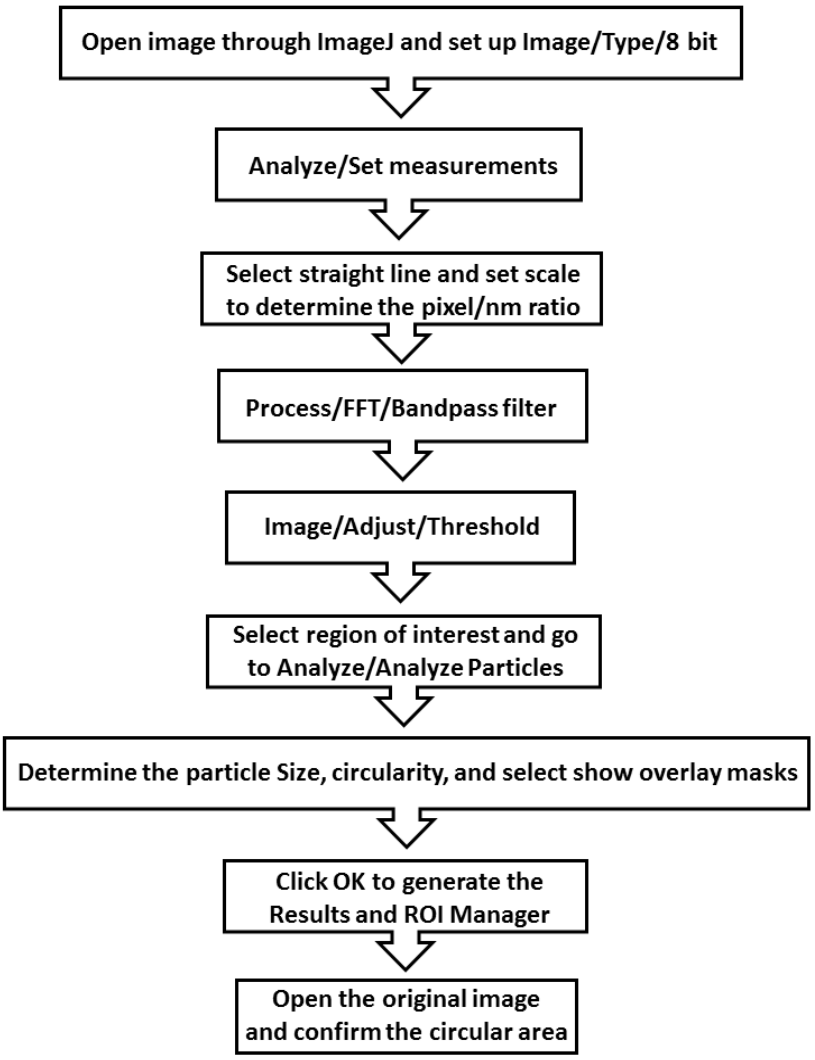

Figure 3.18. Analytic steps of TEM images using Fiji software.

3.5.3. Fibril Detection System

The distribution curve of collagen fibrils was assessed with a bespoke MATLAB codes. Briefly, the original images were converted to binary using an adaptive thresholding method and a custom-designed collagen fibril detection system, using the Circular Hough Transform (CHT) based algorithm (Yuen, Princen et al. 1990, Atherton and Kerbyson 1999), was established to analyse the radius of circular objects in frontal profiles of TEM images. The frequency was calculated for circular spots in each group, data was exported and pooled. Distribution curves were generated by plotting the frequency in 2-nm increments against fibril radius.

3.6. Fourier Transform Infrared Spectroscopy (FTIR)

To further determine the reaction mechanism, infrared spectroscopy would be able to help researchers to identify the newly formed or diminished chemical bonding. Molecules excited by infrared light with specific frequencies will start to vibrate. Infrared spectroscopy is to record the vibrational mode of molecule and the relative intensity of absorbed light to the infrared light wavelength. Each molecule will only absorb the infrared light with frequencies characteristic of their structure and vibrational modes (Williams 1945). Therefore, infrared spectroscopy not only assist researchers to understand the structure of molecules but also to identify the existence and content of a compound. In this section, the effects of the Dresden protocol were examined using infrared spectroscopy technique to evaluate the role of dextran and overall effect of UVA/riboflavin CXL in alternations of structure and formation of new chemical bonds.

3.6.1. Experimental Procedure

Eighteen fresh porcine corneas were treated as above with either PBS, 0.1% riboflavin in 20% dextran or the full Dresden protocol (n = 6 per group). Specimens were lyophilized for 3 days prior to scanning, then measured with FTIR spectra using Nicolet 6700 FTIR spectrometer (Thermo Scientific, MA, USA) with attenuated total reflection (ATR) module. Sixty-four accumulative scans were taken with a resolution of 4 cm^{-1} between 800 and 4000 cm^{-1}. Data was collected using OMNIC software

(Thermo Scientific, MA, USA). Analyses of FTIR spectra of each condition were obtained with a combination of four spectral intervals [ν (C=O) absorption of amide I (1,680–1,630 cm^{-1}), δ (NH_2) absorptions of amide II (1,570–1,515 cm^{-1}), ν (C–N) absorptions of amide III (1,350–1,200 cm^{-1}), and ν (C–O) absorptions of carbohydrate moieties (1,150–1,000 cm^{-1})]. Area under the curve at each interval was analyzed using KnowItAll® ID Expert™ software (Bio-Rad, CA, USA).

3.7. Protein Analysis of PGs using Mass Spectrometry and Western Blotting

This section describes an approach for the quantification and characterization of a targeted set of proteins when considering the complexity of biological tissue. In-gel digestion of gel-separated proteins followed by liquid chromatography-mass spectrometry (LC-MS) analysis is a powerful tool for protein identification (figure 3.19). Using this method, proteins can then be analysed either as intact proteins for molecular weight determination or as peptides generated by proteolysis. The western blotting protein analysis is used to obtain comparable or more specific results than with in-gel digestion. PGs that may be involved in CXL treatment were examined using both LC-MS and western blotting analysis in order to confirm the above findings based on TEM and FTIR, providing further structural information and protein compositions.

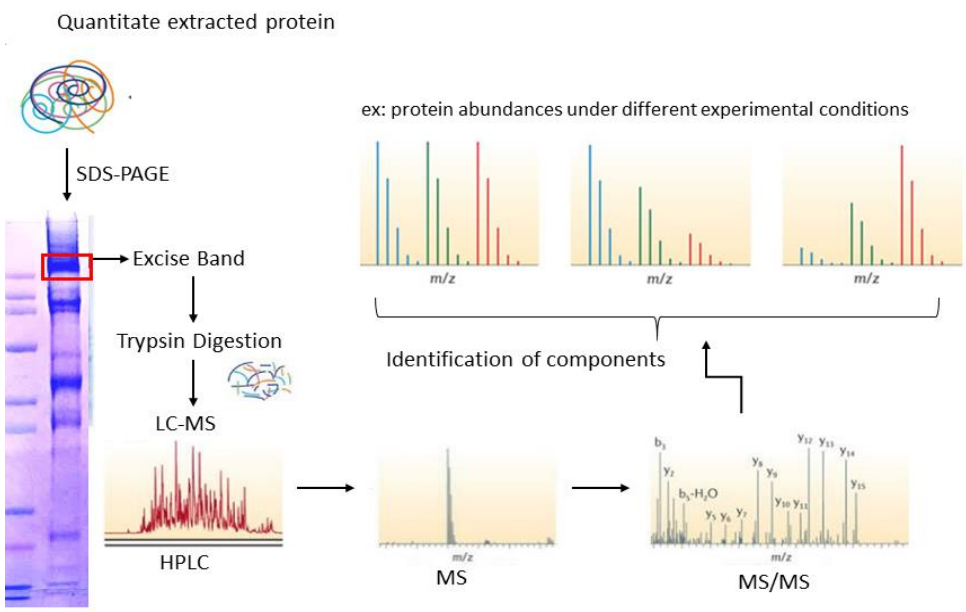

Figure 3.19. In-gel digestion followed by liquid chromatography-mass spectrometry (LC-MS) analysis for protein identification.

3.7.1. Experimental Procedure and Protein Preparation

A total of eighteen porcine eyes were obtained for ECM protein extractions. The de-epithelialized corneas were tested with either PBS, 0.1% riboflavin in 20% dextran or the full Dresden protocol (n = 6 per group). The specimens of experimental or control groups were frozen by liquid nitrogen and ready for ECM protein extraction. The frozen specimens were pulverized and homogenized in 4 M guanidine-HCl containing protease inhibitor, and incubated for 24h at 4°C with gentle agitation. The tissue residue was removed by centrifugation and supernatant was collected as the ECM extracts. The collect extracts were applied to dialysis for desalting, and harvested by lyophiliation. The dried proteins were then weighted and re-solubilized in 7M urea solution with 1% sodium dodecyl sulfate (SDS) in 25 mM Tris-HCl (pH7.0) and 2 mM phenylmethylsulfonyl fluoride (PMSF) (Sigma, USA). Samples were sonicated for 30 s and the concentration was determined using the BCA Protein Assay Kit (Bio-Rad, USA) according to the manufacturer's protocol. A colorimetric analysis was performed with a SpectraMax Plus plate reader. The protein lysates were then separated into two batches for further digestions with Chondroitinase ABC (ChonABC) and Keratanase (Kase) (Sigma, USA). The samples were boiled at 95°C for 5 min and prepared for sodium dodecyl sulfate polyacrylamide gel electrophoresis (SDS-PAGE) analysis for protein identification. The procedure was illustrated in figure 3.20.

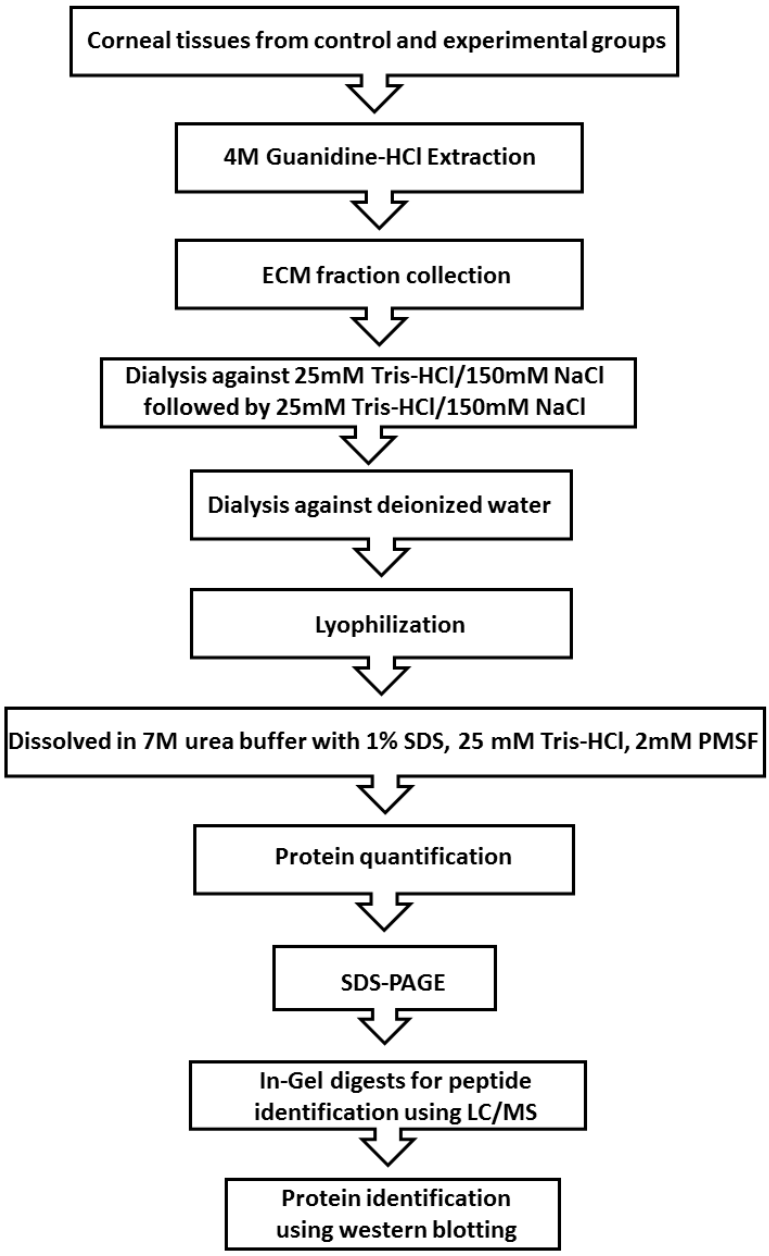

Figure 3.20. Flow chart of ECM preparation, solubilisation and analysis.

3.7.2. SDS-PAGE Analysis and In-Gel Digests for Mass Spectrometry

Mass spectrometry was applied for determining the ECM proteins that may be involved in CXL. The protein lysates were loaded onto 4-12% gradient gels (NuPAGE Novex BisTris precast gel; Invitrogen, USA) and subjected to electrophoresis (100 V for 60 min) under reducing conditions. When the gel electrophoresis was finished, the gels were stained with 0.1% (w/v) Coomassie Brilliant Blue R-250. The potential cross-linked proteins were observed at the top of the gel in lane c and the amount of proteins around 50 kDa and 115 kDa up to 270 kDa were reduced (figure 3.21). These gel-

separated proteins in PBS condition were excised, destained, and digested with trypsin (Sigma, USA) for 16 h at 37°C. Protein peptides were then extracted from gel pieces with 50% acetonitrile (Thermo Fisher, USA). The peptide samples were dried and re-suspended in 0.1% dormic acid (Thermo Fisher, USA) for LC-MS analysis. Fractions were separated using chromatography system coupled with an LTQ Orbitrap Velo Pro mass spectrometer. Mass data acquired and analyzed using Proteome Discoverer version 1.3 (Thermo Scientific, USA) and the Mascot search engine (Version 2.3.02). Three individual batches of ECM proteins were analysed in two independent runs. The numbers of unique peptides were acquired and counted for protein identification.

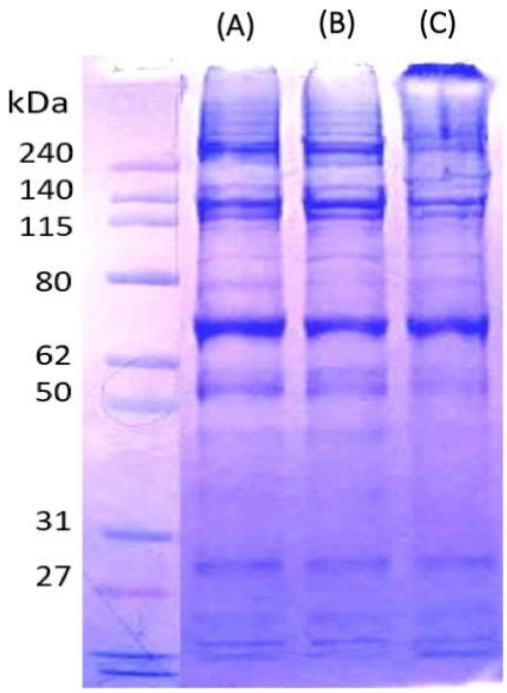

Figure 3.21. Coomassie blue staining of cross-linked and non-cross-linked ECM proteins. (A) PBS, (B) 0.1% riboflavin in 20% dextran, (C) full Dresden protocol.

3.7.3. Protein Identification by Western Blotting Analysis

The PGs identified by LC-MS was further examined using western blotting to detect the changes in expression of specific PGs after CXL. Following the electrophoresis, proteins were transferred to polyvinylidene difluoride (PVDF) membrane (Bio-Rad, USA) using a semidry electrophoretic

transfer system (150 V for 45 min). Protein blocking and immune-detection was performed subsequently. Antibodies to each of PGs were used to assess the possible CXL of PG core proteins. The membranes were probed using anti-decorin antibody (ab138492, Abcam), anti-keratocan antibody (ab128304, Abcam), and anti-lumican antibody (ab108286, Abcam) at room temperature for 2 h, followed by appropriate secondary antibodies conjugated with horseradish peroxidase. Immuno-reactive bands were detected using an enhanced chemiluminescence system.

3.8. Meta-analysis on Clinical trials

Although Dresden protocol is widely adopted, alternative protocols have been developed due to different purposes. Such efforts have resulted in the development of accelerated CXL protocols. Accelerated CXL has become popular due to its advantage of time reduction in this time consuming procedure (Kymionis, Tsoulnaras et al. 2014). These accelerated techniques maintain the original energy density of the standard corneal CXL procedure (5.4 J/cm^2) by creating different combinations of irradiance levels and exposure time lengths (Touboul, Efron et al. 2012, Hammer, Richoz et al. 2014). According to Bunsen-Roscoe law of reciprocity, the photochemical process of CXL should depend on the accumulated radiation dose and its biological effect is proportional to the total energy dose (Brindley 1952). It is supposed to achieve similar effectiveness between conventional Dresden and accelerated protocols. However, the reported outcome showed no consistence and is still under debate (Konstantopoulos and Mehta 2015, Shetty, Pahuja et al. 2015, Waszczykowska and Jurowski 2015, Sadoughi, Einollahi et al. 2018). Therefore, this meta-analysis aimed to compare the effectiveness of conventional Dresden protocol (3 mW/cm^2, 30 min) and other different accelerated protocols including 9 mW/cm^2, 18 mW/cm^2, and 30 mW/cm^2 irradiances. The compared follow-up duration is at 12 months through the direct comparison clinical trials on the changes in refractive powers and topographic outcomes for progressive keratoconus.

3.8.1. Methods

3.8.1.1. Search strategy

This systematic review and meta-analysis is based on PRISMA guidelines recommendations (Moher, Shamseer et al. 2015). The primary source of data was MEDLINE " (United States National Library of Medicine), using the “PubMed" search engine and using the search terms "keratoconus" AND “CXL” AND "riboflavin". The Cochrane database was also searched.

3.8.1.2. Study selection and data extraction

Inclusion criteria were all studies comparing the effects of using conventional CXL versus accelerated CXL protocols on patients with keratoconus. Studies were included if the following criteria is fulfilled; (1) they were written in English, (2) the study included more than ten patients for CXL procedures, (3) the patients aged older than 14 years. Records were excluded if the population were pediatrics. The process of electronic databases searching was outlined in figure 3.22.

3.8.1.3. Data extraction and quality assessment

Two independent observers extracted the following data by use of a predetermined Excel sheet, in addition, any conflicts were resolved via consensus or advisor opinion. The defined data encompassing author, year of publication, number of patients, number of eyes, patient characteristics (age, sex), definition of keratoconus, longest follow up time, intensity of irradiation, total energy applied and riboflavin application techniques. Moreover, the data extraction included the outcomes of the different treatment techniques. The primary outcomes were the change in maximum keratometry (Kmax) at the longest follow up point (12 months). The secondary outcomes included the change in uncorrected visual acuity (UCVA), corrected distance visual acuity (CDVA), mean refractive spherical equivalent (MRSE), minimum keratometry (Kmin), mean keratometry (Kmean), and central corneal thickness (CCT) at one year. Articles that were eligible for inclusion but specific data extraction was not given were marked as “NA” (not available).

The quality of the included studies in this meta-analysis was assessed according to the Newcastle-Ottawa Quality Assessment Scale (NOS) (Stang 2010), as presented in Table 3.3. Studies with an

NOS score ≤ 5 were considered “medium” quality studies. “High” quality studies were defined as having a quality score > 5. The maximum NOS score was 8.

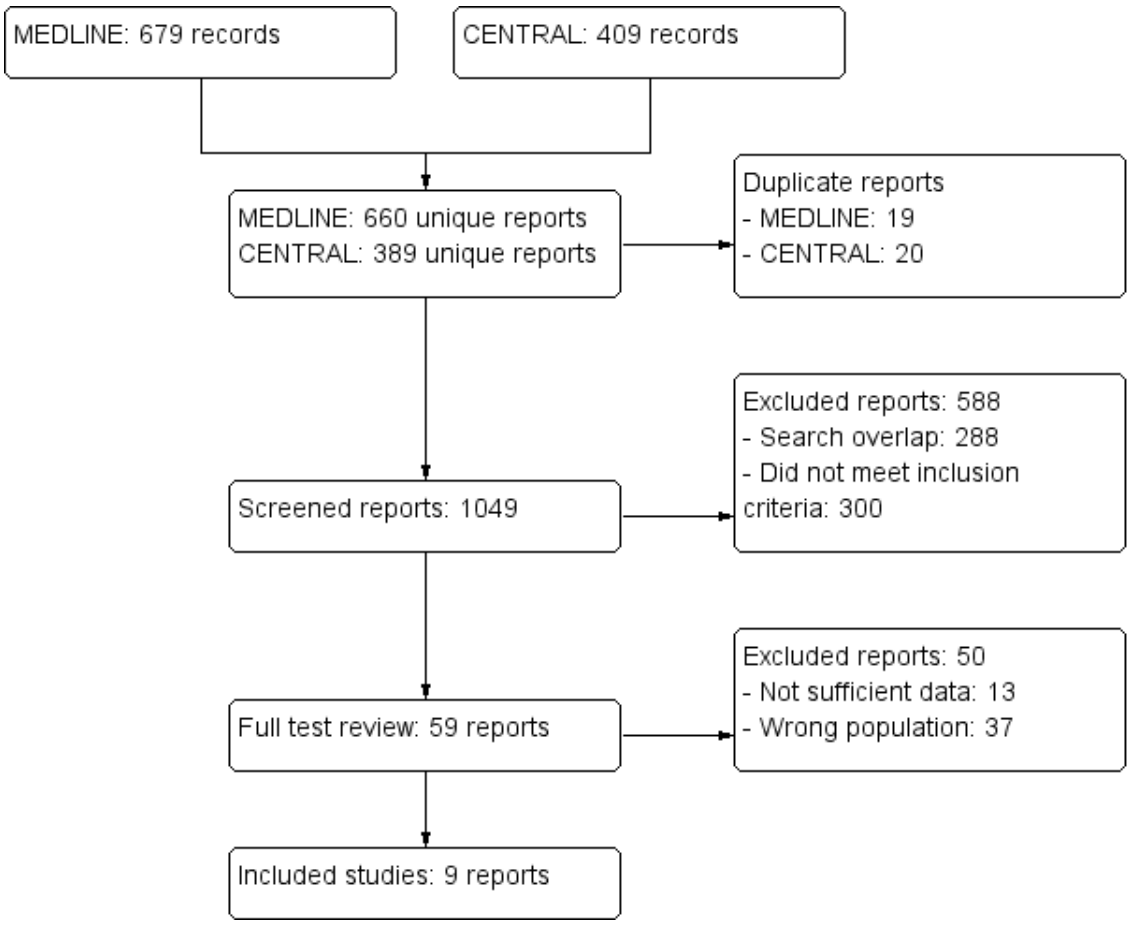

Figure 3.22. Flow diagram for the study analysis.

Table 3.3. Quality assessment of studies included in meta-analyses using a modified Newcastle–Ottawa Quality Assessment Scale.

Author (year)	Selection	Comparability	Exposure	Total points	Quality assessment rating [a]
Brittingham et al. (2014)	4	2	1	7	High
Choi et al. (2017)	4	2	2	8	High
Chow et al. (2015)	4	2	2	8	High
Cinar et al. (2014)	4	2	2	8	High
Hashemi et al. (2015)	4	2	2	8	High
Hashemian et al. (2014)	4	2	2	8	High
Jiang et al. (2017)	4	2	2	8	High
Tomita et al. (2014)	4	2	2	8	High
Woo et al. (2017)	4	2	2	8	High

[a]Studies with an NOS score ≤5 were considered "medium" quality studies. "High" quality studies were defined as having a quality score >5.

3.9. Statistical Analysis

For all the mechanical and ultrastructural measurements, the statistical evaluation was performed using SPSS software version 18.0 (IBM Corp. USA). Results are presented as mean ± standard deviation (SD) and statistical significance calculated using one-way analysis of variance (ANOVA) with Turkey's HSD post-hoc test. Mann-Whitney U test (two-tailed) was used for analysing the statistical difference of the fibril distribution curves which are not normally distributed. Significance differences accepted where $p < 0.05$.

The Statistical analysis was performed using RevMan 5 version 5.3 (Cochrane Collaboration, Copenhagen, 2014) for meta-analysis study. The heterogeneity of the qualitative analysis was assessed visually and using Chi-square test and computing the quantity I^2 statistic. I^2 greater than 50% was considered to state significant heterogeneity. If $p > 0.1$, a fixed model was used, and if $p < 0.1$, a

random effect model was used. Sensitivity analyses were conducted to assess the heterogeneity and robustness of the pooled results. Significance differences accepted where $p < 0.05$.

Chapter 4. Results

4.1. Introduction

The efficacy of corneal CXL is believed to be dependent on the mechanical properties induced through modifying the characteristics of collagen fibrils, with the overall level of effect being dependent on treatment depth. Previous studies have attempted to evaluate mechanical properties and the effective CXL penetration depth by specifically examining anterior and posterior corneal layers (Kohlhaas, Spoerl et al. 2006, Seifert, Hammer et al. 2014). Morphologically, the diameter of collagen fibrils was measured in normal healthy rabbit corneas and in human keratoconic corneas *ex vivo* before and after CXL (Wollensak, Spoerl et al. 2003, Akhtar, Almubrad et al. 2013). TEM images show an increase of 12.2% in collagen fibril diameters within anterior region but only 4.6% increase in posterior segments (Wollensak, Wilsch et al. 2004). These studies demonstrated that the CXL effect is predominantly located within anterior stroma but did not specify the parameters that may be involved in determining and defining the amount of the tissue stiffening induced. Indeed, the relationship between the mechanical behaviour of the cross-linked cornea and its ultrastructure is poorly explored, and the specific contribution of the dextran within the riboflavin solution has not been reported (Choi, Lee et al. 2013, Seifert, Hammer et al. 2014). In addition, the relationship of protein interactions is hard to identify due to the complexity of biological tissue. This chapter presents the main results from the experimental phase of the study obtained using the afore-mentioned techniques. The current study systematically investigates the role of dextran and the effect of UVA/riboflavin CXL in inducing mechanical and ultrastructural changes, as well as the protein interactions in the porcine corneas.

4.2. Thickness measurement

Thickness measurement is of importance for the precise evaluations of mechanical properties and ultrastructure analysis of biological tissue. On comparing the thickness following the CXL treatments on halved corneal strips which were followed by tensile testing and ultrastructural analysis, a statistically significant reduction in tissue thickness was observed in dextran-treated specimens and Dresden protocol compared with their controls. The mean thickness of riboflavin in dextran was 0.79 ± 0.04 mm, while the PBS control was 1.05 ± 0.04 mm ($p = 1.39E-06$). The mean thickness measured after treatment with Dresden protocol was 0.83 ± 0.06 mm, no significant difference was detected comparing to its dextran control (0.81 ± 0.05 mm, $p = 0.63$). The measurements taken on four comparison groups (PBS vs PBS, riboflavin+PBS vs PBS, riboflavin+dextran vs PBS and riboflavin+dextran+UVA vs dextran) were demonstrated in Table 4.1.

For the intact eye globes subjected to inflation test, the thickness variations across the cornea obtained along the eight meridian lines (figure 3.8) were shown in Table 4.2. Four points per line across the cornea were identified as the central cornea, central-peripheral, peripheral-limbus, and limbus. The mean thickness measurements following CXL treatment from central to limbus were 1.3 ± 0.08 mm, 1.19 ± 0.05 mm, 1.17 ± 0.06 mm and 1.18 ± 0.06 mm. Comparing to the control eyes, the measurements were recorded as 0.95 ± 0.08 mm (central, $p = 0.003$), 1.03 ± 0.07 mm (central-peripheral, $p = 0.03$), 1.02 ± 0.06 mm (peripheral-limbus, $p = 0.03$) and 1.03 ± 0.08 mm (limbus, $p = 0.06$) accordingly (Table 4.2). The result demonstrated a statistically significant reduction in thickness in the central and peripheral areas which are affected by CXL.

Table 4.1. Average thickness measurements of halved corneal strips followed by tensile testing and ultrastructural analysis.

Experimental corneal strips / Control corneal strips	No. of Samples	Thickness (mm)	p value
PBS / PBS	6	1.04 ± 0.05 / 1.05 ± 0.03	0.75
Riboflavin + PBS / PBS	6	1.06 ± 0.04 / 1.05 ± 0.04	0.89
Riboflavin + Dextran / PBS	6	0.79 ± 0.04 / 1.05 ± 0.04	0.00
Riboflavin + Dextran + UVA / Dextran	10	0.83 ± 0.06 / 0.81 ± 0.05	0.63

Table 4.2. Average thickness measurements across the whole cornea at four different points. The thickness was measured after the inflation test.

Corneal regions	No. of Samples	Thickness of PBS Control Eye (mm)	Thickness of Cross-linked Eye (mm)	p value
Central cornea	7	1.3 ± 0.08	0.95 ± 0.08	0.003
Central-peripheral	7	1.19 ± 0.05	1.03 ± 0.07	0.03
Peripheral-limbus	7	1.17 ± 0.06	1.02 ± 0.06	0.03
Limbus	7	1.18 ± 0.06	1.03 ± 0.08	0.06

4.3. Ultrastructural Results

4.3.1. Transmission Electron Microscopy (TEM) and Imaging Analysis

The changes to the collagen ultrastructure of specimens were measured at five different depth intervals using TEM as shown in figure 4.1 and figure 4.2 (representative images at 80 to 150 μm) and the obtained images were used to determine collagen fibril diameter (Table 4.3 and figure 4.4 A), inter-fibrillar spacing (Table 4.4), and fibril number per unit area (density) (Table 4.5). The relative value of these ultrastructural measurements following Dresden was demonstrated in figure 4.3 B-D. The overall morphologies of the collagen ultrastructure did not change following PBS or riboflavin in PBS treatment in the absence of UVA (figure 4.1 A and 4.1 B). However, the dextran treatment led to significantly thinner collagen fibrils (figure 4.2), as well as reduced inter-fibrillar spacing and denser packing at all depth intervals compared to its PBS control. Because dextran causes loss of tissue hydration, analysis of fibril diameter at each depth interval revealed a reduction in the diameter of collagen fibrils compared to PBS treatment in the uncorrected data.

In analysing the effect of the Dresden UVA/riboflavin CXL protocol on corneal ultrastructure, both segments within our intra-eye comparisons were treated with dextran. Therefore, any residual difference between the internal controlled comparison groups reflected a true effect of the CXL procedure. Analysis revealed a small but statistically significant increase in collagen fibril diameter in the CXL group at 80 to 150 μm (5% ± 2%, $p < 0.01$) and 200 to 250 μm depths (6% ± 3%, $p < 0.01$), with no differences observed at any other depth intervals (figure 4.1 B, Table 4.3). No statistical differences in inter-fibrillar spacing between treatments were observed at any depths (Table 4.4), but the Dresden protocol caused a decrease in the number of fibrils per unit area in the anterior 250 μm of the tissue (0 to 50 μm: 6% ± 5%, $p < 0.05$; 80 to 150 μm: 11% ± 7%, $p < 0.01$; 200 to 250 μm: 11% ± 5%, $p < 0.01$) (Table 4.5). All together, these data indicated that the UVA/riboflavin CXL procedure created relatively small, depth-localized changes to the collagen ultrastructure.

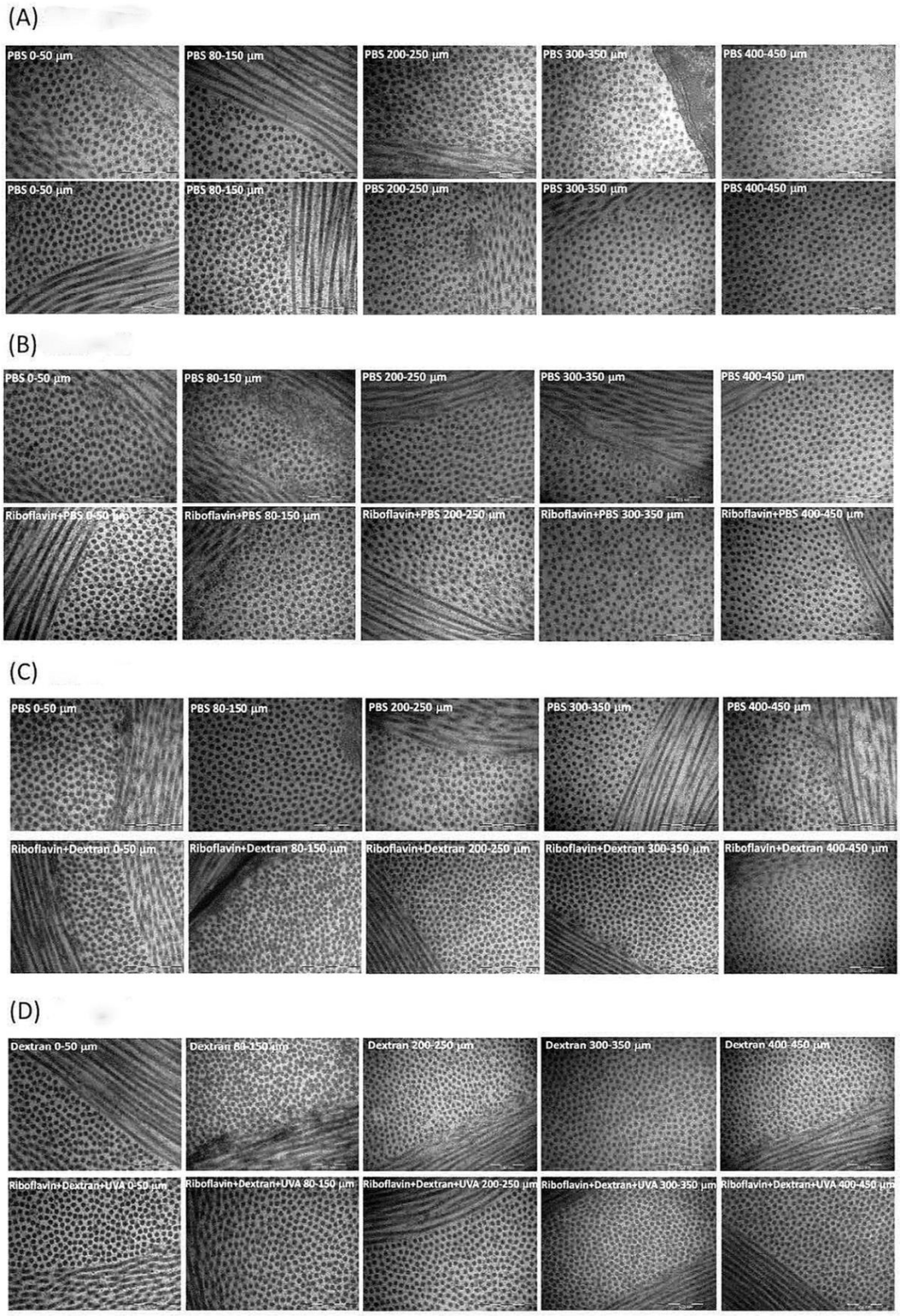

Figure 4.1. Transmission electron microscope (TEM) images of each treatment at different depth intervals. Representative TEM images of (A) PBS vs PBS, (B) Riboflavin+PBS vs PBS, (C) Riboflavin+Dextran vs PBS and (D) Riboflavin+Dextran+UVA vs Dextran. The images were obtained at five depth intervals of 0-50µm, 80-150µm, 200-250µm, 300-350µm, 400-450µm. Bar = 500 nm.

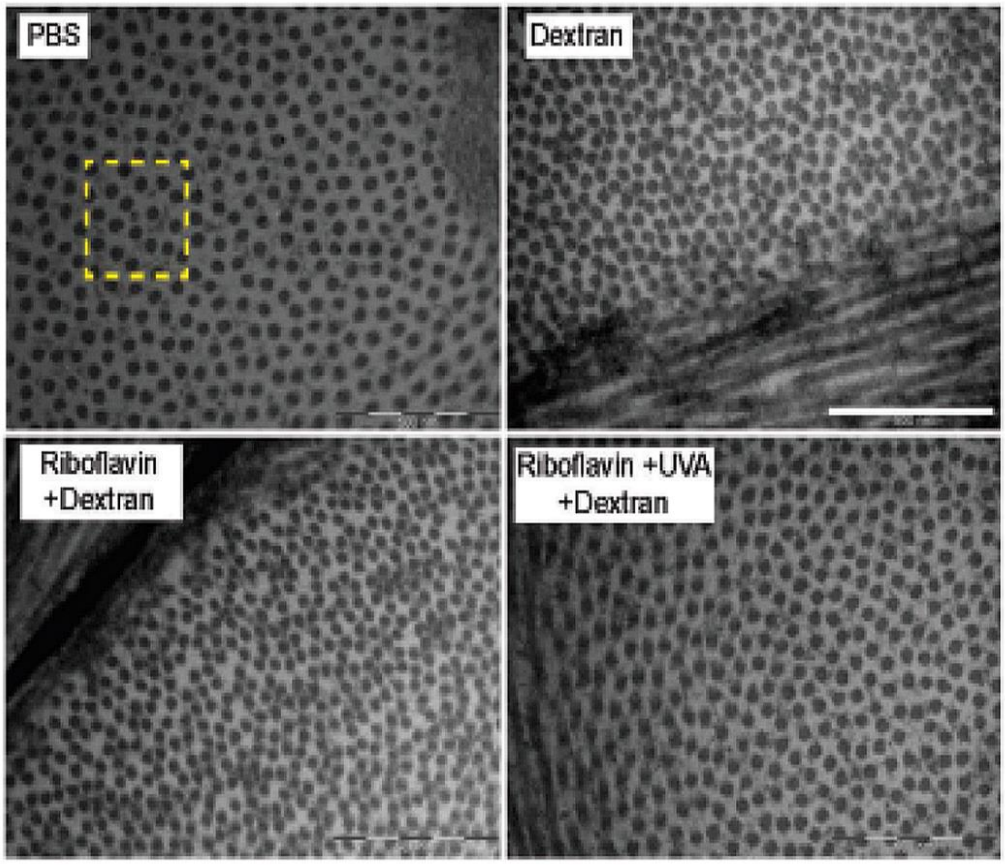

Figure 4.2. Transmission electron microscopy (TEM) images of porcine corneas imaged at a depth of 80 to 150 μm. Representation TEM images of PBS, riboflavin in dextran, dextran only and riboflavin/dextran/UVA cross-linked corneas. An area of 300 x 300 nm^2 (yellow dashed square) is shown for the measurement of the area and density of collagen fibrils. Bar = 500 nm.

Table 4.3. Mean diameter of collagen fibrils of corneal segments at different depth intervals.

Experimental groups	Number of Sample	Depth Range	Mean Diameter of Collagen (nm)		
PBS vs PBS	6	0-50 μm	39.64±1.13		38.69±1.54
		80-150 μm	37.25±1.10		36.41±1.42
		200-250 μm	35.31±1.15	vs	34.84±1.16
		300-350 μm	32.02±1.08		32.02±1.32
		400-450 μm	30.68±0.89		30.27±1.17
PBS vs Riboflavin+PBS	6	0-50 μm	38.63±1.34		38.83±1.11
		80-150 μm	35.61±1.38		35.95±0.66
		200-250 μm	34.34±1.63	vs	34.32±1.15
		300-350 μm	31.18±1.45		30.99±0.92
		400-450 μm	30.28±0.98		30.23±0.52
PBS vs Riboflavin+Dextran	6	0-50 μm	38.78±1.68		34.68±0.63**
		80-150 μm	36.02±1.52		31.85±0.97**
		200-250 μm	34.51±1.11	vs	30.36±1.63**
		300-350 μm	31.11±1.20		29.83±0.86*
		400-450 μm	30.62±1.92		29.45±0.52
Dextran vs Riboflavin+Dextran+UVA	10	0-50 μm	35.85±1.70		36.75±1.03
		80-150 μm	32.74±1.39		34.32±1.23**
		200-250 μm	30.75±1.05	vs	32.50±1.19**
		300-350 μm	30.47±1.36		30.46±1.42
		400-450 μm	30.38±1.17		30.21±0.80

Values are presented as mean ± SD.

Asterisks denote significant differences from control groups, with one asterisk ($p < 0.05$) or two asterisks ($p < 0.01$).

Red asterisks indicate increase compared with control, green represents decrease compared with control.

Table 4.4. Inter-fibrillar spacing of collagen fibrils of corneal segments at different depth intervals.

Experimental groups	Number of Sample	Depth Range	Inter-fibillar Spacing (nm)		
PBS vs PBS	6	0-50 μm	29.84±2.12		30.25±0.70
		80-150 μm	30.52±1.64		30.78±0.69
		200-250 μm	31.32±1.71	vs	30.03±1.17
		300-350 μm	32.03±1.49		31.31±1.11
		400-450 μm	32.38±1.26		31.52±1.34
PBS vs Riboflavin+PBS	6	0-50 μm	30.24±0.63		30.55±0.94
		80-150 μm	30.75±0.59		31.22±1.48
		200-250 μm	30.65±1.65	vs	30.39±0.98
		300-350 μm	31.38±1.29		32.30±0.76
		400-450 μm	31.10±0.97		31.95±1.70
PBS vs Riboflavin+Dextran	6	0-50 μm	30.83±1.35		21.68±2.20**
		80-150 μm	30.77±1.13		21.59±1.34**
		200-250 μm	30.49±0.94	vs	22.93±1.69**
		300-350 μm	31.10±0.92		23.41±0.96**
		400-450 μm	31.19±1.21		23.95±0.68
Dextran vs Riboflavin+Dextran+UVA	10	0-50 μm	20.53±1.83		22.43±3.49
		80-150 μm	21.92±1.55		22.93±2.95
		200-250 μm	22.52±1.97	vs	23.37±2.71
		300-350 μm	23.23±1.81		22.11±1.32
		400-450 μm	23.75±1.68		22.89±2.21

Values are presented as mean ± SD.

Asterisks denote significant differences from control groups, with one asterisk ($p < 0.05$) or two asterisks ($p < 0.01$).

Red asterisks indicate increase compared with control, green represents decrease compared with control.

Table 4.5. Density of collagen fibrils of corneal segments at different depth intervals.

Experimental groups	Number of Sample	Depth Range	Density of Collagen (N/300*300 nm^2)		
PBS vs PBS	6	0-50 μm	18.98±1.56		19.56±1.37
		80-150 μm	18.36±1.17		19.25±2.00
		200-250 μm	20.13±1.56	vs	20.47±1.81
		300-350 μm	19.99±2.08		19.93±1.46
		400-450 μm	20.22±2.59		19.55±2.08
PBS vs Riboflavin+PBS	6	0-50 μm	19.70±1.54		19.90±1.04
		80-150 μm	19.47±1.86		19.18±2.00
		200-250 μm	20.06±0.81	vs	20.09±1.22
		300-350 μm	21.42±0.76		20.91±1.19
		400-450 μm	21.71±1.18		20.82±1.48
PBS vs Riboflavin+Dextran	6	0-50 μm	20.82±1.23		28.42±1.03**
		80-150 μm	18.82±1.96		27.14±1.83**
		200-250 μm	19.21±1.42	vs	28.20±1.39**
		300-350 μm	20.11±1.24		26.40±1.79**
		400-450 μm	20.15±0.93		27.07±1.17**
Dextran vs Riboflavin+Dextran+UVA	10	0-50 μm	28.03±1.74		26.31±1.42*
		80-150 μm	28.44±1.32		25.46±1.71**
		200-250 μm	28.34±1.41	vs	25.24±1.61**
		300-350 μm	26.69±1.94		27.03±1.78
		400-450 μm	26.79±1.77		27.34±1.82

Values are presented as mean ± SD.

Asterisks denote significant differences from control groups, with one asterisk ($p < 0.05$) or two asterisks ($p < 0.01$).

Red asterisks indicate increase compared with control, green represents decrease compared with control.

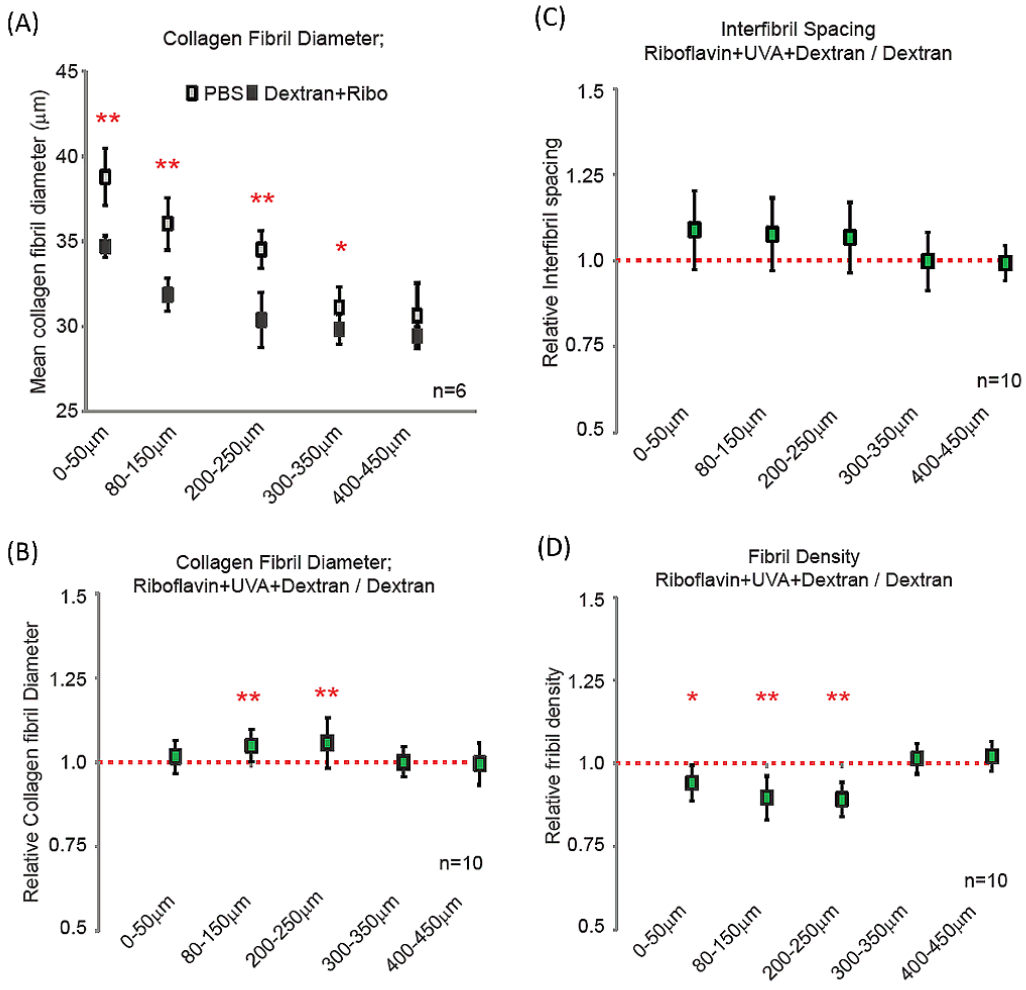

Figure 4.3. Measurement of ultrastructural parameters and relative values at different depth intervals following CXL. (A) Mean collagen fibril diameters of PBS and riboflavin in dextran at each depth interval. (B) Relative collagen fibril diameter. (C) Relative inter-fibrillar spacing. (D) Relative collagen density of the corneal CXL group relative to its dextran group at each depth interval. Values are plotted as mean ± SD from n = 6 (A) or n = 10 (B, C, D). Red asterisks denote significant differences from control groups, with one asterisk ($p < 0.05$) or two asterisks ($p < 0.01$).

4.3.2. The Distribution Curves of Collagen Fibrils

The distribution curve displayed the collagen framework and frequency of fibril diameter at different depth intervals. Most of the collagen fibril radius values in control PBS were in the range between 16-24 nm. The overlaid curve was performed for detecting the variations in the frequency of large collagen fibrils between control and experimental groups. It showed no significant changes following PBS or riboflavin in PBS treatment (figure 4.4 and 4.5). However, the dextran led to significantly thinner collagen fibrils and lower frequency of large fibrils up to 250 μm depths comparing to it PBS control (figure 4.6 C). The smaller collagen fibrils do not seem to be significantly affected by dextran. In the group of Dresden protocol, both segments were treated with dextran, the distribution curve demonstrated the true effect of CXL. In the comparison with dextran control, CXL caused a higher frequency of large fibrils in anterior stroma as shown in figure 4.7C ($p < 0.01$). The findings reveal that the larger collagen fibrils induced by CXL may result from the resistance to dehydration within a stromal depth of 250 μm where CXL affects.

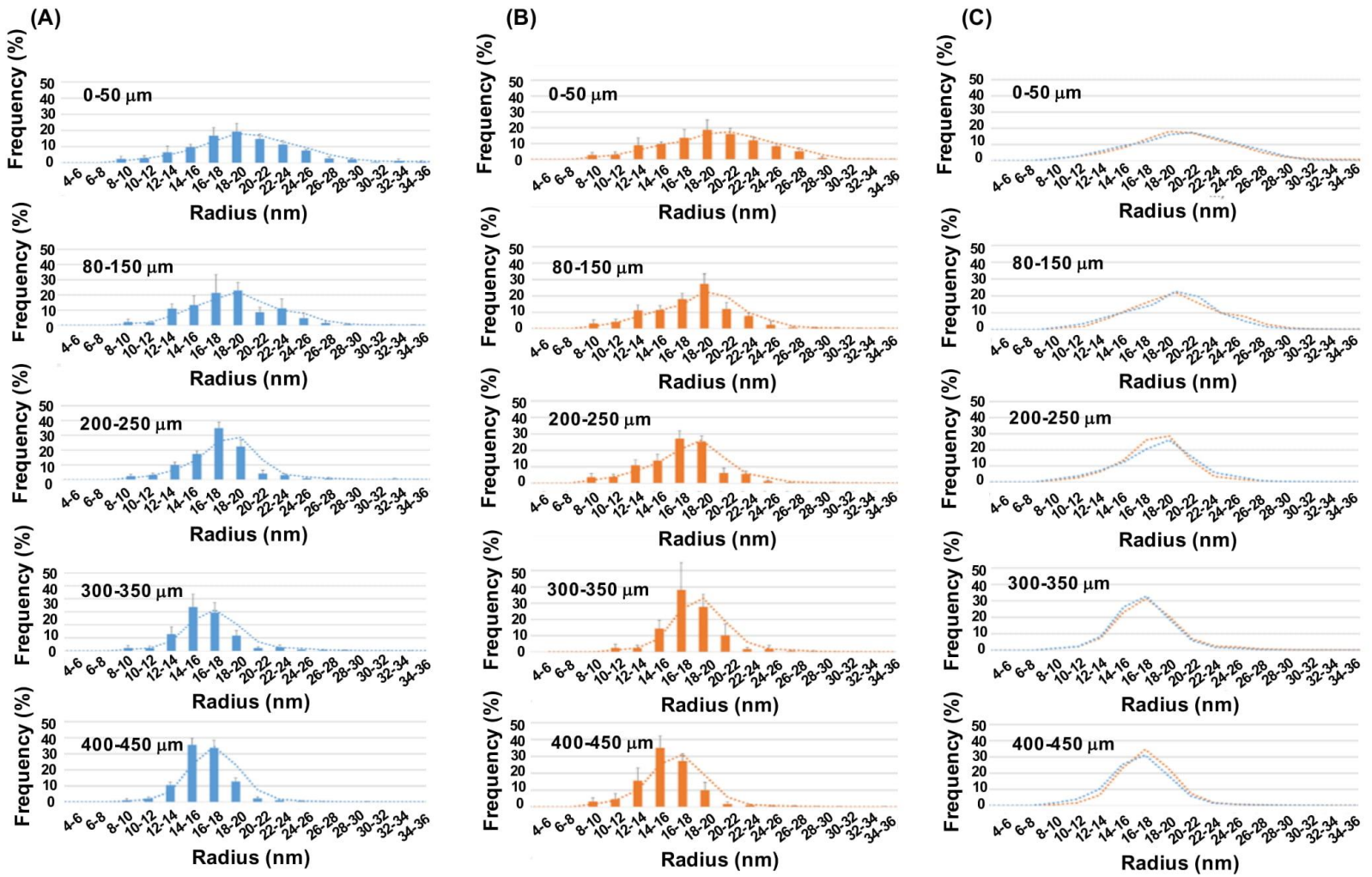

Figure 4.4. The distribution of collagen fibrils following PBS at different depth intervals. (A) left-hand corneal strips in PBS, (B) right-hand corneal strips in PBS, (C) the overlaid curves. The dash lines represent the trend curves. Data were obtained at five depth intervals of 0-50μm, 80-150μm, 200-250μm, 300-350μm, 400-450μm.

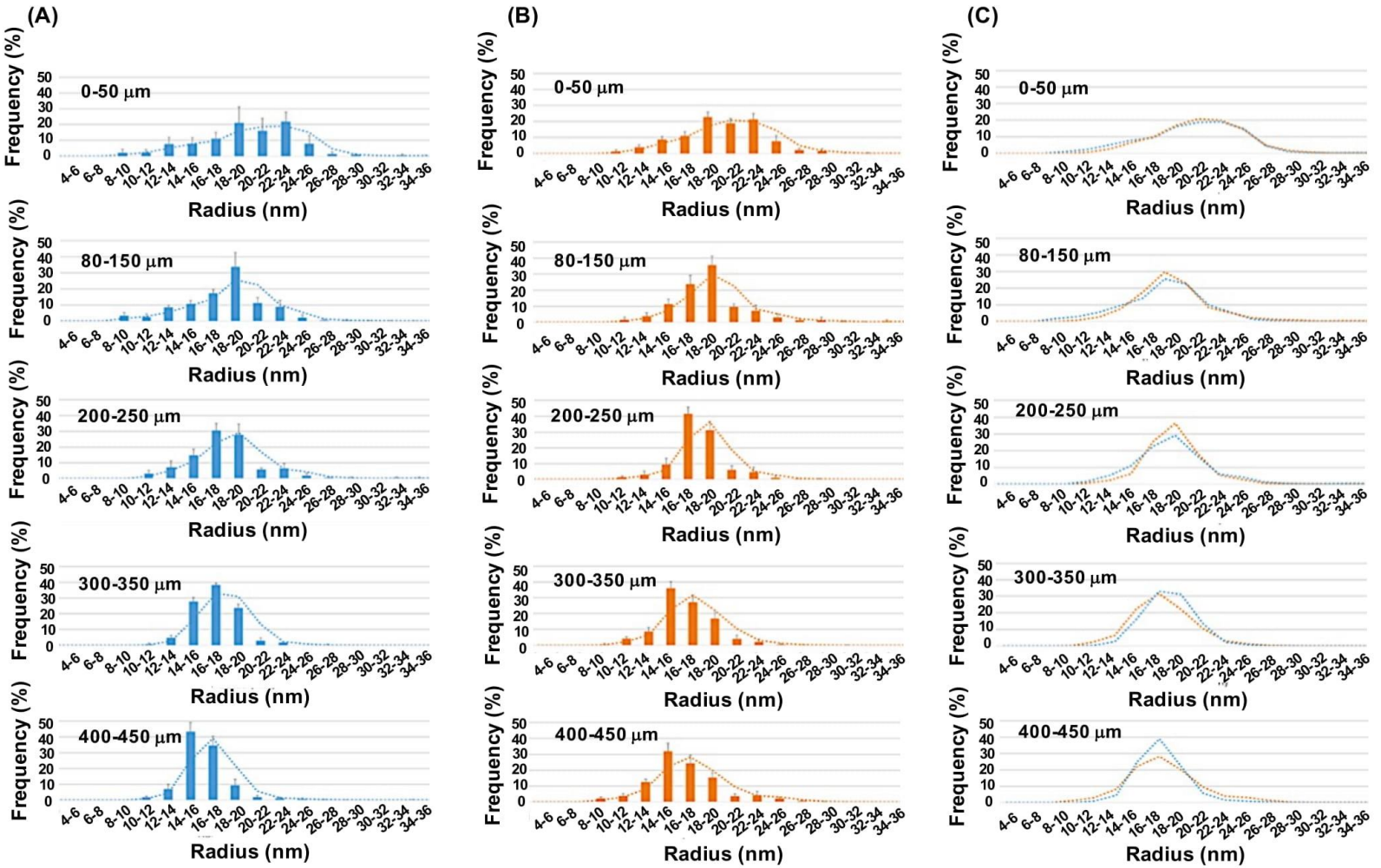

Figure 4.5. The distribution of collagen fibrils following riboflavin at different depth intervals. (A) left-hand corneal strips in PBS, (B) right-hand corneal strips in riboflavin+PBS, (C) The overlaid curves. The dash lines represent the trend curves. Data were obtained at five depth intervals of 0-50μm, 80-150μm, 200-250μm, 300-350μm, 400-450μm.

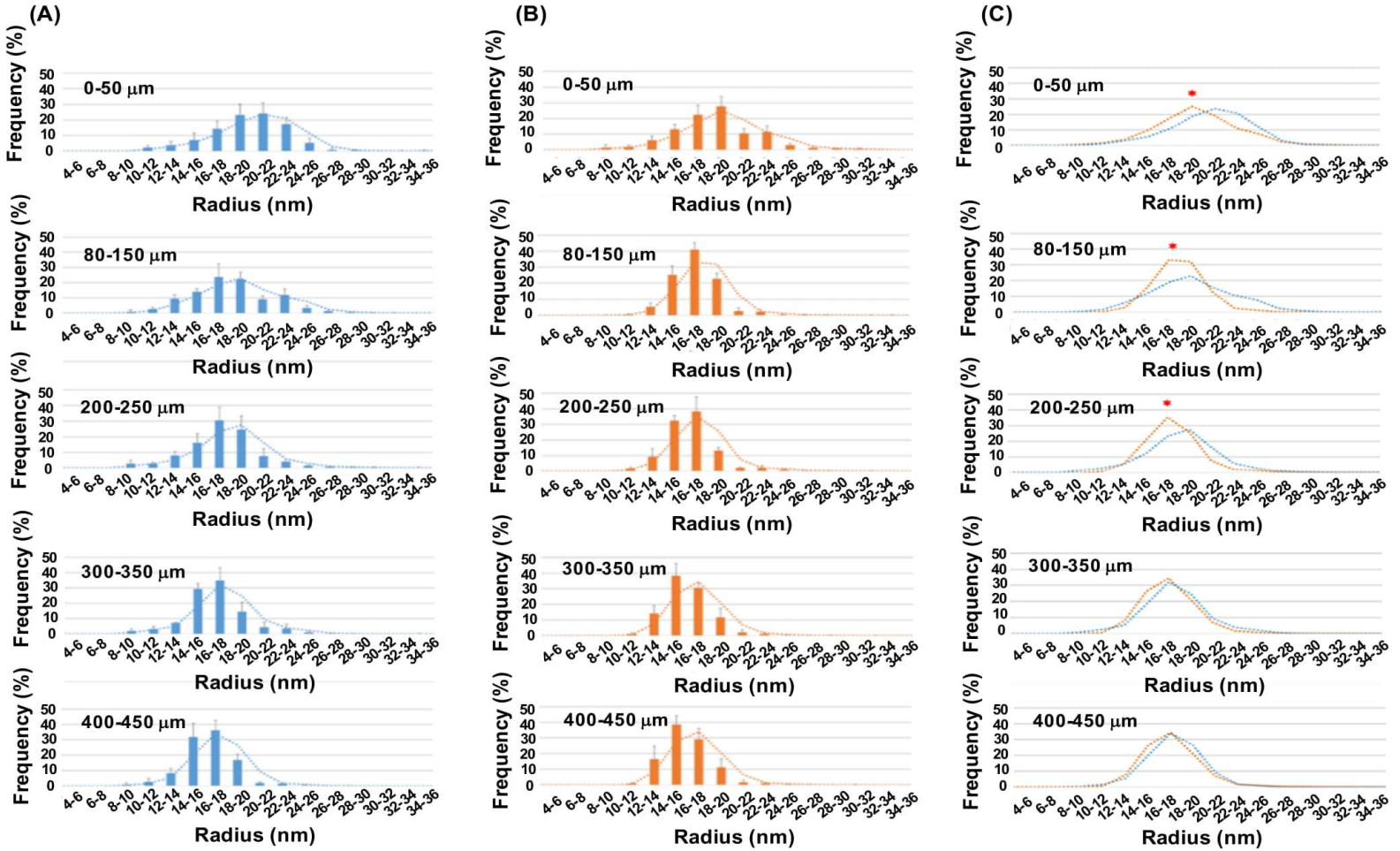

Figure 4.6. The distribution of collagen fibrils following dextran at different depth intervals. (A) left-hand corneal strips in PBS, (B) right-hand corneal strips in riboflavin+dextran, (C) The overlaid curves. The dash lines represent the trend curves. Data were obtained at five depth intervals of 0-50μm, 80-150μm, 200-250μm, 300-350μm, 400-450μm. Asterisks denote significant differences from control groups, with one asterisk ($p < 0.05$) or two asterisks ($p < 0.01$).

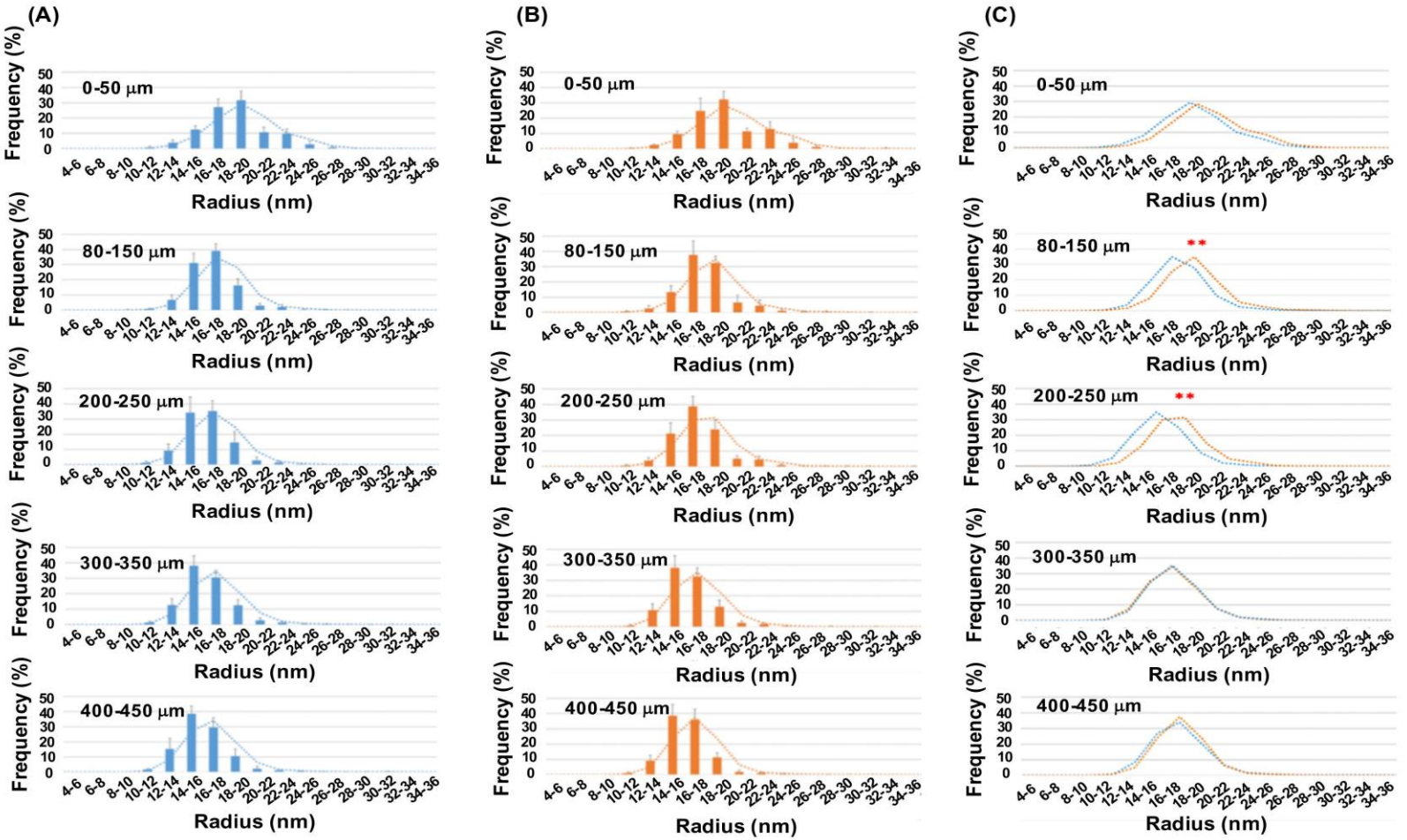

Figure 4.7. The distribution of collagen fibrils following Dresden protocol at different depth intervals. (A) left-hand corneal strips in dextran, (B) right-hand corneal strips in riboflavin+dextran+UVA, (C) The overlaid curves. The dash lines represent the trend curves. Data were obtained at five depth intervals of 0-50μm, 80-150μm, 200-250μm, 300-350μm, 400-450μm. Asterisks denote significant differences from control groups, with one asterisk ($p < 0.05$) or two asterisks ($p < 0.01$).

4.3.3. Fourier Transform Infrared Spectroscopy (FTIR)

To assess the detailed chemical reactions and the conversion of chemical bonds within the corneal tissue after UVA/riboflavin CXL, FTIR spectroscopy measurements were performed on corneas treated with either PBS, riboflavin+dextran, or riboflavin+dextran+UVA (figure 4.8 A and 4.8 B). The relevant characteristic bands were: amide I C = O stretching vibration (1,680 to 1,630 cm^{-1}), amide II NH_2 bending vibration (1,570 to 1,515 cm^{-1}), amide III C-N stretching vibration (1,350 to 1,200 cm^{-1}), and C-O bond stretching vibration (1,150 to 1,000 cm^{-1}). The area under each band was calculated, and the deformation vibrations of CH_2 (1,485 to 1,360 cm^{-1}) were used as an internal standard to determine the intensity ratios (figure 4.8 C and Table 4.5). These analyses revealed significant increases in the C-O stretch peak, increased C-N stretch, and decreased NH_2 deformation following CXL (figure 4.8 C). Plotting the ratio of C-N stretch to NH_2 deformation suggests that the decrease intensities of amide II infrared absorption bands are likely to be accompanied by an increase in the formation of amide III bonds (riboflavin+dextran+UVA = 2.5 ± 0.5; PBS = 1.7 ± 0.3; riboflavin+dextran = 1.8 ± 0.2; figure 4.8 D, Table 4.6).

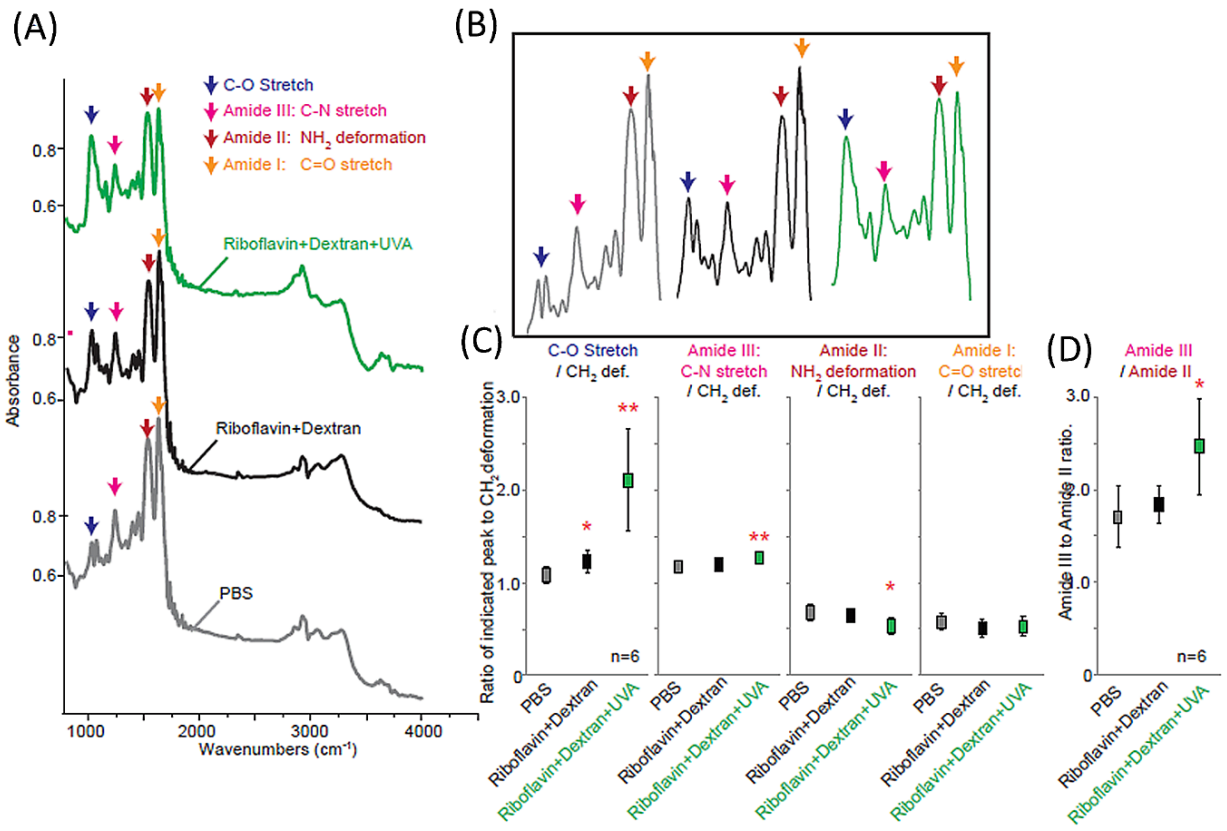

Figure 4.8. Absorption Fourier transform infrared (FTIR) spectra of porcine corneas following corneal CXL treatments. (A) Representative FTIR spectra of corneas treated with PBS (bottom, gray), riboflavin+dextran (middle, black), or riboflavin+dextran+UVA (top, green). (B) Regions where the characteristic bands are located shown at higher magnification and regions of interest indicated amide I (1,680 to 1,630 cm^{-1}), amide II (1,570 to 1, 515 cm^{-1}), amide III (1,350 to 1,200 cm^{-1}), and CO absorption band (1,150 to 1,000 cm^{-1}). (C) Relative intensity ratio of each characteristic band and (D) conversion rate of amide II to amide III. Red asterisks denote significant differences from PBS control groups, with one asterisk ($p < 0.05$) or two asterisks ($p < 0.01$).

Table 4.6. Area ratio corresponding to indicated characteristic bands in FTIR spectra.

Ratio	PBS	Riboflavin+Dextran	Riboflavin+Dextran+UVA
Number of Samples	6	6	6
C-O stretch /-(CH_2)-deformation	1.08±0.09	1.23±0.12*	2.10±0.55**
Amide II /-(CH_2)-deformation	0.67±0.08	0.64±0.06	0.52±0.08*
Amide III /-(CH_2)-deformation	1.16±0.02	1.19±0.02	1.26±0.04**
Amide I /-(CH_2)-deformation	0.57±0.09	0.50±0.09	0.52±0.10
Amide III / Amide I	1.70±0.33	1.84±0.20	2.47±0.51*

Values are presented as mean ± SD.

Asterisks denote significant differences from control groups, with one asterisk ($p < 0.05$) or two asterisks ($p < 0.01$).

Red asterisks indicate increase compared with control, green represents decrease compared with control.

4.4. Mechanical Results

4.4.1. Uniaxial Tensile Testing

UVA/riboflavin treatment and dextran-mediated dehydration both cause the changes in ultrastructure as demonstrated above. To isolate the effect of the individual components of UVA/riboflavin CXL, uniaxial tensile experiments and TEM both were conducted on a set of porcine eyes split into paired comparison groups. To account for inter-animal variability, each cornea was cut into two and half treated with the treatment and compared against the control (tensile measurements and ultrastructural analyses were performed on the same cornea).

The tangent modulus (Et) versus stress (σ) for each corneal strip was determined and the overall stiffening effect indicated by the ratio of the tangent modulus ($Et_{experimental}$ / $Et_{control}$). Comparisons

concentrated on tangent modulus ratios at a stress of 0.03 MPa, which is equivalent to a physiological IOP of approximately 25 mmHg. As expected, no significant differences were observed where both corneal segments were treated identically with PBS, confirming the validity of our intra-eye control system. The Et-σ curves of each corneal strip treated with PBS and ratio of the tangent modulus ($Et_{experimental\ PBS}$ / $Et_{control\ PBS}$) were demonstrated in figure 4.9 and figure 4.10, respectively. The stiffening ratio was calculated as 1.06 ± 0.07 ($Et_{experimental\ PBS}$ vs $Et_{control\ PBS}$: 1.45 ± 0.15 vs 1.38 ± 0.17, p = 0.075, Table 4.7). Riboflavin in PBS treatment also caused no stiffening with the ratio of 1.05 ± 0.14 ($Et_{riboflavin\ in\ PBS}$ vs Et_{PBS}: 1.36 ± 0.32 vs 1.43 ± 0.30, p = 0.448, Table 4.7). However, the riboflavin+dextran group displayed a 13% ± 9% tangent modulus increase compared to their internal PBS control ($Et_{riboflavin\ in\ dextran}$: 1.52 ± 0.17 vs Et_{PBS}: 1.34 ± 0.18, p = 0.011, Table 4.7). Comparing the effect of the full Dresden CXL protocol to the effect of dextran treatment alone, tangent modulus was observed to increase by 28% ± 17% in the corneal segments treated by the Dresden protocol ($Et_{riboflavin+dextran+UVA}$: 2.09 ± 0.17 vs $Et_{dextran}$: 1.62 ± 0.18, p = 5.67E-05, Table 4.7).

The increased tangent modulus observed with dextran alone consists with previous publications (Hatami-Marbini and Rahimi 2016). However, on comparing the tissue thicknesses following treatments, a statistically significant reduced thicknesses in the dextran-treated samples compared with their PBS controls were observed and indicative of dehydration (mean thickness of riboflavin in dextran: 0.79 ± 0.04 mm, PBS: 1.05 ± 0.39 mm, p = 1.39E-06) (Table 4.1). Correcting the tangent modulus readings with these thickness measurements removed the apparent dextran effects (Table 4.7). Together, these data demonstrate that dextran treatment alone causes dehydration and therefore an apparently increased stiffening, whereas corneas treated with UVA/riboflavin exhibit further increased stiffening beyond that caused by the dextran treatment alone.

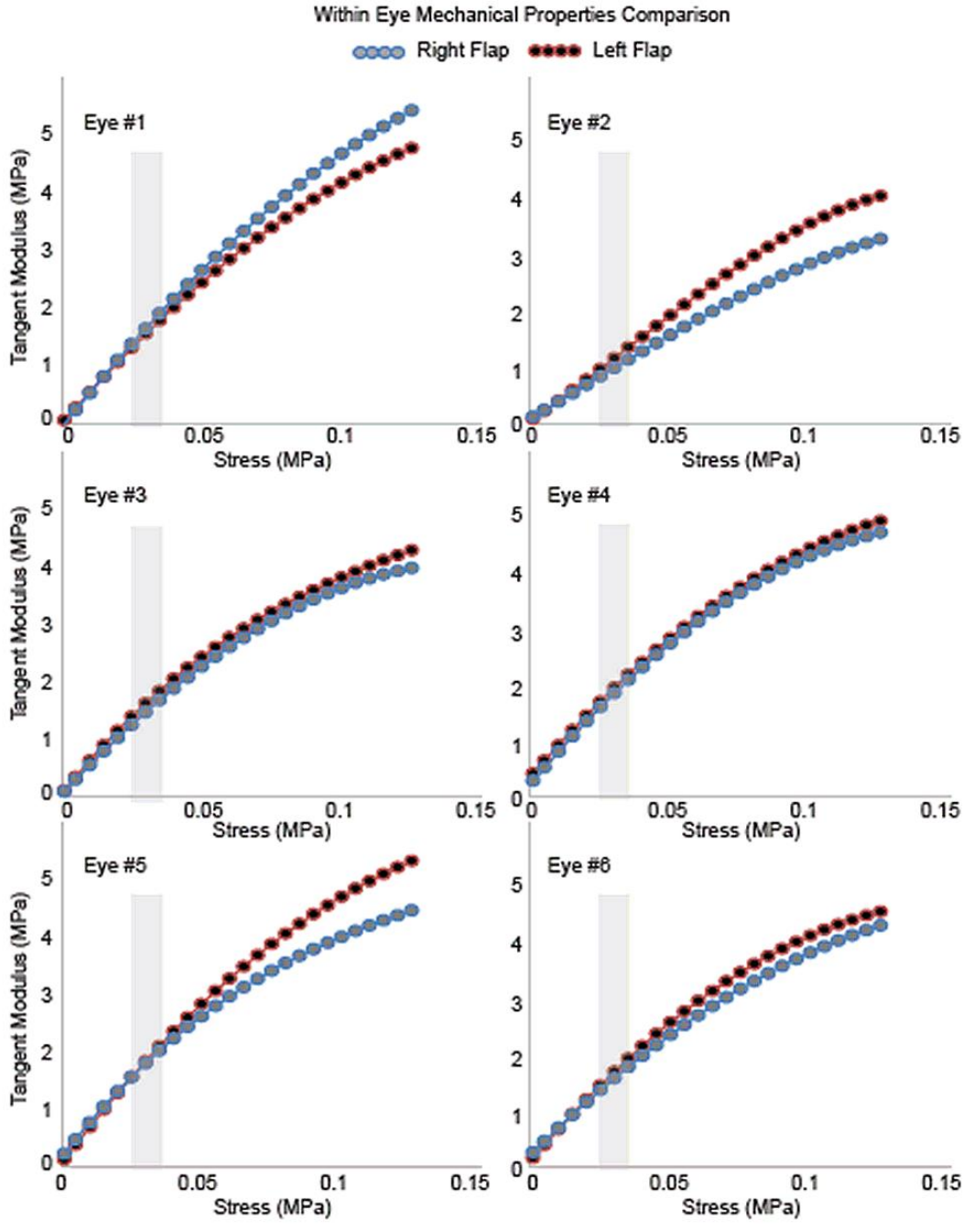

Figure 4.9. The tangent modulus (Et) versus stress (σ) behaviour of paired samples. The tangent modulus vs stress behaviour of right-hand corneal strips vs left-hand strips from 6 corneas are plotted. Both strips were identically treated by soaking in PBS. Gray shaded region represents 0.03 MPa.

(A)

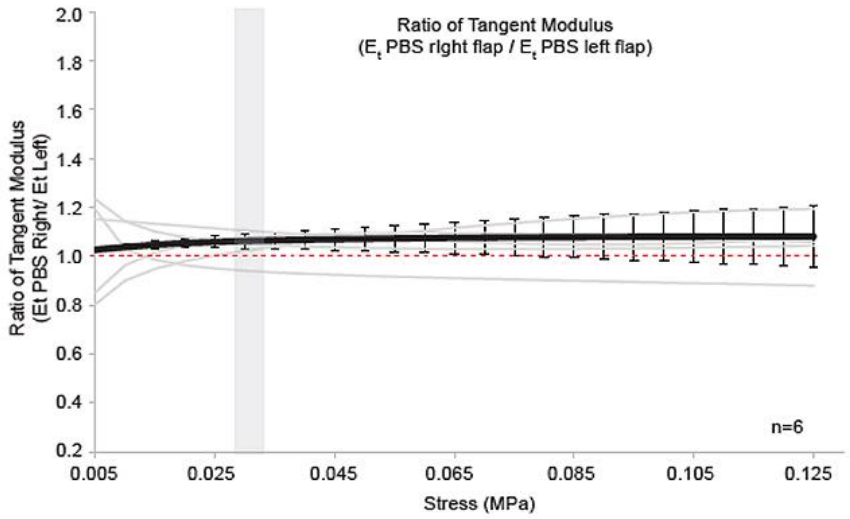
Ratio of Tangent Modulus
(Et PBS right flap / Et PBS left flap)
Ratio of Tangent Modulus
(Et PBS Right/ Et Left)
2.0
1.8
1.6
1.4
1.2
1.0
0.8
0.6
0.4
0.2
n=6
0.005
0.025
0.045
0.065
0.085
0.105
0.125
Stress (MPa)

(B)

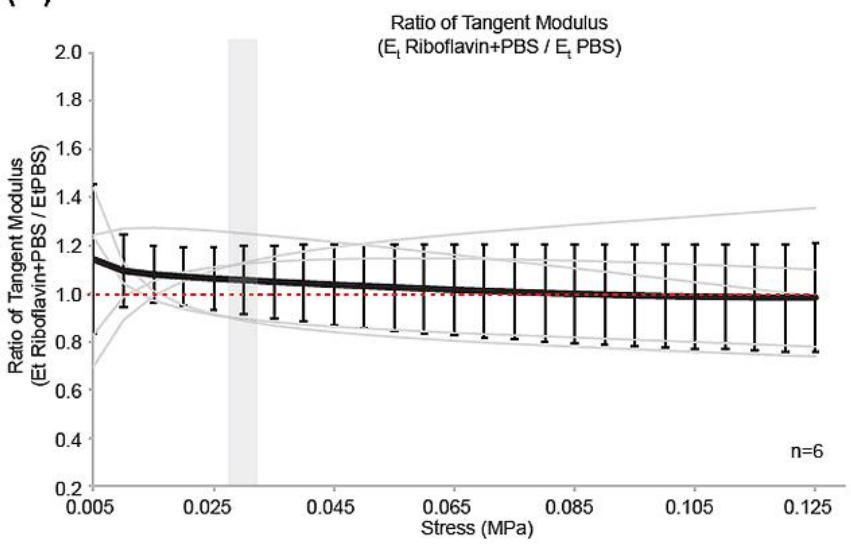
Ratio of Tangent Modulus
(Et Riboflavin+PBS / Et PBS)
Ratio of Tangent Modulus
(Et Riboflavin+PBS / EtPBS)
2.0
1.8
1.6
1.4
1.2
1.0
0.8
0.6
0.4
0.2
n=6
0.005
0.025
0.045
0.065
0.085
0.105
0.125
Stress (MPa)

(Continue)

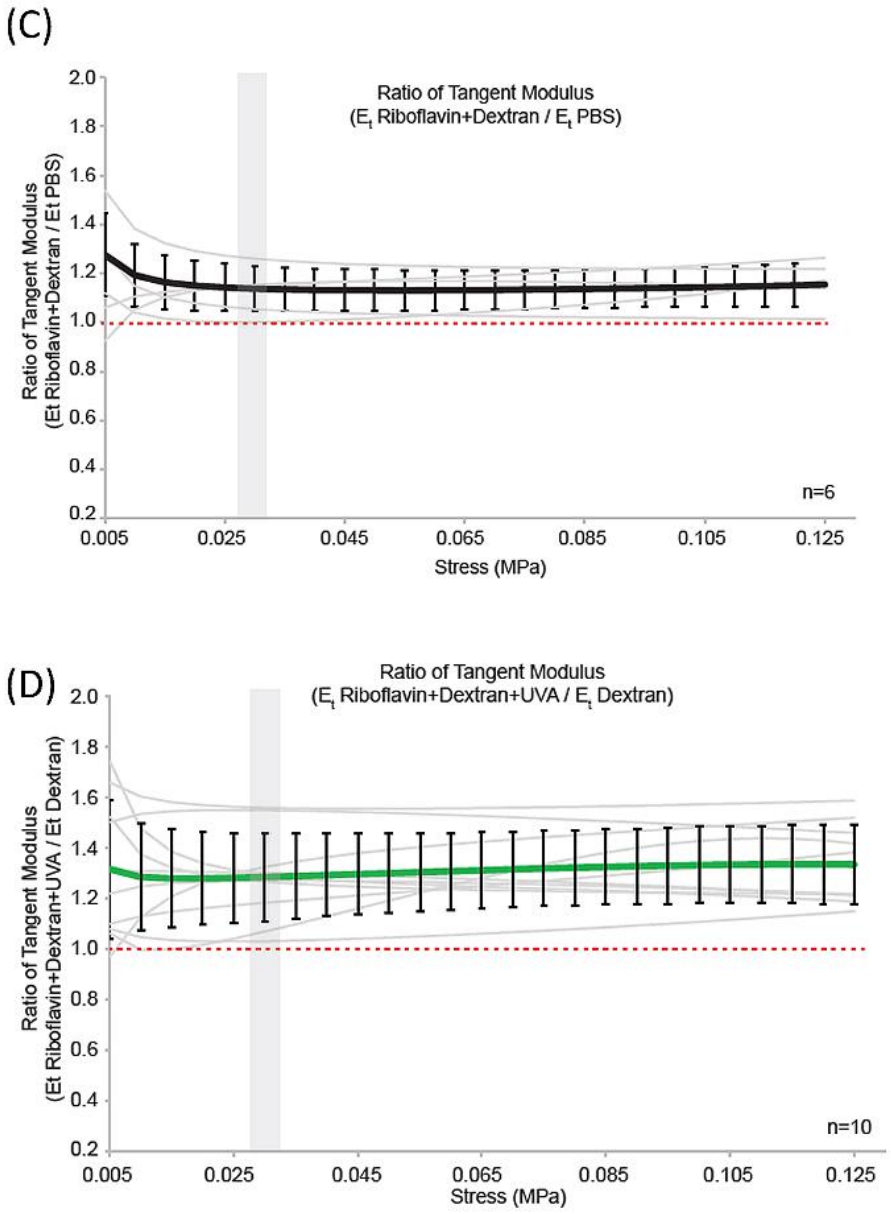

Figure 4.10. The ratio of tangent modulus of porcine eyes. (A) the ratio of tangent modulus between PBS vs PBS (n = 6), (B) riboflavin+PBS vs PBS, (C) riboflavin+dextran vs PBS, and (D) riboflavin+dextran+UVA vs dextran only. Values from each individual cornea pair tested are indicated by gray lines. Average stiffening ratio (mean ± SD) indicated by the bold line and error bars. The red dashed line represented the value of 1 (ie, no difference between paired samples). Gray shaded region represents 0.03 MPa.

Table 4.7. Average stiffening ratio at 0.03 MPa of each group before and after thickness correction.

Parameters	No. of Samples	Average Stiffening Ratio at 0.03 MPa Stress	
		Before Thickness Correction	After Thickness Correction
$Et_{experimental\ PBS}$ / $Et_{control\ PBS}$	6	1.06 ± 0.07	1.04 ± 0.08
$Et_{riboflavin+PBS}$ / Et_{PBS}	6	1.05 ± 0.14	1.04 ± 0.15
$Et_{riboflavin+dextran}$ / Et_{PBS}	6	1.13 ± 0.09*	1.09 ± 0.08
$Et_{riboflavin+dextran+UVA}$ / $Et_{dextran}$	10	1.28 ± 0.17**	1.29 ± 0.16**

Values are presented as mean ± SD.

Asterisks denotes significant differences from control groups, with one asterisk ($p < 0.05$) or two asterisks ($p < 0.01$).

4.4.2. Inflation Testing

To compare the controlled and cross-linked specimens, the material representations have been derived for corneal regions. It can be considered by the numerical parameters α and μ, in which μ is relating to the initial shear modulus and α to the non-linearity. The optimised corneal material parameters α and μ for all specimens using the inverse modelling procedure were generated and shown in Table 4.8. The FE model aimed to provide a match of the displacements measured from the experiment. Experimental and numerical results were provided up to an IOP of 27.25 mmHg, which demonstrated the progressive increase in corneal apex displacement as shown in figure 4.11. The numerical results obtained from the porcine corneas revealed that the corneal material properties were relatively consistent in response to IOP. The comparison showed that the model predictions closely matched the experimental results. A RMS error between the displacement predictions of numerical model and experimental data of was less than 10 % (5.58 ± 1.79%).

By providing a measurement of displacement of the corneal apex with respect to IOP, the pressure readings indicate the response of the cornea. At the IOP of 27.25, the average displacements of corneal

apex were 307 ± 65 μm and 437 ± 63 μm ($p = 0.02$) in CXL and PBS corneas, respectively. Additionally, the average values of μ were 0.02 ± 0.012 and 0.01 ± 0.002 ($p = 0.157$), and the average values of α were 94.3 ± 28.9 and 65.1 ± 15.9 ($p = 0.037$) in CXL and PBS control, respectively.

The corneal stress and strain values were then extracted from the FE models and tangent modulus was calculated from the resulting stress-strain behaviour. All specimens demonstrated an initial low tangent modulus increasing gradually under higher stress. The tangent modulus (Et) versus stress (σ) curve for each cornea was shown in figure 4.12 A. The overall stiffening effect indicated by the ratio of the tangent modulus ($Et_{\text{Cross-linking}}$ / $Et_{\text{Control PBS}}$) was calculated and presented in figure 4.12B. Comparisons concentrated on tangent modulus ratios at a stress of 0.03 MPa, a 43 % ± 24% increase in tangent modulus was observed in the corneas treated with the Dresden protocol ($Et_{\text{Cross-linking}}$: 2.48 ± 0.69 vs $Et_{\text{Control PBS}}$: 1.73 ± 0.40, $p = 0.029$). These data demonstrate that corneal material properties can be well-described using this inflation methods following CXL treatment.

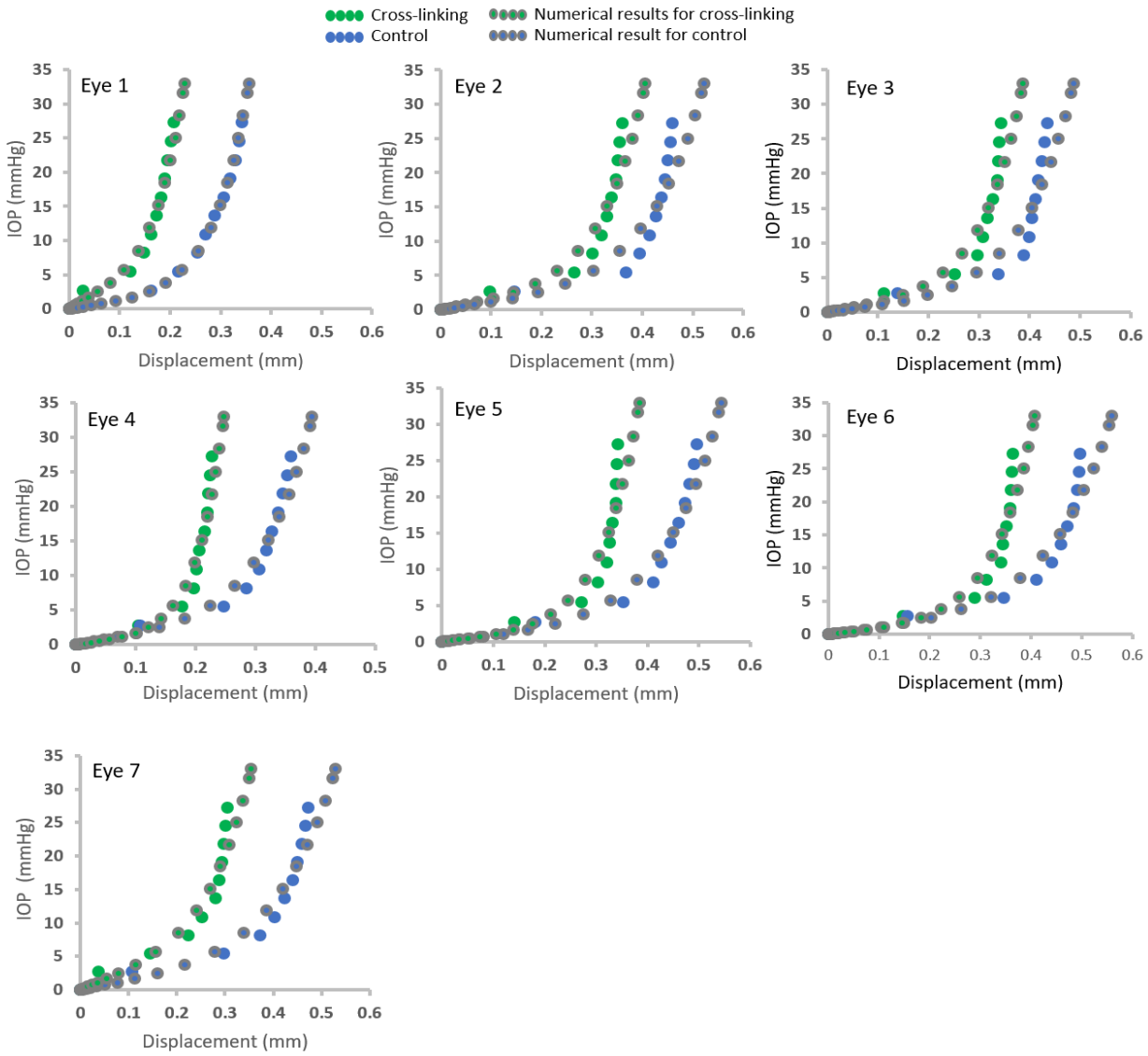

Figure 4.11. IOP-displacement curves of experimental and numerical results for each individual paired eye.

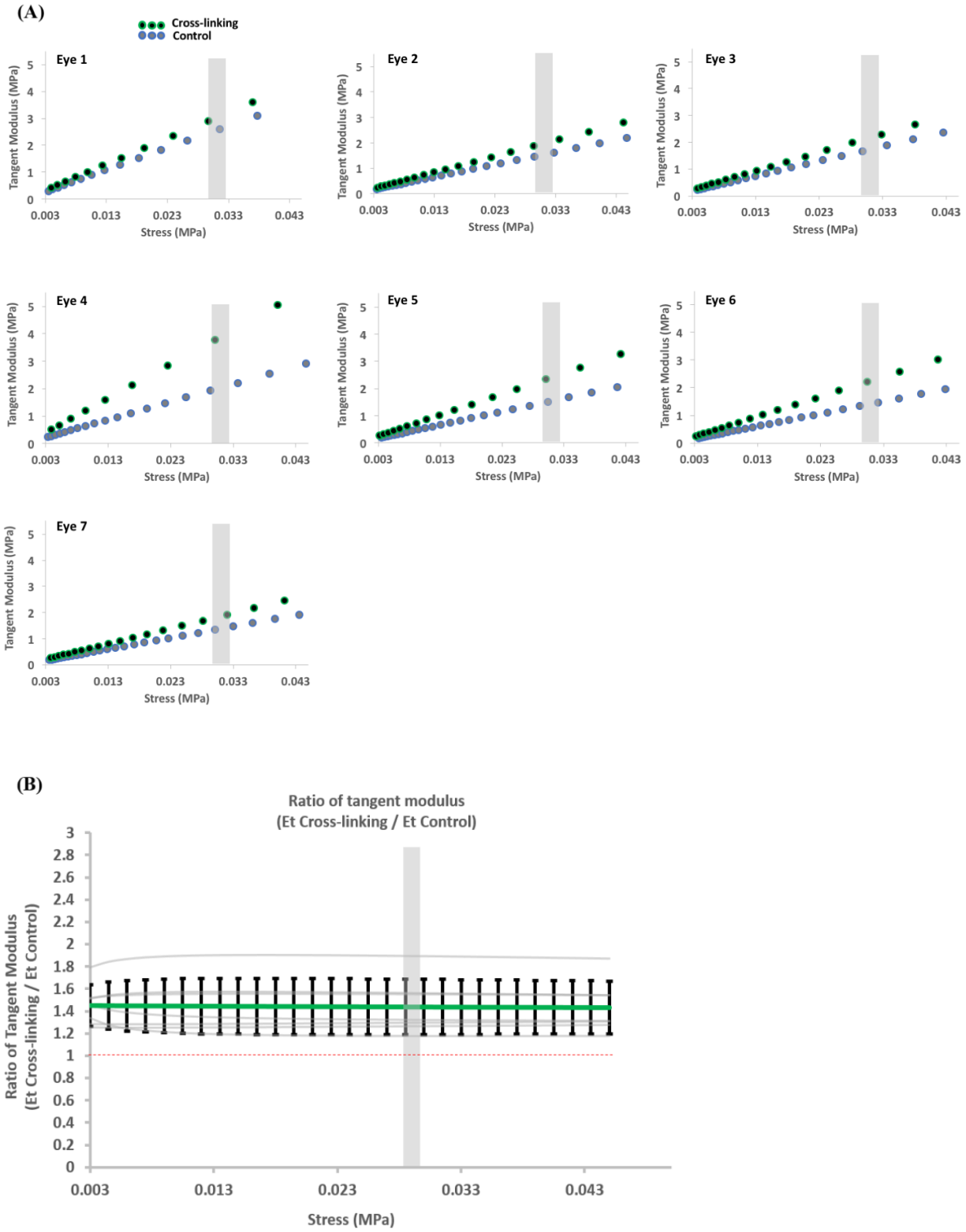

Figure 4.12. The ratio of tangent modulus of paired samples. (A) the tangent modulus vs stress behaviour of right and left eye from 7 paired eyes, (B) the ratio of tangent modulus between control and CXL (n = 7). Values from each individual pair eye tested are indicated by gray lines. Average stiffening ratio (mean ± SD) indicated by the bold line and error bars. The red dashed line represented the value of 1. Gray shaded region represents 0.03 MPa.

Table 4.8. Optimised material parameters α and μ obtained for all specimens from the corneal region using inverse modelling procedure.

	Control (left eye)		CXL (right eye)	
Parameters	**μ**	**α**	**μ**	**α**
EYE1	0.0102	96.07	0.0403	112.54
EYE2	0.0100	57.30	0.0139	73.31
EYE3	0.0091	64.69	0.0126	80.93
EYE4	0.0144	75.52	0.0112	151.22
EYE5	0.0082	57.65	0.0088	90.42
EYE6	0.0096	53.10	0.0085	84.40
EYE7	0.0133	51.36	0.0288	67.62

4.5. Further Investigation of the Stiffening Effects Based on Ultrastructural Evidence Following Dresden CXL

Because the tangent modulus and ultrastructural measurements were performed on the same eye, it was able to directly compare the values obtained (figure 4.13). Comparisons were made between mechanical outcomes measured at 0.03 MPa stress and structural parameters were determined from tissues in relaxed states following Dresden protocol. In this comparison group, both segments within the intra-eye comparisons were treated with dextran. Therefore, dextran-mediated dehydration would not cause difference between the control and experimental segments. At the depth of 80 to 150 μm, collagen fibril diameter increases, inter-fibrillar spacing increases, and collagen fibril density decreases each displayed correlation with tangent modulus increases across the test population (diameter: r^2 =0.23, figure 4.14 A; spacing: r^2 = 0.39, figure 4.14 B; density: r^2 = 0.52, figure 4.13 C). When percentage change on an individual eye basis was plotted, none of the individual ultrastructural parameters were independently indicative of the overall tissue stiffness (figure 4.13D).

However, when considered in combination, the ultrastructural measurements performed better, with a positive correlation of 0.177 (collagen fibril diameter + fibril density – inter-fibrillar spacing, figure 4.13 E). The results should be noted that the ultrastructural changes which were measured in this study do not fully account for the mechanical effects, suggesting that collagen fibril diameter and spacing are not the only aspects of stromal biology affected by UVA/riboflavin CXL.

Because dextran also causes loss of tissue hydration, a mathematical method was used to correct for dehydration effects to identify the true structural changes when evaluating the dextran-mediated effect (Hatami-Marbini and Rahimi 2016). The relationship between thickness (T) and hydration (H) was modelled using the equation: $T = 0.2*e^{0.33*H}$, which has been shown to be effective for these types of calculation (Hatami-Marbini, Etebu et al. 2013). The reduction in thickness followed an exponential decrease in tissue hydration, which was used to calculate the hydration state of the tissues and therefore calculate swelling factors at each depth interval (Table 4.9). Analysis of fibril diameter at each depth interval revealed that although dextran treatment caused a reduction in diameter compared to PBS treatment in the uncorrected data, when correction for swelling factors was included, no significant differences were detected in the distribution curve of collagen fibrils (figure 4.14 C and Table 4.9). The rationale was to compensate for the loss of hydration between and within fibrils and to understand whether the overall framework of ultrastructure has been changed due to dehydrating. The distribution curve after mathematical correction resulted in a higher frequency of larger fibrils and eliminated the statistical variation, indicating that dextran treatment alone has no effect on fibril diameter. Since UVA/riboflavin CXL alone did not affect the thickness significantly comparing to its dextran control, the observed ultrastructural alterations were not correctable and represent the true treatment effect of the corneal CXL procedure (figure 4.15).

The dextran-mediated dehydration not only contributes to overall structure but also the mechanical property changes in the uncorrected data. Therefore, correcting the tangent modulus readings with these thickness measurements removed the apparent dextran effects, whereas residual stiffening effect was still observed in the samples treated with the Dresden protocol after correction (figure 4.14 A and 4.14 B).

However, the mathematical method used for correcting hydration is not applicable to the outcomes of inflation test. As the Thickness-Hydration (T-H) equation was generated by restricted controlled thickness and hydration following tensile test. There are many parameters involved in the specimen preparation for inflation procedure. Therefore, in the experimental design in inflation, this study only performed the PBS and full Dresden as two comparison groups. Although the comparison groups are different in two mechanical tests (CXL vs dextran and CXL vs PBS for tensile and inflation, respectively), it was possible to compare the outcome measurements (Et) from inflation and tensile tests at the same stress (0.03 MPa). The measurements of $Et_{\text{Cross-linking}}$ were 2.09 ± 0.17 and 2.48 ± 0.69 at 0.03 MPa from tensile and inflation, respectively. The outcome measured by tensile and inflation testing did not show statistically differences ($p = 0.187$).

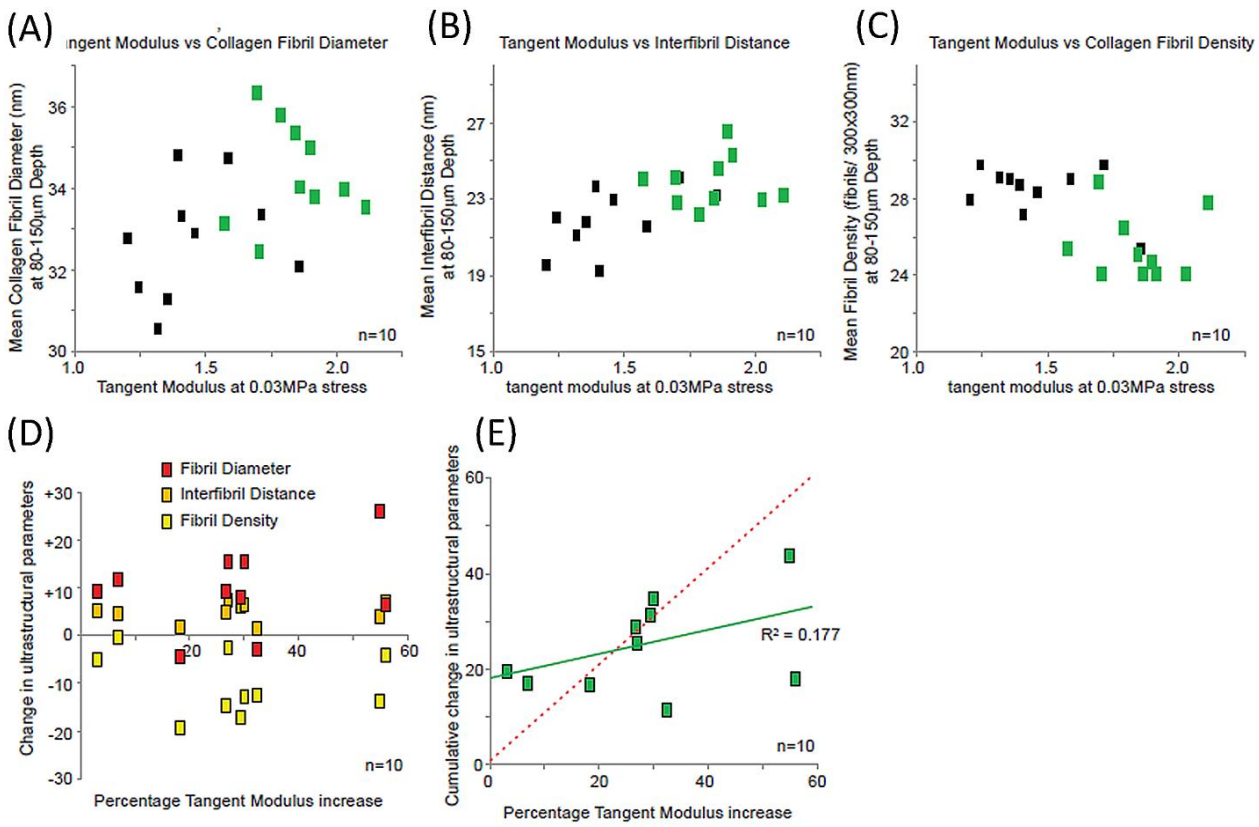

Figure 4.13. Correlation between ultrastructural parameters and tangent modulus following Dresden. Tangent modulus at 0.03 MPa versus (A) collagen fibril diameter, (B) inter-fibrillar spacing, and (C) collagen fibril density. Black boxes = dextran treated eyes; green boxes = riboflavin+dextran+UVA treated eyes. (D) Percentage change in tangent modulus versus percentage change in each ultrastructural parameter. Each box represents the measurements from one eye for either fibril diameter (red), inter-fibrillar distance (orange), or fibril density (yellow). (E) Percentage change in tangent modulus plotted against the cumulative effects of percentage change in fibril diameter + inter-fibrillar spacing – fibril density. Each box represents one eye. Green line = linear line of best fit; red dotted line = 100% correlation.

Table 4.9. Parameters Used in Correction of the Collagen Fibril Radius Distribution Curves.

Depth / Correction Parameter	0-50 μm	80-150 μm	200-250 μm	300-350 μm	400-450 μm
Decreased % of collagen diameter	10.41%	12.83%	14.12%	4.18%	3.01%
Decreased % of inter-fibillar spacing	29.03%	28.06%	27.39%	27.70%	26.91%
Decreased % of collagen diameter on overall loss	26.39%	31.01%	34.02%	13.11%	10.06%
Decreased % of inter-fibillar spacing on overall loss	73.61%	68.99%	65.98%	86.89%	89.94%
Hydration loss % of collagen diameter	4.46%	5.24%	5.75%	2.21%	1.70%
Hydration loss % of inter-fibillar spacing	12.45%	11.67%	11.16%	14.70%	15.21%
Remaining hydration % of collagen diameter	95.54%	94.76%	94.25%	97.79%	98.30%
Remaining hydration % of inter-fibillar spacing	87.55%	88.33%	88.84%	85.30%	84.79%
Swelling factor for correction of distribution of collagen diameter	1.05	1.06	1.06	1.02	1.02

Overall tissue dehydration % = 16.91%

(T: 1.047mm thickness/ H: 5.01; T: 0.791mm/ H: 4.16)

Thickness-Hydration (T-H) relationship of porcine cornea: T = 0.2*e^(0.33*H)

Swelling factor: 1 / Remaining tissue hydration

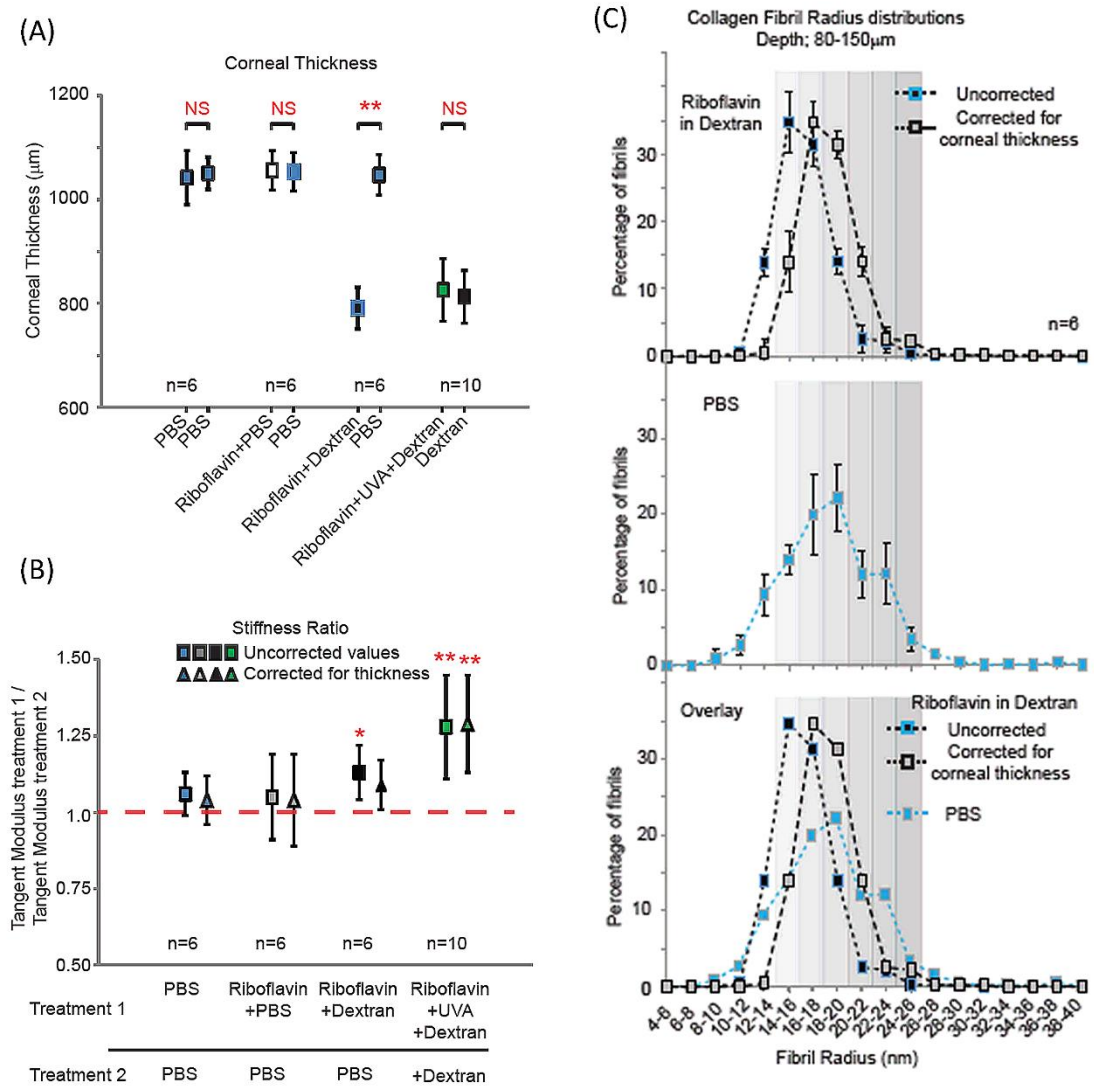

Figure 4.14. The dehydration effect with and without correction for tissue thickness on ultrastructural changes and mechanical outcomes. (A) Average thickness measurement of each comparison group after treatment. (B) The stiffening ratio at 0.03 MPa with and without correction for tissue thickness changes. (C) Collagen fibril diameter distributions plotted as either uncorrected values from the riboflavin+dextran group (top panel, black filled squares) or corrected for dehydration (top panel, gray filled squares) or its corresponding PBS control (middle panel, blue filled squares). Traces are shown overlaid in bottom panels. Gray filled background added to aid visualization. Value in (A) and (B) denote mean ± SD. Red asterisks denote significant differences from control groups, with one asterisk ($p < 0.05$) or two asterisks ($p < 0.01$). NS = not significant.

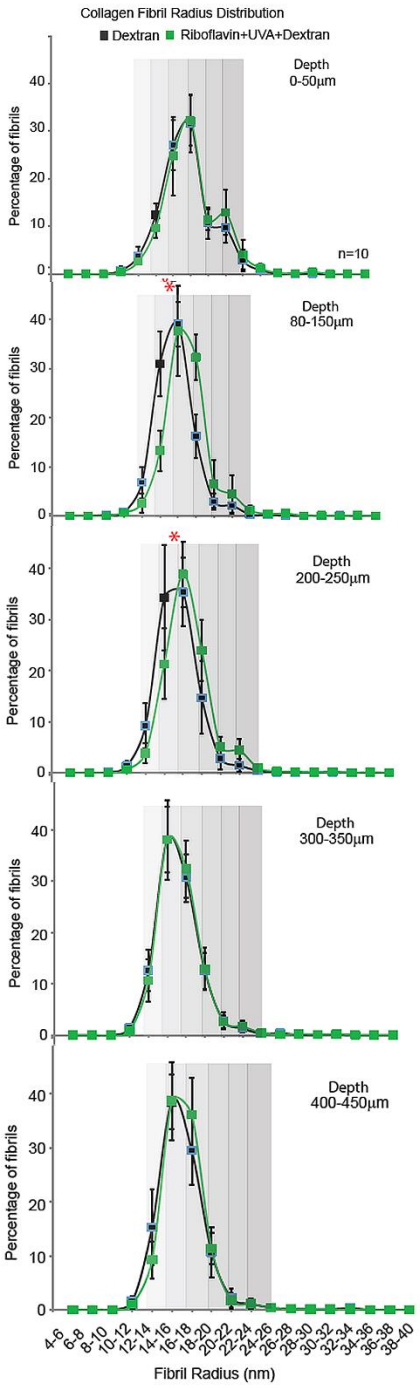

Figure 4.15. Collagen fibril diameter distribution curve of corneal CXL and its corresponding dehydrated control. Collagen fibril diameter distribution curve of riboflavin+dextran+UVA (green boxes) and its dextran control (black boxes) at each depth interval. Gray filled background added to aid visualization. Red asterisks denote significant differences from control groups, with one asterisk ($p < 0.05$) or two asterisks ($p < 0.01$).

4.6. Mass Spectrometry and Protein Analysis

To determine if PGs are involved in UVA/riboflavin CXL, liquid chromatography-mass spectrometry (LC-MS) was used to analyse the SDS-gel samples. Most of proteins were observed stacking at the top of separating gel after CXL (in lane C, figure 4.16) in Coomassie blue staining. It may be due to the large molecular weight of cross-linked proteins which could not be separated into SDS gel. The proteins that may be involved in CXL were around 50 kDa, and from 115 kDa to 240 kDa as shown in lane (A) in figure 4.16. Therefore, these proteins were analysed using LC-MS and listed in Table 4.10 and 4.11. Collagen I, decorin, keratocan, lumican and minecan were all detected, suggesting these proteins may involve in UVA/riboflavin CXL. Therefore, we further studied on these LC-MS-detected PGs by using Chondrotinase ABC and Keratanase which remove keratin sulfate (KS) and chondroitin sulfate (CS) to examine whether these GAGs were affected during CXL process (figure 4.16). The results showed that the amount of proteins larger than 140 kDa was reduced in Coomassie blue-stained SDS gel after enzyme digestion (figure 4.16 D-F), indicating that these cross-linked proteins were glycosylated, which may result in the conformational changes in proteins (Zhang, Conrad et al. 2011). Furthermore, the specific PG core proteins were examined by performing western blot (figure 4.17). Decorin was not observed in large molecular size (dimers or trimers) but was detected at around 115 kDa and 240 kDa after CXL. Lumican and keratocan both showed reduced amount at around or less than 50 kDa, comparing to their PBS and riboflavin+dextran control groups. Although it showed that dextran caused a slightly smeared protein pattern in Coomassie blue-stained SDS gel (figure 4.16 B), it did not induce further protein interactions on PG core proteins (figure 4.17).

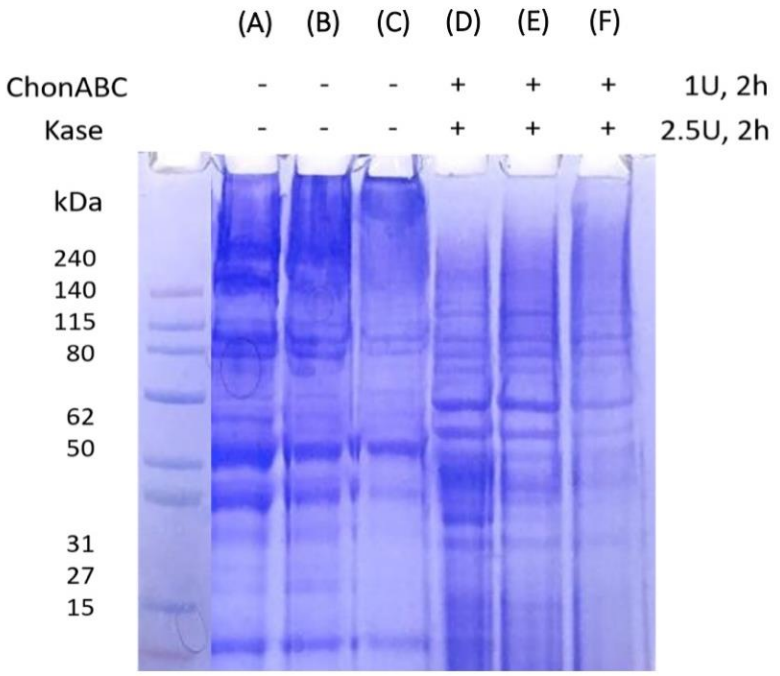

Figure 4.16. Coomassie blue staining of cross-linked and non-cross-linked ECM proteins from whole cornea *ex vivo*. (A, D) PBS, (B, E) 0.1% riboflavin in 20% dextran, (C,F) full Dresden protocol. ChonABC = Chondrotinase ABC; Kase = Keratanase.

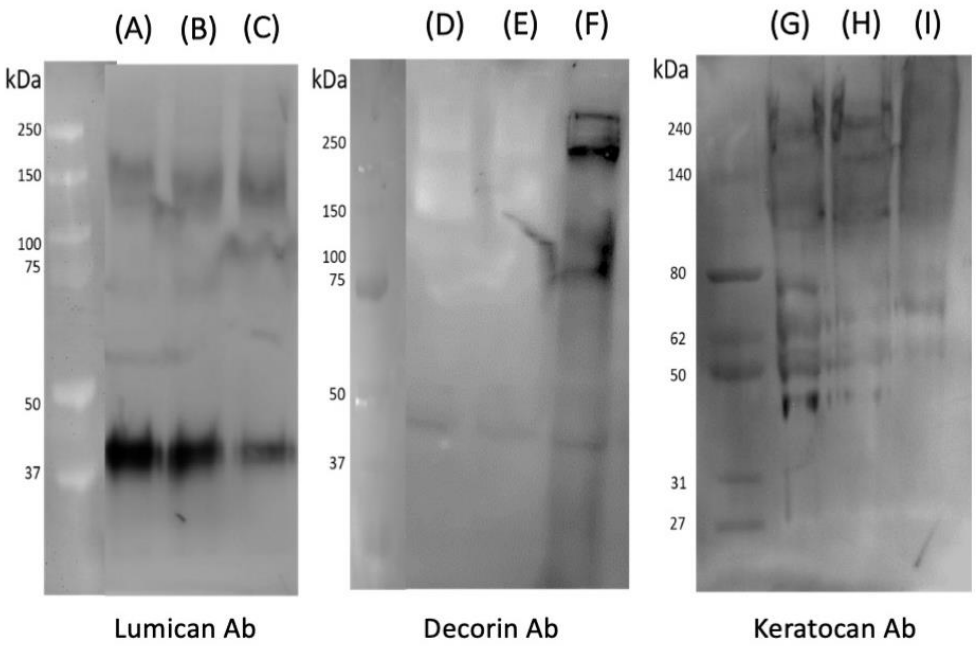

Figure 4.17. Western blot patterns of PG core proteins from cross-linked and non-cross-linked whole cornea *ex vivo*. (A,D,G) PBS, (B,E,H) 0.1% riboflavin in 20% dextran, (C,F,I) full Dresden protocol. Ab = antibody.

Table 4.10. ECM proteins with molecular weight around 115-250 kDa identified by LC-MS.

Identify ECM proteins/PGs	Molecular weight (kDa)	Total peptide spectral counts	Unique peptides
Collagen alpha-1(I) chain	138.9	21	GPPGPMGPPGLAGPPGESGR GSPGADGPAGAPGTPGPQGIAGQ GFPGLPGPSGEPGK GQAGVMGFPGPK DGEAGAQGPPGPAGPAGER GETGPAGPTGPVGPVGAR SGDRGETGPAGPTGPVGPVGAR GVPGPPGAVGPAGK
Collagen alpha-2(I) chain	137.9	19	GELGPVGNPGPAGPAGPR GEPGPAGSVGPVGAVGPR GEVGPAGPNGFAGPAGSAGQP GPKGENGIVGPTGPVGAAGPSGPNGPPGPAGSR
Collagen alpha-1(VI) chain	108.5	5	VPSYQALLR IALVITDGR GLEQLLVGGSHLK VFSVAITPDHLEPR
Decorin	39.9	35	GELGPVGNPGPAGPAGPR GEPGPAGSVGPVGAVGPR GEVGPAGPNGFAGPAGSAGQP GPKGENGIVGPTGPVGAAGPSGPNGPPGPAGSR
Keratocan	40.4	20	NLMQLNMAK LLDNAFQR SLEQLQLAR
Lumican	38.7	11	SLVDLQLTNNK ISNIPDEYFK ILGPLSYSK SVPMVPPGIK

Table 4.11. ECM proteins with molecular weight around or less than 50 kDa identified by LC-MS.

Identify ECM proteins/PGs	Molecular weight (kDa)	Total peptide spectral counts	Unique peptides
Minecan	34.2	23	DFADIPNLR LPVLPPK RLPIGSYI LTLFNAK
Decorin	39.9	19	GELGPVGNPGPAGPAGPR GEPGPAGSVGPVGAVGPR GEVGPAGPNGFAGPAGSAGQP GPKGENGIVGPTGPVGAAGPSGPNGPPGPAGSR
Keratocan	40.4	5	NLMQLNMAK LLDNAFQR SLEQLQLAR
Lumican	38.7	7	SLVDLQLTNNK ISNIPDEYFK ILGPLSYSK SVPMVPPGIK

4.7. Summary of CXL Impact on Extracellular Matrix

The transparency of the human cornea is known to be regulated by the uniform distribution of the collagen fibrils, and hydration is maintained by PGs (Meek and Knupp 2015). Lumican, keratocan, and mimecan are PG core proteins to carry a keratin sulfate chain, where decorin and biglycan carry a chondroitin sulfate chain (Dunlevy, Beales et al. 2000, Ho, Harris et al. 2014). Few studies have investigated the effects of CXL on PGs in cornea (Zhang, Conrad et al. 2011, Akhtar, Almubrad et al. 2013, Sharif, Fowler et al. 2018). It is reported that the expression levels of PG core proteins can be upregulated following CXL in an *in vitro* model (Sharif, Fowler et al. 2018). In addition, keratocan and lumican may interact with collagen in a different manner compared to mimecan and decorin (Zhang, Conrad et al. 2011). CXL appears to be an effective treatment in modulating PGs. However, no evidence has proven that the effect of CXL on PGs leads to the strengthening effect to the corneal ECM.

This study demonstrated the correlation between mechanical property and ultrastructure. The combination of ultrastructural parameters including collagen fibril diameter, density and inter-fibrillar spacing result in the overall tissue stiffness. However, effects on other stromal proteins and particularly the interactions of collagen with PGs could also be contributing to the stiffening. PGs within the corneal stroma have been proposed to play a pivotal role in regulating the fibril-fibril spacing and hydration-dehydration properties (Hahn and Birk 1992), but the dehydration-induced decrease in inter-fibrillar spacing has prevented us from being able to determine the sole effect of CXL on proteoglycans within the current experimental system.

Together with the FTIR results and protein analysis, dextran induces an increase in C-O stretching force compared with PBS controls, indicating that dextran may result in structural changes. However, dextran did not cause additional protein interactions on PGs or collagens according to the western blot analysis and Coomassie blue staining. Indeed, tissue hydration states have been reported to affect the stiffness of CXL treatment (Hatami-Marbini and Rahimi 2016); therefore, hydration states and the osmolarity during CXL procedure could be important factors to consider its contribution on PGs

and the resulting stiffening effect. Further study is warranted to determine and better understand the ultrastructural alterations and protein interactions induced by CXL when applied on keratoconic corneas. Continuation of these studies will pave the way for personalised CXL treatment that will ultimately benefit the patients with keratoconus.

4.8. Evaluation of Conventional CXL and Accelerated CXL in Clinical Trials by Meta-Analysis

A total of 1047 unique reports were retrieved from online search. There was no disagreement about the number of eligible studies for inclusion between authors. The current study identified 9 studies examining 603 eyes of 571 patients which were included in the meta-analysis in this review. Of these, two compared the effect of conventional Dresden protocol (3 mW/cm^2 irradiance for 30 min) with accelerated protocol (9 mW/cm^2 irradiance for 10 min) (Brittingham, Tappeiner et al. 2014), two compared the effect of conventional protocol (3 mW/cm^2 irradiance for 30 min) with accelerated protocol (18 mW/cm^2 irradiance for 5 min) (Chow, Chan et al. 2015, Hashemi, Miraftab et al. 2015), three compared the effect of conventional protocol (3 mW/cm^2 irradiance for 30 min) with accelerated protocol (30 mW/cm^2 irradiance for 3 min) (Hashemian, Jabbarvand et al. 2014, Tomita, Mita et al. 2014, Choi, Kim et al. 2017), two compared the effect of conventional protocol (3 mW/cm^2 irradiance for 30 min) with accelerated protocol (30 mW/cm^2 irradiance for 4min) (Woo, Iyer et al. 2017). The details of all studies included in the meta-analysis was reported in Table 4.12.

This study identified a further eight studies that compared the effect of conventional CXL with accelerated CXL (Kanellopoulos 2012, Sherif 2014, Chow, Chan et al. 2015, Shetty, Pahuja et al. 2015, Cummings, McQuaid et al. 2016, Kortuem, Vounotrypidis et al. 2017, Sadoughi, Einollahi et al. 2018, Zaheer, Khan et al. 2018). However, these studies were excluded from this review because it is not possible to obtain separate data for the mean change of the clinical effects of the accelerated CXL and conventional CXL. Furthermore, two studies were also excluded from this review. In one article, the follow up data were given as a mean of 13.9 ± 6.3 months and the follow up data of 12 months was not available (Ng, Chan et al. 2016). In the second article, the follow up data were given

as a mean of 20.5 ± 6.3 months for accelerated CXL and 20.5 ± 5.6 for conventional CXL, but the follow up data of 12 months was not available (Males and Viswanathan 2018). The methodological quality assessment of the included studies showed that 100% of the articles were of high quality.

Table 4.12. The baseline characteristic of trials included in the meta-analysis.

Author	Country	Study design	Eyes (n)		Gender (male %)		Mean age (y)		Intensity (mW/cm^2)		Total energy (J/cm2)		Riboflavin solution	
			C	A	C	A	C	A	C	A	C	A	C	A
Brittingham et al. (2014)	Switzerland	RCS	81	50	NA	NA	28.62 ±10.53	26.14±10.25	3 for 30 min	9 for 10 min	5.4	5.4	0.1% riboflavin with 20% dextran	0.1% riboflavin with 20% dextran
Choi et al. (2017)	South Korea	RCT	15	13	60	61.5	25.6±3.7	23.7±4.4	3 for 30 min	30 for 3 min 40 sec	5.4	6.6	0.1% riboflavin with 20% dextran	0.1% riboflavin with HPMC
Chow et al. (2015)	China	PCS	19	19	94.7	63.16	27.8±10.9	26.3±3.7	3 for 30 min	18 for 5 min	5.4	5.4	0.1% riboflavin with 20% dextran	0.1% riboflavin with 20% dextran
Cinar et al. (2014)	Turkey	PCS	13	13	46.2	15.4	17±2.7	18.8±4.5	3 for 30 min	9 for 10 min	5.4	5.4	0.1% riboflavin with 20% dextran	0.1% dextran free riboflavin
Hashemi et al. (2015)	Iran	RTC	31	31	NA	NA	NA	NA	3 for 30 min	18 for 5 min	5.4	5.4	0.1% riboflavin with 20% dextran	0.1% riboflavin with 20% dextran
Hashemian et al. (2014)	Iran	RCT	76	77	50	41.6	22.3±4	22.6±4	3 for 30 min	30 for 3 min	5.4	5.4	0.1% riboflavin with 20% dextran	0.1% riboflavin with 20% dextran
Jiang et al. (2017)	China	PCS	36	36	58.06	48.15	26.86±5.28	25.03±5.2	3 for 30 min	30 for 4 min	5.4	7.2	0.1% riboflavin with 20% dextran	0.1% riboflavin with HPMC
Tomita et al. (2014)	Japan	PCS	18	30	NA	NA	30.83±5.2	31.17±5.5	3 for 30 min	30 for 3 min	5.4	5.4	0.1% riboflavin with 20% dextran	0.1% riboflavin with HPMC
Woo et al. (2017)	Singapore	RCT	29	47	72.4	78.7	29±7	28±7	3 for 30 min	30 for 4 min	5.4	7.2	0.1% riboflavin with 20% dextran	0.1% dextran free riboflavin

PCS = Prospective cohort study; RCS = Retrospective cohort study; RCT = Randomized controlled trial; C = conventional CXL; A = accelerated CXL

4.8.1. Primary Outcomes

4.8.1.1. Maximum Keratometry (Kmax)

The data related the mean change of Kmax at 12 months were pooled across six studies (Brittingham, Tappeiner et al. 2014, Hashemian, Jabbarvand et al. 2014, Tomita, Mita et al. 2014, Chow, Chan et al. 2015, Jiang, Jiang et al. 2017, Woo, Iyer et al. 2017). The meta-analysis results are presented in figure 5.2. No significant difference was observed between the two treatment methods (SMD 0.07; 95% CI, -0.86 to 1.00; p = 0.21; figure 4.18). There was significant heterogeneity between studies (p < 0.001, I^2 = 96%). Each study used different UVA intensities, one study (Brittingham, Tappeiner et al. 2014) used 9 mW/cm^2 for 10 min and the other study (Chow, Chan et al. 2015) used 18 mW/cm^2 for 5 min. The rest of four studies used 30 mW/cm^2 for 3 or 4 minutes in their accelerated CXL treatment arm (Hashemian, Jabbarvand et al. 2014, Tomita, Mita et al. 2014, Jiang, Jiang et al. 2017, Woo, Iyer et al. 2017). However, subgroup analysis for those four studies did not reveal significant difference between two groups with severe heterogeneity (SMD -0.39; 95% CI, -1.47 to 0.69; p = 0.48; I^2 = 95%).

4.8.2. Secondary Outcomes

4.8.2.1. Uncorrected Visual Acuity (UCVA)

The mean change of UCVA at 12 months was evaluated in three studies (Hashemian, Jabbarvand et al. 2014, Chow, Chan et al. 2015, Jiang, Jiang et al. 2017). The meta-analysis revealed no significant different between both groups (SMD -0.01; 95% CI, -0.04 to 0.0; p = 0.79; figure 4.19). There was substantial heterogeneity between studies (p < 0.001, I^2 = 89%). This heterogeneity was attributed to the one study (Chow, Chan et al. 2015). This study used accelerated protocol with intensity of 18mW/cm^2 for 5 min, while the other two studies used accelerated protocol with intensity of 30mW/cm^2 for 3 min (Hashemian, Jabbarvand et al. 2014, Jiang, Jiang et al. 2017). Subgroup analysis of these two studies showed that mean change of UCVA was significantly lower in accelerated CXL (30mW/cm^2 for 3 min) than in conventional CXL (SMD -0.48; 95% CI, -0.74 to -2.1; p < 0.001).

4.8.2.2. Corrected Distant Visual Acuity (CDVA)

The mean change of CDVA at 12 months in patients treated with conventional CXL and accelerated CXL were pooled across three studies. As shown in figure 4.20, analysis revealed significant difference favoring accelerated CXL (SMD -1.74; 95% CI, -3.35 to -0.12; p = 0.04). There was a substantial heterogeneity between studies (p < 0.001; I^2 = 96%).

4.8.2.3. Minimum Keratometry (Kmin)

Three studies reported Kmin data at 12 months (Brittingham, Tappeiner et al. 2014, Chow, Chan et al. 2015, Woo, Iyer et al. 2017). Analysis found no significant difference between the two treatment arms with severe heterogeneity (SMD = 0.89; 95% CI: -0.23 to 2.02; p = 0.12; I^2 = 93%; figure 4.21). This heterogeneity was attributed to one study that used irradiation intensity of 18 mW/cm^2 for 5 min in accelerated CXL arm (Chow, Chan et al. 2015). After removal, the pool estimate of the other two studies (Brittingham, Tappeiner et al. 2014, Woo, Iyer et al. 2017), that used irradiation intensity of 30 mW/cm^2 for 3 or 4 min in their accelerated CXL treatment arm, didn't favor any treatment arm with no evidence of heterogeneity (SMD = 0.12; 95% CI: -0.16 to 0.40; p = 0.39; I^2 = 0%).

4.8.2.4. Spherical Equivalence (SE)

Three studies reported SE data at 12 months. Analysis found no significant difference between the two treatment arms with severe heterogeneity (SMD = 0.57; 95% CI: -0.38 to 1.52; p = 0.24; I^2 = 87%; Fig 4.22). This heterogeneity was attributed to one study that used irradiation intensity of 18 mW/cm^2 for 5 min in accelerated CXL arm (Chow, Chan et al. 2015). After removal, the pool estimate of the other two studies (Tomita, Mita et al. 2014, Jiang, Jiang et al. 2017), that used irradiation intensity of 30 mW/cm^2 for 3 or 4 min in their accelerated CXL treatment arm, did not favor any treatment arm with no evidence of heterogeneity (SMD = 0.04; 95% CI: -0.32 to 0.40; p = 0.83; I^2 = 0%).

4.8.2.5. Mean Keratometry (Kmean)

The data related to Kmean at 12 months was reported in only two studies (Tomita, Mita et al. 2014, Woo, Iyer et al. 2017). Analysis revealed no significant difference between the two treatment arms with significant heterogeneity (SMD = 0.27; 95% CI: -0.53 to 1.08; p = 0.51; I^2 = 78%; Fig 4.23).

4.8.2.6. Central Corneal Thickness (CCT)

Only one study reported the data of CCT at 12 months (Chow, Chan et al. 2015). Analysis revealed no significant difference between the two treatment arms (SMD = 0.13; 95% CI: 0.13 to 0.77; p = 0.68).

4.8.2.7. Sensitivity Analysis and Publication Bias

The potential publication bias investigated by funnel plots was generated based on the results of Kmax analysis. The plot did not reveal any obvious asymmetry, suggesting no evidence for publication bias. The robustness of the results was assisted by sensitivity analysis, which revealed the effect of each individual study predominantly affected the overall SMD in each clinical outcome.

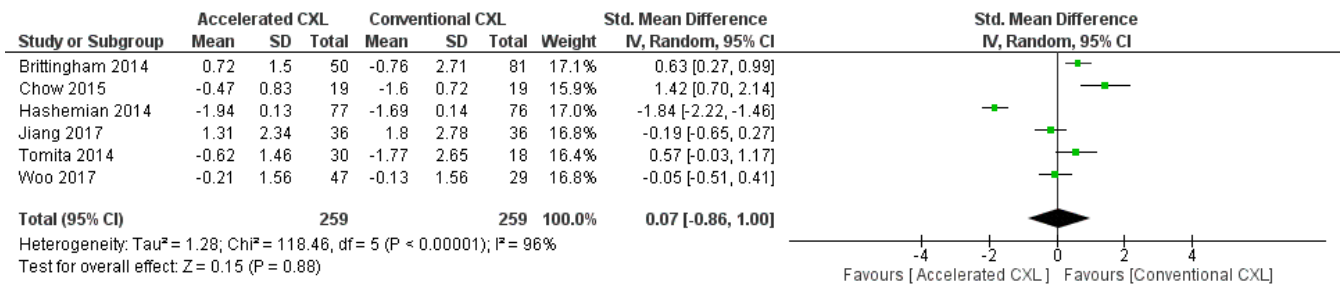

Figure 4.18. Table and forest plot illustrating the standard mean differences for mean change of Kmax for accelerated CXL and conventional CXL after 12 months of follow-up.

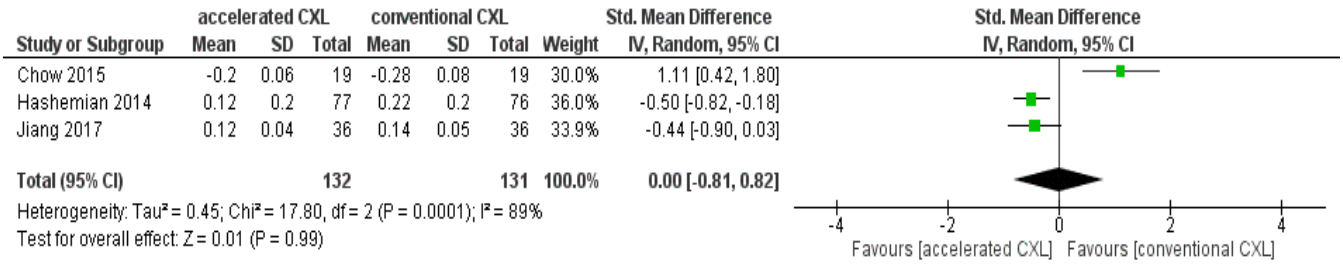

Figure 4.19. Table and forest plot illustrating the standard mean differences for mean change of UCVA for accelerated CXL and conventional CXL after 12 months of follow-up.

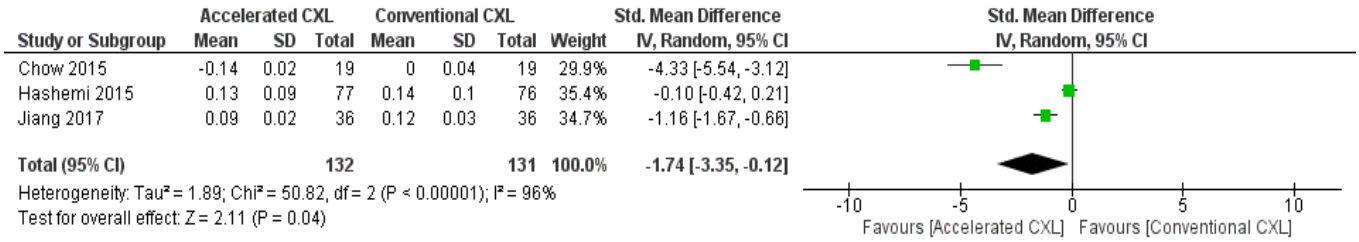

Figure 4.20. Table and forest plot illustrating the standard mean differences for mean change of CDVA for accelerated CXL and conventional CXL after 12 months of follow-up.

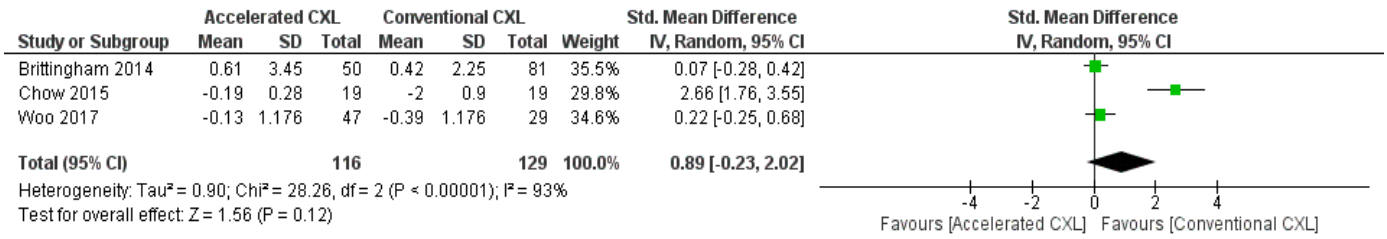

Figure 4.21. Table and forest plot illustrating the standard mean differences for mean change of Kmin for accelerated CXL and conventional CXL after 12 months of follow-up.

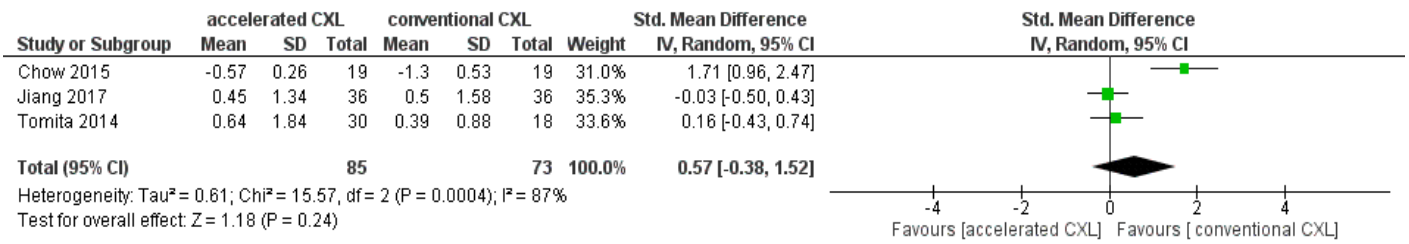

Figure 4.22. Table and forest plot illustrating the standard mean differences for mean change of MRSE for accelerated CXL and conventional CXL after 12 months of follow-up.

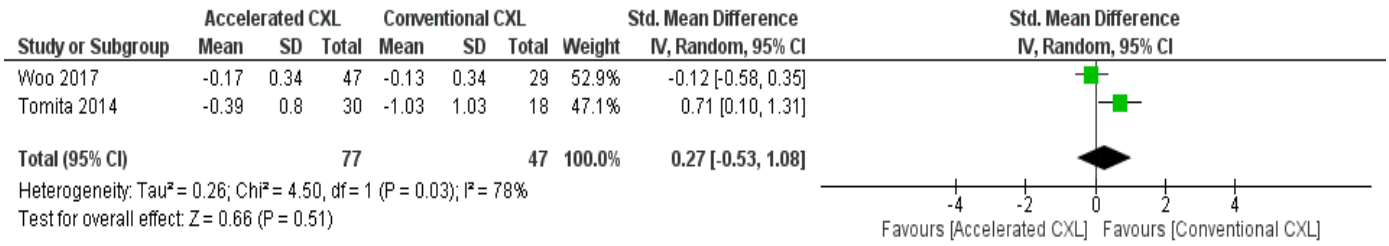

Figure 4.23. Table and forest plot illustrating the standard mean differences for mean change of Kmean for accelerated CXL and conventional CXL after 12 months of follow-up.

4.9. Summary of Meta-Analysis

Both conventional and accelerated protocols showed promising for slowing or halting keratoconus. However, the optimal treatment modality regarding the duration and dosage is still under investigation. This study aimed to assemble the efficacy between the different protocols. From the current meta-analysis, pooled data showed equivalent effect in halting Kmax deterioration and stabilising corneal topography for the treatment of conventional and accelerated CXL in progressive keratoconus at one year. In terms of visual acuity outcomes, the current study found improvement in CDVA for accelerated protocol but equal results in UCVA. With regard to secondary outcome parameters including Kmin, Kmean and MRSE, conventional and accelerated protocols appear to achieve similar results. The findings demonstrated that the two modalities show equivalent efficacy at 12 months after the treatment.

Chapter 5. Discussion and Conclusions

5.1. Overview

A substantially higher number of eyes has been reported to derive the statistical differences when applying tensile testing (Schumacher, Oeftiger et al. 2011, Wernli, Schumacher et al. 2013). In the current study, porcine tissues were used to investigate the intra-animal difference in mechanical response, and between the left and right eyes. Tensile test was performed and compared within individual cornea to avoid the variations, whereas inflation was performed on paired eyes. In order to characterise the biomechanical behaviour over the entire cornea, whole eye globes were used in generating the corneal FE model. The IFE method used to optimise material behaviour parameters from the raw data was found to provide an adequate fit between the experimental and numerical pressure-displacement behaviour.

The current study characterised how corneal mechanical properties relate to ultrastructural changes following the Dresden protocol treatment and identified the contribution of the different components of the protocol to observed effects. In addition, this study evaluated different protocols which were performed in clinical trials and showed equivalent effects of Dresden and accelerated methods on halting progression of keratoconus at one year. Specifically, the data demonstrate that the increases in corneal stiffness measured following Dresden protocol treatment arise from a combination of dextran-mediated dehydration and UVA/riboflavin induced new bond formation and depth-dependent increases in collagen fibril diameter. However, dextran did not cause additional interactions between PGs and collagens.

5.2. The Effect of Dextran on Tensile Measurements

Uniaxial tensile test is the most commonly used technique in a comparative study following CXL treatment. Using this technique, the stiffening effect of cross-linked porcine cornea was found to be increase by a factor of 1.13 in dextran only, which is almost half the amount compared to the measurement after full CXL treatment (a factor of 1.29) at 0.03 MPa stress. The results were

consistent with previous findings which demonstrated a hydration-dependent tensile measurement (Hatami-Marbini and Rahimi 2016). However, in Wollensak et al.'s study, they showed that the tensile properties of CXL-treated porcine corneas significantly increased by a factor of 1.8 at 6% strain compared with untreated corneas (Wollensak, Spoerl et al. 2003). The increase factor they reported was significant higher than the measurement from the current study. There are some differences that can be found in experimental settings and their comparison groups. Firstly, the slenderness ratio (14 mm: 4 mm) for their tensile test was higher than the ratio used in the current study (6 mm: 3 mm). It was reported that a higher slenderness ratio may result in a stiffer stress-strain behaviour (Bagheri, Buj-Corral et al. 2018). However, the high stiffness of cornea found in Wollensak's study was due to the PBS used for control groups. The tensile stress is usually calculated by dividing the measured axial force by the cross-sectional area of the specimens. Therefore, the swollen or dehydrated corneas could result in the significant outcome measurements.

The dextran-treated dehydrated specimens may cause the higher stress values which are measured in smaller cross-sectional area. This present study performed thickness correction by using the non-dehydrated thickness measurement to examine the effect of dextran and sole effect of CXL treatment. The finding suggests that the increased tangent modulus caused by dextran can be corrected, and the values show no significant differences compared to PBS controls. Previous research has proposed that the hydration-dependent tensile behaviour of cornea may be due to the resistance pressure of PGs (Hatami-Marbini and Rahimi 2016). Therefore, the effective loading capability of the PG matrix decreases, yielding an increased tensile response. The results indicate that almost half of the measured stiffening effect of the Dresden protocol comes from the dextran component of the CXL protocol using tensile test, and these effects can be explained due to the dehydration effects.

5.3. The Effect of Dextran on Corneal Hydration and Structures

In addition to providing the mechanical data, ultrastructural analysis using TEM and FTIR offered a more accurate estimate in the parameters that may be helpful to define the measured mechanical response. Although the present study showed limited results of interactions of ECM proteins

including the changed expression of PGs following CXL. The aim of all these experiments is to improve the understanding of UVA/riboflavin CXL, the current clinical setting Dresden protocol, hence to obtain more clear insights toward improved treatment design when evaluating modifications of keratoconus treatment.

5.3.1. Hydration Behaviour Following UVA/Riboflavin CXL

Collagen CXL using the conventional Dresden protocol is initially thought to affect the ultrastructure, mechanical properties, hydrodynamic and enzymatic behaviour of the cornea (Wollensak, Aurich et al. 2007, Kling, Remon et al. 2010, Chai, Gaster et al. 2011, Zhang, Conrad et al. 2011, Akhtar, Almubrad et al. 2013, Wang, Huang et al. 2015). However, it has been reported that dextran used in the original Dresden protocol affects the measurements obtained from tensile testing (Hatami-Marbini and Rahimi 2016). In the conventional Dresden CXL protocol, 20% dextran is used as the de-swelling agent during the application of riboflavin solution, which significantly reduced ($p < 0.01$) the corneal thickness after CXL treatment (Hatami-Marbini and Rahimi 2016). The higher tensile stiffness is observed in less hydrated corneal specimens, and part of this stiffening effects following corneal CXL could be due to the changes in corneal hydration state instead of CXL therapy.

Tissue stiffness is considered a combination of the internal geometry of the tissue and the properties of the material itself. Dextran caused a reduction in tissue hydration and therefore a reduction in thickness which significantly affected the outcomes of uniaxial tensile test and the overall ultrastructure of the treated corneas. In order to correct for the effect of dextran dehydration, a mathematical correction based on the relationship of thickness (T) and hydration (H) was performed in the present study. The correlation of thickness (T) and hydration (H) in the porcine cornea has previously been reported and depicted by the equation $T = 0.2*e^{0.33*H}$ (Hatami-Marbini, Etebu et al. 2013). The reduction in thickness followed an exponential decrease in tissue hydration, which can be used to calculate the hydration state of tissues at different thickness. This study for the first time assessed and corrected for the dehydrating effect of dextran by evaluating the tissue hydration at

different stromal depth intervals. The dehydration of ultrastructure due to dextran dehydration can, therefore, be corrected successfully in this mathematical method.

According to the presented equation ($T = 0.2*e^{0.33*H}$) for the *ex vivo* porcine specimens, the hydration of cornea was around H = 5 and 4 in PBS control and dextran solution, respectively. Previous studies have demonstrated that the hydration of cornea at *in vivo* physiological thickness is close to H = 3.0 to 3.5 for most species (Hatami-Marbini, Etebu et al. 2013). The increase in diameter of collagen fibril, inter-fibrillar spacing and inter-molecular spacing have been observed when the hydration of cornea is increased (Meek, Fullwood et al. 1991, Hayes, White et al. 2017). However, the water entering corneal stroma at normal physiological hydration state does not distribute equally within and between fibrils, proportionally less water is absorbed into the fibrils. Indeed, the current study observed similar results that the changes in diameter of collagen fibril were ranging from 10% to 30%, whereas 70% to 90% water entered the inter-fibrillar spacing thus moving the fibrils apart when the hydration increased from H = 4 to H = 5. The proportional water partition has become the idea that the current study applied to correct the tissue hydration which had been affected by dextran in order to understand the true structural changes in the fibril diameter induced by CXL. The physiological hydration of cornea is believed to be mainly regulated by density of proteoglycans (Chakravarti, Petroll et al. 2000, Kao and Liu 2002). A positive linear correlation is reported between stromal hydration and inter-fibrillar spacing squared in porcine corneas (Hayes, White et al. 2017). In addition, the relationship between hydration and inter-fibrillar spacing depends on the ionic components of the bathing medium and its pH values. Therefore, it is important to keep these parameters constant during the CXL procedure.

5.3.2. Structural and Biochemical Changes Following UVA/Riboflavin CXL

The current study have demonstrated the role of dextran during CXL procedure by examining the tensile mechanical property, ultrastructure and protein interactions. Although this study observed an increase in C-O stretching force in dextran-treated corneas compared with PBS controls, it may indicate that dextran does itself induce inter- or intra-collagen fibril changes. A potential explanation

for the C-O stretching is that the dextran-induced dehydration increases the swelling pressure of tissue and therefore the resistance pressure of proteoglycan matrix, giving rise to intermolecular forces (Hodson and Mayes 1978, Hatami-Marbini, Etebu et al. 2013). The current study has investigated the structural response of corneal collagen to tensile load using TEM technique to probe hierarchies ranging from molecular to fibrils. Although the comparison was made in same cornea to reduce the individual variations, the structural changes is measured under relaxed states after CXL. The current study demonstrated a 5% increase ($p < 0.01$) in the diameter of collagen fibrils and an approximately 10% decrease in fibril density after CXL, in the comparison with dextran controls. The fibril density was calculated as 222, 300, and 277 fibrils/μm^2 in PBS, dextran, and CXL groups, respectively. Previous studies have reported the increased diameter, increased density but reduced interfibrillar spacing in rabbit cornea after CXL (Wang, Huang et al. 2015). Although a higher density (277 fibrils/μm^2) compared to PBS controls (222 fibrils/μm^2) was observed, the sole effect of CXL on ultrastructure can only be examined when the comparison is made in the presence of dextran. Therefore, the real structural changes induced by CXL was evaluated and the density of fibril was reduced compared to dextran (300 fibrils/μm^2). Indeed, the dextran-involved structural changes are most likely a consequence of treatment-induced changes in tissue hydration rather than CXL itself (Hayes, Boote et al. 2011). The present study provides a mathematical method for the evaluation of structural changes by dextran.

The rationale behind UVA/riboflavin CXL is that photo-polymerization, in the presence of the photosensitizer, leads to creation of chemical bonds between substrates within the corneal stroma, including between collagens and proteoglycans and other stromal proteins (Wollensak, Spoerl et al. 2003, Brummer, Littlechild et al. 2011). Studies have showed and compared molar percentage of amino acids in collagen before and after UVA/riboflavin CXL, the decreases in molar percentages of Met, Tyr, His, Hlys, and Lys in cross-linked collagens are observed. The results suggest that these amino acids may be involved in the photo-polymerisation reaction (Zhang, Mao et al. 2013).

The FTIR data revealed significant changes in conversion rate of amide bonds following the full Dresden protocol. Lysine-based cross-links following UVA/riboflavin CXL have previously been postulated but not been found chemically (Spoerl, Huhle et al. 1998, Wollensak, Spoerl et al. 2003), and it has been proposed that cross-links form through endogenous carbonyl groups including imidazole formation (figure 5.1) (McCall, Kraft et al. 2010). The results support a model where the increased swelling pressure and the involvement of endogenous carbonyls (allysine) leads to the new bond formation (Boyce, Jones et al. 2007). This leads to a broader mechanism where UVA/riboflavin–induced intra-fibrillar bonds present as thickened collagen fibrils and less dense overall structure and drive the increased tissue mechanical strength and resistance to dehydration (figure 5.2).

It should be noted that the ultrastructural parameters the current study measured can not fully account for the mechanical effects. In addition, the measurements are largely dependent on the experimental design system. The effects on other stromal proteins and the interactions of collagen with proteoglycans could be involved in CXL therefore contributing to the stiffening. Previous studies have demonstrated that lumican-deficient posterior stroma displayed a pronounced increase in fibril diameter, altered inter-fibrillar spacing and significant reduction in keratan sulfate (KS) (Chakravarti, Petroll et al. 2000). To further clarify the interrelations of GAGs, PG core proteins and collagens during CXL treatment, the formation of cross-links between each other have been examined (Zhang, Conrad et al. 2011). The effects of CXL on the protein interactions were designed and revealed in solution *in vitro* study (Zhang, Conrad et al. 2011). The GAGs including KS and CS were reported to interrupt the CXL formation between collagens and PG core proteins. However, their results were not consistent with the *ex vivo* outcomes, which keratocan and lumican both form cross-links with collagen. This might be due to the presence of KS chains that affect the conformation of PG core proteins binding to collagens (Zhang, Conrad et al. 2011). This study has also demonstrated the formation of higher molecular weight of keratocan, which may be due to the cross-linked GAGs to form dimers or trimers.

The mechanical role of proteoglycans has also been increasingly studied in recent years. Proteoglycans usually adopt a linear conformation filling the space between collagen fibrils networks, which is proposed to contribute to a damping function by providing viscous resistance or cohesive force to the sliding of the collagen fibrils (Lewis, Krawczak et al. 2010, Wollensak, Sporl et al. 2011). GAGs covalently bonded to PGs are responsible for about 70% water content in cornea due to their negatively charged sulfated groups which are believed to attract water through osmotic effects (Comper and Laurent 1978, Elliott, Goodfellow et al. 1980, Brown, Vural et al. 1994). Therefore, they are important in regulating fibril-fibril spacing through hydration (swelling), charge repulsion, and their interaction with water giving compressive stiffness to the tissue (Hahn and Birk 1992). However, the swelling pressure is restricted by the elasticity of the collagen network and the size of GAGs that form repulsion force or anti-parallel interactions, creating more or less space for free water uptake (Bettelheim and Plessy 1975, Lewis, Pinali et al. 2010). According to previous studies, it was hypothesised that the PGs and GAGs matrix between the spring-like structures of collagen lamellae possibly act against their straightening (Scott 1992, Winkler, Chai et al. 2011, Hatami-Marbini 2014). The effective resistance and loading capability of the PG matrix reduces when the hydration increases, and the collagen lamellae move further apart from each other, therefore a softer mechanical property was observed. It may be helpful to explain some of the apparently contradictory reports in the literature (Wollensak, Aurich et al. 2007, Zhang, Conrad et al. 2011, Akhtar, Almubrad et al. 2013, Hayes, Kamma-Lorger et al. 2013, Wang, Huang et al. 2015). Therefore, the hydration states and the osmolarity of the riboflavin solutions could be important factors to consider in CLX protocol modifications used in clinical practice.

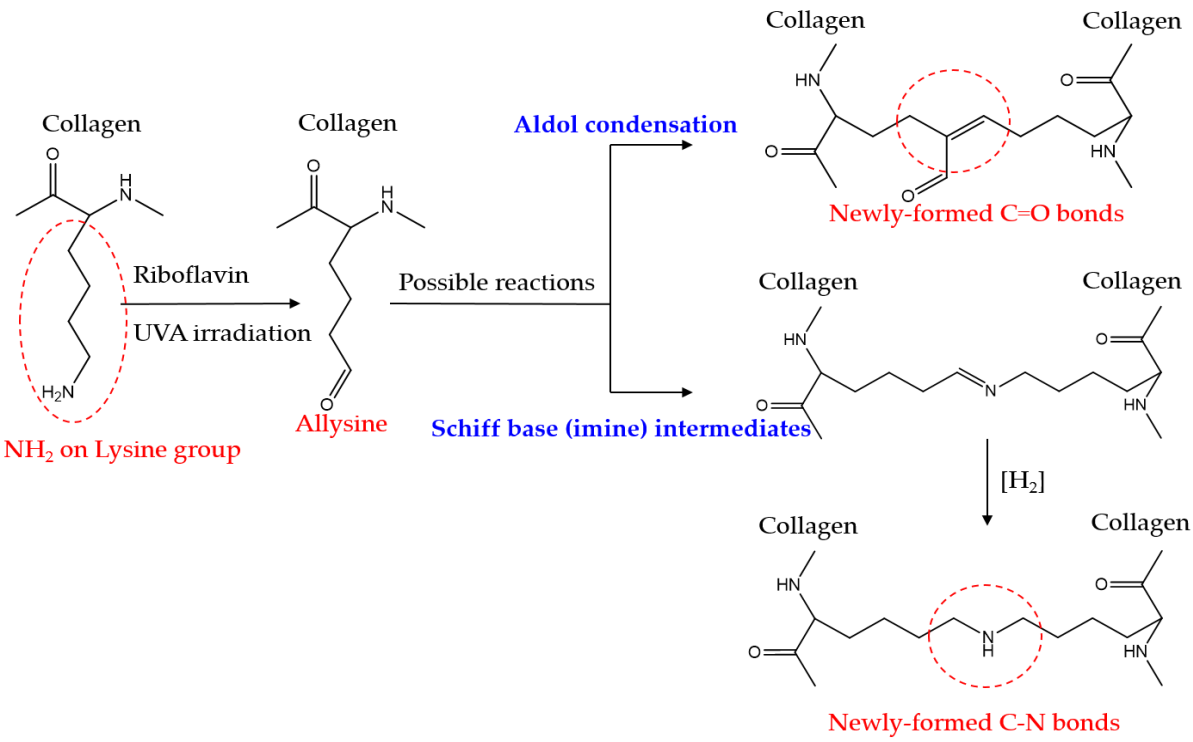

Figure 5.1. Proposed mechanisms by which riboflavin can induce CXL of collagen molecules in the presence of UVA.

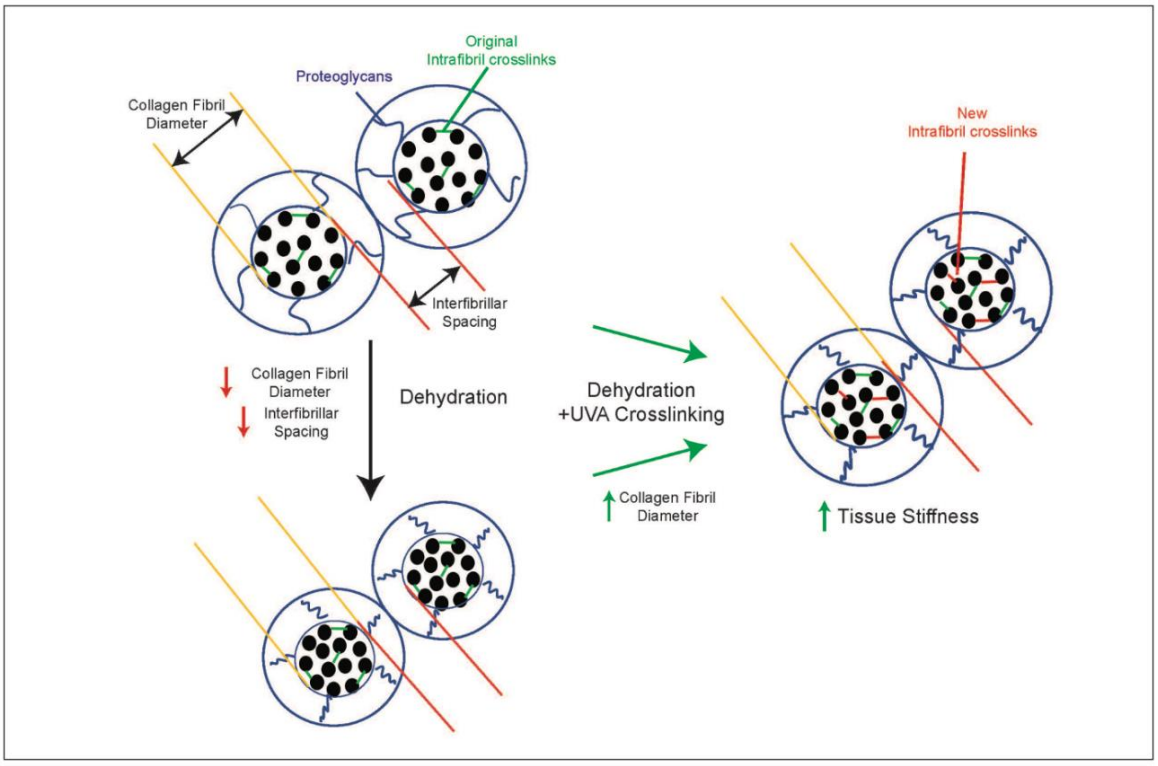

Figure 5.2. Proposed model of UVA/riboflavin CXL with the presence of dextran. The black solid circle, blue solid line, green solid line and red solid line represented collagen molecule, proteoglycans, original cross-links formed between collagen molecules and additional cross-links induced by UVA/riboflavin CXL treatment, respectively.

5.4. Mechanical Behaviours of Porcine Corneas Under Inflation

Mechanical testing including uniaxial tensile test and inflation test were utilised to determine the desired characteristics of the corneal materials and mechanical response following CXL treatment. Due to the anisotropic and viscoelastic nature of the corneal tissue, careful control of specimen preparation, dissection and precise loading rates during the testing were of importance for comparable outcomes. The technique used for measuring mechanical property of whole eye rather than of corneal strips is inflation test which has become one of the most desirable *ex vivo* experimental setting available to researchers. It stems from the similarities between the way in which the tissue is loaded and observed *in vivo*. The corneal thickness and curvature change in response to the changes in IOP. In the meantime, this stretching within the cornea induces a stress to prevent additional extension to the corneal surface (Kling, Remon et al. 2010).

To measure more precisely the contribution of CXL treatment *ex vivo* on mechanical properties, and a more accurate analysis procedure regarding the structural changes while considering the actual effects in clinical treatment, a physiologically realistic loading regime is needed. In the current study, all the comparisons of mechanical measurements were made under physiological state (25 mmHg IOP). This is different from previous studies in which the measurements of mechanical behaviours were usually performed at very high stress (>100 mmHg IOP) or until the specimen ruptured (Elsheikh and Anderson 2005). The procedure involved in tensile test has some inherent deficiencies such as non-uniform stress distribution across the curved corneal strips, which have reduced the reliability of this method especially when the measurements are performed under high stress or maximum loading (Elsheikh and Anderson 2005). Therefore, inflation is considered more suitable for determining material properties than tensile test due to its experimental setting and design that is representative of *in vivo* condition (Elsheikh and Anderson 2005, Whitford, Studer et al. 2015). However, the accuracy of results and variations in mechanical response of corneas can depend on the experimental strain rate, the regions analysed, tissues' anisotropy, and the constitutive models presented. Additionally, interpretation of the results should be careful when comparing stiffness

considering tangent modulus that was calculated at same level of stress in different regions. In the current study, the stress-strain behaviour of specimens subjected to tensile testing was from half cornea strips instead of intact cornea. The results generated in inflation was from corneal model using whole eye globe.

Another superior benefit of inflation could be the loading directions. The corneal strength is explained not only through the variations in the structure of collagen and its interactions with extracellular matrix, but also through the orientation of collagen fibrils according to the direction of the load. Collagen fibrils re-orientate themselves to the direction of the applied load (Bell, Hayes et al. 2018). It has been reported that longitudinal fibrils are found in regions supporting tensile loads, and transverse fibrils corresponds to regions under compressive loading or loading in orthogonal direction (Martin and Boardman 1993, Bell, Hayes et al. 2018). Tensile and inflation testing follow different loading orientations in measurement of corneal mechanical properties. Tensile testing induces a change in collagen fibrils' alignment towards the load direction. In the inflation testing, as the tissue is loaded similar to *in vivo* conditions, no change in the fibrils' orientation would be expected.

The current study observed a significant increase in stiffness after CXL and a 29% reduction in corneal apical rise with increase IOP during inflation. The present results showed that the tangent modulus from tensile testing were comparable and in agreement with the outcomes using inflation. The tangent modulus measured in the corneas treated with full Dresden protocol ($Et_{Cross\text{-}linking}$) were 2.09 ± 0.17 and 2.48 ± 0.69 using tensile and inflation tests, with a 28 ± 17% and 43 ± 24% increase compared to their corresponding control, respectively. Although the measurement from inflation showed 18.6% higher than the stiffness measured from tensile testing, the results did not show statistical differences between two methods. Similar stress-strain and tangent modulus behaviours were observed in all specimens at low stress level (0.03 MPa) when using both tensile and inflation methods. Previous studies have reported an overestimated tangent modulus using tensile testing when comparing with inflation. However, this study did not observe any significant difference on the measurements. A possible explanation could be due to the too low loading stress (0.03 MPa) to

observe the changes in polar distribution of fibril networks (reflecting straightening of crimp or reorientation of lamellae). It has been reported that CXL significantly increased the stiffness of porcine corneas by about 42% when subjected to high pressure (300 mmHg) using inflation, but no significant difference was observed under physiological range of pressure (15 mmHg) (Matteoli, Virga et al. 2016). Additionally, the mathematical analysis of the present inflation testing was built on a number of assumptions of corneal material which was modelled as a homogenous, non-linear anisotropic and hyper-elastic material properties. The analysis in the current study did not take into account the variation of material stiffness between the corneal epithelium, endothelium and stroma (Elsheikh, Alhasso et al. 2008), and the preferred orientation of collagen fibrils (Hayes, Boote et al. 2007). For these reasons, the analysis is expected to produce the characteristic behaviours of intact corneas which was considered as a whole in numerical simulations process. However, the overestimated mechanical measurements reported in the literature may be explained due to the high stress used in the experimental setting, therefore no significant difference was found when evaluating the stiffness under low or physiological states. As keratoconus is regarded as a degenerative disease affecting the corneal collagen networks, in which a degeneration of the collagen fibril structure and an increased propensity of fibril sliding could give rise to altered macroscopic morphology (Holmes, Gilpin et al. 2001, Koster, Leach et al. 2007). Using different methodologies may have profound impacts on the mechanical outcome measured, especially for the comparison of normal and diseased tissue.

5.5. Meta-Analysis in Clinical Study

Keratometric change represents the progression of keratoconus, studies have report that conventional CXL results in a more pronounced decrease of keratometry and provides higher corneal flattening effect than accelerated CXL (Shetty, Pahuja et al. 2015, Cummings, McQuaid et al. 2016). However, the current meta-analysis presented no significant difference between the two treatment methods comparing at 12 months. Although severe heterogeneity was displayed, the variation may be due to the different patients' baseline, the varied irradiation intensity and treating time from three different

accelerated protocols. In addition, conventional CXL may be effective in halting the progress of keratoconus for at least 12 months (Chunyu, Xiujun et al. 2014), which may explain the contradictory reports in clinical trials when comparing the efficacy of two treatment modalities (Konstantopoulos and Mehta 2015, Shetty, Pahuja et al. 2015, Medeiros, Giacomin et al. 2016). Only one study demonstrated the outcome at 18 months following accelerated CXL in the included studies (Hashemi, Miraftab et al. 2015), therefore, further studies are needed to confirm the long-term effect.

A minimum of 400 μm CCT is included in the present meta-analysis, the CCT at 12 months was only available from one study and showed no significant difference (Chow, Chan et al. 2015). However, in most clinical trials, CCT is reported to be reduced after CXL in both treatment modalities (Hafezi, Kanellopoulos et al. 2007, Spoerl, Mrochen et al. 2007, Vinciguerra, Albe et al. 2009, Caporossi, Mazzotta et al. 2010). It was explained due to the compactness of cornea fibrils after CXL caused by thermal and photochemical effects (Greenstein, Shah et al. 2011), but other studies attribute this to measurement errors from different instruments (Touboul, Efron et al. 2012). Indeed, CCT was reduced after CXL but often returned to preoperative value after 12 to 18 months (Shetty, Pahuja et al. 2015).

The major limitation of the present study was the short follow-up time and limited number of cases. The range of follow-up for accelerated protocols was 6 to 18 months. Moreover, the definition criteria for progressive keratoconus, demographic baseline and follow-up period varied within the included studies. Lastly, different UVA instruments, riboflavin ingredients, surgical procedures and postoperative medications were used in these studies, which also resulted in severe heterogeneity. Although riboflavin in 20 % dextran is used by default in conventional CXL, the use of riboflavin with hydroxypropyl methylcellulose (HPMC) is performed in accelerated CXL as it was shown to increase the diffusion rate of fluorescein (Waltman and Patrowicz 1970). Hence it allows for better penetration of riboflavin and may benefit for shorter treatment in accelerated CXL, especially for the accelerated CXL with intensity of 30 mW/cm^2 also included in this meta-analysis.

Previous laboratory studies have reported inconsistent outcomes when comparing the conventional CXL and accelerated CXL, which did not follow the Bunsen-Roscoe law. Irradiating with higher intensities for shorter time duration to achieve the same cumulative dose of 5.4 J/cm^2, resulted in the reduced tangent modulus and thus less stiffening effect compared to conventional CXL (Hammer, Richoz et al. 2014). The delivered cumulative dose does not seem to be the only factor to affect the corneal properties. In this meta-analysis, no difference was observed between conventional CXL and accelerated CXL with a follow-up of 12 months, which both showed comparable results in halting the progression of keratoconus, with improvement in visual acuity. Although the laboratory studies have demonstrated unequal measurements following different protocols, effects of CXL is considered to mainly reflect the biomechanical impact on stiffening and the thinning cornea rather than reforming cornea shape and refractive power (Liu, Liu et al. 2017). However, the decrease in efficacy with higher irradiation still has been concerned and may result in less stabilization of keratoconus. Therefore, some studies using a higher cumulative dose of 6.6 J/cm^2 or 7.8 J/cm^2 (Sherif 2014, Choi, Kim et al. 2017). It should be remarked that the cumulative dose duration of riboflavin instillation before and during the irradiation can differ among the included studies in this meta-analysis. As the statistical reliability may be reduced when evaluating the parameters if too few studies were included in this meta-analysis.

In addition, accelerated CXL is more favourable for paediatrics due to its short duration. Accompanied by more participants enrolled in randomised clinical trials and by standardisation for measuring apparatus as well as riboflavin ingredients, more reliable outcomes and convinced conclusions could be obtained in future.

5.6. Limitations and Future Work

Understanding the stabilisation mechanism of UVA/riboflavin CXL is clinically relevant when evaluating modifications to the Dresden protocol and developing optimal protocols or new keratoconus treatments. In this thesis, the effect of UVA/riboflavin was characterised mainly on mechanical properties and ultrastructural changes. Collagen properties interact with several other

determinants of matrix strength, which may contribute to the mechanical properties of corneas. The interactions between these different parameters limit the mechanical analysis of the sole contribution of corneal collagen, especially the biochemical modifications on corneal matrix following CXL. These complex interrelationships create a challenge in investigating the independent role of collagen properties as a determinant of corneal strength. Any change in the swelling pressure affects the pre-stressed condition of the collagen network and subsequently the measured macroscopic mechanical properties.

During corneal dehydration with dextran, water is lost from within and between the collagen fibrils. The current study performed a mathematical method to correct the fibril distribution based on the same proportional water partition. The changed hydration ratio on overall thickness was applied and interpolated into each depth interval, resulting in the same shifting frames. However, the corneal hydration/dehydration behaviour is depth-dependent and relied on the collagen structures and ratio of PGs (Lee and Wilson 1981, Castoro, Bettelheim et al. 1988, Cristol, Edelhauser et al. 1992, Muller, Pels et al. 2001). Additionally, the ratio of UVA-induced structural changes will not be able to evaluated in this study. The current study proposed that the additional cross-links induced by UVA/riboflavin CXL contributed to an increased tissue mechanical strength and a resultant resistance to ultrastructural change which lead to the thickened fibril bundles and a less dense structure comparing to its dextran controls. However, it is unable to comment on the effect of riboflavin/UVA CXL on other matrix components such as the interactions of collagen-PGs and PGs-PGs in the current study design. PGs within the corneal stroma have been proposed to play a pivotal role in regulating the fibril-fibril spacing and hydration-dehydration properties (Hahn and Birk 1992). The results showed that the inter-fibrillar spacing was slightly increased after CXL but not significantly. The inter-fibrillar spacing decreased dramatically due to the dehydrating effect of dextran which made it difficult to determine the sole effect of CXL on proteoglycans in the current experimental system.

Previous inflation study on trephination specimens which showed a rise in the apex as a function of increased IOP was very similar to the observations in porcine corneas (Elsheikh and Anderson 2005).

Although the current study cannot rule out a contribution of the entire eye motion to the apical radius displacement, the behaviour which was observed in corneal apical rise was consistent in 7 pairs of eye globes. It was reported that non-cross-linked corneas did not fully return to the initial apical position after pressurized. However, cross-linked corneas tended to return to the original values both for apical position and corneal thickness, showing a more elastic behaviour than then non-cross-linked cornea (Kling, Remon et al. 2010). The current study did not examine the hysteresis properties before and after CXL, but the results are consistent with the cross-linked cornea being stiffer.

Further work will be needed to evaluate the effects on keratoconic corneas instead of normal corneas. Although several ex vivo estasia models have been established by using chondroitinase and collagenase to induce a disordered ultrastructure (Hong, Sinha-Roy et al. 2012, Wang, Huang et al. 2015, Qiao, Li et al. 2018), keratoconic animal model has not yet been well-established. Spontaneous Mutant with Keratoconus-affected Corneas and Japanese Keratoconus mice which were developed by a Japan group studying the progression of disease was reported to have similar clinical characteristics of keratoconus, including conical shape, apoptosis of keratocytes, and higher expression of c-Fos protein (Tachibana, Okamoto et al. 2002). However, these symptoms only occurred on male mice and were found to relate to lymphocyte infiltration and inflammation on the keratoconus-affected corneas. Understanding the interactions between cellular behaviour with cross-linked ECM is of importance to evaluate the long-term effect of UVA/riboflavin CXL treatment especially for keratoconic eyes.

The major effect during CXL treatment is the decrease of corneal thickness after riboflavin instillation, which was caused by the hyper-osmolarity of the riboflavin-dextran solution. Decreased corneal thickness in patients has been reported with a 18.7% reduction in a clinical study (Kymionis, Kounis et al. 2009), in which corneal pachymetry was monitored with Scheimpflug imaging immediately after riboflavin instillation. Therefore, the use of alternative iso- or hypo-smolar riboflavin solution has been proposed to maintain or increase the effective corneal thickness (Hafezi, Mrochen et al. 2009). Although it was reported that behaviour of the corneal response to pressure was independent to the hydration or swelling effects (Kling, Remon et al. 2010). The results from

restricted thickness will be of importance to further improve the current understanding of corneal mechanics and provide a more precise representation of its material parameters for numerical models. In this study, PBS was used as a bathing solution, which may become the main drawback for the experimental design. As the corneal strips were subjected to tensile experiments, the tissue hydration may affect the tensile properties assessed. Glycerol or mineral oil should be concerned in the future work in order to prevent the thickness changes of specimens and keep their states (swelling or dehydration) constant during the mechanical tests (Lari, Schultz et al. 2012, Hatami-Marbini 2014).

For the inflation experiment, although this study used a corneal model instead of a whole eye model, the limbal junction is allowed to move, which is thought to be crucial to establish a biomechanical model mimicking the optical function of a real eye (Woo, Kobayashi et al. 1972, Shin, Vito et al. 1997, Srodka and Iskander 2008). The full parametric characterization of human corneal deformation as a function of pressure will be valuable to enhance the predictability of FE modelling of the cornea and ultimately the predictability of the procedure. Open questions such as the apparent anisotropy of the intact porcine cornea in the biomechanical response and in response to treatment are yet to be confirmed in humans and of interest in pathologic or keratoconic corneas.

5.7. Conclusions

Overall, this study has enhanced comprehensive insight on the efficacy of corneal CXL treatment with riboflavin and UVA through the systematic analysis with correction for corneal tissue hydration at each depth interval, which provides a robust method to evaluate the ultrastructural impact of corneal CXL. The current study has established the standards in terms of mechanical, chemical, and structure/biological changes induced by the Dresden protocol, as well as the proteins that may be involved in. The present work proposes a model where fibril diameter and structural density are important parameters in determining tissue stiffness. The comparisons of stiffness and analysis of IFE modelling presented in this study provided important information relating to the effectiveness of CXL in biomechanical behaviour across the corneas, which can be useful in applications where the prediction of the modifications of CXL protocol in corneal material stiffness is required.

The first aim, the current study defined the characteristics of corneal mechanical properties by using tensile and inflation testing.

The purpose of applying two different mechanical measurements is due to the anisotropic and viscoelastic properties of the ocular tissue. Tensile and inflation tests follow different loading orientations in the measurement of corneal mechanical properties. The current study has provided experimental data of the significant changes in corneal thickness, ratio of tangent modulus and apical rise with increased IOP after CXL. The thickness was significantly reduced in the presence of dextran, however the increased tangent modulus caused by dextran can be corrected. The sole effect of CXL can then be estimated. The results showed that the tangent modulus from tensile testing was comparable and in agreement with the outcomes using inflation. Although only corneal model was performed in this study, the experimental data are valuable input parameters in FE models that will allow a better understanding and increased predictability of the CXL treatment.

The second aim, the current study identified the alterations in corneal ultrastructure in the presence of dextran following CXL, and possible interactions between Extracellular Matrix (ECM) proteins following CXL

Based on the analysis results of the ultrastructural parameters including the diameter of collagen fibrils, inter-fibrillar spacing and density of collagen using the TEM, this study has observed an altered collagen architecture within the first 300 μm of stromal depth consisting of 5% increase in the diameter of collagen fibrils with no significant changes to inter-fibrillar spacing, resulting in a 10% decrease in number of fibril per unit area. Furthermore, Fourier Transform Infrared Spectroscopy confirmed the formation of inter-fibrillar amide bonds induced by UVA/riboflavin CXL. Although dextran contributed to a significant increase in stiffness accompanied with a reduced fibrillar thickness and potential C-O stretching force, it did not cause additional protein interactions on proteoglycans or collagens according to the western blot analysis and Coomassie blue staining. The

current study assessed and corrected the dehydrating effect of dextran by evaluating the tissue hydration at different stromal depth intervals. The dehydration of ultrastructure due to dextran dehydration can be corrected successfully in a mathematical method.

The third aim, the current study performed the correlation between biomechanical behaviour and structural parameters that may be important for defining the amount of stiffening.

Understanding the mechanical behaviour of the cornea and its corresponding biological and ultrastructural alterations is clinically relevant. Combined studies of ultrastructural analysis of the collagen fibrils and biomechanical approaches are required. Therefore, in the third aim, this study compared the tangent modulus and ultrastructural measurements obtained from the experimental data following Dresden protocol. The combination of the ultrastructural measurements (collagen fibril diameter + fibril density – inter-fibrillar spacing) displayed a positive correlation of 0.177 with tangent modulus increases across the test population. Although the results should be noted that the measured ultrastructural changes which were measured do not fully account for the mechanical effects. The data support a model wherein collagen fibril diameter and structural density are fundamental parameters in defining tissue stiffening following UVA/riboflavin corneal CXL, and provide the key benchmarks against which modifications to the Dresden CXL protocol can be evaluated.

The forth aim, the current study evaluated the efficacy of the CXL in clinical practice, and compared conventional and accelerated CXL by Meta-analysis.

No difference was observed in this meta-analysis on the efficacy between conventional CXL and accelerated CXL with a follow-up of 12 months, which both showed comparable results in halting the progression of keratoconus, with improvement in visual acuity. Although the laboratory studies have demonstrated unsuccessful for the Bunsen-Roscoe law on biomechanical impact on stiffening and the thinning cornea with higher irradiation, efficacy of CXL is considered mainly on the reforming cornea shape and refractive power in clinical practice. The current study performed the same methodology on porcine specimens, so that it would be able to relate some experimental

findings on inflation to clinical data reported in patients, which will provide further insight into the mechanisms of CXL and predictability of the treatment.

Chapter 6. References

Abad, J. C. (2008). "Management of slipped laser in situ keratomileusis flap following intrastromal corneal ring implantation in post-LASIK ectasia." J Cataract Refract Surg 34(12): 2177-2181.

Abahussin, M., S. Hayes, N. E. Knox Cartwright, C. S. Kamma-Lorger, Y. Khan, J. Marshall and K. M. Meek (2009). "3D collagen orientation study of the human cornea using X-ray diffraction and femtosecond laser technology." Invest Ophthalmol Vis Sci 50(11): 5159-5164.

Ahearne, M., Y. Yang, K. Y. Then and K. K. Liu (2007). "An indentation technique to characterize the mechanical and viscoelastic properties of human and porcine corneas." Ann Biomed Eng 35(9): 1608-1616.

Ahearne, M., Y. Yang, K. Y. Then and K. K. Liu (2008). "Non-destructive mechanical characterisation of UVA/riboflavin crosslinked collagen hydrogels." Br J Ophthalmol 92(2): 268-271.

Akhtar, S., T. Almubrad, I. Paladini and R. Mencucci (2013). "Keratoconus corneal architecture after riboflavin/ultraviolet A cross-linking: ultrastructural studies." Mol Vis 19: 1526-1537.

Al-Yousuf, N., I. Mavrikakis, E. Mavrikakis and S. M. Daya (2004). "Penetrating keratoplasty: indications over a 10 year period." Br J Ophthalmol 88(8): 998-1001.

Alanazi, S. A., T. Almubrad, A. I. AlIbrahim, A. A. Khan and S. Akhtar (2015). "Ultrastructure Organization of Collagen Fibrils and Proteoglycans of Stingray and Shark Corneal Stroma." J Ophthalmol 2015: 686914.

Alastrue, V., B. Calvo, E. Pena and M. Doblare (2006). "Biomechanical modeling of refractive corneal surgery." J Biomech Eng 128(1): 150-160.

Aldahlawi, A. M., M. F. Elshal, L. A. Damiaiti, L. H. Damanhori and S. M. Bahlas (2016). "Analysis of CD95 and CCR7 expression on circulating CD4(+) lymphocytes revealed disparate immunoregulatory potentials in systemic lupus erythematosus." Saudi J Biol Sci 23(1): 101-107.

Aldahlawi, N. H., S. Hayes, D. P. O'Brart, A. Akhbanbetova, S. L. Littlechild and K. M. Meek (2016). "Enzymatic Resistance of Corneas Crosslinked Using Riboflavin in Conjunction With Low Energy, High Energy, and Pulsed UVA Irradiation Modes." Invest Ophthalmol Vis Sci 57(4): 1547-1552.

Aldahlawi, N. H., S. Hayes, D. P. S. O'Brart, A. Akhbanbetova, S. L. Littlechild and K. M. Meek (2016). "Enzymatic Resistance of Corneas Crosslinked Using Riboflavin in Conjunction With Low Energy, High Energy, and Pulsed UVA Irradiation ModesCorneal Enzymatic Resistance Following Crosslinking." Investigative Ophthalmology & Visual Science 57(4): 1547-1552.

Alhayek, A. and P. R. Lu (2015). "Corneal collagen crosslinking in keratoconus and other eye disease." Int J Ophthalmol 8(2): 407-418.

Alio, J. L., D. P. Pinero and A. Daxer (2011). "Clinical outcomes after complete ring implantation in corneal ectasia using the femtosecond technology: a pilot study." Ophthalmology 118(7): 1282-1290.

Alio, J. L., M. H. Shabayek and A. Artola (2006). "Intracorneal ring segments for keratoconus correction: long-term follow-up." J Cataract Refract Surg 32(6): 978-985.

Ambekar, R., K. C. Toussaint, Jr. and A. Wagoner Johnson (2011). "The effect of keratoconus on the structural, mechanical, and optical properties of the cornea." J Mech Behav Biomed Mater 4(3): 223-236.

Anderson, K., A. El-Sheikh and T. Newson (2004). "Application of structural analysis to the mechanical behaviour of the cornea." J R Soc Interface 1(1): 3-15.

Andreassen, T. T., A. H. Simonsen and H. Oxlund (1980). "Biomechanical properties of keratoconus and normal corneas." Exp Eye Res 31(4): 435-441.

Angunawela, R. I., F. Arnalich-Montiel and B. D. Allan (2009). "Peripheral sterile corneal infiltrates and melting after collagen crosslinking for keratoconus." J Cataract Refract Surg 35(3): 606-607.

Annaka, M. (2012). "Salt effect on microscopic structure and stability of colloidal complex obtained from neutral/polyelectrolyte block copolymer and oppositely charged surfactant." Colloids Surf B Biointerfaces 99: 127-135.

Arbelaez, M. C., M. B. Sekito, C. Vidal and S. R. Choudhury (2009). "Collagen cross-linking with riboflavin and ultraviolet-A light in keratoconus: One-year results." Oman J Ophthalmol 2(1): 33-38.

Arora, R., D. Gupta, J. L. Goyal and P. Jain (2012). "Results of corneal collagen cross-linking in pediatric patients." J Refract Surg 28(11): 759-762.
Asri, D., D. Touboul, P. Fournie, F. Malet, C. Garra, A. Gallois, F. Malecaze and J. Colin (2011). "Corneal collagen crosslinking in progressive keratoconus: multicenter results from the French National Reference Center for Keratoconus." J Cataract Refract Surg 37(12): 2137-2143.
Atherton, T. J. and D. J. Kerbyson (1999). "Size invariant circle detection." Image and Vision computing 17(11): 795-803.
Bagheri, A., I. Buj-Corral, M. Ferrer, M. M. Pastor and F. Roure (2018). "Determination of the Elasticity Modulus of 3D-Printed Octet-Truss Structures for Use in Porous Prosthesis Implants." Materials (Basel) 11(12).
Balasubramanian, S. A., S. Mohan, D. C. Pye and M. D. Willcox (2012). "Proteases, proteolysis and inflammatory molecules in the tears of people with keratoconus." Acta Ophthalmol 90(4): e303-309.
Bell, J. S., S. Hayes, C. Whitford, J. Sanchez-Weatherby, O. Shebanova, C. Vergari, C. P. Winlove, N. Terrill, T. Sorensen, A. Elsheikh and K. M. Meek (2018). "The hierarchical response of human corneal collagen to load." Acta Biomater 65: 216-225.
Bergmanson, J. P., T. M. Sheldon and J. D. Goosey (1999). "Fuchs' endothelial dystrophy: a fresh look at an aging disease." Ophthalmic Physiol Opt 19(3): 210-222.
Beshtawi, I. M., R. Akhtar, M. C. Hillarby, C. O'Donnell, X. Zhao, A. Brahma, F. Carley, B. Derby and H. Radhakrishnan (2013). "Scanning acoustic microscopy for mapping the microelastic properties of human corneal tissue." Curr Eye Res 38(4): 437-444.
Beshtawi, I. M., R. Akhtar, M. C. Hillarby, C. O'Donnell, X. Zhao, A. Brahma, F. Carley, B. Derby and H. Radhakrishnan (2014). "Biomechanical changes after repeated collagen cross-linking on human corneas assessed in vitro using scanning acoustic microscopy." Invest Ophthalmol Vis Sci 55(3): 1549-1554.
Bettelheim, F. A. and B. Plessy (1975). "The hydration of proteoglycans of bovine cornea." Biochim Biophys Acta 381(1): 203-214.
Bettelheim, F. A. and B. Plessy (1975). "The hydration of proteoglycans of bovine cornea." Biochimica et Biophysica Acta (BBA) - General Subjects 381(1): 203-214.
Birk, D. E., J. M. Fitch, J. P. Babiarz and T. F. Linsenmayer (1988). "Collagen type I and type V are present in the same fibril in the avian corneal stroma." J Cell Biol 106(3): 999-1008.
Boote, C., S. Dennis, Y. Huang, A. J. Quantock and K. M. Meek (2005). "Lamellar orientation in human cornea in relation to mechanical properties." J Struct Biol 149(1): 1-6.
Boote, C., S. Dennis, R. H. Newton, H. Puri and K. M. Meek (2003). "Collagen fibrils appear more closely packed in the prepupillary cornea: optical and biomechanical implications." Invest Ophthalmol Vis Sci 44(7): 2941-2948.
Bottos, K. M., A. L. Hofling-Lima, M. C. Barbosa, J. B. Barbosa, Jr., J. L. Dreyfuss, P. Schor and H. B. Nader (2010). "Effect of collagen cross-linking in stromal fibril organization in edematous human corneas." Cornea 29(7): 789-793.
Bouheraoua, N., L. Jouve, M. El Sanharawi, O. Sandali, C. Temstet, P. Loriaut, E. Basli, V. Borderie and L. Laroche (2014). "Optical coherence tomography and confocal microscopy following three different protocols of corneal collagen-crosslinking in keratoconus." Invest Ophthalmol Vis Sci 55(11): 7601-7609.
Bourne, W. M. (2003). "Biology of the corneal endothelium in health and disease." Eye (Lond) 17(8): 912-918.
Boyce, B., R. Jones, T. Nguyen and J. Grazier (2007). "Stress-controlled viscoelastic tensile response of bovine cornea." Journal of biomechanics 40(11): 2367-2376.
Boyce, B. L., J. M. Grazier, R. E. Jones and T. D. Nguyen (2008). "Full-field deformation of bovine cornea under constrained inflation conditions." Biomaterials 29(28): 3896-3904.
Boyce, B. L., R. E. Jones, T. D. Nguyen and J. M. Grazier (2007). "Stress-controlled viscoelastic tensile response of bovine cornea." J Biomech 40(11): 2367-2376.
Brindley, G. S. (1952). "The Bunsen-Roscoe law for the human eye at very short durations." J Physiol 118(1): 135-139.

Brittingham, S., C. Tappeiner and B. E. Frueh (2014). "Corneal cross-linking in keratoconus using the standard and rapid treatment protocol: differences in demarcation line and 12-month outcomes." Invest Ophthalmol Vis Sci 55(12): 8371-8376.
Brown, C. T., M. Vural, M. Johnson and V. Trinkaus-Randall (1994). "Age-related changes of scleral hydration and sulfated glycosaminoglycans." Mech Ageing Dev 77(2): 97-107.
Brummer, G., S. Littlechild, S. McCall, Y. Zhang and G. W. Conrad (2011). "The role of nonenzymatic glycation and carbonyls in collagen cross-linking for the treatment of keratoconus." Invest Ophthalmol Vis Sci 52(9): 6363-6369.
Cabrera Fernandez, D., A. M. Niazy, R. M. Kurtz, G. P. Djotyan and T. Juhasz (2006). "Biomechanical model of corneal transplantation." J Refract Surg 22(3): 293-302.
Campbell, F. W. and R. W. Gubisch (1966). "Optical quality of the human eye." J Physiol 186(3): 558-578.
Cannon, D. J. and C. S. Foster (1978). "Collagen crosslinking in keratoconus." Invest Ophthalmol Vis Sci 17(1): 63-65.
Caporossi, A., C. Mazzotta, S. Baiocchi and T. Caporossi (2010). "Long-term results of riboflavin ultraviolet a corneal collagen cross-linking for keratoconus in Italy: the Siena eye cross study." Am J Ophthalmol 149(4): 585-593.
Castoro, J. A., A. A. Bettelheim and F. A. Bettelheim (1988). "Water gradients across bovine cornea." Invest Ophthalmol Vis Sci 29(6): 963-968.
Chai, D., R. N. Gaster, R. Roizenblatt, T. Juhasz, D. J. Brown and J. V. Jester (2011). "Quantitative assessment of UVA-riboflavin corneal cross-linking using nonlinear optical microscopy." Invest Ophthalmol Vis Sci 52(7): 4231-4238.
Chakravarti, S., W. M. Petroll, J. R. Hassell, J. V. Jester, J. H. Lass, J. Paul and D. E. Birk (2000). "Corneal opacity in lumican-null mice: defects in collagen fibril structure and packing in the posterior stroma." Invest Ophthalmol Vis Sci 41(11): 3365-3373.
Chan, C. C., D. G. Cogan, F. S. Bucci, D. Barsky, Q. Li and M. A. Crawford (1993). "Anterior corneal dystrophy with dyscollagenosis (Reis-Bucklers type?)." Cornea 12(5): 451-460.
Chan, C. C., M. Sharma and B. S. Wachler (2007). "Effect of inferior-segment Intacs with and without C3-R on keratoconus." J Cataract Refract Surg 33(1): 75-80.
Chen, S., M. J. Mienaltowski and D. E. Birk (2015). "Regulation of corneal stroma extracellular matrix assembly." Exp Eye Res 133: 69-80.
Choe, E. and D. B. Min (2006). "Chemistry and reactions of reactive oxygen species in foods." Crit Rev Food Sci Nutr 46(1): 1-22.
Choi, M., J. Kim, E. K. Kim, K. Y. Seo and T. I. Kim (2017). "Comparison of the Conventional Dresden Protocol and Accelerated Protocol With Higher Ultraviolet Intensity in Corneal Collagen Cross-Linking for Keratoconus." Cornea 36(5): 523-529.
Choi, S., S. C. Lee, Y. Cheong, J. H. Shin, K. H. Jin and H. K. Park (2013). "Nanostructural response of mitomycin C application on human scleral tissues." J Biomed Nanotechnol 9(8): 1393-1397.
Choi, S., S. C. Lee, H. J. Lee, Y. Cheong, G. B. Jung, K. H. Jin and H. K. Park (2013). "Structural response of human corneal and scleral tissues to collagen cross-linking treatment with riboflavin and ultraviolet A light." Lasers Med Sci 28(5): 1289-1296.
Chow, V. W., T. C. Chan, M. Yu, V. W. Wong and V. Jhanji (2015). "One-year outcomes of conventional and accelerated collagen crosslinking in progressive keratoconus." Sci Rep 5: 14425.
Chunyu, T., P. Xiujun, F. Zhengjun, Z. Xia and Z. Feihu (2014). "Corneal collagen cross-linking in keratoconus: a systematic review and meta-analysis." Sci Rep 4: 5652.
Cinar, Y., A. K. Cingu, F. M. Turkcu, T. Cinar, H. Yuksel, Z. G. Ozkurt and I. Caca (2014). "Comparison of accelerated and conventional corneal collagen cross-linking for progressive keratoconus." Cutan Ocul Toxicol 33(3): 218-222.
Collier, S. A. (2001). "Is the corneal degradation in keratoconus caused by matrix-metalloproteinases?" Clinical & Experimental Ophthalmology 29(6): 340-344.
Comper, W. D. and T. C. Laurent (1978). "Physiological function of connective tissue polysaccharides." Physiol Rev 58(1): 255-315.

Cordeiro Barbosa, M. M., J. B. Barbosa, Jr., F. E. Hirai and A. L. Hofling-Lima (2010). "Effect of cross-linking on corneal thickness in patients with corneal edema." Cornea 29(6): 613-617.
Coskunseven, E., M. R. Jankov, 2nd and F. Hafezi (2009). "Contralateral eye study of corneal collagen cross-linking with riboflavin and UVA irradiation in patients with keratoconus." J Refract Surg 25(4): 371-376.
Cristol, S. M., H. F. Edelhauser and M. J. Lynn (1992). "A comparison of corneal stromal edema induced from the anterior or the posterior surface." Refract Corneal Surg 8(3): 224-229.
Cummings, A. B., R. McQuaid, S. Naughton, E. Brennan and M. Mrochen (2016). "Optimizing Corneal Cross-Linking in the Treatment of Keratoconus: A Comparison of Outcomes After Standard- and High-Intensity Protocols." Cornea 35(6): 814-822.
D'Agati, V., S. F. Yan, R. Ramasamy and A. M. Schmidt (2010). "RAGE, glomerulosclerosis and proteinuria: roles in podocytes and endothelial cells." Trends Endocrinol Metab 21(1): 50-56.
Dahl, B. J., E. Spotts and J. Q. Truong (2012). "Corneal collagen cross-linking: an introduction and literature review." Optometry 83(1): 33-42.
Davidson, A. E., S. Hayes, A. J. Hardcastle and S. J. Tuft (2014). "The pathogenesis of keratoconus." Eye 28(2): 189-195.
Daxer, A. and P. Fratzl (1997). "Collagen fibril orientation in the human corneal stroma and its implication in keratoconus." Invest Ophthalmol Vis Sci 38(1): 121-129.
DelMonte, D. W. and T. Kim (2011). "Anatomy and physiology of the cornea." J Cataract Refract Surg 37(3): 588-598.
Depalle, B., Z. Qin, S. J. Shefelbine and M. J. Buehler (2015). "Influence of cross-link structure, density and mechanical properties in the mesoscale deformation mechanisms of collagen fibrils." J Mech Behav Biomed Mater 52: 1-13.
Dhawan, S., K. Rao and S. Natrajan (2011). "Complications of corneal collagen cross-linking." J Ophthalmol 2011: 869015.
Dias, J., V. F. Diakonis, V. P. Kankariya, S. H. Yoo and N. M. Ziebarth (2013). "Anterior and posterior corneal stroma elasticity after corneal collagen crosslinking treatment." Exp Eye Res 116: 58-62.
Doillon, C. J., M. A. Watsky, M. Hakim, J. Wang, R. Munger, N. Laycock, R. Osborne and M. Griffith (2003). "A collagen-based scaffold for a tissue engineered human cornea: physical and physiological properties." Int J Artif Organs 26(8): 764-773.
Downs, J. C., J. K. Suh, K. A. Thomas, A. J. Bellezza, C. F. Burgoyne and R. T. Hart (2003). "Viscoelastic characterization of peripapillary sclera: material properties by quadrant in rabbit and monkey eyes." J Biomech Eng 125(1): 124-131.
Dudakova, L., P. Liskova, T. Trojek, M. Palos, S. Kalasova and K. Jirsova (2012). "Changes in lysyl oxidase (LOX) distribution and its decreased activity in keratoconus corneas." Exp Eye Res 104: 74-81.
Duke-Elder, S. (1965). "Moorfields and British Ophthalmology." Proc R Soc Med 58(7): 541-545.
Dunlevy, J. R., M. P. Beales, B. L. Berryhill, P. K. Cornuet and J. R. Hassell (2000). "Expression of the keratan sulfate proteoglycans lumican, keratocan and osteoglycin/mimecan during chick corneal development." Exp Eye Res 70(3): 349-362.
Dupps, W. J., Jr. and S. E. Wilson (2006). "Biomechanics and wound healing in the cornea." Exp Eye Res 83(4): 709-720.
Eberwein, P., C. Auw-Hadrich, F. Birnbaum, P. C. Maier and T. Reinhard (2008). "Corneal melting after cross-linking and deep lamellar keratoplasty in a keratoconus patient." Klin Monbl Augenheilkd 225(1): 96-98.
Edmund, C. (1988). "Corneal elasticity and ocular rigidity in normal and keratoconic eyes." Acta Ophthalmol (Copenh) 66(2): 134-140.
Ehlers, N. and J. Hjortdal (2008). "Riboflavin-ultraviolet light induced cross-linking in endothelial decompensation." Acta Ophthalmol 86(5): 549-551.
Elliott, G. F., J. M. Goodfellow and A. E. Woolgar (1980). "Swelling studies of bovine corneal stroma without bounding membranes." J Physiol 298: 453-470.

Elsheikh, A., D. Alhasso and P. Rama (2008). "Assessment of the epithelium's contribution to corneal biomechanics." Exp Eye Res 86(2): 445-451.
Elsheikh, A., D. Alhasso and P. Rama (2008). "Biomechanical properties of human and porcine corneas." Exp Eye Res 86(5): 783-790.
Elsheikh, A. and K. Anderson (2005). "Comparative study of corneal strip extensometry and inflation tests." J R Soc Interface 2(3): 177-185.
Elsheikh, A., M. Brown, D. Alhasso, P. Rama, M. Campanelli and D. Garway-Heath (2008). "Experimental assessment of corneal anisotropy." J Refract Surg 24(2): 178-187.
Elsheikh, A., B. Geraghty, D. Alhasso, J. Knappett, M. Campanelli and P. Rama (2010). "Regional variation in the biomechanical properties of the human sclera." Exp Eye Res 90(5): 624-633.
Elsheikh, A., D. Wang, M. Brown, P. Rama, M. Campanelli and D. Pye (2007). "Assessment of corneal biomechanical properties and their variation with age." Curr Eye Res 32(1): 11-19.
Erskine, L. and E. Herrera (2014). "Connecting the retina to the brain." ASN Neuro 6(6).
Ertan, A., H. Karacal and G. Kamburoglu (2009). "Refractive and topographic results of transepithelial cross-linking treatment in eyes with intacs." Cornea 28(7): 719-723.
Eyre, D. (1987). "Collagen cross-linking amino acids." Methods Enzymol 144: 115-139.
Eysteinsson, T., F. Jonasson, H. Sasaki, A. Arnarsson, T. Sverrisson, K. Sasaki, E. Stefansson and G. Reykjavik Eye Study (2002). "Central corneal thickness, radius of the corneal curvature and intraocular pressure in normal subjects using non-contact techniques: Reykjavik Eye Study." Acta Ophthalmol Scand 80(1): 11-15.
Ferrer, R. L. (1998). "Graphical methods for detecting bias in meta-analysis." Fam Med 30(8): 579-583.
Freed, A. D. and T. C. Doehring (2005). "Elastic model for crimped collagen fibrils." J Biomech Eng 127(4): 587-593.
Freund, D. E., R. L. McCally, R. A. Farrell, S. M. Cristol, N. L. L'Hernault and H. F. Edelhauser (1995). "Ultrastructure in anterior and posterior stroma of perfused human and rabbit corneas. Relation to transparency." Invest Ophthalmol Vis Sci 36(8): 1508-1523.
Fullwood, N. J., K. M. Meek, N. S. Malik and S. J. Tuft (1990). "A comparison of proteoglycan arrangement in normal and keratoconus human corneas." Biochem Soc Trans 18(5): 961-962.
Funderburgh, J. L. and G. W. Conrad (1990). "Isoforms of corneal keratan sulfate proteoglycan." J Biol Chem 265(14): 8297-8303.
Geraghty, B. (2012). "Biomechanical behaviour of the cornea and sclera." Unpublished doctoral dissertation, University of Dundee, United Kingdom.
Geraghty, B., S. W. Jones, P. Rama, R. Akhtar and A. Elsheikh (2012). "Age-related variations in the biomechanical properties of human sclera." J Mech Behav Biomed Mater 16: 181-191.
Girard, G. and S. Rigali (2011). "Role of the phenazine-inducing protein Pip in stress resistance of Pseudomonas chlororaphis." Microbiology 157(Pt 2): 398-407.
Girard, M., J. K. Suh, R. T. Hart, C. F. Burgoyne and J. C. Downs (2007). "Effects of storage time on the mechanical properties of rabbit peripapillary sclera after enucleation." Curr Eye Res 32(5): 465-470.
Girard, M. J., J. K. Suh, M. Bottlang, C. F. Burgoyne and J. C. Downs (2009). "Scleral biomechanics in the aging monkey eye." Invest Ophthalmol Vis Sci 50(11): 5226-5237.
Godefrooij, D. A., G. A. de Wit, C. S. Uiterwaal, S. M. Imhof and R. P. Wisse (2017). "Age-specific Incidence and Prevalence of Keratoconus: A Nationwide Registration Study." Am J Ophthalmol 175: 169-172.
Goldich, Y., A. L. Marcovich, Y. Barkana, Y. Mandel, A. Hirsh, Y. Morad, I. Avni and D. Zadok (2012). "Clinical and corneal biomechanical changes after collagen cross-linking with riboflavin and UV irradiation in patients with progressive keratoconus: results after 2 years of follow-up." Cornea 31(6): 609-614.
Gordon-Shaag, A., M. Millodot, E. Shneor and Y. Liu (2015). "The genetic and environmental factors for keratoconus." Biomed Res Int 2015: 795738.

Greenstein, S. A., V. P. Shah, K. L. Fry and P. S. Hersh (2011). "Corneal thickness changes after corneal collagen crosslinking for keratoconus and corneal ectasia: one-year results." J Cataract Refract Surg 37(4): 691-700.
Grytz, R. and G. Meschke (2010). "A computational remodeling approach to predict the physiological architecture of the collagen fibril network in corneo-scleral shells." Biomech Model Mechanobiol 9(2): 225-235.
Hafezi, F., P. Dejica and F. Majo (2010). "Modified corneal collagen crosslinking reduces corneal oedema and diurnal visual fluctuations in Fuchs dystrophy." Br J Ophthalmol 94(5): 660-661.
Hafezi, F. and H. P. Iseli (2008). "Pregnancy-related exacerbation of iatrogenic keratectasia despite corneal collagen crosslinking." J Cataract Refract Surg 34(7): 1219-1221.
Hafezi, F., J. Kanellopoulos, R. Wiltfang and T. Seiler (2007). "Corneal collagen crosslinking with riboflavin and ultraviolet A to treat induced keratectasia after laser in situ keratomileusis." J Cataract Refract Surg 33(12): 2035-2040.
Hafezi, F., M. Mrochen, H. P. Iseli and T. Seiler (2009). "Collagen crosslinking with ultraviolet-A and hypoosmolar riboflavin solution in thin corneas." J Cataract Refract Surg 35(4): 621-624.
Hahn, R. A. and D. E. Birk (1992). "beta-D xyloside alters dermatan sulfate proteoglycan synthesis and the organization of the developing avian corneal stroma." Development 115(2): 383-393.
Hammer, A., O. Richoz, S. Arba Mosquera, D. Tabibian, F. Hoogewoud and F. Hafezi (2014). "Corneal biomechanical properties at different corneal cross-linking (CXL) irradiances." Invest Ophthalmol Vis Sci 55(5): 2881-2884.
Hanna, K. D., F. E. Jouve, G. O. Waring, 3rd and P. G. Ciarlet (1992). "Computer simulation of arcuate keratotomy for astigmatism." Refract Corneal Surg 8(2): 152-163.
Hashemi, H., M. Miraftab, M. A. Seyedian, F. Hafezi, H. Bahrmandy, S. Heidarian, K. Amanzadeh, H. Nikbin, A. Fotouhi and S. Asgari (2015). "Long-term Results of an Accelerated Corneal Cross-linking Protocol (18 mW/cm2) for the Treatment of Progressive Keratoconus." Am J Ophthalmol 160(6): 1164-1170 e1161.
Hashemian, H., M. Jabbarvand, M. Khodaparast and K. Ameli (2014). "Evaluation of corneal changes after conventional versus accelerated corneal cross-linking: a randomized controlled trial." J Refract Surg 30(12): 837-842.
Hatami-Marbini, H. (2014). "Hydration dependent viscoelastic tensile behavior of cornea." Ann Biomed Eng 42(8): 1740-1748.
Hatami-Marbini, H. (2014). "Viscoelastic shear properties of the corneal stroma." J Biomech 47(3): 723-728.
Hatami-Marbini, H., E. Etebu and A. Rahimi (2013). "Swelling pressure and hydration behavior of porcine corneal stroma." Curr Eye Res 38(11): 1124-1132.
Hatami-Marbini, H. and A. Rahimi (2016). "Interrelation of Hydration, Collagen Cross-Linking Treatment, and Biomechanical Properties of the Cornea." Curr Eye Res 41(5): 616-622.
Hayashi, S., T. Osawa and K. Tohyama (2002). "Comparative observations on corneas, with special reference to Bowman's layer and Descemet's membrane in mammals and amphibians." J Morphol 254(3): 247-258.
Hayes, S., C. Boote, C. S. Kamma-Lorger, M. S. Rajan, J. Harris, E. Dooley, N. Hawksworth, J. Hiller, N. J. Terill, F. Hafezi, A. K. Brahma, A. J. Quantock and K. M. Meek (2011). "Riboflavin/UVA collagen cross-linking-induced changes in normal and keratoconus corneal stroma." PLoS One 6(8): e22405.
Hayes, S., C. Boote, J. Lewis, J. Sheppard, M. Abahussin, A. J. Quantock, C. Purslow, M. Votruba and K. M. Meek (2007). "Comparative study of fibrillar collagen arrangement in the corneas of primates and other mammals." Anat Rec (Hoboken) 290(12): 1542-1550.
Hayes, S., C. Boote, S. J. Tuft, A. J. Quantock and K. M. Meek (2007). "A study of corneal thickness, shape and collagen organisation in keratoconus using videokeratography and X-ray scattering techniques." Exp Eye Res 84(3): 423-434.
Hayes, S., C. S. Kamma-Lorger, C. Boote, R. D. Young, A. J. Quantock, A. Rost, Y. Khatib, J. Harris, N. Yagi, N. Terrill and K. M. Meek (2013). "The effect of riboflavin/UVA collagen cross-linking

therapy on the structure and hydrodynamic behaviour of the ungulate and rabbit corneal stroma." PLoS One 8(1): e52860.
Hayes, S., C. Kamma-Lorger Cs Fau - Boote, R. D. Boote C Fau - Young, A. J. Young Rd Fau - Quantock, A. Quantock Aj Fau - Rost, Y. Rost A Fau - Khatib, J. Khatib Y Fau - Harris, N. Harris J Fau - Yagi, N. Yagi N Fau - Terrill, K. M. Terrill N Fau - Meek and K. M. Meek (2013). "The effect of riboflavin/UVA collagen cross-linking therapy on the structure and hydrodynamic behaviour of the ungulate and rabbit corneal stroma." PLoS ONE 8(1932-6203 (Electronic)).
Hayes, S., T. White, C. Boote, C. S. Kamma-Lorger, J. Bell, T. Sorenson, N. Terrill, O. Shebanova and K. M. Meek (2017). "The structural response of the cornea to changes in stromal hydration." J R Soc Interface 14(131).
Hedbys, B. O. (1961). "The role of polysaccharides in corneal swelling." Experimental Eye Research 1(1): 81-91.
Hersh, P. S., S. A. Greenstein and K. L. Fry (2011). "Corneal collagen crosslinking for keratoconus and corneal ectasia: One-year results." J Cataract Refract Surg 37(1): 149-160.
Higgins, J. P., S. G. Thompson, J. J. Deeks and D. G. Altman (2003). "Measuring inconsistency in meta-analyses." BMJ 327(7414): 557-560.
Ho, L. T., A. M. Harris, H. Tanioka, N. Yagi, S. Kinoshita, B. Caterson, A. J. Quantock, R. D. Young and K. M. Meek (2014). "A comparison of glycosaminoglycan distributions, keratan sulphate sulphation patterns and collagen fibril architecture from central to peripheral regions of the bovine cornea." Matrix Biol 38: 59-68.
Hodson, S. A. and K. R. Mayes (1978). "Intercellular spaces and coupled water transport in the rabbit cornea [proceedings]." J Physiol 284: 146P.
Hoeltzel, D. A., P. Altman, K. Buzard and K. Choe (1992). "Strip extensiometry for comparison of the mechanical response of bovine, rabbit, and human corneas." J Biomech Eng 114(2): 202-215.
Holmes, D. F., C. J. Gilpin, C. Baldock, U. Ziese, A. J. Koster and K. E. Kadler (2001). "Corneal collagen fibril structure in three dimensions: Structural insights into fibril assembly, mechanical properties, and tissue organization." Proc Natl Acad Sci U S A 98(13): 7307-7312.
Hong, C. W., A. Sinha-Roy, L. Schoenfield, J. T. McMahon and W. J. Dupps, Jr. (2012). "Collagenase-mediated tissue modeling of corneal ectasia and collagen cross-linking treatments." Invest Ophthalmol Vis Sci 53(4): 2321-2327.
Hovakimyan, M., R. Guthoff, S. Knappe, A. Zhivov, A. Wree, A. Kruger, A. Heisterkamp and O. Stachs (2011). "Short-term corneal response to cross-linking in rabbit eyes assessed by in vivo confocal laser scanning microscopy and histology." Cornea 30(2): 196-203.
Hovakimyan, M., R. F. Guthoff and O. Stachs (2012). "Collagen cross-linking: current status and future directions." J Ophthalmol 2012: 406850.
Huang, R., H. J. Kim and D. B. Min (2006). "Photosensitizing effect of riboflavin, lumiflavin, and lumichrome on the generation of volatiles in soy milk." J Agric Food Chem 54(6): 2359-2364.
Huang, Y. and K. M. Meek (1999). "Swelling studies on the cornea and sclera: the effects of pH and ionic strength." Biophys J 77(3): 1655-1665.
Ihalainen, A., T. Salo, H. Forsius and L. Peltonen (1986). "Increase in type I and type IV collagenolytic activity in primary cultures of keratoconus cornea." Eur J Clin Invest 16(1): 78-84.
Iozzo, R. V. (1999). "The biology of the small leucine-rich proteoglycans. Functional network of interactive proteins." J Biol Chem 274(27): 18843-18846.
Iseli, H. P., M. Popp, T. Seiler, E. Spoerl and M. Mrochen (2011). "Laboratory measurement of the absorption coefficient of riboflavin for ultraviolet light (365 nm)." J Refract Surg 27(3): 195-201.
Iseli, H. P., M. A. Thiel, F. Hafezi, J. Kampmeier and T. Seiler (2008). "Ultraviolet A/riboflavin corneal cross-linking for infectious keratitis associated with corneal melts." Cornea 27(5): 590-594.
Ivarsen, A. and J. Hjortdal (2013). "Collagen cross-linking for advanced progressive keratoconus." Cornea 32(7): 903-906.
Ivekovic, S., E. Trucco and Y. R. Petillot (2008). "Human body pose estimation with particle swarm optimisation." Evol Comput 16(4): 509-528.
Jester, J. V., W. M. Petroll and H. D. Cavanagh (1999). "Corneal stromal wound healing in refractive surgery: the role of myofibroblasts." Prog Retin Eye Res 18(3): 311-356.

Jiang, L. Z., W. Jiang and S. Y. Qiu (2017). "Conventional vs. pulsed-light accelerated corneal collagen cross-linking for the treatment of progressive keratoconus: 12-month results from a prospective study." Exp Ther Med 14(5): 4238-4244.
Jones, L. R., N. W. Preyer, H. C. Wolfsen, D. M. Reynolds, M. A. Davis and M. B. Wallace (2009). "Monte carlo model of stricture formation in photodynamic therapy of normal pig esophagus." Photochem Photobiol 85(1): 341-346.
Jue, B. and D. M. Maurice (1986). "The mechanical properties of the rabbit and human cornea." J Biomech 19(10): 847-853.
Kamaev, P., M. D. Friedman, E. Sherr and D. Muller (2012). "Photochemical kinetics of corneal cross-linking with riboflavin." Invest Ophthalmol Vis Sci 53(4): 2360-2367.
Kampik, D., M. Koch, K. Kampik and G. Geerling (2011). "[Corneal riboflavin/UV-A collagen cross-linking (CXL) in keratoconus: two-year results]." Klin Monbl Augenheilkd 228(6): 525-530.
Kanellopoulos, A. J. (2012). "Long term results of a prospective randomized bilateral eye comparison trial of higher fluence, shorter duration ultraviolet A radiation, and riboflavin collagen cross linking for progressive keratoconus." Clin Ophthalmol 6: 97-101.
Kanellopoulos, A. J. and P. S. Binder (2007). "Collagen cross-linking (CCL) with sequential topography-guided PRK: a temporizing alternative for keratoconus to penetrating keratoplasty." Cornea 26(7): 891-895.
Kao, W. W. and C. Y. Liu (2002). "Roles of lumican and keratocan on corneal transparency." Glycoconj J 19(4-5): 275-285.
Kato, M., H. Wang, M. Bernfield, J. T. Gallagher and J. E. Turnbull (1994). "Cell surface syndecan-1 on distinct cell types differs in fine structure and ligand binding of its heparan sulfate chains." J Biol Chem 269(29): 18881-18890.
Kennedy, R. H., W. M. Bourne and J. A. Dyer (1986). "A 48-year clinical and epidemiologic study of keratoconus." Am J Ophthalmol 101(3): 267-273.
Kim, W. J., Y. S. Rabinowitz, D. M. Meisler and S. E. Wilson (1999). "Keratocyte apoptosis associated with keratoconus." Exp Eye Res 69(5): 475-481.
Kissner, A., E. Spoerl, R. Jung, K. Spekl, L. E. Pillunat and F. Raiskup (2010). "Pharmacological modification of the epithelial permeability by benzalkonium chloride in UVA/Riboflavin corneal collagen cross-linking." Curr Eye Res 35(8): 715-721.
Kling, S., L. Remon, A. Perez-Escudero, J. Merayo-Lloves and S. Marcos (2010). "Corneal biomechanical changes after collagen cross-linking from porcine eye inflation experiments." Invest Ophthalmol Vis Sci 51(8): 3961-3968.
Kohgo, H., H. Isoda, H. Takeda, S. Inagawa, K. Sugiyama, S. Yamashita and H. Sakahara (2006). "Visualization of spinal cord motion associated with the cardiac pulse by tagged magnetic resonance imaging with particle image velocimetry software." J Comput Assist Tomogr 30(1): 111-115.
Kohlhaas, M., E. Spoerl, T. Schilde, G. Unger, C. Wittig and L. E. Pillunat (2006). "Biomechanical evidence of the distribution of cross-links in corneas treated with riboflavin and ultraviolet A light." J Cataract Refract Surg 32(2): 279-283.
Kohlhaas, M., E. Spoerl, A. Speck, T. Schilde, D. Sandner and L. E. Pillunat (2005). "[A new treatment of keratectasia after LASIK by using collagen with riboflavin/UVA light cross-linking]." Klin Monbl Augenheilkd 222(5): 430-436.
Koller, T., M. Mrochen and T. Seiler (2009). "Complication and failure rates after corneal crosslinking." J Cataract Refract Surg 35(8): 1358-1362.
Komai, Y. and T. Ushiki (1991). "The three-dimensional organization of collagen fibrils in the human cornea and sclera." Invest Ophthalmol Vis Sci 32(8): 2244-2258.
Konstantopoulos, A. and J. S. Mehta (2015). "Conventional versus accelerated collagen cross-linking for keratoconus." Eye Contact Lens 41(2): 65-71.
Koppen, C., J. C. Vryghem, L. Gobin (2009). "Keratitis and corneal scarring after UVA/ riboflavin cross-linking for keratoconus." J Refract Surg 25(9):S819–S823.
Kortuem, K. U., E. Vounotrypidis, A. Athanasiou, M. Muller, A. Babenko, C. Kern, S. Priglinger and W. J. Mayer (2017). "Differences in corneal clinical findings after standard and accelerated cross-linking in patients with progressive keratoconus." BMC Ophthalmol 17(1): 222.

Koster, S., J. B. Leach, B. Struth, T. Pfohl and J. Y. Wong (2007). "Visualization of flow-aligned type I collagen self-assembly in tunable pH gradients." Langmuir 23(2): 357-359.
Kozobolis, V., G. Labiris, M. Gkika, H. Sideroudi, E. Kaloghianni, D. Papadopoulou and G. Toufexis (2010). "UV-A Collagen Cross-Linking Treatment of Bullous Keratopathy Combined With Corneal Ulcer." Cornea 29(2): 235-238.
Krachmer, J. H., R. S. Feder and M. W. Belin (1984). "Keratoconus and related noninflammatory corneal thinning disorders." Surv Ophthalmol 28(4): 293-322.
Krueger, R. R. and J. C. Ramos-Esteban (2007). "How might corneal elasticity help us understand diabetes and intraocular pressure?" J Refract Surg 23(1): 85-88.
Kuo, I. C., A. Broman, A. Pirouzmanesh and M. Melia (2006). "Is there an association between diabetes and keratoconus?" Ophthalmology 113(2): 184-190.
Kymionis, G. D., D. I. Bouzoukis, V. F. Diakonis (2007). "Diffuse lamellar keratitis after corneal collagen crosslinking in a patient with post-laser in situ keratomileusis corneal ectasia." J Cataract Refract Surg 33(12):2135–2137.
Kymionis, G. D., M. A. Grentzelos, G. A. Kounis, D. M. Portaliou, E. T. Detorakis, M. Magarakis, V. E. Karampatakis and I. G. Pallikaris (2010). "Intraocular pressure measurements after corneal collagen crosslinking with riboflavin and ultraviolet A in eyes with keratoconus." J Cataract Refract Surg 36(10): 1724-1727.
Kymionis, G. D., G. A. Kounis, D. M. Portaliou, M. A. Grentzelos, A. E. Karavitaki, E. Coskunseven, M. R. Jankov and I. G. Pallikaris (2009). "Intraoperative pachymetric measurements during corneal collagen cross-linking with riboflavin and ultraviolet A irradiation." Ophthalmology 116(12): 2336-2339.
Kymionis, G. D., D. M. Portaliou, D. I. Bouzoukis (2007). "Herpetic keratitis with iritis after corneal crosslinking with riboflavin and ultraviolet A for keratoconus." J Cataract Refract Surg 33(11):1982–1984.
Kymionis, G. D., D. M. Portaliou, V. F. Diakonis, A. E. Karavitaki, S. I. Panagopoulou, M. R. Jankov Ii and E. Coskunseven (2011). "Management of post laser in situ keratomileusis ectasia with simultaneous topography guided photorefractive keratectomy and collagen cross-linking." Open Ophthalmol J 5: 11-13.
Kymionis, G. D., K. I. Tsoulnaras, M. A. Grentzelos, D. A. Liakopoulos, N. G. Tsakalis, S. V. Blazaki, T. A. Paraskevopoulos and M. K. Tsilimbaris (2014). "Evaluation of corneal stromal demarcation line depth following standard and a modified-accelerated collagen cross-linking protocol." Am J Ophthalmol 158(4): 671-675 e671.
Kymionis, G. D., K. I. Tsoulnaras, M. A. Grentzelos, A. D. Plaka, D. G. Mikropoulos, D. A. Liakopoulos, N. G. Tsakalis and I. G. Pallikaris (2014). "Corneal stroma demarcation line after standard and high-intensity collagen crosslinking determined with anterior segment optical coherence tomography." J Cataract Refract Surg 40(5): 736-740.
Laggner, M., A. Pollreisz, G. Schmidinger, R. A. Byrne, C. Scheinecker, U. Schmidt-Erfurth and Y. T. Chen (2015). "Author Response: Analytic Formulas on Factors Determining the Safety and Efficacy in UV-Light-Sensitized Corneal Cross-Linking." Invest Ophthalmol Vis Sci 56(10): 5742.
Lanchares, E., M. A. del Buey, J. A. Cristobal, L. Lavilla and B. Calvo (2011). "Biomechanical property analysis after corneal collagen cross-linking in relation to ultraviolet A irradiation time." Graefes Arch Clin Exp Ophthalmol 249(8): 1223-1227.
Land, M. (2015). "Focusing by shape change in the lens of the eye: a commentary on Young (1801) 'On the mechanism of the eye'." Philos Trans R Soc Lond B Biol Sci 370(1666).
Lapolla, A., P. Traldi and D. Fedele (2005). "Importance of measuring products of non-enzymatic glycation of proteins." Clin Biochem 38(2): 103-115.
Lari, D. R., D. S. Schultz, A. S. Wang, O. T. Lee and J. M. Stewart (2012). "Scleral mechanics: comparing whole globe inflation and uniaxial testing." Exp Eye Res 94(1): 128-135.
Lau, J., J. P. Ioannidis and C. H. Schmid (1998). "Summing up evidence: one answer is not always enough." Lancet 351(9096): 123-127.
Lee, D. and G. Wilson (1981). "Non-uniform swelling properties of the corneal stroma." Curr Eye Res 1(8): 457-461.

Letko, E., P. A. Majmudar, S. L. Forstot, R. J. Epstein and R. S. Rubinfeld (2011). "UVA-light and riboflavin-medicated corneal collagen cross-linking." Int Ophthalmol Clin 51(2): 63-76.
Lewis, J. L., D. A. Krawczak, T. R. Oegema, Jr. and J. J. Westendorf (2010). "Effect of decorin and dermatan sulfate on the mechanical properties of a neocartilage." Connect Tissue Res 51(2): 159-170.
Lewis, P. N., C. Pinali, R. D. Young, K. M. Meek, A. J. Quantock and C. Knupp (2010). "Structural interactions between collagen and proteoglycans are elucidated by three-dimensional electron tomography of bovine cornea." Structure 18(2): 239-245.
Lim, K. S., S. Buyamin, A. Ahmad, M. I. Shapiai, F. Naim, M. Mubin and D. H. Kim (2014). "Improving vector evaluated particle swarm optimisation using multiple nondominated leaders." ScientificWorldJournal 2014: 364179.
Lin, J. T. (2015). "Analytic Formulas on Factors Determining the Safety and Efficacy in UV-Light-Sensitized Corneal Cross-Linking." Invest Ophthalmol Vis Sci 56(10): 5740-5741.
Linder-Ganz, E., G. Yarnitzky, Z. Yizhar, I. Siev-Ner and A. Gefen (2009). "Real-time finite element monitoring of sub-dermal tissue stresses in individuals with spinal cord injury: toward prevention of pressure ulcers." Ann Biomed Eng 37(2): 387-400.
Liu, Y., Y. Liu, Y. N. Zhang, A. P. Li, J. Zhang, Q. F. Liang, Y. Jie and Z. Q. Pan (2017). "Systematic review and Meta-analysis comparing modified cross-linking and standard cross-linking for progressive keratoconus." Int J Ophthalmol 10(9): 1419-1429.
Lombardo, G., S. Serrao, M. Rosati and M. Lombardo (2014). "Analysis of the viscoelastic properties of the human cornea using Scheimpflug imaging in inflation experiment of eye globes." PLoS One 9(11): e112169.
Lombardo, M., S. Serrao, M. Rosati, P. Ducoli and G. Lombardo (2014). "Biomechanical changes in the human cornea after transepithelial corneal crosslinking using iontophoresis." J Cataract Refract Surg 40(10): 1706-1715.
Lubart, R., R. Lavi, H. Friedmann and S. Rochkind (2006). "Photochemistry and photobiology of light absorption by living cells." Photomed Laser Surg 24(2): 179-185.
Luce, D. A. (2005). "Determining in vivo biomechanical properties of the cornea with an ocular response analyzer." J Cataract Refract Surg 31(1): 156-162.
Makdoumi, K., J. Mortensen and S. Crafoord (2010). "Infectious keratitis treated with corneal crosslinking." Cornea 29(12): 1353-1358.
Males, J. J. and D. Viswanathan (2018). "Comparative study of long-term outcomes of accelerated and conventional collagen crosslinking for progressive keratoconus." Eye (Lond) 32(1): 32-38.
Mao, J. R. and J. Bristow (2001). "The Ehlers-Danlos syndrome: on beyond collagens." J Clin Invest 107(9): 1063-1069.
Martin, R. B. and D. L. Boardman (1993). "The effects of collagen fiber orientation, porosity, density, and mineralization on bovine cortical bone bending properties." J Biomech 26(9): 1047-1054.
Martins, S. A., J. C. Combs, G. Noguera, W. Camacho, P. Wittmann, R. Walther, M. Cano, J. Dick and A. Behrens (2008). "Antimicrobial efficacy of riboflavin/UVA combination (365 nm) in vitro for bacterial and fungal isolates: a potential new treatment for infectious keratitis." Invest Ophthalmol Vis Sci 49(8): 3402-3408.
Mason, S. L., R. M. Stewart, V. R. Kearns, R. L. Williams and C. M. Sheridan (2011). "Ocular epithelial transplantation: current uses and future potential." Regen Med 6(6): 767-782.
Matteoli, S., A. Virga, I. Paladini, R. Mencucci and A. Corvi (2016). "Investigation into the elastic properties of ex vivo porcine corneas subjected to inflation test after cross-linking treatment." J Appl Biomater Funct Mater 14(2): e163-170.
Maurice, D. M. (1957). "The structure and transparency of the cornea." J Physiol 136(2): 263-286.
Maurice, D. M. and F. Monroe (1990). "Cohesive strength of corneal lamellae." Exp Eye Res 50(1): 59-63.
Mazzotta, C., A. Balestrazzi, S. Baiocchi, C. Traversi and A. Caporossi (2007). "Stromal haze after combined riboflavin-UVA corneal collagen cross-linking in keratoconus: in vivo confocal microscopic evaluation." Clin Exp Ophthalmol 35(6): 580-582.

Mazzotta, C., C. Traversi, A. L. Paradiso, M. E. Latronico and M. Rechichi (2014). "Pulsed Light Accelerated Crosslinking versus Continuous Light Accelerated Crosslinking: One-Year Results." J Ophthalmol 2014: 604731.
McCall, A. S., S. Kraft, H. F. Edelhauser, G. W. Kidder, R. R. Lundquist, H. E. Bradshaw, Z. Dedeic, M. J. Dionne, E. M. Clement and G. W. Conrad (2010). "Mechanisms of corneal tissue cross-linking in response to treatment with topical riboflavin and long-wavelength ultraviolet radiation (UVA)." Invest Ophthalmol Vis Sci 51(1): 129-138.
McMonnies, C. W. (2008). "The evidentiary significance of case reports: eye rubbing and keratoconus." Optom Vis Sci 85(4): 262-269.
Medeiros, C. S., N. T. Giacomin, R. L. Bueno, R. C. Ghanem, H. V. Moraes, Jr. and M. R. Santhiago (2016). "Accelerated corneal collagen crosslinking: Technique, efficacy, safety, and applications." J Cataract Refract Surg 42(12): 1826-1835.
Medeiros, F. A. and R. N. Weinreb (2006). "Evaluation of the influence of corneal biomechanical properties on intraocular pressure measurements using the ocular response analyzer." J Glaucoma 15(5): 364-370.
Meek, K. M. (2009). "Corneal collagen-its role in maintaining corneal shape and transparency." Biophys Rev 1(2): 83-93.
Meek, K. M. and C. Boote (2009). "The use of X-ray scattering techniques to quantify the orientation and distribution of collagen in the corneal stroma." Prog Retin Eye Res 28(5): 369-392.
Meek, K. M., N. J. Fullwood, P. H. Cooke, G. F. Elliott, D. M. Maurice, A. J. Quantock, R. S. Wall and C. R. Worthington (1991). "Synchrotron x-ray diffraction studies of the cornea, with implications for stromal hydration." Biophys J 60(2): 467-474.
Meek, K. M. and C. Knupp (2015). "Corneal structure and transparency." Prog Retin Eye Res 49: 1-16.
Meek, K. M. and R. H. Newton (1999). "Organization of collagen fibrils in the corneal stroma in relation to mechanical properties and surgical practice." J Refract Surg 15(6): 695-699.
Meek, K. M., S. J. Tuft, Y. Huang, P. S. Gill, S. Hayes, R. H. Newton and A. J. Bron (2005). "Changes in collagen orientation and distribution in keratoconus corneas." Invest Ophthalmol Vis Sci 46(6): 1948-1956.
Mencucci, R., S. Ambrosini, C. Ponchietti, M. Marini, G. B. Vannelli and U. Menchini (2005). "Ultrasound thermal damage to rabbit corneas after simulated phacoemulsification." J Cataract Refract Surg 31(11): 2180-2186.
Mencucci, R., M. Marini, I. Paladini, E. Sarchielli, E. Sgambati, U. Menchini and G. B. Vannelli (2010). "Effects of riboflavin/UVA corneal cross-linking on keratocytes and collagen fibres in human cornea." Clin Exp Ophthalmol 38(1): 49-56.
Mencucci, R., C. Mazzotta, F. Rossi, C. Ponchietti, R. Pini, S. Baiocchi, A. Caporossi and U. Menchini (2007). "Riboflavin and ultraviolet A collagen crosslinking: in vivo thermographic analysis of the corneal surface." J Cataract Refract Surg 33(6): 1005-1008.
Micelli Ferrari, T., M. Leozappa, M. Lorusso, E. Epifani and L. Micelli Ferrari (2009). "Escherichia coli keratitis treated with ultraviolet A/riboflavin corneal cross-linking: a case report." Eur J Ophthalmol 19(2): 295-297.
Michelacci, Y. M. (2003). "Collagens and proteoglycans of the corneal extracellular matrix." Braz J Med Biol Res 36(8): 1037-1046.
Mohammadpour, M., A. Masoumi, M. Mirghorbani, K. Shahraki and H. Hashemi (2017). "Updates on corneal collagen cross-linking: Indications, techniques and clinical outcomes." J Curr Ophthalmol 29(4): 235-247.
Moher, D., L. Shamseer, M. Clarke, D. Ghersi, A. Liberati, M. Petticrew, P. Shekelle, L. A. Stewart and P.-P. Group (2015). "Preferred reporting items for systematic review and meta-analysis protocols (PRISMA-P) 2015 statement." Syst Rev 4: 1.
Moren, H., M. Malmsjo, J. Mortensen and A. Ohrstrom (2010). "Riboflavin and ultraviolet a collagen crosslinking of the cornea for the treatment of keratitis." Cornea 29(1): 102-104.

Morishige, N., Y. Takagi, T. Chikama, A. Takahara and T. Nishida (2011). "Three-dimensional analysis of collagen lamellae in the anterior stroma of the human cornea visualized by second harmonic generation imaging microscopy." Invest Ophthalmol Vis Sci 52(2): 911-915.
Morishige, N., A. J. Wahlert, M. C. Kenney, D. J. Brown, K. Kawamoto, T. Chikama, T. Nishida and J. V. Jester (2007). "Second-harmonic imaging microscopy of normal human and keratoconus cornea." Invest Ophthalmol Vis Sci 48(3): 1087-1094.
Muller, L. J., E. Pels and G. F. Vrensen (2001). "The specific architecture of the anterior stroma accounts for maintenance of corneal curvature." Br J Ophthalmol 85(4): 437-443.
Myers, K. M., B. Coudrillier, B. L. Boyce and T. D. Nguyen (2010). "The inflation response of the posterior bovine sclera." Acta Biomater 6(11): 4327-4335.
Nan, M. and Q. He (2013). "Study on the effect of blood content on diffuse reflectance spectra of basal cell carcinoma skin tissue." ScientificWorldJournal 2013: 192495.
Nash, I. S., P. R. Greene and C. S. Foster (1982). "Comparison of mechanical properties of keratoconus and normal corneas." Exp Eye Res 35(5): 413-424.
Newton, R. H. and K. M. Meek (1998). "The integration of the corneal and limbal fibrils in the human eye." Biophys J 75(5): 2508-2512.
Ng, A. L., T. C. Chan and A. C. Cheng (2016). "Conventional versus accelerated corneal collagen cross-linking in the treatment of keratoconus." Clin Exp Ophthalmol 44(1): 8-14.
Nguyen, T. D., R. E. Jones and B. L. Boyce (2008). "A nonlinear anisotropic viscoelastic model for the tensile behavior of the corneal stroma." J Biomech Eng 130(4): 041020.
Nguyen, T. M., J. F. Aubry, M. Fink, J. Bercoff and M. Tanter (2014). "In vivo evidence of porcine cornea anisotropy using supersonic shear wave imaging." Invest Ophthalmol Vis Sci 55(11): 7545-7552.
Nyquist, G. W. (1968). "Rheology of the cornea: experimental techniques and results." Exp Eye Res 7(2): 183-188.
O'Brart, D. P., E. Chan, K. Samaras, P. Patel and S. P. Shah (2011). "A randomised, prospective study to investigate the efficacy of riboflavin/ultraviolet A (370 nm) corneal collagen cross-linkage to halt the progression of keratoconus." Br J Ophthalmol 95(11): 1519-1524.
O'Brart, N. A. L., D. P. S. O'Brart, N. H. Aldahlawi, S. Hayes and K. M. Meek (2018). "An Investigation of the Effects of Riboflavin Concentration on the Efficacy of Corneal Cross-Linking Using an Enzymatic Resistance Model in Porcine Corneas." Invest Ophthalmol Vis Sci 59(2): 1058-1065.
Paik, D. C., Q. Wen, R. E. Braunstein, S. Airiani and S. L. Trokel (2009). "Initial studies using aliphatic beta-nitro alcohols for therapeutic corneal cross-linking." Invest Ophthalmol Vis Sci 50(3): 1098-1105.
Pandolfi, A. and G. A. Holzapfel (2008). "Three-dimensional modeling and computational analysis of the human cornea considering distributed collagen fibril orientations." J Biomech Eng 130(6): 061006.
Parekh, M., S. Ferrari, C. Sheridan, S. Kaye and S. Ahmad (2016). "Concise Review: An Update on the Culture of Human Corneal Endothelial Cells for Transplantation." Stem Cells Transl Med 5(2): 258-264.
Passaglia, C., F. Dodge, E. Herzog, S. Jackson and R. Barlow (1997). "Deciphering a neural code for vision." Proc Natl Acad Sci U S A 94(23): 12649-12654.
Perez-Santonja, J. J., A. Artola, J. Javaloy, J. L. Alio and J. L. Abad (2009). "Microbial keratitis after corneal collagen crosslinking." J Cataract Refract Surg 35(6): 1138-1140.
Petitti, D. B., R. Contreras, F. H. Ziel, J. Dudl, E. S. Domurat and J. A. Hyatt (2000). "Evaluation of the effect of performance monitoring and feedback on care process, utilization, and outcome." Diabetes Care 23(2): 192-196.
Pinsky, P. M. and D. V. Datye (1992). "Numerical modeling of radial, astigmatic, and hexagonal keratotomy." Refract Corneal Surg 8(2): 164-172.
Polisetti, N. and N. C. Joyce (2013). "The culture of limbal stromal cells and corneal endothelial cells." Methods Mol Biol 1014: 131-139.

Pollhammer, M. and C. Cursiefen (2009). "Bacterial keratitis early after corneal crosslinking with riboflavin and ultraviolet-A." J Cataract Refract Surg 35(3): 588-589.
Qiao, J., H. Li, Y. Tang, W. Song, B. Rong, S. Yang, Y. Wu and X. Yan (2018). "A rabbit model of corneal Ectasia generated by treatment with collagenase type II." BMC Ophthalmol 18(1): 94.
Qu, J., C. Macaulay, S. Lam and B. Palcic (1994). "Optical properties of normal and carcinomatous bronchial tissue." Appl Opt 33(31): 7397-7405.
Quantock, A. J. and R. D. Young (2008). "Development of the corneal stroma, and the collagen-proteoglycan associations that help define its structure and function." Dev Dyn 237(10): 2607-2621.
Rabinowitz, Y. S. (1998). "Keratoconus." Surv Ophthalmol 42(4): 297-319.
Raiskup, F., A. Hoyer and E. Spoerl (2009). "Permanent corneal haze after riboflavin-UVA-induced cross-linking in keratoconus." J Refract Surg 25(9): S824-828.
Raiskup, F. and E. Spoerl (2013). "Corneal crosslinking with riboflavin and ultraviolet A. I. Principles." Ocul Surf 11(2): 65-74.
Raiskup, F. and E. Spoerl (2013). "Corneal crosslinking with riboflavin and ultraviolet A. Part II. Clinical indications and results." Ocul Surf 11(2): 93-108.
Raiskup-Wolf, F., A. Hoyer, E. Spoerl and L. E. Pillunat (2008). "Collagen crosslinking with riboflavin and ultraviolet-A light in keratoconus: long-term results." J Cataract Refract Surg 34(5): 796-801.
Rama, P., F. Di Matteo, S. Matuska (2009). "Acanthamoeba keratitis with perforation after corneal collagen crosslinking and bandage contact lens." J Cataract Refract Surg 35(4):788–791.
Randers, E., J. H. Kristensen, E. J. Erlandsen and H. Danielsen (1998). "Serum cystatin C as a marker of the renal function." Scand J Clin Lab Invest 58(7): 585-592.
Rehany, U., M. Lahav and S. Shoshan (1982). "Collagenolytic activity in keratoconus." Ann Ophthalmol 14(8): 751-754.
Richoz, O., S. Kling, S. Zandi, A. Hammer, E. Spoerl and F. Hafezi (2014). "A constant-force technique to measure corneal biomechanical changes after collagen cross-linking." PLoS One 9(8): e105095.
Riley, G. P., R. L. Harrall, P. G. Watson, T. E. Cawston and B. L. Hazleman (1995). "Collagenase (MMP-1) and TIMP-1 in destructive corneal disease associated with rheumatoid arthritis." Eye 9(6): 703-718.
Rocha, K. M., J. C. Ramos-Esteban, Y. Qian, S. Herekar and R. R. Krueger (2008). "Comparative study of riboflavin-UVA cross-linking and "flash-linking" using surface wave elastometry." J Refract Surg 24(7): S748-751.
Ruberti, J. W., A. Sinha Roy and C. J. Roberts (2011). "Corneal biomechanics and biomaterials." Annu Rev Biomed Eng 13: 269-295.
Rubinoff, C. H. and E. H. Greener (1985). "Physical properties of an experimental periodontal dressing material." Dent Mater 1(1): 3-6.
Sadoughi, M. M., B. Einollahi, A. Baradaran-Rafii, D. Roshandel, H. Hasani and M. Nazeri (2018). "Accelerated versus conventional corneal collagen cross-linking in patients with keratoconus: an intrapatient comparative study." Int Ophthalmol 38(1): 67-74.
Salomao, M. Q., S. S. Chaurasia, A. Sinha-Roy, R. Ambrosio, Jr., A. Esposito, R. Sepulveda, V. Agrawal and S. E. Wilson (2011). "Corneal wound healing after ultraviolet-A/riboflavin collagen cross-linking: a rabbit study." J Refract Surg 27(6): 401-407.
Sawaguchi, T. (1998). "Attenuation of delay-period activity of monkey prefrontal neurons by an alpha2-adrenergic antagonist during an oculomotor delayed-response task." J Neurophysiol 80(4): 2200-2205.
Schumacher, S., M. Mrochen, J. Wernli, M. Bueeler and T. Seiler (2012). "Optimization model for UV-riboflavin corneal cross-linking." Invest Ophthalmol Vis Sci 53(2): 762-769.
Schumacher, S., L. Oeftiger and M. Mrochen (2011). "Equivalence of biomechanical changes induced by rapid and standard corneal cross-linking, using riboflavin and ultraviolet radiation." Invest Ophthalmol Vis Sci 52(12): 9048-9052.

Scott, J. E. (1992). "Morphometry of cupromeronic blue-stained proteoglycan molecules in animal corneas, versus that of purified proteoglycans stained in vitro, implies that tertiary structures contribute to corneal ultrastructure." Journal of Anatomy 180(Pt 1): 155-164.
Scott, J. E. (1992). "Morphometry of cupromeronic blue-stained proteoglycan molecules in animal corneas, versus that of purified proteoglycans stained in vitro, implies that tertiary structures contribute to corneal ultrastructure." J Anat 180 (Pt 1): 155-164.
Scroggs, M. W. and A. D. Proia (1992). "Histopathological variation in keratoconus." Cornea 11(6): 553-559.
Seifert, J., C. M. Hammer, J. Rheinlaender, S. Sel, M. Scholz, F. Paulsen and T. E. Schaffer (2014). "Distribution of Young's modulus in porcine corneas after riboflavin/UVA-induced collagen cross-linking as measured by atomic force microscopy." PLoS One 9(1): e88186.
Seiler, T., S. Huhle, E. Spoerl and H. Kunath (2000). "Manifest diabetes and keratoconus: a retrospective case-control study." Graefes Arch Clin Exp Ophthalmol 238(10): 822-825.
Shah, S., M. Laiquzzaman, R. Bhojwani, S. Mantry and I. Cunliffe (2007). "Assessment of the biomechanical properties of the cornea with the ocular response analyzer in normal and keratoconic eyes." Invest Ophthalmol Vis Sci 48(7): 3026-3031.
Sharif, R., B. Fowler and D. Karamichos (2018). "Collagen cross-linking impact on keratoconus extracellular matrix." PLoS One 13(7): e0200704.
Sharma, N., P. Maharana, G. Singh and J. S. Titiyal (2010). "Pseudomonas keratitis after collagen crosslinking for keratoconus: case report and review of literature." J Cataract Refract Surg 36(3): 517-520.
Sherif, A. M. (2014). "Accelerated versus conventional corneal collagen cross-linking in the treatment of mild keratoconus: a comparative study." Clin Ophthalmol 8: 1435-1440.
Sherwin, C. P., T. P. Labuza, A. McCormick and B. Chen (2002). "Cross-polarization/magic angle spinning NMR to study glucose mobility in a model intermediate-moisture food system." J Agric Food Chem 50(26): 7677-7683.
Shetty, R., N. K. Pahuja, R. M. Nuijts, A. Ajani, C. Jayadev, C. Sharma and H. Nagaraja (2015). "Current Protocols of Corneal Collagen Cross-Linking: Visual, Refractive, and Tomographic Outcomes." Am J Ophthalmol 160(2): 243-249.
Shetty, R., A. Sathyanarayanamoorthy, R. A. Ramachandra, V. Arora, A. Ghosh, P. R. Srivatsa, N. Pahuja, R. M. M. A. Nuijts, A. Sinha-Roy, R. R. Mohan and A. Ghosh (2015). "Attenuation of lysyl oxidase and collagen gene expression in keratoconus patient corneal epithelium corresponds to disease severity." Molecular Vision 21: 12-25.
Shin, T. J., R. P. Vito, L. W. Johnson and B. E. McCarey (1997). "The distribution of strain in the human cornea." J Biomech 30(5): 497-503.
Sinha Roy, A. and W. J. Dupps, Jr. (2011). "Patient-specific modeling of corneal refractive surgery outcomes and inverse estimation of elastic property changes." J Biomech Eng 133(1): 011002.
Sinha Roy, A., K. M. Rocha, J. B. Randleman, R. D. Stulting and W. J. Dupps, Jr. (2013). "Inverse computational analysis of in vivo corneal elastic modulus change after collagen crosslinking for keratoconus." Exp Eye Res 113: 92-104.
Smolek, M. K., T. Oshika, S. D. Klyce, N. Maeda, D. H. Haight and M. B. McDonald (1998). "Topographic assessment of irregular astigmatism after photorefractive keratectomy." J Cataract Refract Surg 24(8): 1079-1086.
Snedeker, J. G. and A. Gautieri (2014). "The role of collagen crosslinks in ageing and diabetes - the good, the bad, and the ugly." Muscles, Ligaments and Tendons Journal 4(3): 303-308.
Snyder, M. C., J. P. Bergmanson and M. J. Doughty (1998). "Keratocytes: no more the quiet cells." J Am Optom Assoc 69(3): 180-187.
Sondergaard, A. P., A. Ivarsen and J. Hjortdal (2013). "Corneal resistance to shear force after UVA-riboflavin cross-linking." Invest Ophthalmol Vis Sci 54(7): 5059-5069.
Spoerl, E., M. Huhle and T. Seiler (1998). "Induction of cross-links in corneal tissue." Exp Eye Res 66(1): 97-103.
Spoerl, E., M. Mrochen, D. Sliney, S. Trokel and T. Seiler (2007). "Safety of UVA-riboflavin cross-linking of the cornea." Cornea 26(4): 385-389.

Spoerl, E. and T. Seiler (1999). "Techniques for stiffening the cornea." J Refract Surg 15(6): 711-713.
Spoerl, E., G. Wollensak, D. D. Dittert and T. Seiler (2004). "Thermomechanical behavior of collagen-cross-linked porcine cornea." Ophthalmologica 218(2): 136-140.
Spoerl, E., T. Wollensak G Fau - Seiler and T. Seiler (2009). "Increased resistance of crosslinked cornea against enzymatic digestion." Current Eye Research 29(0271-3683 (Print)).
Spoerl, E., G. Wollensak and T. Seiler (2004). "Increased resistance of crosslinked cornea against enzymatic digestion." Curr Eye Res 29(1): 35-40.
Sridhar, M. S. (2018). "Anatomy of cornea and ocular surface." Indian J Ophthalmol 66(2): 190-194.
Srodka, W. and D. R. Iskander (2008). "Optically inspired biomechanical model of the human eyeball." J Biomed Opt 13(4): 044034.
Stang, A. (2010). "Critical evaluation of the Newcastle-Ottawa scale for the assessment of the quality of nonrandomized studies in meta-analyses." Eur J Epidemiol 25(9): 603-605.
Steven, P., M. Hovakimyan, R. F. Guthoff, G. Huttmann and O. Stachs (2010). "Imaging corneal crosslinking by autofluorescence 2-photon microscopy, second harmonic generation, and fluorescence lifetime measurements." J Cataract Refract Surg 36(12): 2150-2159.
Stewart, J. M., D. S. Schultz, O. T. Lee and M. L. Trinidad (2009). "Collagen cross-links reduce corneal permeability." Invest Ophthalmol Vis Sci 50(4): 1606-1612.
Stramer, B. M., J. D. Zieske, J. C. Jung, J. S. Austin and M. E. Fini (2003). "Molecular mechanisms controlling the fibrotic repair phenotype in cornea: implications for surgical outcomes." Invest Ophthalmol Vis Sci 44(10): 4237-4246.
Stryer, L. (1987). "The molecules of visual excitation." Sci Am 257(1): 42-50.
Studer, H., X. Larrea, H. Riedwyl and P. Buchler (2010). "Biomechanical model of human cornea based on stromal microstructure." J Biomech 43(5): 836-842.
Subasinghe, S. K., K. C. Ogbuehi and G. J. Dias (2018). "Current perspectives on corneal collagen crosslinking (CXL)." Graefes Arch Clin Exp Ophthalmol 256(8): 1363-1384.
Sung, H. W., W. H. Chang, C. Y. Ma and M. H. Lee (2003). "Crosslinking of biological tissues using genipin and/or carbodiimide." J Biomed Mater Res A 64(3): 427-438.
Tabbara, K. F., O. M. Al-Omar, H. F. El-Sheikh and N. Sharara (1999). "The long term effects of unilateral corneal scars." Doc Ophthalmol 98(3): 267-272.
Tachibana, M., M. Okamoto, M. Sakamoto and Y. Matsushima (2002). "Hereditary keratoconus-like keratopathy in Japanese wild mice mapped to mouse Chromosome 13." Mamm Genome 13(12): 692-695.
Takahashi, K., A. Murakami and S. Okisaka (1999). "[Kerato-epithelin mutation (R 555 Q) in a case of Reis-Bucklers corneal dystrophy]." Nippon Ganka Gakkai Zasshi 103(10): 761-764.
Takaoka, A., N. Babar, J. Hogan, M. Kim, M. O. Price, J. F. W. Price, S. L. Trokel and D. C. Paik (2016). "An Evaluation of Lysyl Oxidase–Derived Cross-Linking in Keratoconus by Liquid Chromatography/Mass SpectrometryCross-Linking Evaluation in Keratoconus by LC/MS." Investigative Ophthalmology & Visual Science 57(1): 126-136.
Tanter, M., D. Touboul, J. L. Gennisson, J. Bercoff and M. Fink (2009). "High-resolution quantitative imaging of cornea elasticity using supersonic shear imaging." IEEE Trans Med Imaging 28(12): 1881-1893.
Tomita, M., M. Mita and T. Huseynova (2014). "Accelerated versus conventional corneal collagen crosslinking." J Cataract Refract Surg 40(6): 1013-1020.
Touboul, D., N. Efron, D. Smadja, D. Praud, F. Malet and J. Colin (2012). "Corneal confocal microscopy following conventional, transepithelial, and accelerated corneal collagen cross-linking procedures for keratoconus." J Refract Surg 28(11): 769-776.
Twa, M. D., J. Li, S. Vantipalli, M. Singh, S. Aglyamov, S. Emelianov and K. V. Larin (2014). "Spatial characterization of corneal biomechanical properties with optical coherence elastography after UV cross-linking." Biomed Opt Express 5(5): 1419-1427.
Uchio, E., S. Ohno, J. Kudoh, K. Aoki and L. T. Kisielewicz (1999). "Simulation model of an eyeball based on finite element analysis on a supercomputer." Br J Ophthalmol 83(10): 1106-1111.

Vinciguerra, P., E. Albe, B. E. Frueh, S. Trazza and D. Epstein (2012). "Two-year corneal cross-linking results in patients younger than 18 years with documented progressive keratoconus." Am J Ophthalmol 154(3): 520-526.
Vinciguerra, P., E. Albe, A. M. Mahmoud, S. Trazza, F. Hafezi and C. J. Roberts (2010). "Intra- and postoperative variation in ocular response analyzer parameters in keratoconic eyes after corneal cross-linking." J Refract Surg 26(9): 669-676.
Vinciguerra, P., E. Albe, S. Trazza, T. Seiler and D. Epstein (2009). "Intraoperative and postoperative effects of corneal collagen cross-linking on progressive keratoconus." Arch Ophthalmol 127(10): 1258-1265.
Waller, S. G., R. F. Steinert and M. D. Wagoner (1995). "Long-term results of epikeratoplasty for keratoconus." Cornea 14(1): 84-88.
Waltman, S. R. and T. C. Patrowicz (1970). "Effects of hydroxypropyl methylcellulose and polyvinyl alcohol on intraocular penetration of topical fluorescein in man." Invest Ophthalmol 9(12): 966-970.
Wang, X., Y. Huang, S. Jastaneiah, S. Majumdar, J. U. Kang, S. C. Yiu, W. Stark and J. H. Elisseeff (2015). "Protective Effects of Soluble Collagen during Ultraviolet-A Crosslinking on Enzyme-Mediated Corneal Ectatic Models." PLoS One 10(9): e0136999.
Wang, Y., Y. S. Rabinowitz, J. I. Rotter and H. Yang (2000). "Genetic epidemiological study of keratoconus: evidence for major gene determination." Am J Med Genet 93(5): 403-409.
Waszczykowska, A. and P. Jurowski (2015). "Two-year accelerated corneal cross-linking outcome in patients with progressive keratoconus." Biomed Res Int 2015: 325157.
Watson, P. G. and R. D. Young (2004). "Scleral structure, organisation and disease. A review." Exp Eye Res 78(3): 609-623.
Wernli, J., S. Schumacher, E. Spoerl and M. Mrochen (2013). "The efficacy of corneal cross-linking shows a sudden decrease with very high intensity UV light and short treatment time." Invest Ophthalmol Vis Sci 54(2): 1176-1180.
White, T. L., P. N. Lewis, R. D. Young, K. Kitazawa, T. Inatomi, S. Kinoshita and K. M. Meek (2017). "Elastic microfibril distribution in the cornea: Differences between normal and keratoconic stroma." Exp Eye Res 159: 40-48.
Whitford, C., A. Joda, S. Jones, F. Bao, P. Rama and A. Elsheikh (2016). "Ex vivo testing of intact eye globes under inflation conditions to determine regional variation of mechanical stiffness." Eye Vis (Lond) 3: 21.
Whitford, C., N. V. Movchan, H. Studer and A. Elsheikh (2018). "A viscoelastic anisotropic hyperelastic constitutive model of the human cornea." Biomech Model Mechanobiol 17(1): 19-29.
Whitford, C., H. Studer, C. Boote, K. M. Meek and A. Elsheikh (2015). "Biomechanical model of the human cornea: considering shear stiffness and regional variation of collagen anisotropy and density." J Mech Behav Biomed Mater 42: 76-87.
Williams, V. Z. (1945). "Infrared and Raman Spectra of Polyatomic Molecules (Herzberg, Gerhard)." Journal of Chemical Education 22(11): 572.
Wilson, S. E., Y. G. He, J. Weng, Q. Li, A. W. McDowall, M. Vital and E. L. Chwang (1996). "Epithelial injury induces keratocyte apoptosis: hypothesized role for the interleukin-1 system in the modulation of corneal tissue organization and wound healing." Exp Eye Res 62(4): 325-327.
Wilson, S. E. and J. W. Hong (2000). "Bowman's layer structure and function: critical or dispensable to corneal function? A hypothesis." Cornea 19(4): 417-420.
Winkler, M., D. Chai, S. Kriling, C. J. Nien, D. J. Brown, B. Jester, T. Juhasz and J. V. Jester (2011). "Nonlinear optical macroscopic assessment of 3-D corneal collagen organization and axial biomechanics." Invest Ophthalmol Vis Sci 52(12): 8818-8827.
Wittig-Silva, C., E. Chan, F. M. Islam, T. Wu, M. Whiting and G. R. Snibson (2014). "A randomized, controlled trial of corneal collagen cross-linking in progressive keratoconus: three-year results." Ophthalmology 121(4): 812-821.
Wollensak, G. (2006). "Crosslinking treatment of progressive keratoconus: new hope." Curr Opin Ophthalmol 17(4): 356-360.
Wollensak, G. (2010). "Histological changes in human cornea after cross-linking with riboflavin and ultraviolet A." Acta Ophthalmol 88(2): e17-18.

Wollensak, G., H. Aurich, D. T. Pham and C. Wirbelauer (2007). "Hydration behavior of porcine cornea crosslinked with riboflavin and ultraviolet A." J Cataract Refract Surg 33(3): 516-521.
Wollensak, G., H. Aurich, C. Wirbelauer and D. T. Pham (2009). "Potential use of riboflavin/UVA cross-linking in bullous keratopathy." Ophthalmic Res 41(2): 114-117.
Wollensak, G., H. Aurich, C. Wirbelauer and S. Sel (2010). "Significance of the riboflavin film in corneal collagen crosslinking." J Cataract Refract Surg 36(1): 114-120.
Wollensak, G. and E. Iomdina (2008). "Crosslinking of scleral collagen in the rabbit using glyceraldehyde." J Cataract Refract Surg 34(4): 651-656.
Wollensak, G. and E. Iomdina (2009). "Biomechanical and histological changes after corneal crosslinking with and without epithelial debridement." J Cataract Refract Surg 35(3): 540-546.
Wollensak, G. and E. Iomdina (2009). "Long-term biomechanical properties of rabbit cornea after photodynamic collagen crosslinking." Acta Ophthalmol 87(1): 48-51.
Wollensak, G., E. Iomdina, D. D. Dittert and H. Herbst (2007). "Wound healing in the rabbit cornea after corneal collagen cross-linking with riboflavin and UVA." Cornea 26(5): 600-605.
Wollensak, G. and B. Redl (2008). "Gel electrophoretic analysis of corneal collagen after photodynamic cross-linking treatment." Cornea 27(3): 353-356.
Wollensak, G., E. Spoerl, F. Reber and T. Seiler (2004). "Keratocyte cytotoxicity of riboflavin/UVA-treatment in vitro." Eye (Lond) 18(7): 718-722.
Wollensak, G., E. Spoerl and T. Seiler (2003). "Riboflavin/ultraviolet-a-induced collagen crosslinking for the treatment of keratoconus." Am J Ophthalmol 135(5): 620-627.
Wollensak, G., E. Spoerl and T. Seiler (2003). "Stress-strain measurements of human and porcine corneas after riboflavin-ultraviolet-A-induced cross-linking." J Cataract Refract Surg 29(9): 1780-1785.
Wollensak, G., E. Spoerl, M. Wilsch and T. Seiler (2004). "Keratocyte apoptosis after corneal collagen cross-linking using riboflavin/UVA treatment." Cornea 23(1): 43-49.
Wollensak, G., E. Sporl, C. Mazzotta, T. Kalinski and S. Sel (2011). "Interlamellar cohesion after corneal crosslinking using riboflavin and ultraviolet A light." Br J Ophthalmol 95(6): 876-880.
Wollensak, G., E. Sporl, F. Reber, L. Pillunat and R. Funk (2003). "Corneal endothelial cytotoxicity of riboflavin/UVA treatment in vitro." Ophthalmic Res 35(6): 324-328.
Wollensak, G., M. Wilsch, E. Spoerl and T. Seiler (2004). "Collagen fiber diameter in the rabbit cornea after collagen crosslinking by riboflavin/UVA." Cornea 23(5): 503-507.
Wollensak, J. and E. Buddecke (1990). "Biochemical studies on human corneal proteoglycans--a comparison of normal and keratoconic eyes." Graefes Arch Clin Exp Ophthalmol 228(6): 517-523.
Wong, T. T., C. Sethi, J. T. Daniels, G. A. Limb, G. Murphy and P. T. Khaw (2002). "Matrix metalloproteinases in disease and repair processes in the anterior segment." Surv Ophthalmol 47(3): 239-256.
Woo, J. H., J. V. Iyer, L. Lim, M. H. Hla, J. S. Mehta, C. M. Chan and D. T. Tan (2017). "Conventional Versus Accelerated Collagen Cross-Linking for Keratoconus: A Comparison of Visual, Refractive, Topographic and Biomechanical Outcomes." Open Ophthalmol J 11: 262-272.
Woo, S. L., A. S. Kobayashi, W. A. Schlegel and C. Lawrence (1972). "Nonlinear material properties of intact cornea and sclera." Exp Eye Res 14(1): 29-39.
Woodward, M. A., T. S. Blachley and J. D. Stein (2016). "The Association Between Sociodemographic Factors, Common Systemic Diseases, and Keratoconus: An Analysis of a Nationwide Heath Care Claims Database." Ophthalmology 123(3): 457-465 e452.
Wright, A., W. A. Bubb, C. L. Hawkins and M. J. Davies (2002). "Singlet oxygen-mediated protein oxidation: evidence for the formation of reactive side chain peroxides on tyrosine residues." Photochem Photobiol 76(1): 35-46.
Xi Cheng, Hamed Hatami-Marbini and P. M. Pinsky (2013). Modeling Collagen-Proteoglycan Structural Interactions in the Human Cornea. Protein and Cell Mechanics. Dordrecht, Springer: 11-24.
Xu, Y. (2009). "Thermal stability of collagen triple helix." Methods Enzymol 466: 211-232.
Young, R. D. (1985). "The ultrastructural organization of proteoglycans and collagen in human and rabbit scleral matrix." J Cell Sci 74: 95-104.

Yu, J. G., F. J. Bao, Y. F. Feng, C. Whitford, T. Ye, Y. B. Huang, Q. M. Wang and A. Elsheikh (2013). "Assessment of corneal biomechanical behavior under posterior and anterior pressure." J Refract Surg 29(1): 64-70.
Yuen, H., J. Princen, J. Illingworth and J. Kittler (1990). "Comparative study of Hough transform methods for circle finding." Image and vision computing 8(1): 71-77.
Zaheer, N., W. A. Khan, S. Khan and M. A. M. Khan (2018). "Comparison of Changes in Central Corneal Thickness During Corneal Collagen Cross-Linking, Using Isotonic Riboflavin Solutions With and Without Dextran, in the Treatment of Progressive Keratoconus." Cornea 37(3): 340-346.
Zamora, K. V., J. J. Males (2009). "Polymicrobial keratitis after a collagen crosslinking procedure with postoperative use of a contact lens: a case report." Cornea 28(4): 474–476.
Zeng, Y., J. Yang, K. Huang, Z. Lee and X. Lee (2001). "A comparison of biomechanical properties between human and porcine cornea." J Biomech 34(4): 533-537.
Zhang, Y., A. H. Conrad and G. W. Conrad (2011). "Effects of Ultraviolet-A and Riboflavin on the Interaction of Collagen and Proteoglycans during Corneal Cross-linking." The Journal of Biological Chemistry 286(15): 13011-13022.
Zhang, Y., A. H. Conrad and G. W. Conrad (2011). "Effects of ultraviolet-A and riboflavin on the interaction of collagen and proteoglycans during corneal cross-linking." J Biol Chem 286(15): 13011-13022.
Zhang, Y., X. Mao, T. Schwend, S. Littlechild and G. W. Conrad (2013). "Resistance of Corneal RFUVA–Cross-Linked Collagens and Small Leucine-Rich Proteoglycans to Degradation by Matrix Metalloproteinases." Investigative Ophthalmology & Visual Science 54(2): 1014-1025.
Zhou, L., S. Sawaguchi, S. S. Twining, J. Sugar, R. S. Feder and B. Y. Yue (1998). "Expression of degradative enzymes and protease inhibitors in corneas with keratoconus." Invest Ophthalmol Vis Sci 39(7): 1117-1124.